# ABSTRACT

## SYNTHESIS, MOLECULAR AND SOLID STATE STRUCTURES, AND MAGNETIC PROPERTIES OF SANDWICH LANTHANIDE PHTHALOCYANINES LACKING C-H BONDS

**by**
**Wycliffe A. Graham**

A new class of sandwich phthalocyanine (Pc) compounds without C-H bonds was synthesized and characterized. They are the bis[octakis(perfluoro $i$-$C_3F_7$) octakis(perfluoro)phthalocyaninato(2−)]M(III) complexes, formulated as $(F_{64}Pc)_2MH$, M = Tb, Dy, Lu, Y. Single molecular magnetic (SMM) behavior in the $(F_{64}Pc)_2TbH$ and $(F_{64}Pc)_2DyH$ complexes was confirmed through slowed relaxation response of their magnetization in an applied time varying magnetic field during alternating current (AC) magnetic testing in the range 2 - 50 K. The energy barrier to magnetic reversal, $\Delta = 215$ $cm^{-1}$ and the pre-exponential factor, $\tau_0^{-1} = 2.7 \times 10^7$ $s^{-1}$ were estimated for the undiluted $(F_{64}Pc)_2TbH$ with direct current bias magnetic field ($H$dc) of 1000 Oe applied. Undiluted $(F_{64}Pc)_2DyH$ gave estimated values of $\Delta = 31$ $cm^{-1}$ and $\tau_0^{-1} = 1.6 \times 10^5$ $s^{-1}$ at $H$dc = 500 Oe. These respective values are within the range observed for the unsubstituted Tb and Dy analogues. Magnetic hysteresis testing at 0.04 K exhibited hysteresis in both of these complexes. Magnetic circular dichroism (MCD) tests on $(F_{64}Pc)_2Tb$ frozen in acetone at 1.8-1.9 K exhibited a "butterfly shaped" hysteresis which appeared to depend on the oxidation state of the complex and which also provided evidence of quantum tunneling of magnetization. The chemical tuning of the Pc macrocycle of these complexes through the replacement of the H atoms with the electron withdrawing fluorine atom and $i$-$C_3F_7$ group has created additional functionalities.

Thermal analysis in the forms of thermogravimetric analysis and differential scanning calorimetry showed the complexes to be stable up to 450°C in air and N$_2$. Cyclic voltammetry revealed four reduced and one oxidized states, the oxidized state occurring at > 1.2 V, showing the complexes' resistance to oxidation. The (F$_{64}$Pc)$_2$MH compounds derive their uniqueness as [(F$_{64}$Pc)$_2$M]$^-$ sandwich phthalocyanine complexes with exceptional thermal and oxidative stability.

# SYNTHESIS, MOLECULA R AND SOLID STATE STRUCTURES, AND MAGNETIC PROPERTIES OF SANDWICH LANTHANIDE PHTHALOCYANINES LACKING C-H BONDS

by
Wycliffe A. Graham

**A Dissertation**
**Submitted to the Faculty of**
**New Jersey Institute of Technology**
**in Partial Fulfillment of the Requirements for the Degree of**
**Doctor of Philosophy in Materials Science and Engineering**

**Interdisciplinary Program in Materials Science and Engineering**

**May 2012**

**APPROVAL PAGE**

**SYNTHESIS, MOLECULAR AND SOLID STATE STRUCTURES, AND
MAGNETIC PROPERTIES OF SANDWICH LANTHANIDE
PHTHALOCYANINES LACKING
C-H BONDS**

**Wycliffe A. Graham**

| | |
|---|---|
| Dr. Joseph Bozzelli, Dissertation Co-Advisor | Date |
| Distinguished Professor of Chemistry and Environmental Science, NJIT | |

| | |
|---|---|
| Dr. Trevor Tyson, Dissertation Co-Advisor | Date |
| Distinguished Professor of Physics, NJIT | |

| | |
|---|---|
| Dr. Nuggehalli Ravindra, Committee Chairman | Date |
| Professor of Physics, NJIT | |

| | |
|---|---|
| Dr. Steve Greenbaum, Committee Member | Date |
| Professor of Physics, Hunter College, CUNY, New York | |

| | |
|---|---|
| Dr. Keun Ahn, Committee Member | Date |
| Assistant Professor of Physics, NJIT | |

| | |
|---|---|
| Dr. Haidong Huang, Committee Member | Date |
| Assistant Professor of Chemistry and Environmental Science, NJIT | |

# BIOGRAPHICAL SKETCH

**Author:**         Wycliffe A. Graham

**Degree:**         Doctor of Philosophy

**Date:**           January 2012

## Undergraduate and Graduate Education:

- Doctor of Philosophy in Materials Science and Engineering,
  New Jersey Institute of Technology, Newark, NJ, 2012

- Master of Philosophy (M.Phil.) in Physics, University of the West Indies,
  Mona, Jamaica West Indies, 1989

- Bachelor of Science in Natural Sciences, University of the West Indies,
  Mona, Jamaica West Indies, 1983

### Professional Education

- Construction Technology and Management, The Chartered Institute of Building,
  Englemere, U.K., 1992

**Major:** Materials Science and Engineering

## Presentations and Publications:

Pinnock, W.R.; Graham, W. A., Radioactivity in Jamaican Bauxite
    Waste, in Bauxite Tailings, Proceedings of an International Conference on
    Bauxite Waste, Kingston, Jamaica, Eds. Wagh, A.S.; Desai. P., 1986,113-117.

Graham, W.A., Building Materials Standards in Jamaica Today, JBI Journal, 10

Graham, W.A., Aggregates for Concrete, Builder's Magazine, Jamaica, 1995,
    7, 13 – 17.

Graham, W.A., New Monitoring Procedures for Aggregates Used in
    Concrete, in Proceedings of the Quarry Operators Seminar, Kingston,
    Jamaica, 25-33.

Graham,  W.A.,  Phthalocyanine Synthesis,  Poster presentation at
    CUNY-AGEP 11th Annual CUNY Conference in Science and Engineering,
    New York, 2008

Graham, W.A.; Gorun, S.M. Synthesis, X-ray Structures and Magnetic Properties of
    the first fluorophthalocyanine sandwich  complexes.  Poster presentation at
    Targeted Fellowship Luncheon, NJIT. 2008.

Graham, W.A.; Gorun, S.M. Magnetism in Some
    bis[octakis(perfluoro i-$C_3F_7$) (perfluoro)phthalocyninato] M(III) Complexes,
    Oral  presentation at the CUNY-AGEP 13th Annual CUNY Conference in
    Science and  Engineering,  New York, 2010

Graham, W.A.; Gorun, S.M., Synthesis, X-ray Structures and Magnetism of Lanthanide
    Sandwich complexes with H-Free, Internally Stabilized Closed-Shell Ligands,
    Manuscript Submitted to Angewandte Chemie, 2011

Liao, M.-S.; Graham, W.; Gorun, S. M.; Huang, M.-J.; Watts, J. D., Electronic
    Structure, Bonding, And Optical Spectra Of Unsubstituted and Fluorinated
    Yttrium and Lutetium Bis(Phthalocyanines). 2011;  Manuscript in Preparation.

Gonidec, M.; Davies, S. E.; Graham, W.; McMaster, J.; Vidal-Gancedo, J.; Gorun, S.
    M., Slow Magnetic Relaxation Of Highly Reduced States Of A Double-Decker
    Phthalocyanine Terbium (III) Complex. Barcelona, 2011;  Manuscript in
    Preparation.

To my family,
for their patience, love, support and encouragement.

# ACKNOWLEDGMENT

**TABLE OF CONTENTS**

**TABLE OF CONTENTS**
**(Continued)**

**TABLE OF CONTENTS**
**(Continued)**

# TABLE OF CONTENTS
## (Continued)

**TABLE OF CONTENTS**
**(Continued**

**TABLE OF CONTENTS**
**(Continued)**

# TABLE OF CONTENTS
## (Continued)

**TABLE OF CONTENTS**
**(Continued)**

## LIST OF TABLES

**LIST OF TABLES**
**(Continued)**

# LIST OF TABLES
## (Continued)

# LIST OF TABLES

## (Continued)

# LIST OF FIGURES

**LIST OF FIGURES**
**(Continued)**

# LIST OF FIGURES
## (Continued)

**LIST OF FIGURES**
**(Continued)**

## LIST OF FIGURES
### (Continued)

## LIST OF FIGURES
### (Continued)

# LIST OF FIGURES
## (Continued)

# LIST OF FIGURES
## (Continued)

# LIST OF FIGURES
## (Continued)

**LIST OF FIGURES**
**(Continued)**

**CHAPTER 1**

**INTRODUCTION**

### 1.1 Rationale

Research in molecular magnetism can be defined as the discipline which conceives, realizes, studies and uses new molecular materials bearing new but predictable magnetic and other physical properties.[1] This new and exciting discipline is one in which chemists and other interdisciplinary scientists are designing molecular assemblies with many varied properties so that they may eventually be part of multifunctional and possibly, miniature devices. One of these properties is magnetic bistability which describes a magnetic core that can be in either of two possible states of magnetization ($\geq$ 2 "stable" magnetic states are desired). Other properties include transparency, optical changes (linear and/or nonlinear), semi-conductivity, magnetostrictive response, biocompatibility, solubility, redox activity, magneto-optic response, large polarizabilities and low density.[2] From an engineering viewpoint, the high magnetic susceptibilities and magnetizations that can be achieved with these materials are balanced by the possibility of their fabrication and processiblity at low temperature and with low environmental contamination. For organic or organometallic magnets, modulation and/or tuning of properties via chemical manipulation presents a promising developmental pathway. In fact, since the development of molecular magnetism, not only known quantum effects have been associated with some of these new materials, but other new attributes and effects have also been discovered.

Molecular magnets are more varied in composition than traditional bulk magnets. They can be composed of charge transfer and metal complexes, radical salts, neutral radicals and polymers with unpaired spins.[3]   They can be classified into four main categories, namely inorganic magnets, organic-inorganic magnets, organic magnets and molecular clusters.  Single Molecular Magnets (SMMs) are molecular magnets in which each molecule behaves as a magnet.  They are potential candidates for the preparation of high capacity magnetic storage and quantum computing devices.

The thrust of the work presented here is to use the versatile and tunable phthalocyanine (Pc) ring with the paramagnetic lanthanide (Ln) center in designing multifunctional SMMs. This idea is not new. Several of the sandwich lanthanide phthalocyanines ($Pc_2Ln$) have been reported to have SMM behavior; these include both the un-substituted $Pc_2Ln$[4]   and substituted $Pc'_2Ln$.[5]   Furthermore, magnetic behavior has been reported in the binuclear lanthanide phthalocyanines, $Pc_3Ln_2$ [6] and tetra-butyl ammonium (TBA) salts of the $Pc_2Ln$ anions such as $TBA[Pc_2Ln]$.[7]

It has been reported[8] that lanthanide(III)-Pc molecules showing SMM behavior have large axial magnetic anisotropies and the ligand field of the lanthanide ion controls the anisotropy.[9]   The sandwich lanthanide perfluorophthalocyanine complexes are being synthesized for two main reasons: 1)  To investigate the effect of "tuning" the Pc ring with electron-withdrawing F atoms on these complexes' crystal structure, thereby modifying their solubility, robustness, optical, surface and redox properties;    2) to influence the crystal field around the $Ln^{3+}$ ion thereby improving their SMM properties. It is anticipated that a change in the magnetic behavior of these complexes will improve the SMM properties along with their other attributes such as the solubility and robustness.

## 1.2 Specific Goals

The primary goal of this project was to synthesize Pc complexes suitable for the development of multifunctional SMMs from fluorine substituted lanthanide phthalocyanines and/or compounds derived from them. While compounds of the type $Pc_2Ln$, $Pc_3Ln_2$, $[Pc_2Ln]^-M^+$ and $[Pc_2Ln]^+M^-$ are known, their perfluorinated analogues, $(F_{64}Pc)_2Ln$, $(F_{64}Pc)_3Ln_2$, $[(F_{64}Pc)_2 Ln]^-M^+$ and $[ (F_{64}Pc)_2 Ln]^+M^-$ , ($M^-$ = anion, $M^+$ = cation), to the best of my knowledge, are not known. Halogenation is critical in depressing frontier orbitals' energies and thus stabilizes the $F_{64}Pc^{\bullet-}$ radical anion, if present, in $(F_{64}Pc)_2Ln$ complexes,[10] while also tuning intermolecular, steric and magnetic interactions. Synthesis, characterization and identification of the magnetic properties, particularly the SMM behavior of these fluorinated compounds were the primary goals. Secondary goals included spectroscopic characterization, redox and magnetic circular dichroism studies, and comparison of experimental observations with calculated results from Density Functional Theory (DFT). The target molecules were the bis[octakis(*i*-$C_3F_7$) octakis(perfluoro)phthalocyaninatoM(III)] abbreviated as $(F_{64}Pc)_2M$ (M= Tb, Dy, Y, Lu). Their typical structure is shown in Figure 1.1.

## 1.3 Phthalocyanines

The invention of phthalocyanines was accidental. In 1907, two scientists Braun and Tcherniac first produced this blue solid when they heated o-cyanobenzamide.[11] At the Imperial Chemical Industries, Scotland, in 1928, another accidental synthesis occurred which energized industrial applications of phthalocyanines. The phthalocyanines were then used as dyes, paints, colors for metal surfaces, fabrics and plastics.[12] Professor

Reginald P. Linstead was the first elucidate its structure the decade of the 1930s.   He
went on to name this class of compounds "phthalocyanine" by the combination of two
prefixes: "phthal" to emphasize the association with various phthalic acid derivatives and
Greek "cyanine" for blue.[13-19]
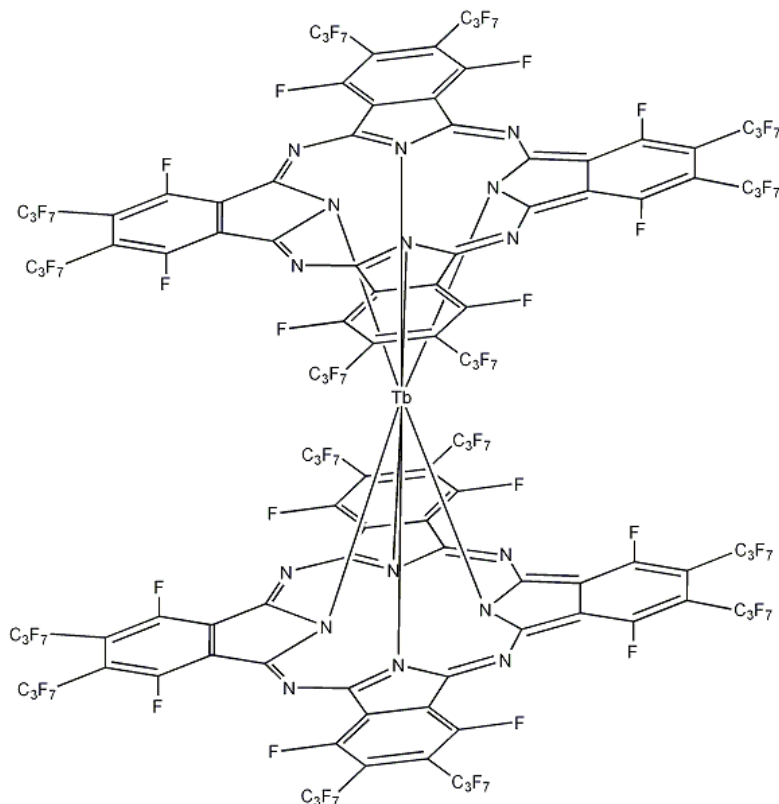


**Figure 1.1** Structure of $(F_{64}Pc)_2Tb$.

Phthalocyanine is a highly symmetrical, planar conjugated system consisting of
an 18 $\pi$ electron aromatic macrocycle made up of four iminoisoindoline units. The
general structure is shown in Figure. 1.2. It bears some resemblance to the naturally
occurring porphyrin ring system, but phthalocyanines are not found in nature. It is
unlikely that phthalocyanines would ever be produced in nature because the absence of
their principal precursors. Phthalocyanines have been prepared in the laboratory from

phthalonitriles,[20-23] phthalimides, phthalic anhydrides,[24] diiminoisoindolines,[25] and phthalic acids[26] as the starting materials. The center may consist of two hydrogen atoms or a metal. A metal from every group of the periodic table has been used and up to 40 different metals have been used in the center. The four benzene rings allow for up to sixteen sites of substitution possible in phthalocyanines.
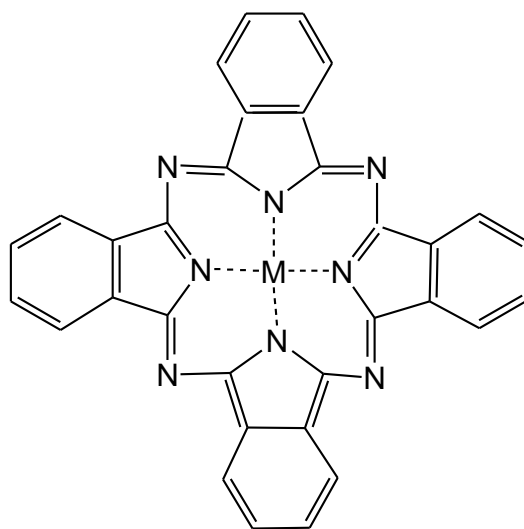
**Figure 1.2** The phthalocyanine ring with metal center, M.

## 1.4 Lanthanides and Yttrium

The general chemistry of the lanthanide elements has been extensively covered in many standard textbooks in organic chemistry. The lanthanides comprise the group of elements from La to Lu in the periodic table. They are characterized by the gradual filling of the 4f sub-shell. The electronic configurations of the neutral atoms show some irregularities, particularly for the stable $4f^7$ configurations found in Eu and Gd. The trivalent cations of

the lanthanides however, show strict regularity, all having the $4f^n5d^06s^0$ electronic configuration.[27]

The chemistry of yttrium is usually reported with that of the lanthanides because it lies above lanthanum in group 3 of the periodic table. It has no 4f electrons, but forms a +3 ion with the Kr noble gas core and the size of both its atomic and ionic radii are comparable to Tb and Dy. It is also generally found in nature along with the lanthanides and resembles the Tb(III) and Dy(III) compounds in its compounds.[28] The absence of 4f electrons and the closed shell of Y(III) ion means the metallic core of its compounds are diamagnetic in nature and they therefore provide a good comparative study of magnetic phenomena in the lanthanides.

The characteristic oxidation state of the lanthanides is the +3, but the +2 oxidation state is also important with the $Eu^{+2}$ and $Yb^{+2}$ being the most stable of the di-positive ions. Although higher oxidation states occur, they are not usual. Cerium forms a stable +4 species in aqueous solution. Dy, Tb, Pr, and Nd also form the +4 species.[29]

There is a reduction in atomic size with an increase in atomic number in the lanthanides, the so called lanthanide contraction. [30] This trend is even more apparent in the radii of the trivalent ions. The reduction in size is due to the poor shielding of the 4f electrons as the nuclear charge increases.

The electrons responsible for the properties of the lanthanide ions are the 4f electrons and the 4f orbitals are effectively shielded from the influence of external forces by the overlying $5s^2$ and $5p^6$ shells.[28] The result is that the electronic states arising from the various $4f^n$ configurations are not significantly affected by surrounding ions and do not vary much for a given ion in all its compounds.

The Russell-Saunders[28, 31] coupling gives a good approximation for the electronic states of the $4f^n$ configurations. Spin-orbit coupling is present in lanthanide ions with non-zero orbital angular momentum. The spin-orbit couplings are also very large. This result in most of the lanthanide ions having ground states with well-defined values of total angular momentum, J, and the next lowest J state at energies many times the product of Boltzmann constant and temperature (k$T$). The magnetic susceptibilities and magnetic moments are for most part calculated from the well defined ground state and are in good agreement with experiment. For the lanthanides, the external fields do not either appreciably split the free ion terms or quench orbital angular momentum.[28] In forming complexes the lanthanides have a preference for coordination numbers greater than 6. The most common co-ordination numbers of the $Ln^{3+}$ ions are 8 and 9.[28]

## 1.5 Molecular Magnets

Traditionally, magnetic materials are bulk materials based on atoms with d or f orbital based spin sites and has extended network bonding in three dimensions. Molecular magnets are associated with new phenomena that are not associated with traditional magnets. Some of these include macroscopic quantum tunneling, quantum coherence, quantum hysteresis, and magnetic bistabilities within the clusters, large magnetorestriction, magnetoresistance, and magnetocaloric effects to name a few.[32-39] Recently, molecule based magnets and particularly single molecular chased magnets have gained prominence due to their many attributes.[2] These include large spin, small size, intrinsic memory effect[40], semiconductivity, flexibility, low density, self assembly[4] and the Kondo effect.[41]

Four of the main classes of molecular magnets are inorganic magnets, organic-inorganic magnets, organic magnets and molecular clusters. Inorganic magnets include $Fe^{III}_4[Fe(CN)_6]_3 \bullet 15H_2O$, which is a mixed valence compound containing the iron ions in two different oxidation states. In addition to its long range ferromagnetic ordering it is important due to its optical properties.[42]

The combination of transition metal complexes and organic radicals forming organometallic compounds has produced several organic-inorganic magnets.[43-45] These compounds are developed using a paramagnetic center being the transition metal or rare earth ion, and an organic radical.[3, 43] Miller and his team successfully produced ferromagnets exceeding the magnetization of iron metal with Curie's temperature ($T_c$) at room temperature using the tetracyanoethylene (TCNE) anion bound to various metal ions.[45-47] They produced compounds such as $[Fe(C_5Me_5)_2][TCNE]$ with $T_c$ of about 4.8 K and a $V(TCNE)_xY$(solvent) which has a $T_c$ of 400 K.[43-45, 47]

The development of a purely organic molecular magnet provides exciting possibilities because apart from being magnetic, the molecule would also have properties specific to the organic compounds. These organic based compounds will have the metal ion absent and will derive magnetism solely from the spins of the electrons from the s and p orbitals.[39, 42] While these types are not in the scope of the present project, it may be possible to isolate metal-free isomers during the synthesis procedure.

Molecular clusters include those molecules than contain a finite number of magnetic centers which may display high spin values in their ground state.[37, 38] The $Mn_{12}$-Acetate complex formulated as $[Mn_{12}O_{12}(CH_3COO)_{16}(H_20)_4]$ $2CH_3COOH \bullet 4H_2O$ is an example of this class of molecules. This molecule contains eight $Mn^{III}$, and four

$Mn^{IV}$ ions which are antiferromagnetically coupled and six molecules of solvation (four $H_2O$ and two $CH_3COOH$). The crystal's unit cell has a ferromagnetic core consisting of $Mn_{12}O_{12}$ clusters. The clusters in different unit cells are separated from each other by nonmagnetic acetate ligands, coordinated water, and other non-interacting molecules of solvation.[35, 37, 38, 43]

Molecular magnets have several potential uses, including the use in high capacity magnetic storage media[40, 48, 49] and quantum bits (qubits) applicable to quantum computers.[50, 51]

## 1.6 Lanthanide Phthalocyanines

### 1.6.1 General Types of Lanthanide Phthalocyanines

Three general subgroups of the lanthanide phthalocyanines derivatives are known. They are the lanthanide monophthalocyanines, the bisphthalocyanines and the dilanthanide tris-phthalocyanines.[52] For the monophthalocyanines, the $Ln^{3+}$ is coordinated to one dianionic tetradentate phthalocyanine ligand and can have axial ligands which are mono-anionic and can be either mono- or bi-dentate. Other neutral ligand(s) can then complete coordination environment which is often 8.

The bisphthalocyanine, sometimes called the double-decker or sandwich complexes consists of two of Pc ligands. For the $Ln^{3+}$ ion, one of the Pc ligands is dianionic and the other can be radical anionic. It has been argued that some of the lanthanides may form the $Ln^{4+}$ and is instead coordinated to two dianionic Pc ligands.[53]

The dilanthanide tris-phthalocyanines have two metal cations sandwiched between three Pc rings. This would make the regular Pc ligands dianionic. Several

variations in the double deckers and triple deckers are possible.[52]   For example, sandwich complexes have been synthesized with dissimilar Pc rings.  That is, each ring has different substituents attached to it, and such bisphthalocyanines have been called heteroleptic.  Dilanthanide tris-phthalocyanines, with the same two cations are referred to as homonuclear and with different cations, heteronuclear.  These triple deckers can also be heteronuclear and heteroleptic.

### 1.6.2 Synthesis Methods

There have been several reported methods for the preparation of bisphthalocyanines.  A popular method of synthesis is the solid state reaction of the substituted or un-substituted o-phthalonitriles and the lanthanide salt such as the as the acetate.  These reactions are a template reaction resulting in cyclic tetramerization of the phthalonitrile using the metal center.[54]   Reported difficulties with purifying the products of the solid state reaction, probably led to the development of solution reactions in which cyclotetramerization of the phthalonitrile occurred in alcohol with the presence of a strong organic base such as 1,8-diazabicyclo-[5,4,0]-undec-7-ene (DBU)[55, 56] or in dimethylethanolamine.[56]    The sandwich molecules can also be prepared from metal insertion into the metal free phthalocyanine analogues.[57]   There are several established methods for the synthesis of metal free phthalocyanines.  These also involve the cyclotetramerization of the respective phthalonitrile and include methods such as the cerium promoted synthesis,[58]    lithium metal in alcohol (followed by acid work-up),[59]    and the use of ionic liquids such as 1,1,3,3-tetramethylguaninidinium trifluoracetate (TMGT).[60]

The synthesis of the heteroleptic double deckers poses a greater challenge.  It can be achieved by the reaction of one LnPc′ and the phthalonitrile necessary for the second

substituted lanthanide phthalocyanine ring (Pc″), forming the (Pc′)Ln( Pc″) complex. The reaction of an alkali metal salt, with two different macrocycles and the lanthanide salt produces the heteroleptic as well as homoleptic species.[61, 62]

### 1.6.3 Oxidized and Reduced Bisphthalocyanines

The lanthanide phthalocyaninate anions, $[(Pc_2 Ln)]^-$ was first made by Konami et al.[63] This synthesis method used was cyclic tetramerization of phthalonitrile in the presence of the lanthanide salt and sodium carbonate. Separation of the sodium salts $Na[Pc_2Ln]$ and the addition of $NBu_4Br$ yielded the TBA salts $NBu_4[Pc_2Ln]$. The sandwich compound has been reduced with hydrazine in the presence of tetrabutylammonium perchlorate and it yielded $NBu_4[Pc_2Ln]$.[64]

The oxidized double decker $[Pc_2Ln]^+$ species has been reportedly synthesized as the compound $SbCl_6[Pc_2Ln]$. This complex is expected to contain two Pc radical anionic macrocycles.[65] The synthesis and characterization of the $SbCl_6^-$ precursor has been reported.[66, 67]

The first triple decker containing only the Pc macrocycle reported was the $Pc_3Y_2$ synthesized as a side product in the synthesis of $Pc_2Y$ by Kasuga in 1986.[68] Since then triple decker lanthanide phthalocyanines have been reported synthesized and characterized. These include both the homonuclear-homoleptic[62, 69-71] and homo-nuclear-heteroleptic[61, 72] as well heteronuclear-heteroleptic species.[6] The triple decker complexes are composed of three dianionic ligands and two trivalent lanthanide ions.[6] Oxidation of these complexes via electron loss from the macrocycles have been achieved forming compounds such as the $[Pc_3Ln_2]^+M^-$. Several species have been synthesized and characterized.[73-75]

### 1.6.4 Deposited Films

The bisphthalocyanines have been deposited on several different substrates using different deposition techniques in which electronic semiconductor devices and optical coatings were the major applications. The deposition techniques included Langmuir Blodgett films,[76-81] sublimed films,[82, 83] spin coating,[84] molecular beam expitaxy,[85] and an electrophoretic deposition technique.[84] Langmuir Blodgett technique for film deposition of phthalocyanines appears to be most popular because according to Jones et al.,[76] the technique promises better control over film thickness than the traditional methods of vacuum sublimation and spin coating. Bai et al.,[84] claims that electrophoretic deposition is a low cost and rapid method of film deposition compared to the others.

### 1.6.5 Magnetism in Sandwich Lanthanide Complexes

Some $Pc_2Ln$ have also been reported to have ferromagnetic and/or antiferromagnetic ground states due to strong magnetic interaction between the lanthanide f electrons and phthalocyanine radical electron.[86] 2D self-assembly of the substituted terbium bisphthalocyanine on Highly Oriented Pyrolytic Graphite (HOPG) has been reported.[4] A lanthanide polymeric coordination compound $[Tm^{III}(hfac)_3(NITPhOPh)]_\infty$ has been reportedly synthesized and belongs to a group of so called 1D single chain magnets family.[87] Magnetism on the reduced and oxidized species of the lanthanide phthalocyanine complexes has been investigated.[65, 88] Some of the triple decker lanthanide phthalocyanines have been shown to exhibit antiferromagnetic and ferromagnetic interactions between the f electrons of the lanthanides.[6] Several of the

reduced species of the double decker lanthanide phthalocyanines and the neutral species of some dilanthanide trisphthalocyanines have exhibited SMM behavior.[89-91]

### 1.6.6 Applications of Some Lanthanide Phthalocyanines

The general phthalocyanines have many applications, but there are some specific applications for the lanthanide double and triple decker phthalocyanines. These are electrochromic displays,[78-80, 92, 93] conducting materials,[94] sensors,[95] field effect transistors,[96, 97] optical nonlinear materials,[98] Liquid crystalline molecular semi-conductors,[99, 100] and molecular electronic components for information storage and processing.[101]

<div align="center">

### 1.7 Summary

</div>

The survey of the literature on lanthanide phthalocyanines indicates a wealth of diverse research areas with many new products being synthesized and characterized. This adds to many actual and potential applications of lanthanide phthalocyanines. While there are many substituted lanthanide monophthalocyanines, bisphthalocyanines and dilanthanide trisphthalocyanines synthesized, to the best of our knowledge, there are no published examples of the lanthanide phthalocyanines containing the nearly complete surrounding of the center by fluorine atoms attached to the Pc macrocycle. The possibility of improved Pc magnets and their research and commercial applications shows it to be a prime area of research.

# CHAPTER 2

# EXPERIMENTAL

## 2.1 Overall Synthesis Method and Purification

The synthesis of the desired fluorine substituted lanthanide phthalocyanines was done in several steps. These were;

1. Synthesis of phthalonitrile precursor.

2. Microwave assisted synthesis of lanthanide and yttrium phthalocyanine mixtures.

3. Separation and individual purification of targeted lanthanide phthalocyanine molecules.

4. Preparation of crystals for X-ray and other testing.

In order to assist in the characterization and analysis of the $(F_{64}Pc)_2MH$ complexes, the known, un-substituted, bis(phthalocynaninato)yttrium(III) complex, $Pc_2Y$ was synthesized. It was synthesized using a modification of a method by Sleven et al.[56] In the method, phthalonitrile was reacted with 1/8 part of yttrium(III) acetate hydrate and ½ part of 1,8-diazabicyclo[5.4.0]undec-7-ene (DBU) in 1-hexanol. In this synthesis, the one electron reduced species, $[Pc_2Y]^-$ and the monophthalocyanine $YPcL_n$ (where L = neutral monodentate or bidentate ligands and n = 2 or 3) were produced in the reaction.

## 2.2 Reagents

All the solvents and chemicals were ACS grade with the exception of the chloroform used for liquid chromatography, which was technical grade. The following chemicals were obtained from Fisher Scientific; ethyl acetate, $C_4H_8O_2$, (99.9%); Hexanes, $C_6H_{14}$, (99.8%), containing 4.2%, methyl pentanes; chloroform, $CHCl_3$, (containing 0.75%

ethanol as preservative), technical grade; acetone, $C_3H_6O$, (99.6%),; toluene, $C_6H_5CH_3$;

methyl ethyl ketone, $C_4H_8O$, (99.8%); n-amyl alcohol, $CH_3(CH_2)_3CH_2OH$, (99.6%);

reagent alcohol, histological grade of a mixture of ethanol, methanol and isopropyl

alcohols; methanol, $CH_3OH$ (99.85%), anhydrous silica gel, grade 60, 70-230 mesh.

Fluorotrichloromethane, $CFCl_3$, (99%). ACS, NMR standard; terbium (III) acetate

hydrate, $Tb(C_2H_3O_2)_3 \cdot xH_2O$, 99.9%; dysprosium (III) acetate hydrate,

$Dy(C_2H_3O_2)_3 \cdot xH_2O$, (99.9%); Cesium fluoride, CsF, (99%) were obtained from Sigma-

Aldrich Inc. 1-hexanol, $CH_3(CH_2)_4CH_2OH$, (99%) was obtained from Alfa Aesar.

Acetonitrile, $C_2H_3N$, (99.5%), ACS grade was obtained from Acros Organics.

Tetrafluorophthalonitrile, $C_8F_4N_2$, (98.0%), ACS grade was obtained from TCI America.

Hexafluoropropene, $C_3F_6$, (98.5%), ACS grade was obtained from Synquest Labs Inc.


## 2.3 Synthesis of Phthalonitrile Precursor Perfluoro-(4,5 di-isopropyl phthalonitrile)

Perfluoro-(4,5 di-isopropyl phthalonitrile), (PFPN) was synthesized using a method by

Gorun et al.[102]   It is the reaction of 1,2-dicyano-3,4,5,6-tetrafluorobenzene (otherwise

called tetrafluorophthalonitrile, (TFP)) and 1,1,2,3,3,3-hexafluoro-1-propene (also known

as hexafluoropropene) in  acetonitrile n the presence of excess CsF.  The structural

equation for the reaction is given in Figure 2.1.
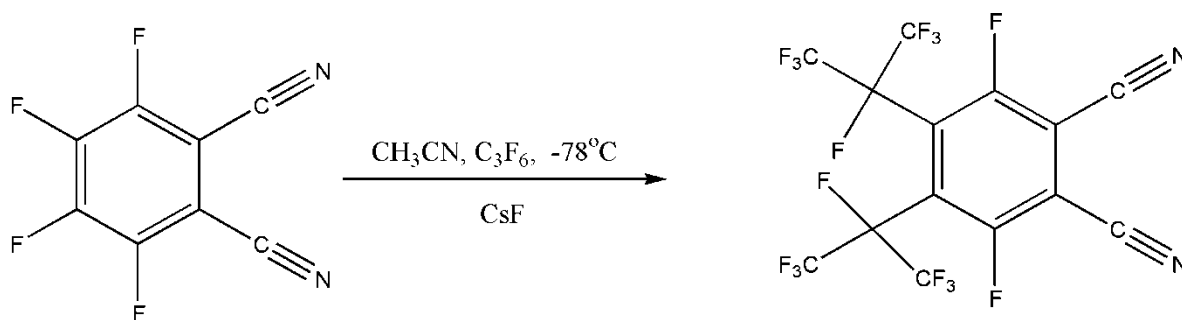


**Figure 2.1** Synthesis of  perfluoro-(4,5 di-isopropyl phthalonitrile).

TFP (1.000 g, 0.50 mmol) and anhydrous CsF (0.7 g, 4.6 mmol) were added to a Fisher-Porter bottle under anhydrous conditions. The Fisher-Porter bottle and its contents were evacuated and dry nitrogen added. Seventy mL of acetonitrile previously dried by refluxing over dry $CaCl_2$, was added to the Fisher-Porter bottle under a nitrogen atmosphere and the bottle and its contents cooled to $-78°C$. At this temperature, an excess of hexafluoropropene (20 mL, 0.24 mol) was added. The cooling bath was then removed allowing the reaction to warm to room temperature.

The reaction was stirred for an additional 45 minutes at room temperature before venting and quenching in 150 mL of saturated brine. The mixture was extracted with ethyl acetate and the desired PFPN isomer was separated using flash chromatography. Liquid chromatography was carried out on a 25.4 mm diameter column using 63-300 micron silica gel with a mobile phase of toluene/hexanes (1:5) to give a 30% yield.

## 2.4 Synthesis of Bis[octakis(perfluoro $i$-$C_3F_7$) octakis(perfluoro) phthalocyaninato]Metal(III) Complex, $(F_{64}Pc)_2MH$. (M = Tb, Dy, Lu,Y)

Perfluoro-(4,5 di-isopropyl phthalonitrile) crystals (300 mg, 0.60 mmol), $M(CH_3COO)_3 \cdot xH_2O$, (60 mg, 0.15±0.03 mmol) and 5 drops of 1-hexanol were added to a glass reaction tube. A teflon coated stirrer was then placed in the tube which was closed before placing in a CEM Discover microwave reactor. The reactants were ramped at a rate of 18°C/min to a temperature of 180°C and then held at this temperature for 15 minutes. During this time, the pressure varied between 20 and 50 psi. At the end of this period, the reaction products were cooled to room temperature before venting and dissolving in ethyl acetate. Excess toluene was then added to the mixture to precipitate most of a blue solid which contains the target product. Both precipitate and filtrate were

then dried and each gel filtered with a filter funnel utilizing 60-200 µm silica gel and a 60% ethyl acetate/hexanes mixture which removes the initial brown impurities and any un-reacted phthalonitrile. The mixture was then changed to 20% then 35% acetone/chloroform to remove green and blue fractions respectively. The blue fraction was then further purified by flash chromatography on 60-200 µm silica gel column using the same train of solvent mixtures. Final product purification was achieved by liquid chromatography on 60-300 µm silica using 20% acetone/chloroform mixture followed by precipitation from an acetone solution with toluene. The precipitate was dried yield a blue powder.

The product $(F_{64}Pc)_2MH$ was then crystallized from the 35% acetone/chloroform mixture, methyl ethyl ketone or methyl ethyl ketone/toluene by slow evaporation at room temperature to produce purple/bronze cuboid crystals. Currently, the yields using this method are as follows;

- Bis[octakis($i$-$C_3F_7$) octakis(perfluoro)phthalocyaninato]lutetium(III), **[1]** or $(F_{64}Pc)_2LuH$, yield, 16 mg (5%):

- Bis[octakis($i$-$C_3F_7$) octakis(perfluoro)phthalocyaninato]yttrium(III), **[2]** or $(F_{64}Pc)_2YH$, yield, 35 mg (12%):

- Bis[octakis($i$-$C_3F_7$) octakis(perfluoro)-phthalocyaninato] terbium(III), **[3]** or $(F_{64}Pc)_2TbH$, yield, 36 mg (12%):

- Bis[octakis($i$-$C_3F_7$) octakis(perfluoro)phthalocyaninato] dysprosium(III), **[4]** or $(F_{64}Pc)_2DyH$, yield, 31 mg (10 %).
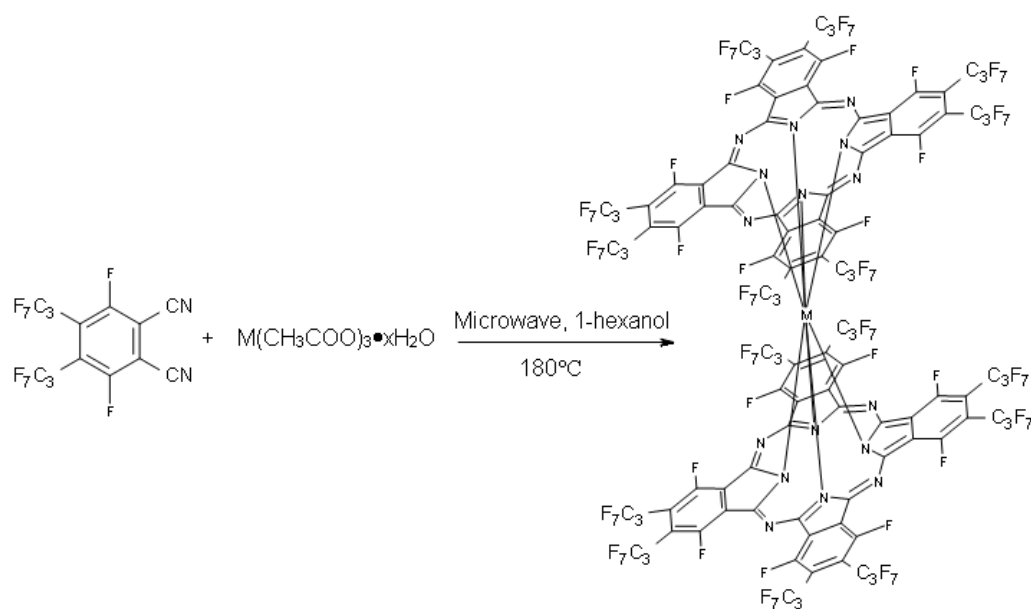
**Figure 2.2** Synthesis of the bis[octakis(perfluoro *i*-C$_3$F$_7$) octakis(perfluoro) phthalocyaninato]Metal(III) molecule, (F$_{64}$Pc)$_2$MH.  (M = Tb, Dy, Lu,Y).


## 2.5 Synthesis of Bis[phthalocynaninato]Yttrium(III) Complex, Pc$_2$Y

Phthalonitrile (500 mg, 3.9 mmol) was added to yttrium(III) acetate hydrate (130 mg, 0.49 mmol) in 50 mL round bottom flask.   The solvent, 1- hexanol (15 mL) was added to the flask and stirred before DBU ( 300 mg,  2.0 mmol) was added.  The entire assembly was then refluxed at 165°C for 24 hours.   The reaction products were then removed from the flask with a minimum of chloroform and precipitated three times by adding an excess of hexanes.  Excess hexanes were removed from the filtrate.  The crude product was then fractionated by flash chromatography on neutral alumina using a 95% chloroform and 5% methanol (v/v) mixture as the mobile phase.  A green fraction, which was the desired product, was the first to elute from the column followed by a blue green fraction.  Repeated chromatography of the green fraction was done to remove traces of the

impurities. The yield of bis(phthalo-cynaninato)yttrium(III), $Pc_2Y$, was 61 mg (11%). The identity of this neutral $Pc_2Y$ complex was confirmed by UV-Vis, NIR[103] and mass spectroscopy (Appendix A).
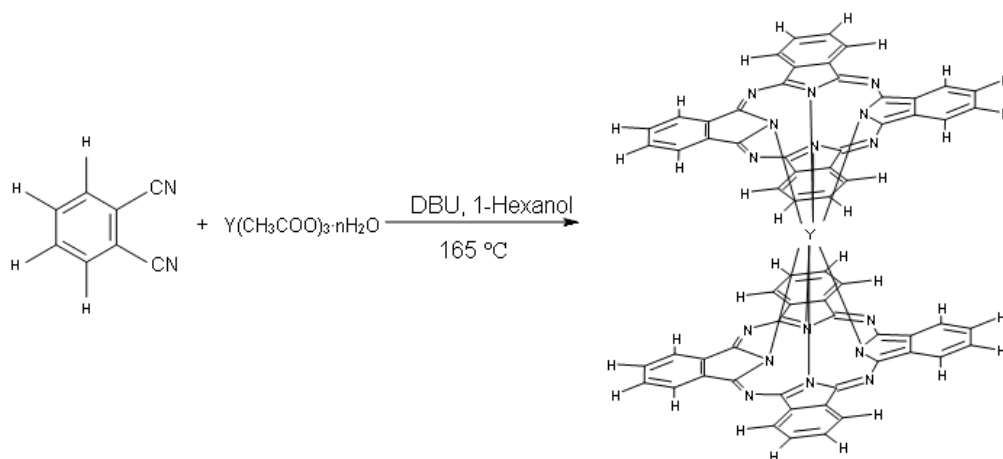


**Figure 2.3** Synthesis of bis(phthalocynaninato)yttrium(III), $Pc_2Y$.

## 2.6 Summary

Four new perfluoro sandwich and one known sandwich phthalocyanine compounds were made from their respective precursor phthalonitriles. The results are summarized on Table 2.1.

Accompanying the synthesis of the desired $(F_{64}Pc)_2MH$ complexes were some by-products whose empirical formula were not ascertained. Attempts were made to purify and characterize three of these byproducts. They were a blue green compound **[2-1]**, a green substance **[2-2], and** a dark green compound **[2-3]**. The green substance, **[2-2]**

sticks to the silica gel and frequently a 1:1 mixture of acetone/chloroform or acetone/ethanol was required for its removal.

**Table 2.1** Summary of Bis(phthalocynaninato)M(III) Complexes Synthesized

| Empirical Formula | Short Formula | Formula Weight | Purity | Yield (%) | Symbol used in Thesis |
|---|---|---|---|---|---|
| $C_{112}F_{128}N_{16}LuH$ | $(F_{64}Pc)_2LuH$ | 4177.08 | >95%* | 5 | **[1]** |
| $C_{112}F_{128}N_{16}YH$ | $(F_{64}Pc)_2YH$ | 4091.02 | >95%* | 12 | **[2]** |
| $C_{112}F_{128}N_{16}TbH$ | $(F_{64}Pc)_2TbH$ | 4161.04 | >95%* | 12 | **[3]** |
| $C_{112}F_{128}N_{16}DyH$ | $(F_{64}Pc)_2DyH$ | 4164.61 | >95%* | 10 | **[4]** |
| $C_{64}H_{32}N_{16}Y$ | $Pc_2Y$ | 1113.95 | >95%† | 11 | $Pc_2Y$ |

* Purity estimated from the absence of peaks from other substances in the ^{19}F NMR spectrum (in acetone-$D_6$) of a solution obtained from crystallized material. See Appendix C.

† Purity estimated from UV-Vis spectra. This is not a new complex.

The purification of the $(F_{64}Pc)_2MH$ was complicated by **[2-3]** which was eluted at the same rate from the liquid chromatography column. This **[2-3]** compound was removed by repeated precipitation in toluene from a solution of $(F_{64}Pc)_2MH$ in acetone. Repeated flash chromatography of the blue compound was carried out using only the 20% and 35% acetone/chloroform mixtures to remove traces of the other products and impurities. The blue $(F_{64}Pc)_2MH$ product was observed as two fractions which were separated by the 20% acetone/chloroform mixture on the silica gel liquid chromatography column. The fraction which crystallized easily was the second purple/bluish product and it was collected and tested for the presence of green impurities in the filtrate after precipitating from an acetone solution with excess toluene.

The synthesis of the $(F_{64}Pc)_2MH$ complexes was hampered by the inability to use DBU as a catalyst to aid in cyclotetramerization. DBU reacted with the precursor perfluoro-(4,5 di-isopropyl phthalonitrile) and appeared to destroy it. Another base

dimethyl ethanol amine (DMEA) was also tried and it too destroyed the precursor during the test. As a result, the use other organic bases such as 1,5-diazabicyclo[4.3.0]non-5-ene (DBN), bis(trimethylsilyl)amine (also known as hexamethyldisilazane, or HMDS) and other amines were not attempted.

Yields were also affected by the many different compounds formed during the synthesis reaction. It is known that this type of reaction results in the formation of monophthalocyanines, metal free phthalocyanine, in addition to reduced and possible oxidized forms of the sandwich complexes.[53, 104] The microwave reaction leaves a fraction of the phthalonitrile unreacted and causes some of its fragmentation. In particular in the reaction, **[2-2]** appears to be very surface active and sticks to the glassware and probably the products as well because it is present in each purification step. These factors made separating the desired products via fractionation in flash chromatography particularly inefficient. The pathway using metalation of the metal-free phthalocyanines was not very successful as it did not give improved yields.

The microwave assisted synthesis described herein gave the best results after attempting metal insertion using the metal free monoisomer, regular refluxing in 1-hexanol, solid state testing in a closed glass ampoule and solid state testing in an open container with thermal heating. When time, energy and yields were considered, microwave assisted synthesis approximately doubled the efficiency relative to the other methods.

# CHAPTER 3

## STRUCTURE AND SPECTROSCOPIC PROPERTIES
## OF (F$_{64}$Pc)$_2$MH COMPLEXES (M = Y, Lu)

### 3.1 Overview

The complexes (F$_{64}$Pc)$_2$LuH and (F$_{64}$Pc)$_2$YH  are closed shell and were designed to precede the study of the Tb and the Dy analogues that are the main candidates for applications as molecular magnets.    Their study should help in the elucidation of the properties of the F$_{64}$Pc ligand in the sandwich environment.  In particular, it may allow a comparison of the interactions of the unpaired 4f electrons in the case of the Dy and Tb analogues with (F$_{64}$Pc)$_2$LuH which has all spin paired electrons in the ground state and with (F$_{64}$Pc)$_2$YH which has no 4f electrons. Furthermore, the closed shell complexes also provide a more manageable set of conditions in the application of Density Functional Theory (DFT) studies.  The closed shell property will also be exploited as a probable diamagnetic matrix for a future study of the dilute mixtures of the paramagnetic **[3]** and **[4]** complexes.  Dilute mixtures are sometimes required to differentiate between SMM and ferromagnetic/ferri-magnetic properties when hysteresis is obtained from AC magnetic studies. The dilution separates the molecules thus making it improbable that any slowed relaxation to the changing magnetic field is due to long range order.

The lutetium(III) ion is the smallest of the lanthanides and its synthesis is important in comparing differences due to the central ion size.  As a bisphthalocyanine, Lu(III) complexes have found several applications in electronics.[78, 80, 93, 96, 97, 99]    Its synthesis, in this study, may also have secondary benefits in providing a complex with enhanced    electronic and electrochromic properties. This enhancement is considered

because of the incorporation of the strong electron withdrawing fluorine substituents on the Pc ring.   The electronic properties of these phthalocyanine complexes are not in the scope of this study.

The effect of the fluorines on the phthalocyanine macrocycle will also be assessed by comparing some of the properties of the regular, un-substituted $Pc_2Y$, with   those of the $(F_{64}Pc)_2MH$.  The yttrium complex was chosen again because of closeness of the size of its Y(III) ion to that of the Tb(III) and the Dy(III) ions in addition to its closed shell electronic structure and lack of 4f electrons.

## 3.2 Mass Spectroscopy

The data for the Mass Spectroscopy (MS) of the complexes was provided by staff at Bremen University in Germany.  It was carried out using their Applied Biosystems Voyager-DE STR MALDI-TOF mass spectrometer. The test method selected was the Matrix Assisted Laser Desorption/Ionization, Time of Flight (MALDI-TOF).   This method was chosen from the other methods such as Electrospray Ionization (ESI) and Electron Impact (EI) because it results in less fragmentation of the complexes and is better suited for large organic and organometallic complexes.  In general, MS machines have three modules: An ion source, a mass analyzer and a detector.  In MALDI, a laser beam is used to achieve ionization. The analyte is usually mixed with a solvent and matrix material before being placed on a plate.   The function of the matrix is two-fold: It protects the molecule from destruction or excessive fragmentation by the laser and facilitates vaporization and ionization of the materials.  Two common mass analyzers for MALDI are time of flight (TOF) and Fourier Transform Ion Cyclotron Resonance

(FTICR) analyzers. They determine the mass to charge (m/z) ratio of the ions arriving at the detector. FTICR has a higher resolution than TOF mass analyzers. Calibration of the mass spectrometer is achieved by external or internal calibration using a material of known m/z ratio and fragmentation pattern. In internal calibration, the calibrant is mixed with analyte, solvent and matrix on the MALDI plate, while for external calibration the calibrant, matrix and solvent are used to calibrate the machine separately. The MALDI spectrometer can be tuned to be operated in the positive or negative ion mode.

The complexes **[1]** and **[2]**, synthesized as described in Section 2.4 were tested using the matrix α-cyano-4-hydroxycinnamic acid, (CCA) and formulated as $HOC_6H_4CH=C(CN)CO_2H$ dissolved in acetonitrile. The machine was calibrated externally. Mass spectral data is shown on Table 3.1. Mass spectroscopy data for these two complexes were collected with the machine operating in the negative ion mode. No useful data was observed for the positive ion mode. This was unfortunate because there was the possibility that the complexes could be the neutral species and thus the observance of the $[M+2H]^+$ species would definitely confirm that a $[M-H]^-$ ion was observed rather than a $M^-$ ion for the m/z results. The fluorinated ring substituents caused the lack of the positive ion mode. Data for the positive mode were obtained for the Tb and Dy complexes and are shown in Chapter 4.

**Table 3.1** Mass Spectroscopy Data for $(F_{64}Pc)_2LuH$ and $(F_{64}Pc)_2YH$

| Complex (empirical formula) | [M⁻] calculated (m/z) | [M-H]⁻ calculated (m/z) | Observed (m/z) | Mass[a] Accuracy (ppm) | Comment |
|---|---|---|---|---|---|
| $C_{112}F_{128}N_{16}YH$ | 4090.7615 | 4089.7537 | 4089.9135 | 39.07 | $[M-H]^-$ |
| $C_{112}F_{128}N_{16}LuH$ | 4176.7964 | 4175.7886 | 4175.8476 | 14.13 | $[M-H]^-$ |

Spectral data is shown for the most abundant peak in the patterns. [a]The mass accuracy is based on the $[M-H]^-$ calculated m/z values.

A comparison of the calculated and observed isotopic patterns is shown in Figure 3.1, while other MS plots and isotopic patterns are found in Appendix A. The calculated patterns coincide for two peaks only: the most abundant and the second most abundant peaks for both complexes. This may be due to the lower resolution of the TOF mass analyzer and the large masses of the complexes.
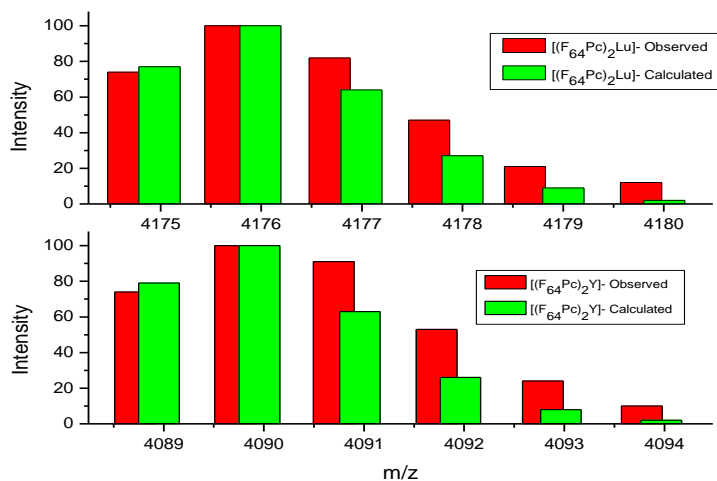


**Figure 3.1** Comparison of the isotopic patterns of $[C_{112}F_{128}N_{16}Y]^-$ and $[C_{112}F_{128}N_{16}Lu]^-$.

### 3.3 X-ray Diffraction

Single crystal X-ray diffraction was carried out on complexes **[1]** and **[2]** in order to determine their structures. The X-ray data was collected on a Bruker Apex II CCD X-ray diffractometer equipped with a variable-temperature nitrogen cold stream using graphite-monochromatic CuK\α radiation ($\lambda$ = 1.54178 Å). The diffractomer is located at the Chemistry Department of Rutgers' University Newark campus. Single crystals were obtained from the slow evaporation of mixture of acetone/chloroform (35%/65%) at room temperature. Table 3.2 summarizes the crystal data for the **[1]** and **[2]**. Detailed data and results can be found in Appendix B.

The X-ray crystallographic data did not fully support the empirical formula obtained in the MS. The MS data suggested that the complexes could be formulated as $([F_{64}Pc]^{2-})_2[M^{3+}]H^+$ and based on this, the proton is missing from the structure.  In fact, there was an on-going controversy as to its existence. At one time, it was thought that the neutral species had this proton and not the $\pi$ radical Pc ligand.  Even in the use of a soft technique such as MALDI, a proton may be easily removed in the MALDI plasma during the acceleration of the ions by the electromagnetic field towards the field-free "time of flight" chamber of the mass analyzer.  On large macromolecules of this type it is also difficult locate this proton in X-ray crystallography.

The X-ray structure confirms the sandwich type geometry of the $(F_{64}Pc)_2MH$ complexes and the staggered conformation of the $[F_{64}Pc]^{2-}$ ligands with respect to each other.   The central metal ion has coordination number of eight with each unit cell having four molecules. The **[1]** and **[2]** complexes are iso-structural.  The tetragonal structure of the $(F_{64}Pc)_2MH$ is shown in Figure 3.2.

The planes formed by the four coordinating isoindoline N atoms (4N planes) are separated by 2.70 and 2.77 Å for **[1]** and **[2]** respectively.  These values are in the 2.68-2.70 and 2.72-2.79 Å range observed for other Lu and Y sandwich complexes.[105]   The metal coordination spheres are distorted square anti-prisms.  Metal--N distances, listed as pairs of trans bonds are also similar to those of non-fluorinated analogues, viz. 2.380(4), 2.394(4) and 2.411(3), 2.421(3) with averages of 2.387 and 2.416 for **[1]** and **[2]** respectively.  The $\phi$ twist angles, (Figure 3.2) of $32.0 \pm 0.5°$, however, indicate a 10° shift toward the eclipsed configuration in comparison with the unsubstituted sandwiches, for which the twist angles  are  42° (45° for a perfectly staggered complex).  This shifts,

given the similarity of Metal--N as well as the 4N inter planar distances with those of the unsubstituted double-deckers, appear counterintuitive considering that, everything else being equal, steric bulkiness disfavors eclipsed configurations.

**Table 3.2** X-ray Crystallography Data for $(F_{64}Pc)_2LuH$ and $(F_{64}Pc)_2YH$

| Empirical Formula | $C_{112}F_{128}N_{16}Y$ | $C_{112}F_{128}N_{16}Lu$ |
|---|---|---|
| Formula weight | 4090.19 | 4176.25 |
| Temperature, K | 253(2) | 100 |
| Wavelength, Å | 1.54178 | 1.54178 |
| Crystal system | Tetragonal | Tetragonal |
| Space group | P4/ncc | P4/ncc |
| Unit cell dimensions | | |
| a, Å | 27.4142(4) | 27.1399(4) |
| b, Å | 27.4142(4) | 27.1399(4) |
| c, Å | 24.3774(10) | 23.7987(10) |
| $\alpha = \beta = \gamma$ | 90° | 90° |
| Volume, Å$^3$ | 18320.6(8) | 17529.5(8) |
| Z | 4 | 4 |
| Density (calc.), g/cm$^3$ | 1.483 | 1.582 |
| F(000) | 7900 | 8028.0 |
| $R_1$ | 0.0732 | 0.0820 |
| $R_2$ | 0.2226 | 0.2319 |
| Crystal size, mm$^3$ | 0.42 x 0.41 x 0.23 | 0.47 x 0.41 x 0.20 |
| θ range for data collection | 3.22 to 67.58° | 4.61 to 57.39°. |
| Refinement method | Full-matrix least-squares on F$^2$ | Full-matrix least-squares on F$^2$ |
| Goodness-of-fit on F$^2$ | 1.058 | 1.115 |

The $i$-$C_3F_7$ groups appeared to be "nesting", favoring the eclipsed configurations. Notably, the absence of substituents could render the energy differences between the eclipsed and staggered configurations small, probably allowing intermolecular interactions to dictate the formation of a quasi-staggered Pc$_2$Ln complex.[106]

(a)          (b)          (c)

(d)          (e)
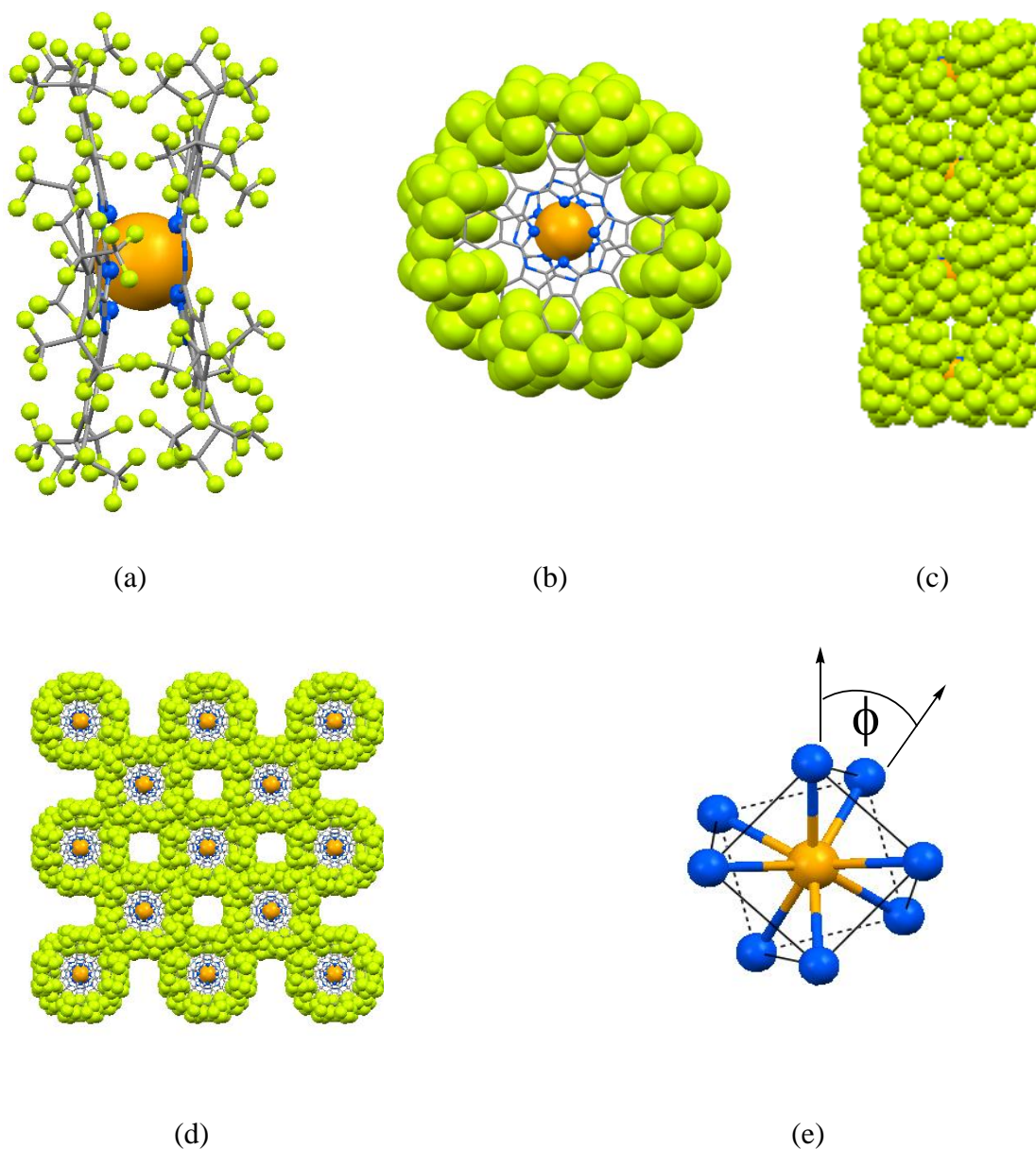
**Figure 3.2**   Single crystal X-ray structural characterizations of the tetragonal $(F_{64}Pc)_2Lu$ and $(F_{64}Pc)_2Y$.  a) View perpendicular to the 4-fold axis.  b) Molecular structure viewed along the 4-fold axis. Metal center, orange, van der Waals representation; C, black, N, blue, $N_8$ coordination sphere: ball and stick representation; F, green, van der Waals representations. c) Columnar stacking viewed along the $a$ axis.   d) Packing diagram viewed along the $c$ axis.   e) The distortion of the square-prismatic $MN_8$ chromophore by the twist angle.

The usual Pc rings convex shapes was noted, but the convexity may not be symmetrical. A proposition is presented to quantify the convexity by estimating the radii of curvature, $R_i$, of circles circumscribed to triangles defined by the geometric centers of two opposite benzene rings and those of the 4N planes, shown in Figure 3.3. $R_i$ is computed as $R_i = AB \cdot BC \cdot AC / 4K$, where $K = s(s-AB)(s-AC)(s-BC)]^{1/2}$ and $s = (AB + BC + AC)/2$.
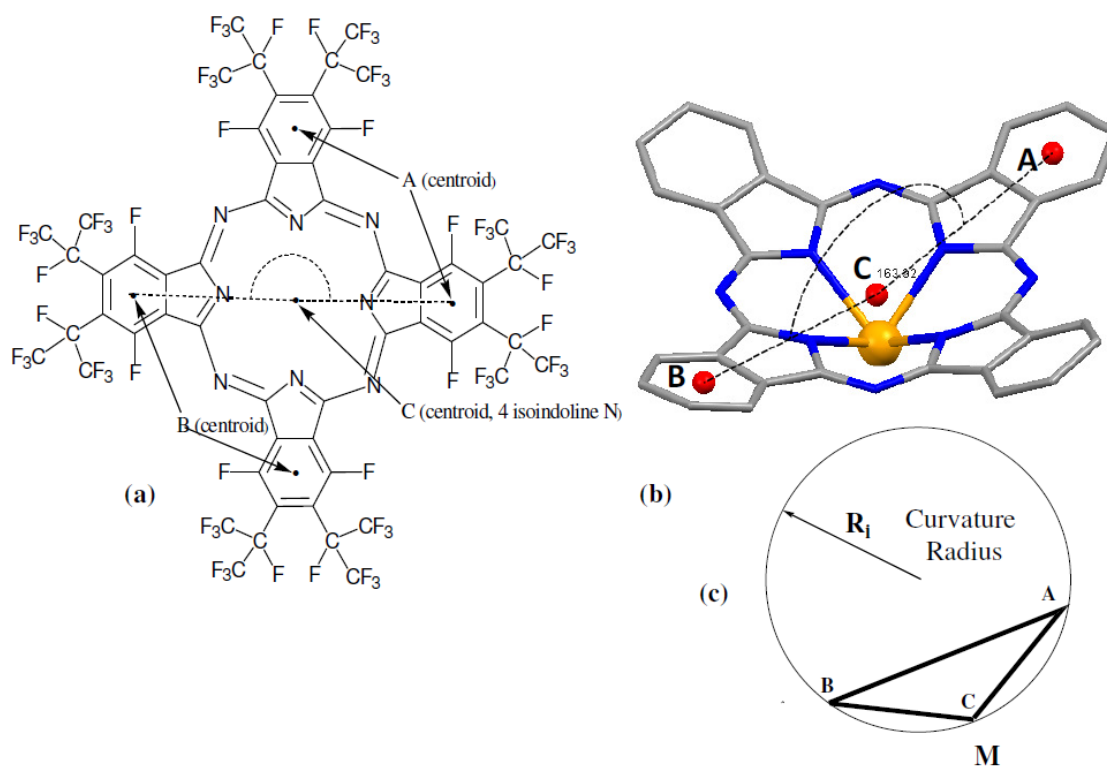


**Figure 3.3** Definition of the four radii of curvature, $R_i$ of the two $F_{64}Pc^{2-}$ rings. (a) The geometric centers of the benzene rings, A and B, and the coordinating isoindole Nitrogen atoms, C. (b) Representation of the ACB triangle defined by the three geometric centers, using an abbreviated Pc ring and the atomic coordinates from the X-ray structure of $(F_{64}Pc)_2M$. Color code: C: black; N: blue; Metal center: orange. (c) The circumscribed circle and its radius, $R_i$. M stands for Metal. The curvature radii, $R_i$, i = 1- 4, may not be equal, depending on the distortions of each Pc ring.

Thus, each complex, which exhibits a 4-fold symmetry axis, is characterized by two independent radii, one for each face of the Pc ring. The associated spheres approximate F-lined pockets, Figure 3.3 b, a, viewed as Non-Covalent Interaction Space (NCIS) which might accommodate other molecules. The sphere radii for each Pc face are: [**1**]: 18.6, 19.5; [**2**]: 17.9, 18.4; averages: 19.0 and 18.2 Å, respectively.

The radii are independent of the degree of rotation of the 8 benzene rings around their centers, measured by the $\gamma$ angle made by the bond that links the two benzene ring C atoms that bear the $i$-$C_3F_7$ groups with the 4N plane. The $\gamma$ values, 1 for each Pc face of the tetragonal complexes are: [**1**]: 4.3, 7.9; [**2**]: 3.5, 8.0. Both the convexity, asymmetry and, especially, $\gamma$ asymmetry suggest that the two Pc(2−) rings of each complex are not perfectly equivalent. This non-equivalency provides a weak yet notable support for the presence of a proton (on a non-coordinating N), a notoriously difficult identification via X-ray diffraction, exacerbated by the 4-fold disorder.[53, 107, 108]

Support for the asymmetry of the complexes was provided in Density Functional Theory (DFT). Both DFT and Time Dependent Density Functional Theory (TDDFT) calculations carried out on [**1**] and [**2**] by Liao et al.,[109] and presented in a draft manuscript. In their work, they modeled geometric structures and calculated electronic and vibration spectra, Mulliken charge distribution, dipole moment, vertical ionization potential, vertical electron affinity and binding energy. Calculated properties for $Pc_2Y$ and $(F_nPc)_2Y$ (n=16,32,64) were carried out based on the X-ray structure as seen without an axial H. The relative energy differences between $D_{4d}$ and $C_{4v}$ structures for $Pc_2Y$ and $(F_nPc)_2Y$ (n=16,32) were also computed in order to assess which would be the lower energy structure. It was shown that the molecules would adopt the lower energy $C_{4v}$

symmetry and not higher $D_{4d}$. Indeed this was supported by the 32° twist angle measured by for the **[1]** and **[2]**.

Following from the geometrical structure optimization calculations on the non-protonated forms of sandwich complexes above, calculations were also done for the $Pc_2YH$ and $(F_nPc)_2YH$ (n=16,32) and $(F_{32}Pc)_2LuH$. Due to the considerable computing effort required to model the $(F_{64}Pc)_2MH$ complexes, and based on results of initial calculations of the non protonated forms showing good consistency, no calculations were done for the $(F_{64}Pc)_2MH$. The results are shown on Figure F.1 in Appendix F and they show that all the defined co-ordinate distances indicate asymmetry due at least in part to the axial proton. In particular the Metal--N distances of the for opposing rings are 2.296, 2.573 Å for $(F_{32}Pc)_2LuH$ and 2.338, 2.611Å for $(F_{32}Pc)_2YH$. The Pc ring with the axial H has the longer distance and although this was also observed for the experimental X-ray structures of **[1]** and **[2],** their quality was inadequate to provide a statistically true difference at the 95% confidence limits.

## 3.4 Nuclear Magnetic Resonance (NMR) Spectroscopy

### 3.4.1 NMR Introduction

In organic chemistry, NMR spectroscopy provides a very powerful technique for the characterization of molecules. In the absence of an X-ray structure, NMR can provide 3-D structural information for any molecule provided that it contains NMR active nuclei. NMR active nuclei that have intrinsic spin include $^1H$, $^{13}C$, $^{19}F$ and $^{31}P$. They possess a magnetic moment, $\mu$ and angular momentum $\hbar I$. Spin is quantized and each of these nuclei posses $I = \frac{1}{2}$. The magnetic moment is given by the equation:

$$\mu = \gamma \, \hbar I \qquad\qquad (3.1)$$

where $\gamma$ is the gyromagnetic ratio, $\hbar = \dfrac{h}{2\pi}$ and h is planks constant.

In a magnetic field these nuclei posses $2I+1$ spin states and since $I = \tfrac{1}{2}$, There are two spin states, referred to as the magnetic quantum numbers $m_l$. The allowed values of $m_l$ are $I$, $I-1$, $I-2$,…..$-I$. For these molecules $m_l$ takes values of $\pm\tfrac{1}{2}$ in the presence of a magnetic field as shown in Figure 3.4. This applied magnetic field removes the degeneracy by interacting with the nucleus, thereby splitting the energy level. The energy of interaction between field and nuclei is given by;

$$E = -\mu B_0 \qquad\qquad (3.2)$$

and since $\mu = \gamma \, \hbar I$

$$E = -\frac{\gamma h \nu_0}{2\pi} B_0 \qquad\qquad (3.3)$$

NMR active nuclei will resonate at characteristic frequencies, $\nu_0$ when they are placed in a magnetic field. Signal intensity, resonant frequency and absorption energy are all proportional to magnetic field strength, $B_0$. The local environment of the nuclei affects the value of the resonant frequency. This change in the value of the resonant frequency is referred to as a chemical shift. The direct relationship between $B_0$ and both the fundamental frequency and its shift, enables this shift to be converted to a dimensionless value. Chemical shift is normally reported in parts per million (ppm) and found from the equation:

$$\delta = \frac{\nu - \nu_0}{\nu_0} \tag{3.4}$$
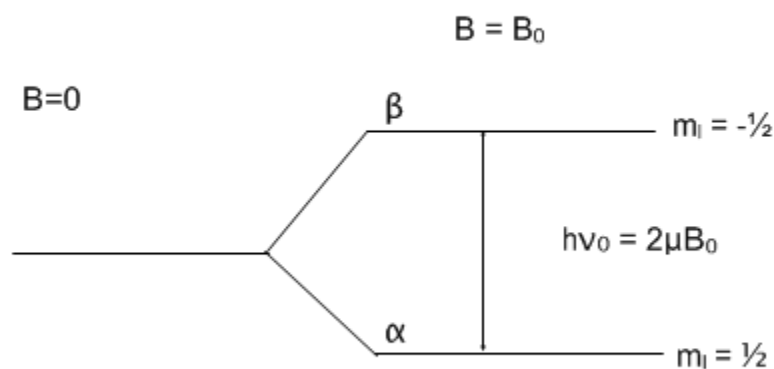


**Figure 3.4** Splitting of the energy level of an NMR active nucleus of spin $I = \frac{1}{2}$ in a magnetic field $B_0$.

A NMR test generates a spectrum which shows the positions, shape and size of the chemical shifts. The chemical shifts carry information about the environment of the nuclei. Active NMR nuclei may couple in a process called scalar coupling which is really a form of spin-spin coupling of the nuclei. The source of this coupling is the interaction of nuclei with different spin states through chemical bonds of the molecule and as a result the signal splits. Coupling to $n$ equivalent (spin $\frac{1}{2}$) nuclei splits the signal into n+1 multiplets with intensity ratios following Pascal triangle. The spacing between the lines of these multiplets is known as the coupling constant and when given in Hz, it is independent of the magnetic field and frequency. The coupling constant J is given by the equation:

$$J = \delta \nu_0 \qquad\qquad (3.5)$$

where the chemical shift, δ is given in ppm and the frequency, $\nu_0$ is given in MHz.

The splitting of the signal into lines with equal intensity due to nuclei with slightly different intensities and that result in a symmetrical signal following the Pascal triangle is an example of first order multiplets, in which chemical shift is represented by the center of the array. However, in a situation where $\Delta\delta\nu_0/J < 10$, second order effects may be seen as the patterns are no longer symmetrical. Second order effects also provide valuable information in the interpretation of the structure of organic molecules.

## 3.4.2  $^{19}$F and $^1$H NMR

Solution $^{19}$F and $^1$H NMR spectroscopy data was collected at NJIT on Bruker ARX 300 machine interfaced to a computer using the Xwin NMR software. $^{19}$F data was collected relative to the NMR reference standard fluorotrichloromethane, $CFCl_3$, (99%). The X-ray structure failed to show the presence of the proton and therefore it was hoped that $^1$H NMR would show the presence of this proton and provide some insight into its environment, thereby elucidating its attachment on the complex. $^{19}$F NMR was carried out to assist in the verification of the structure and glean information on the environment of the fluorine atoms. Initial results of the $^{19}$F spectra confirmed the presence of the fluorine atoms in the structure and integration of the lines revealed an approximate 6:1:1 ratio of primary aliphatic, to aromatic to tertiary aliphatic fluorines. The $^{19}$F NMR spectra also revealed a broad "hump" feature stretching between −135 to −205 ppm, on which the tertiary aliphatic fluorine signal sits. The $^{19}$F spectrum of [2] is shown in Figure 3.5 while that of [1] is shown in Appendix F.

The $^{19}$F NMR of the closed shell $(F_{64}Pc)_2MH$ complexes shown in Table 3.3 have similar chemical shifts to those of $PcF_{64}Zn$, probably indicating the diamagnetic nature of the central metal ion. However, the spectra of **[1]** and **[2]** however contains two significant differences from the spectrum $PcF_{64}Zn$. They are the presence of the hump feature and a doublet which occurs for the primary F in $(F_{64}Pc)_2YH$.
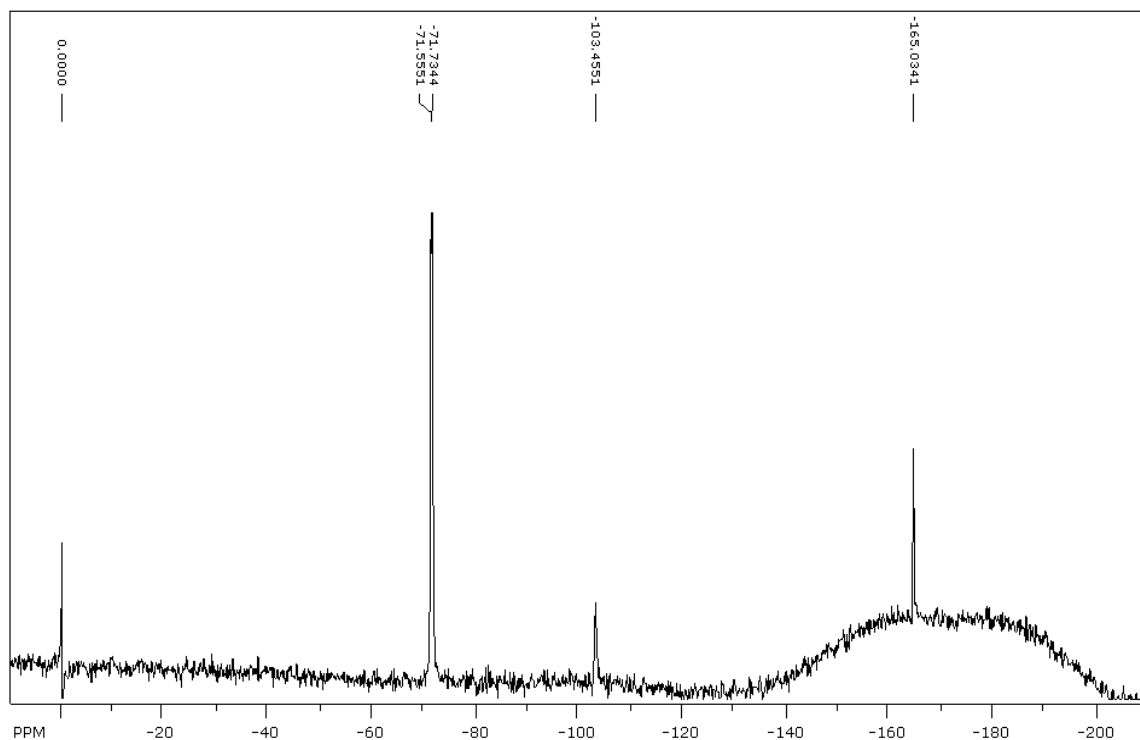


**Figure 3.5** $^{19}$F NMR spectra of $(F_{64}Pc)_2YH$ in acetone $D_6$ showing broad feature.

**Table 3.3** $^{19}$F NMR Spectra of $(F_{64}Pc)_2LuH$ and $(F_{64}Pc)_2YH$ in Acetone $D_6$ Compared with That of $F_{64}PcZn$

| *Complex* | *Primary Aliphatic CF$_3$ shifts, (ppm) and J (Hz)* | *Aromatic F shifts, ppm* | **Tertiary Aliphatic CF shifts, ppm** |
|---|---|---|---|
| $(F_{64}Pc)_2YH$ | $(-71.5, -71.8)$, (J=80) | $-103.5$ | $-165.0$ |
| $(F_{64}Pc)_2$ LuH | $-71.4$ | $-103.7$ | $-165.0$ |
| $F_{64}PcZn^{[110]}$ | $-71.3$ | $-103.8$ | $-164.6$ |

The primary aliphatic fluorines (d, $CF_3$, 6F) of **[2]** appear as an unsymmetrical doublet at the existing resolution of the test method. The chemical shifts and intensities of the doublet are $-71.5$ ppm, 396 and $-71.8$ ppm, 421. The exact nature of the split is currently difficult to elucidate because of the absence of additional data from 2D and other types of NMR analysis. While there is usually weak spin-spin coupling for $^1$H over three bonds[111], this is not necessarily the case for $^{19}$F NMR in some perfluorinated compounds.[112] Perfluorinated chains of certain aliphatic perfluorinated compounds have shown a difference in that $^4$J(F,F) coupling is generally larger than $^3$J(F,F) or $^5$J(F,F) values.[112-114]

In the sandwich Pc environment, the steric interaction between the $i$-$C_3F_7$ moieties and between the $CF_3$ groups may result in hindered rotations, hence forming rotamers. Rotation of the $CF_3$ groups around the C-C bond may change the environment of the F atoms as they may occupy a more *cis* or *trans* orientation. Furthermore, the curvature of the Pc rings indicates intra-molecular steric interactions between the bulky $i$-$C_3F_7$ groups. This steric interaction should result in hindered rotation of especially the $i$-$C_3F_7$ groups around the Ar-C bond. This rotation should also make the tertiary aliphatic F move closer to each other resulting in changes in their interactions. A rotation of one of the $i$-$C_3F_7$ about its Ar-C bond will make the primary aliphatic Fs of adjacent $i$-$C_3F_7$ not only move closer but may cause a cogwheel motion (Figure 4.1) resulting in a rotation of the ring which will change the twist angle momentarily. The molecule should then relax from this higher energy position back to equilibrium position. While the exact nature of the hump feature is not known, the action of the rotamers may be a factor in its observance.

Analysis of the packing of the molecules in the single crystal using the Mercury 2.4 ® software[115] shows that the short van der Waals contacts are between molecules of different stacks, but in solution these effects may be lost.  Solid state NMR would also present an interesting study.

In order to the obtain accurate NMR $^{19}$F peak integrals of **[1]** and **[2]**, a background correction had to be manually applied through Spinworks® software[116] which removes the hump feature.  The $^{19}$F NMR spectrum of **[1]** with background correction is shown in Figure 3.6.

The $^1$H proton NMR was carried out in for $(F_{64}Pc)_2MH$ complexes in the solvents $CDCl_3$, acetone $D_6$ and acetonitrile $D_3$.  In all three cases no signal was observed for the presence of a proton attached to pyrolle nitrogen (N-H).  Spyroulias et al.[117], reported the N-H proton in high field in the region of −8.73 for the $^1$H NMR of $Lu^{(III)}H(TPP)_2$ and $Lu^{(III)}H(TPP)(OEP)$  in $CDCl_3$. They reported differences in the UV-visible spectrum of these porphyrin complexes between $CH_2Cl_2$ and DMF.   The differences were attributed to differences between the protonated and deprotonated forms.[118]  In more basic solvents such as DMF and pyridine, it was reported that the deprotonated form exists.  Despite the differences between the porphyrins and phthalocyanines, it was expected that the $(F_{64}Pc)_2MH$ would have similar behavior.
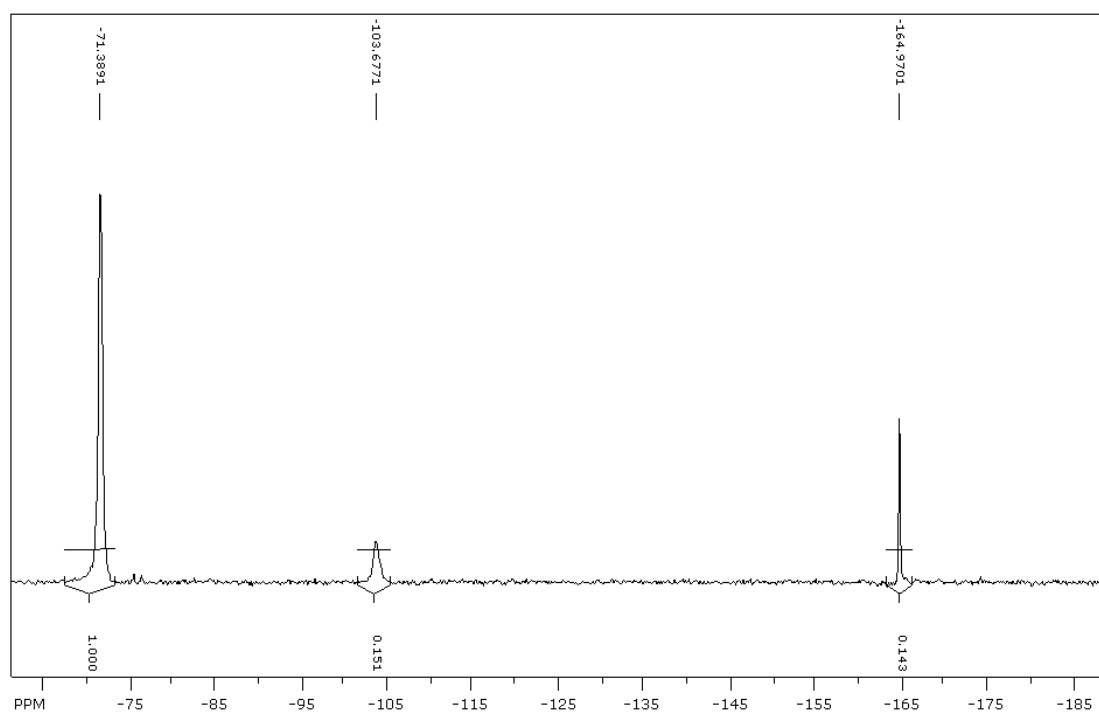
**Figure 3.6** $^{19}$F NMR spectrum of $(F_{64}Pc)_2LuH$ in acetone $D_6$ with background correction showing the calculated peak integrals.

No $^1$H signal was observed in either basic or less basic solvents. In addition, there was no observable difference in the UV-visible spectra between solutions of the complexes in protic solvents such as methanol or basic solvents such as pyridine, except for solvent dependent shifts in peak positions. The absence of the signal is being attributed to the presence of the strong electron withdrawing fluorine atoms on the ring, possible diminishing the effect the field on the proton on the ring of these homoleptic complexes.

## 3.5 Vibration Spectroscopy

### 3.5.1 Theory

Vibrations in chemical bonds can be excited by electromagnetic radiation in the Infrared (IR) region (2-40 μm) of the electromagnetic spectrum. IR spectroscopy which measures these vibrations is a powerful method utilized in the characterization of organic molecules. The atom groups in molecules can vibrate in modes such as bending, symmetrical and anti-symmetrical stretching, scissoring, torsions, wagging, twisting and rocking. Cyclic and ring type molecules can also exhibit a breathing mode. It is also common for combinations (or coupling) of some of these so called normal modes to occur. The motion of the atoms of molecules which include translation, vibration and rotation correspond to the $3N$ degrees of freedom of the atom in a molecule. For example, if one considers the $H_2O$ molecule with three atoms, then there are symmetric and asymmetric stretching of the O-H bonds and a symmetric scissoring bending of the H-O-H structure in addition to the three rotations and three translations. For such non linear molecules with, *n=3*, (*n* = number of atoms) there are *n−1* stretching vibrations and *2n−5* bending vibrations.[119] This accounts for *3n−6* IR frequencies bands in this molecule. In general, the numbers of IR absorptions are calculated by subtracting from the $3N$ translational degrees of freedom of the collections of atoms, the sum of the $3N$ rotational degrees of freedom for the molecule. This results in *3n−6* absorptions for non-linear molecules and *3n−5* for linear molecules.

The energy of the absorbed IR radiation is usually expressed in as:

$$E = \frac{hc}{\lambda}$$

(3.6)

In reporting the IR spectra chemists may report in μm, but it is customary for them to report in wavenumbers, $\bar{v}$ with units of cm$^{-1}$. Wavenumber is defined as: $\bar{v} = {}^{1}/_{\lambda}$. The spectrum of the resonant absorption is usually reported in percent transmission (%T) versus $\bar{v}$. The stretching and other vibrations between two atoms can be described by the classical harmonic oscillator with, $E = \frac{1}{2}kx^2 = hc\bar{v}$. Vibrational frequencies are therefore given by;

$$v = \frac{1}{2\pi}\sqrt{\frac{k}{\mu}}$$

(3.7)

*Where k* is the force constant in units of N/m,

$\mu$ is the reduced mass, $\dfrac{m_1 m_2}{(m_1 + m_2)}$ for two atoms,

$v$ is the frequency of the vibration ($v = {}^{c}/_{\lambda}$)

Vibration motion is quantized and thereby follows rules of quantum mechanics. The allowed transitions are given by the expression, $E = (n + \frac{1}{2})hv$, with n = 1, 2, 3,….

An irradiated molecule will have IR active absorption bands that result from changes in the dipole moment of the molecule during vibrations. As a result, polar molecules with groups such as F, OH and C=O bond are highly IR active. When the vibrations result in a cancellation of the dipole moment in a symmetrical, linear molecule such as O=C=O, that vibration in the molecule is not IR active.

### 3.5.2 IR Spectroscopy

IR data was collected on a Perkin Elmer Instruments Spectrum One FT-IR Spectrometer interfaced to a Dell OptiPlex GXI Pentium III computer using the Spectrum Version 3.02.00 software. The samples were prepared using KBr pellets. The bisphthalocyanine

complexes have 258 atoms therefore the spectra is expected to have many lines. It has been reported that the IR spectroscopic techniques reveal that the frequencies of pyrrole stretching, isoindole breathing, isoindole stretching vibrations, aza stretching vibrations, and coupling of pyrrole and aza stretching vibrations depend on the rare earth ionic size, shifting to higher energy along with the lanthanide contraction due to the increased ring–ring interaction across the lanthanide series.[120] There is only one proton on the ring, but its location is uncertain. However, signals should be obtained from the stretching, bending and wagging of the C-F bonds on the benzene rings and on the $i$-$C_3F_7$ moiety. The IR peaks occurring in the region 1800-700 cm$^{-1}$ for the $(F_{64}Pc)_2LuH$, $(F_{64}Pc)_2YH$ and $Pc_2Y$ is shown in Figure 3.7. The IR peaks occurring in the region 1800-700 cm$^{-1}$ for the $(F_{64}Pc)_2LuH$, $(F_{64}Pc)_2YH$ and $Pc_2Y$ is shown in Figure 3.7. Initial assignments based on the literature [5, 120-123] are set out in Table 3.4:

**Table 3.4** Infrared Peaks and Initial Assignments for $(F_{64}Pc)_2YH$, $(F_{64}Pc)_2YH$ and $Pc_2Y$

| Complex and Some Absorptions (cm$^{-1}$) | | | Assignments |
|---|---|---|---|
| **$(F_{64}Pc)_2$ LuH** | **$(F_{64}Pc)_2$ YH** | **$Pc_2Y$** | |
| 730m, | 730s | 733s | Pc ring breathing |
| 753m | 752m | 768m | |
| 967s | 967s | 884m | |
| 1094s | 1094s | 1062s | Coupling of isoindole deformation and aza stretching |
| | | 1115s | Isoindole breathing coupled with C–H bending |
| 1170s | 1170s | | Symmetric C-F stretch |
| 1249vs | 1247vs | | Anti-symmetric C-F stretch |
| | | 1322vs | Pyrrole stretching (marker for π radical ligand) |
| 1352w | 1352w | 1364s | |
| 1384w | 1384w | 1384m | |
| 1454w | 1453w | 1449s | |
| 1490w | 1485w | 1489w | Isoindole stretching |
| 1637m | 1632m | 1628s | Benzene ring stretch |
| 1747w | 1745w | 1718w | Benzene ring stretch |

Legend: vs = strongest absorption, s = strong, m = medium, w = weak, b = broad.

There is great interest in the region between 1300 and 1460 cm$^{-1}$ due to reports that three dominant vibrations occur in this region for the neutral Pc$_2$Ln[104, 124] and that the most intense of these bands occurring ca. 1313-1322 cm$^{-1}$ is characteristic of the $\pi$ radical ligand.[125]  These vibrations that red shifted with decreasing Ln$^{3+}$ size [La to Lu] are metal dependent and  are assigned to C-N and C-C stretching vibrations of the inner (CN)$_8$  Pc ring.[124]    An intense vibration occurred as a very strong absorption for the reference Pc$_2$Y complex at 1322 cm$^{-1}$, but none was observed in this region for **[1]** and **[2]**.  The absence of this band in **[1]** and **[2]** is attributed to absence of an F$_{64}$Pc$^{\bullet-}$ in these complexes.  It appears unlikely that its absence is due to the strong electron withdrawing fluorine groups because the tetrakis-substituted and the octakis-substituted lanthanide bisphthalocyanines have been reported to generally have the strong band appearing at around 1320 cm$^{-1}$.  A difference is that for  the oxyalkyl substituted species, the intensity of this band decreases while the band appearing at 1377 cm$^{-1}$ gains in intensity.[52]

The [Pc$_2$Ln]$^-$  anions have the principal metal dependent IR bands located around 492, 878, 1398 and 1474 cm$^{-1}$.  A strong  absorbing metal independent band appears at 1329 cm$^{-1}$ in the spectra of [Pc$_2$Ln]$^-$  anions.[125]  Weis and Fischer[52]  propose that this band is related to the presence of the two dianionic phthalocyanine ligands and suggests further that the absence of this band in the neutral Pc$_2$Ln supports the delocalization of the unpaired electron over both rings on the IR time scale.  If this was not the case, this band would be present in the neutral lanthanide bisphthalocyanine complexes.   This strong absorbing band was not found in the IR spectra of **[1]** and **[2]**.  It was unexpected because of the proposed presence of the F$_{64}$Pc$^{2-}$ and metal independence of the vibration.

Asymmetric and symmetric C-F stretching has been assigned to the absorptions at

248 and 1170 cm$^{-1}$ respectively.  IR tables and charts of fluorinated organic compounds[126]  indicate that Ar-F occurs at  1200 – 1100 cm$^{-1}$ due to  ring and C-F stretch and  occurs at 420 – 375 cm$^{-1}$ due  to in-plane C-F deformation vibration.  These tables further indicate that poly-fluorinated compounds have a series of very intense bands in the region 1360-1090 cm$^{-1}$ due to the strong coupling of C-F and C-C stretching vibrations.  While there are several bands in this region it is difficult to assign them to C-F vibrations due to the presence of other characteristic vibrations from the $F_{64}Pc^{2-}$ ring.
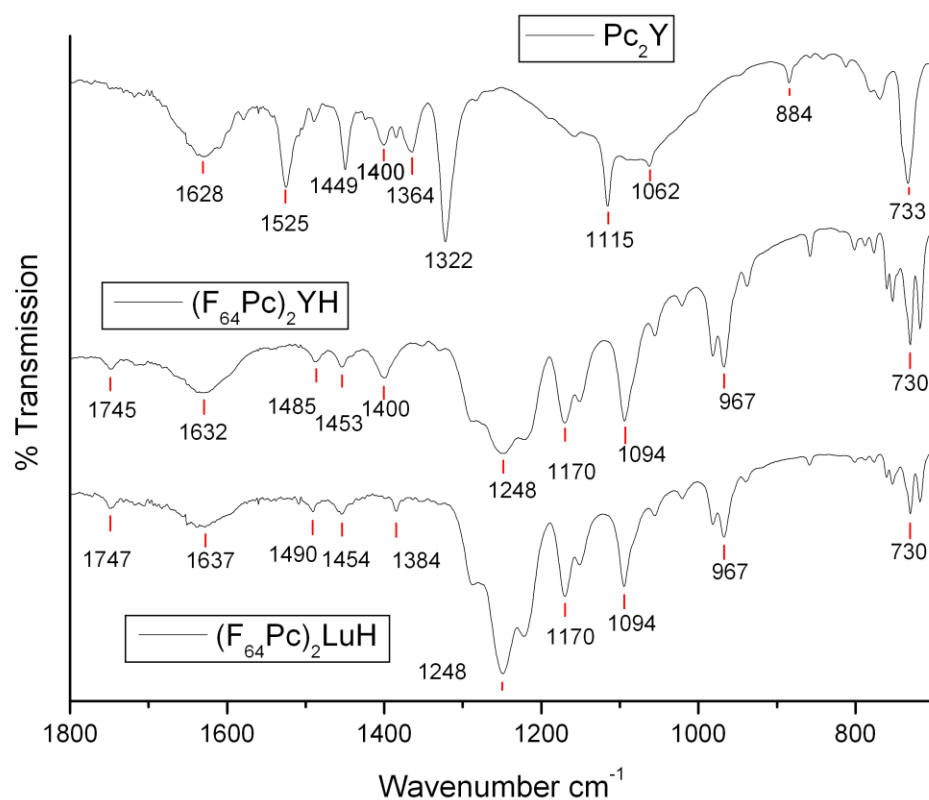


**Figure 3.7** IR spectra of $(F_{64}Pc)_2LuH$, $(F_{64}Pc)_2YH$ and $Pc_2Y$ from KBR discs.

Amine N-H have characteristic stretch vibrations in the range 3300-3500 cm$^{-1}$ and bending vibrations at 1600 cm$^{-1}$.[127]  The N-H pyrrole of vibrations **[1]** and **[2]** are

expected to be close to these values. In fact IR N-H stretching of pyrrole containing compounds have been reported in the range 3316-3335 $cm^{-1}$ using KBr discs.[128]

The IR spectra of both **[1]** and **[2]** showed a strong, broad peak at 3446±1 $cm^{-1}$. The peak due to the N-H stretch is expected to be a single, weak peak, and if it occurs in **[1]** and **[2]**, it could be swamped by this peak, most likely generated by the O-H stretch from the practically unavoidable presence of moisture in the KBr discs. Similarly, a broad, medium to weak absorption occurred between 1628-1637 $cm^{-1}$ in the complexes. Again, this absorption encompasses the region where the benzene ring stretch of the phthalocyanine ring occurs.[120] The occurrence of IR absorptions due to N-H stretch and bending **[1]** and **[2]** requires additional supporting methods such the use of DFT.


### 3.6 Electron Spin Resonance

### 3.6.1 Theory

Electron Spin Resonance (ESR) or electron paramagnetic resonance is one of a series of resonance techniques utilized in the study of materials which have energy absorption effects that are associated with changing the spin angular momentum of electrons and nuclei. Other members of this spectroscopy family include NMR, Magnetic Resonance Imaging (MRI), Nuclear Quadrupole Resonance (NQR) and Ferromagnetic Resonance (FMR).[129] In chemistry ESR is a valuable characterization tool for studying or identifying paramagnetic species such as organometallic complexes containing transition metals, and organic and inorganic free radicals. These chemical species have one or more unpaired electrons. Paramagnetic materials develop an induced magnetization intensity which is greater than that of the applied magnetic field, $B_0$. Although they

contain permanent magnetic dipoles with little or no interaction, they lose their magnetization on removal of $B_0$.

The absorption spectra from ESR involve the species which are excited during the application of $B_0$. An electron has spin S = ½ and a magnetic moment, $\mu_e$ and thus will be aligned parallel or anti-parallel with $B_0$. The magnetic moment is given by:

$$\mu_e = -g_e\mu_B\vec{S} \tag{3.8}$$

where $g_e$=2.0023, and is the electron *g*-factor for a free atom, $\mu_B$ = the electronic Bohr Magneton and $\vec{S}$ the dimensionless electron spin vector. The g-factor is the ratio of the magnetic moment to the angular momentum. The electronic Bohr Magneton, $\mu_B$ is defined as $\mu_B = e\hbar/2m$ and is closely related to the spin magnetic moment of a free electron. S is a quantum number used to represent the electron spin angular momentum. The axial interaction of the magnetic field with the magnetic moment, called the Zeeman Interaction, $\bar{H}_{ZI}$ results in an energy separation which can be expressed by the following Hamiltonian:[130]

$$\bar{H}_{ZI} = \mu_e \bullet \bar{B} = g_e\mu_BS_Z \tag{3.9}$$

The Zeeman Effect is the breaking of degeneracy in atomic energy levels due to the interaction between the magnetic moment of an atom and an external magnetic field. The splitting is described in Figure 3.8. The energy separation $\Delta E$, between the populations aligned parallel and anti-parallel with the applied magnetic field falls within the microwave energy radiation band, typically with frequencies in the range 3.5-95 GHz. Most ESR instruments achieve resonance using a single microwave frequency and sweeping the magnetic field to obtain resonance. Since the upper energy and lower

energy levels relative to the magnetic quantum numbers are given by $E_\beta = \frac{1}{2}g_e\mu_B B_0$ and

$E_\alpha = -\frac{1}{2}g_e\mu_B B_0$ respectively, then:

$$\Delta E = h\nu = g_e\mu_B B_0 \qquad\qquad (3.10)$$

where $\nu$ is the frequency of microwave energy.
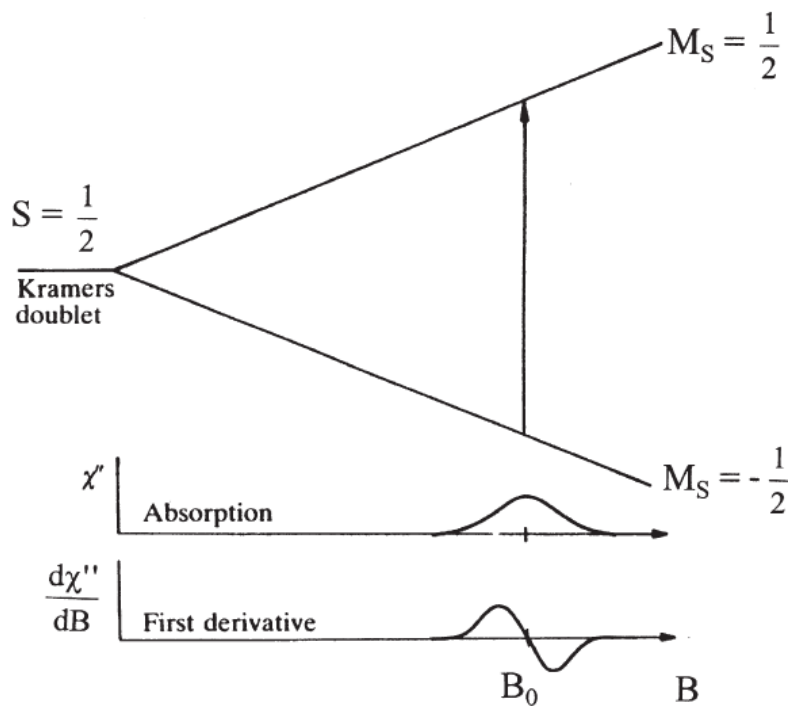


**Figure 3.8** Energy level diagram for an isolated electron in a magnetic field $B_0$ and the corresponding absorption spectrum and first derivative ESR spectrum. [131]

The Zeeman interaction is just one of the interactions that the unpaired electrons experience. Here, molecular and atomic orbitals containing an electron experience a contribution to paramagnetism due to the electron motion in the orbital which has angular

momentum *L*. The two interactions are known as spin-orbit coupling and orbital magnetic field interactions.

These two interactions results in a deviation of the $g_e$ value from the free-electron value and also adds anisotropy which means that the value of $g_e$ will depend on the orientation of the crystalline material with the applied magnetic field. In fact, single crystals are generally used to measure a $g\perp$ and $g\parallel$. The spin-orbit coupling gives rise to a spin-orbit constant and anisotropic $\bar{\bar{g}}$ tensor in the Hamiltonian for the effect of spin-orbit coupling. Nuclei may possess a non-zero spin due to the spin of their nucleons. The coupling interaction of the magnetism of the electron and that of these nuclei is referred to hyperfine coupling and it also adds a term to the overall Hamiltonian. The hyperfine coupling tensor, $\bar{\bar{A}}$, may have alignment with one or more of the principal axes of $\bar{\bar{g}}$ depending on the point group of the molecule. Molecules with multiple unpaired electrons may undergo interactions with the electric field of neighboring atoms due to the geometry of the structure or the crystal or ligand field. Splitting of a degenerate electronic ground state may result in the absence of a magnetic field, the so called "Zero Field Splitting" (ZFS). ZFS results in line splitting of the ESR spectrum. The interaction results in addition to the total Hamiltonian, a field splitting fine structure tensor, $\bar{\bar{D}}$.

In ESR, four different magnetic interactions may occur which can influence the behavior of electrons in a magnetic field They are;[130]

a) the Zeeman interaction, $\bar{H}_{ZI}$

b) the nuclear hyperfine interaction, $\bar{H}_{HF}$

c) the electrostatic quadrupole interaction, $\bar{H}_Q$

d) the zero-field splitting if $S > \frac{1}{2}$, $\bar{H}_{FS}$

The Hamiltonians for each effect are shown in equations 3.11-3.15;

$$\bar{H}_{ZI} = \mu_B \bar{B}(\bar{L} + g_e\bar{S}) + \lambda\bar{L}\bar{S} = \mu_B\bar{B}\bar{\bar{g}}\bar{S} \tag{3.11}$$

where $\lambda$, the spin-orbit coupling constant, $\bar{S}$ the dimensionless spin vector and $g$, the effective $g$-value; and

$$\bar{H}_{HF} = \bar{I}\bar{\bar{A}}\bar{S} \tag{3.12}$$

where $\bar{\bar{A}}$ is the hyperfine coupling tensor and $\bar{I}$ the nuclear spin vector.

$$\bar{H}_Q = \bar{I}\bar{\bar{Q}}\bar{I} \tag{3.13}$$

where $\bar{\bar{Q}}$ is the quadrupole coupling tensor

$$\bar{H}_{FS} = \bar{S}\bar{\bar{D}}\bar{S} \tag{3.14}$$

with the fine structure tensor $\bar{\bar{D}}$; The Hamiltonian for H$_{FS}$ is;[131-133]

$$\bar{H}_{FS} = D\left(\overline{S_z^2} - \frac{S(S+1)}{3}\right) + E(S_x^2 - S_y^2) \tag{3.15}$$

where D denotes the axial fine structure parameter and $E$ describes the orthorhombic fine structure parameter. The total Hamiltonian then becomes

$$\bar{H}_T = \mu_B\bar{B}\bar{\bar{g}}\bar{S} + \bar{I}\bar{\bar{A}}\bar{S} + \bar{I}\bar{\bar{Q}}\bar{I} + \bar{S}\bar{\bar{D}}\bar{S} \tag{3.16}$$

### 3.6.2 Instrumentation

The microwave instrumentation for ESR spectra consist of four important parts.[134] These are;

1. The supply of microwaves. In the Bruker EMX this is controlled by the microwave bridge assembly which supplies, detects and controls microwave

radiation.

2. A sample cavity which receives microwaves via a waveguide and reflects the waves back to the detector,

3. Electromagnets at 90° to the cavity which supply the magnetic field. A small magnetic field oscillating magnetic field is superimposed on the sample cavity via modulation coils. (i.e. via the Hall probe field controller).

4. A detector diode also contained in the microwave bridge assembly in the EMX.

### 3.6.3  ESR Spectra of $(F_{64}Pc)_2LuH$ and $(F_{64}Pc)_2YH$

Electron spin resonance was carried out at the City University of New York (CUNY) on their Bruker EMX EPR spectrometer series (9.5 GHz) EPR machine with magnetic field at 0.3300 T and wavelength (cavity dimensions) of 0.86 cm. The machine is a continuous wave electron spin resonance (CW-ESR) type. Samples were tested in powder form using Wilmad LabGlass® 4 mm outer diameter thin walled quartz tubes 135 and 250 mm long. Low temperature measurements were obtained using a glass Dewar cooled with liquid nitrogen.

Solutions dissolved in chloroform and acetone failed to give a signal at room and liquid nitrogen temperatures. Symmetrical second derivative ESR signals with structure were obtained in the solid state, with average g values of 2.004. The results are shown in Table 3.5 and plots of the spectra in Figure 3.9. No signal was expected from the samples because the central metal ($M^{3+}$) ions are closed shell (no unpaired electrons) and the $F_{64}Pc^{2-}$ ligands are not expected to have radical electrons. The presence of impurities from contamination of [3] and [4] is being ruled out because [3] gave no signal and [4] gave a signal which was very noisy and did not resemble the ESR signal of either [1] or [2]. Contamination with iron and other magnetic impurities was unlikely because these

would result in a signal in solution (or in suspension in the case of insoluble species such as magnetite).

**Table 3.5** ESR Data for $(F_{64}Pc)_2LuH$ and $(F_{64}Pc)_2YH$ in the Solid State

| Complex | Gyromagnetic ratio, g value | Temperature (K) | FWHW (G) | Average Field (G) |
|---|---|---|---|---|
| $(F_{64}Pc)_2YH$ | 2.0037 | 295 | 6.6 | 3470 |
| $(F_{64}Pc)_2YH$ | 2.0042 | 77 | 7.4 | 3355 |
| $(F_{64}Pc)_2LuH$ | 2.0038 | 295 | 6.6 | 3470 |
| $(F_{64}Pc)_2LuH$ | 2.0039 | 77 | 7.4 | 3355 |

In the calculation of the g value of **[1]** and **[2]**, the simplified Equation 3.10 was used. The symmetry of the line shape indicates absence of any large effects other than of the Zeeman interaction. It was not possible to measure $g_\perp$ and $g_\parallel$ due to absence of large crystals and the limits of the existing EPR machine.



(a)  (b)
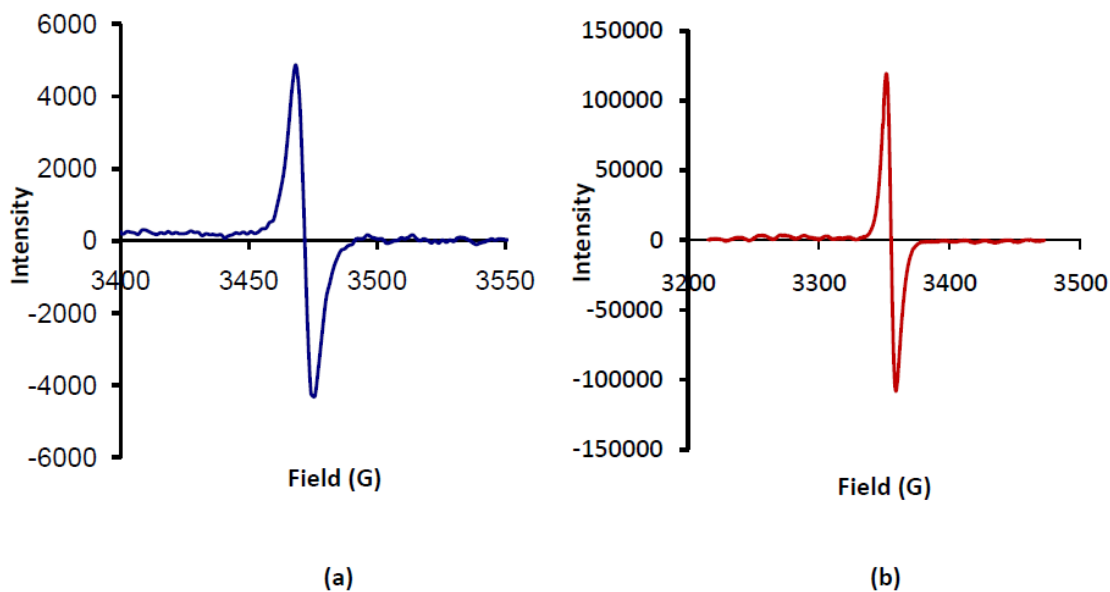
**Figure 3.9** ESR spectra showing symmetry and structure: a) Spectrum of $(F_{64}Pc)_2YH$ and; b) Spectrum of $(F_{64}Pc)_2LuH$.

The g value was greater than that of the free electron ($g_e = 2.0023$) indicating the presence of other interactions. The point group of these complexes is $C_1$ (no symmetry) therefore if the $\bar{\bar{g}}$ and $\bar{\bar{A}}$ tensors exist, they should be non co-incident and the ESR symmetry is triclinic.[130] If however, one considers **[1]** and **[2]** to have the idealized higher $C_{4v}$ symmetry then, $A_{xx}=A_{yy}{\neq}A_{zz}$ and $g_{xx}=g_{yy}{\neq}gzz$, the tensor axes are all co-incident and the ESR symmetry could be axial.

The structure of the line outside of the main peaks has not been interpreted at this time.

## 3.7 Magnetism

### 3.7.1 Diamagnetism, Paramagnetism, Ferromagnetism and Antiferromagnetism

At the macroscopic level, magnetism of a sample is measured as molar magnetism, $M_m$ and molar susceptiblity $\chi_M$. Several forms of magnetism have been classified with the four most common types being diamagnetism, paramagnetism and ferromagnetism and anti-ferromagnetism. This classification is based on measured values of $\chi$ as a function of temperature and applied magnetic field.

Diamagnetism arises because of the magnetic field which is induced by the applied magnetizing field, *H* from circular motion of spin paired electrons. This generated field opposes *H*. According to Langevin, the diamagnetic susceptibility is directly proportional to the number of bonded electrons and the sum of the squared values of the average orbital radius. It is given by the equation:

$$\chi_{Dia} = -\frac{N_A e^2}{6mc^2} \sum_i^n \overline{r_i^2} \qquad (3.17)$$

All materials exhibit diamagnetism.

Paramagnetism, however, results from the presence of unpaired electrons which in the absence of *H* have no permanent magnetization. On the application of *H*, the magnetic moments of the species with unpaired electrons align with the field increasing the magnetization of the sample. The Curie law describes the relationship between $\chi_M$ and temperature, *T*. At fixed applied *H* and high temperature, $\chi_M$ is inversely proportional to *T*. It is given by:

$$\chi_M = \frac{C}{T} \tag{3.18}$$

where C is the Curie constant.

This equation applies to magnetically dilute samples where interaction between ions and molecules is minimized. In many real systems, this is not the case and there are indeed interactions between units that cause neighboring magnetic moments to become aligned or paired. This deviation from the Curie law is compensated for in the Curie-Weiss law. The Curie-Weiss Law is given by:

$$\chi_M = \frac{C}{T - \theta} \tag{3.19}$$

A plot of $\chi_M^{-1}$ vs. *T* is in the Curie Law approximates to an intercept on *T* axis at the origin. For the Curie-Weiss Law, this intercept is non-zero, with a negative value of $\theta$ indicating anti-ferromagnetism and a positive value, ferromagnetism.

Ferromagnetism and anti-ferromagnetism are forms of cooperative magnetism. In ferromagnetism there is spin alignment from dipole-dipole interaction of adjacent atoms/species, while in anti-ferromagnetism there is spin pairing from the dipole-dipole interactions. The relative amount of spin alignment and spin pairing leads to various

degrees of ferrimagnetism.  The relationship of $\chi$ with $T$ for these classifications is shown in Figure 3.10.

**Table 3.6**  Units, Conversions and Values for Physical Quantities of Magnetic Measurements[135]

| Quantity | cgs -emu units[‡] | SI units | Conversion |
|---|---|---|---|
| Magnetic moment | emu, erg/G | $Am^2$, J/T* | $1$ J/T $=10^3$ emu, erg/G |
| Inductance or magnetic flux density | Gauss (G) | T | $1T = 10^4$ G |
| Magnetic field strength  or magnetizing field (H) | Oersted (Oe) | A/m | $1$ A/m $= 4\pi \times 10^{-3}$ Oe |
| Volume magnetization (M) | $emu/cm^3$ | A/m | $1$ A/m $= 10^{-3}$ $emu/cm^3$ |
| Permeability of free-space, $\mu_0$ | 1 G/Oe | $4\pi \times 10^{-7}$ H/m | |
| Molar Susceptibility, $\chi_m$ | emu/mol, $cm^3/mol$ | $m^3/mol$ | $1 cm^3/mol = 4\pi \times 10^{-6}$ $m^3/mol$ |
| Intensity of magnetization, I | $emu/cm^3$ | T | $1$ T$=1/4\pi \times 10^4$ $emu/cm^3$ |

[‡]  emu are electromagnetic units of cgs system, and are often used interchangeably to represent some magnetic units

\* $1$ $Am^2 = 1$J/T

Magnetism data is presented in either the MKS or cgs units.  The cgs system of units is still very popular for describing magnetic parameters.  Table 3.6 gives some units, conversions and values for magnetic materials.

Van Vlecks equation for paramagnetism, Equation 3.36 reduces to the Curie law under the conditions stipulated.  It is given (in cgs units) as:

$$\chi = \frac{N_A \mu_B^2 \mu_{eff}^2}{3kT}$$

(3.20)

where $\mu_{eff}$ is the Bohr Magneton number (effective magnetic moment) and $C = \frac{N_A \mu_B^2}{3k}$. For transition metals and particularly lanthanides, the orbital contribution to the magnetic moment is appreciable and thereby modifies $\mu_{eff}$ and the g values of the species.  In this case the $\mu_{eff}$ (spin-orbit case) is given by:

$$\mu_{eff} = g\sqrt{J(J+1)}$$

(3.21)

with J = L+S.

The gyromagnetic ratio, g value can be estimated in this case by;

$$g = 1 + \frac{S(S+1) - L(L+1) + J(J+1)}{2J(J+1)} \tag{3.22}$$
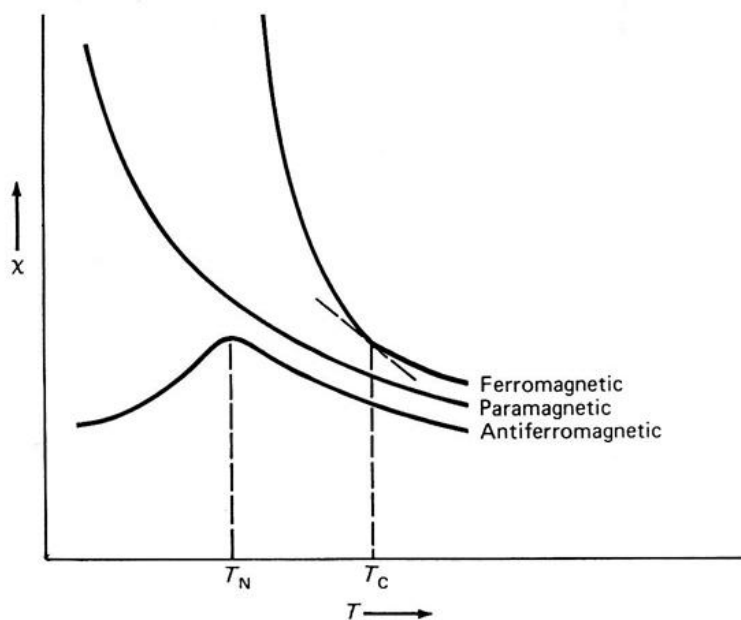


**Figure 3.10** Temperature dependence of ferromagnetic, paramagnetic and antiferromagnetic behavior . $T_C$ = Curie Temperature and $T_N$ = Néel Temperature.[136]

### 3.7.2 Theory

Magnetism refers to the response of a material when placed in a magnetic field. Historically, this response was described mainly through a mechanical movement such as attraction, repulsion or torsion. These macroscopic responses are however, driven by interactions at the atomic or sub-atomic level with the applied magnetic field. The material responds because magnetism is induced inside winthin it by the applied field; it is said to be magnetized. In classical physics, the magnetic moment or magnetic dipole

moment, μ is the strength of the magnetic source.  It can be defined in terms of a bar magnet as the product of the pole strength and the displacement between them.  That is:

$$\mu = px \tag{3.23}$$

where $p$ is pole strength, $x$ is displacement and μ has units of J/T.   Uniform magnetic fields, $H$ can be created within current carrying coils.  The magnetic moment within a planar loop is given by the product of the current $i$ and the area vector $\bar{a}$, such that:

$$\mu = i\bar{a} \tag{3.24}$$

and in this case, μ has units of $Am^2$.  Rotating or gyrating charged objects such as electrons, protons and even large galactic objects have a magnetic moment.

A substance placed in a magnetizing field, $H$ will experience a magnetic induction B which is the sum of the $H$ and the contribution of the intensity of magnetization of the material itself, $M$ such that;

$$B = H + 4\pi M \tag{3.25}$$

 The relationship between B and $H$ is defined by B = $\mu_0 H$, where $\mu_0$ is the permeability of free-space and has value of $4\pi \times 10^{-7}$ Henry/meter.   The ratio $M/H$ is also defined as the magnetic susceptibility, $\chi$.  Inside of a linear isotropic material, B, $H$ and M have the same direction and $\chi$ and μ are scalers and unitless. In this case, μ is the permeability of the material and takes values depending on how the material interacts with the $H$.   In anisotropic materials $\bar{\bar{\chi}}$  and $\bar{\bar{\mu}}$  are 3x3 matrices called the permeability and magnetic susceptibility tensors respectively.  Thus, $\bar{B} = \bar{\bar{\mu}}\bar{H}$ and $\bar{M} = \bar{\bar{\chi}}\bar{H}$. The matrices are related by the Equation 3.26:

$$\mu = \mu_0(I_3 + \chi) \tag{3.26}$$

where $I_3$ is the 3x3 identity matrix. The above classical explanation of the magnetic permeability and susceptibility of a substance contrasts somewhat with the quantum mechanical approach.[137] This leads to a general equation relating the magnetic susceptibility of an atom to the energies of the various energy states that the atom occupies. In this approach μ and χ are defined as:

$$\mu_z = -\frac{\partial E}{\partial H}$$

(3.27)

and

$$\chi = -\frac{1}{H}\frac{\partial E}{\partial H}$$

(3.28)

where $\mu_z$ = the component of the magnetic moment in the field (z) direction and E = the energy of the spin and orbital angular momenta of the atom with the field, depending on *H*.

For a system of non-interacting particles the equation by Van Vleck may be developed. The magnetization intensity, I, can be obtained by considering that each system may be in a number energy levels. Using a Boltzmann distribution function, I can be given by:

$$I = \frac{n\sum_i \mu_i exp\left(-E_i/kT\right)}{\sum_i exp\left(-E_i/kT\right)}$$

(3.29)

The molar susceptibility $\chi_M$ can therefore be given as:

$$\chi_M = \frac{IN}{Hn} = \frac{N \sum_i \frac{\partial E_i}{\partial H} exp\left(-\frac{E_i}{kT}\right)}{\sum_i exp\left(-\frac{E_i}{kT}\right)} \tag{3.30}$$

The expansion of the $E_i$ energy level into a power series gives expressions such

that     $E_i = E_i^0 + HE_i^{(1)} + H^2 E_i^{(2)} + \cdots\cdots$     and     $\mu_{i=} - \frac{\partial E_i}{\partial H} = -E_i^{(1)} - 2E_i^{(2)} - \cdots.$

Substitution of these expansions into equation 3.30 gives an equation for the second

expression as a power series in $H$.  An assumption is made that the exponentials

involving the terms $HE_i^{(1)}$ and $H^2 E_i^{(2)}$ are much smaller than k$T$.  If it is also assumed

that there is no residual moment in the absence of a magnetic field and the terms $HE_i^{(1)}$

and $H^2 E_i^{(2)}$ are expanded and an approximation made by neglecting all terms containing

second orders of $H$, the fundamental expression for the molar susceptibility $\chi_M$ is

expressed as:

$$\chi_M = N \frac{\sum_i \left[\left(E_i^{(1)}\right)^2 / kT - 2E_i^{(2)}\right] exp\left(-\frac{E_i^0}{kT}\right)}{\sum_i exp\left(-\frac{E_i^0}{kT}\right)} \tag{3.31}$$

This is the fundamental Van Vleck equation; to solve it, one needs to know the quantities

$E_i^{(0)}$, $E_i^{(1)}$ and $E_i^{(2)}$.    Theoretically, Van Vleck's equation can be used when the

eigenvalues $E_i^{(0)}$ and eigenfunctions $|n\rangle$ of the Hamiltonian are known at $H$=0, (zero field

condition).  The Hamiltonian for this energy is:

$$\mathcal{H}^0 \psi_i^0 = E_i^0 \psi_i^0 \tag{3.32}$$

where $\psi_i$ is wavefunction of the $i^{\text{th}}$ energy level $E_i^0$ and $\mathcal{H}^0$ is the operator in the zero applied field condition. In a scenario where the applied magnetic field is small enough to cause a perturbation in $\psi_i^0$, this will result in a change in both the wavefunction and energy. Perturbation theory can therefore be used to approximate the new energies. The change in energy along the z-axis may be given by:

$$-H\langle\psi_i^0|\mu_z|\psi_i^0\rangle - H^2 \sum_{ij} \frac{|\langle\psi_i^0|\mu_z|\psi_i^0\rangle|^2}{E_j^0 - E_i^0} \qquad (3.33)$$

which neglects the additional term in $H^2$ (due to diamagnetism). The summation runs over the $i^{\text{th}}$ level with $E_j^0 \neq E_i^0$, knowing $E_i^0$ and replacing $\mu_z$ with the Zeeman operator $\hat{H}_{ZE} = \mu_B \sum_k (L_k + g_e S_k) H$ where $L_k$ and $S_k$ are the orbital and spin momenta of electron $k$ respectively, calculates for $E_i^{(1)}$ and $E_i^{(2)}$. They are given by:

$$E_i^{(1)} = \langle\psi_i^0|\hat{H}_{ZE}|\psi_i^0\rangle \qquad (3.34)$$

$$E_i^{(2)} = \sum_{ij} \frac{|\langle\psi_i^0|\hat{H}_{ZE}|\psi_i^0\rangle|^2}{E_j^0 - E_i^0} \qquad (3.35)$$

A more simplified form of the Van Vleck equation is obtained when all energies $E_i$ are linear in $H$ and the second-order Zeeman coefficients $E_i^{(2)}$ vanish. It is given by:

$$\chi_M = \frac{N_A \sum_i E_i^{(1)^2} \exp\left(-E_i^{(0)}/kT\right)}{kT \sum_i \exp\left(-E_i^{(0)}/kT\right)} \qquad (3.36)$$

### 3.7.3 The Super Conducting Quantum Interference Device (SQUID)

The SQUID is one of the most sensitive magnetic measuring devices available. Its sensitivity is in the order of $10^{-14}$ T.[138] SQUIDs utilize the Josephson junction to measure the magnetic moment of the sample.[139] They work by utilizing the interaction between magnetic flux and the Josephson junction. The sample's magnetic flux modulates the current passing through the Josephson junction which is detected by the system's electronic apparatus.[140]

The Josephson junction is composed of two superconductors separated by a thin insulating layer.[141] Its function is based on quantum mechanics and involves the concept of a quantum of magnetic flux passing through the superconductor. The superconducting current is carried by a Cooper electron pair.[142] This electron pair which is formed by electron phonon interactions can tunnel across a junction. The DC Josephson Effect is when a direct current passes the insulator without being driven by an external electromagnetic field (i.e., tunneling). In general at certain fixed voltages, the junction may carry a direct current whilst acting as a highly sensitive frequency to voltage converter.[140] It is this voltage that can be detected, amplified and characterized in the application of SQUIDs in magnetometers.

A commercial SQUID magnetometer such as those produced by Quantum Design® consists of four main components.[143] They are: (a) superconducting magnet (b) superconducting detection coil which is coupled inductively to the sample; (c) a SQUID connected to the detection coil; (d) superconducting magnetic shield. Magnetic measurements are carried out in the SQUID by moving the sample through the second-order gradiometer. The sample's magnetic moment induces an electric current in the

pick-up coil system. The magnetic flux change in the pick-up coils changes the persistent current in the detection circuit. Changes in the current in the detection coils produce variations in the SQUID output voltage which are proportional the magnetic moment of sample. Figure 3.11 shows an example of a gradiometer superconducting detection coil in a Quantum Designs ® SQUID MPMS XL5.
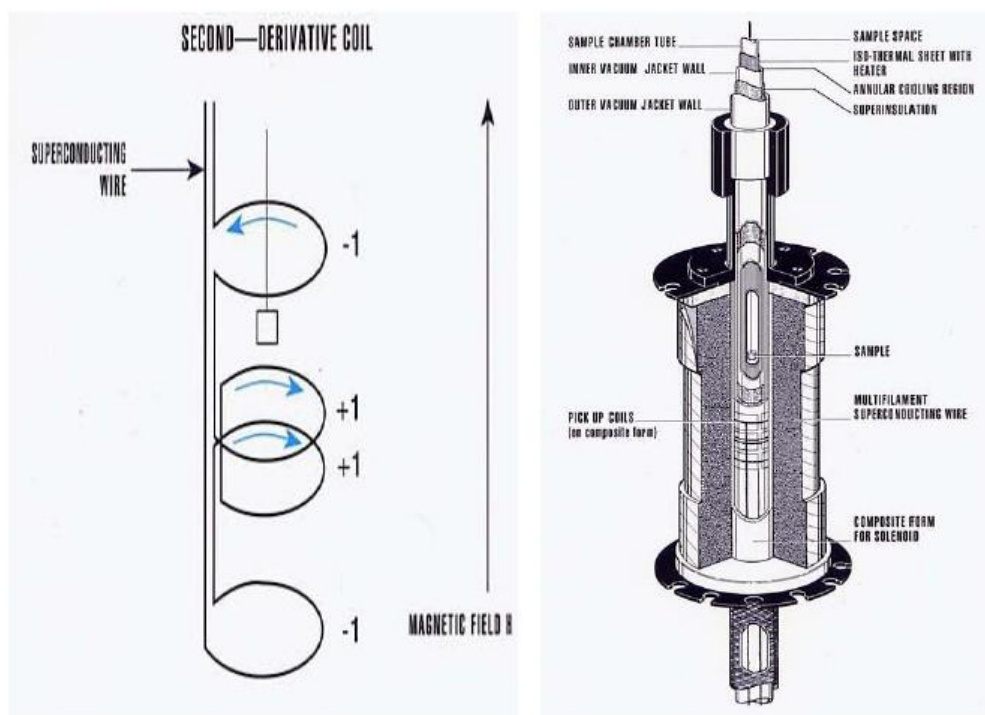


**Figure 3.11** The configuration and location of the second-order gradiometer superconducting detection coil. The coil sits outside the sample space within the liquid helium bath.[143]

### 3.7.4 Direct Current Magnetism

Direct Current (DC) magnetism was carried out on microcrystalline samples of the complexes using the SQUID MPMS-XL magnetometer at Argonne National Laboratory and the raw data provided. Longitudinal moment was measured for hysteresis at temperatures of 5 K, 50 K, 100 K, 150 K, 200 K, 250 K, and 200 K. The Zero Field

Cooled-Field Cooled (ZFC-FC) test also was carried out between 2 K and 300 K. Carrying out the ZFC-FC at low magnetic field helps to identify any special magnetic features in the sample such as irreversibility due to ferromagnetic behavior.[143] The data from the SQUID was processed and the molar magnetization, $M_m$ and the molar susceptibility, $\chi_M$ were calculated. In general, magnetization per unit volume obtained is corrected for background (sample capsule). This is achieved by obtaining the magnetism of the empty capsule under the same conditions under which the sample is tested. The longitudinal moment of the capsule is then subtracted from that of the corresponding sample. Then $\chi_M^{un}$ (uncorrected for diamagnetism) is calculated using the expression;

$$\chi_M^{un} = \frac{Longitudinal\ Moment/Field}{mass\ of\ sample/Formula\ Weight} \tag{3.37}$$

The diamagnetic susceptibility contribution to the measured value was calculated using Pascal's constants.[144] Pascal suggested that the diamagnetism of a molecule can be estimated by summing the diamagnetic susceptibility of every atom $\chi_{Di}$ and $\lambda_i$ of every bond. The molar diamagnetic susceptibility of the molecule is $\chi_D$:

$$\chi_D = \sum_i \chi_{Di} + \sum_i \lambda_i \tag{3.38}$$

where $\chi_{Di}$ and $\lambda_i$ are known as Pascal constants. The values of these Pascal's constants were obtained from standard tables.[145] Diamagnetic susceptibilities of **[1]** and **[2]** were obtained by using the base value of the Pc ring[144] from which the hydrogen atoms were removed and replaced by the F atoms and $i$-$C_3F_7$ moiety. The diamagnetic susceptibility of the neutral $Pc_2Y$ was obtained from the literature value of $H_2Pc$.

The hysteresis magnetic test on **[1]** and **[2]** at 5 K did not reveal any irreversibility. Hysteresis of the **[2]** is shown in Figure 3.12 and that of **[1]** is shown in

Appendix D.  The hysteresis curves in Figure 3.12(a) that are based on the magnetic moment of the raw sample, shows diamagnetism. However when the samples were corrected for the standard diamagnetic contributions (Figure 3.12(b)) both samples were observed to be weakly paramagnetic.
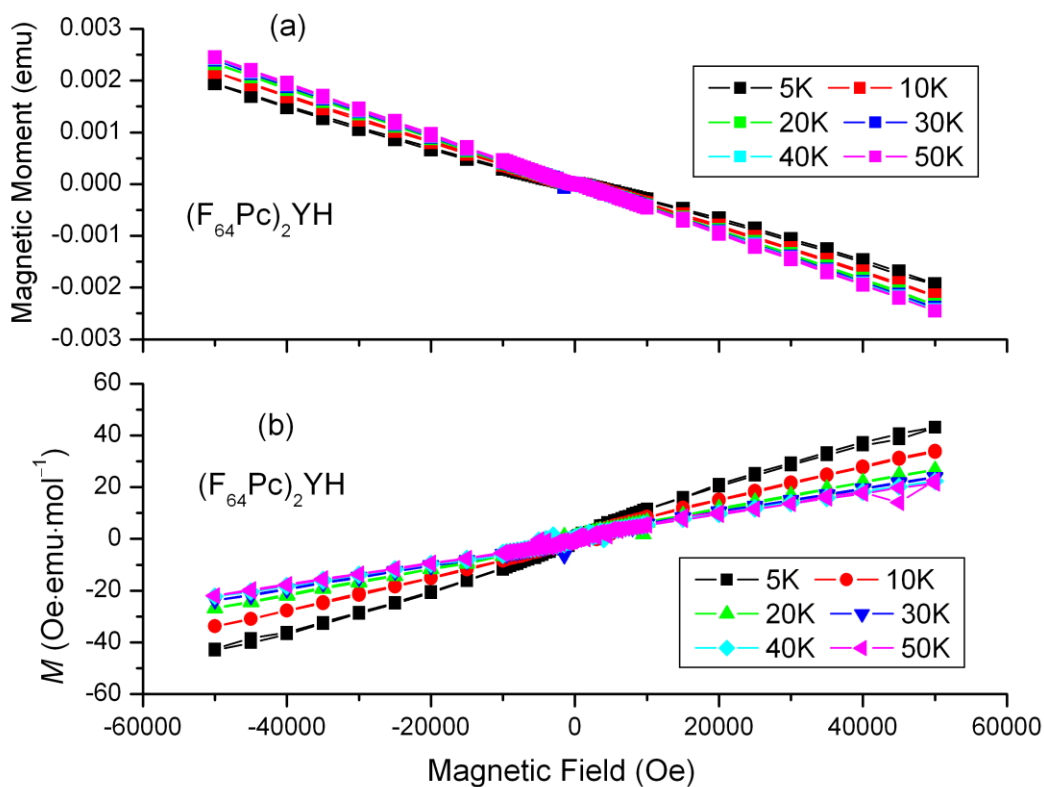


**Figure 3.12** Temperature dependent hysteresis of $(F_{64}Pc)_2YH$; a) Magnetic moment of raw sample. b) Molar magnetization, $M$ of sample corrected for diamagnetism.

Complex **[1]** exhibited higher values of molar magnetization at 5 K and above. Magnetic susceptibility calculations were done for the complexes on the ZFC-FC test carried out between 2 K and 300 K.  The results showed very weak magnetism of **[1]** and **[2]** compared to literature values of the $Pc_2Y$ complex.  These results are shown in Figure 3.13 as plots of $\chi_M$ vs. $T$ and $\chi_M T$ vs. $T$.
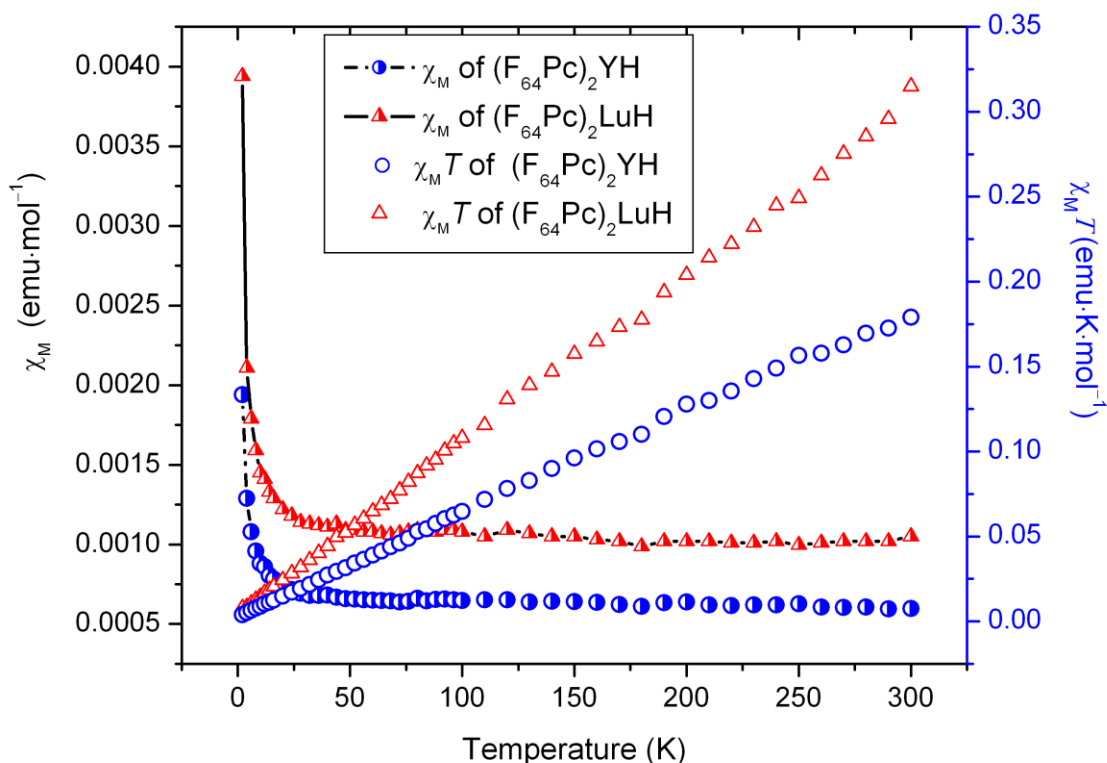
**Figure 3.13** Molar magnetic susceptibility $\chi_M$ and $\chi_M T$ versus temperature, $T$ plots of $(F_{64}Pc)_2LuH$ and $(F_{64}Pc)_2YH$ for the ZFC-FC tests.

An attempt to fit the $\chi_M$ vs. $T$ of **[1]** and **[2]** to the Curie-Weiss law using a non-linear, Levenberg-Marquardt fit was not successful. The plots of the $\chi_M^{-1}$ vs. $T$ did not produce the straight line expected for a Curie-Weiss law behavior. Additional calculations for the effective magnetic moment $\mu_{eff}$ and $\chi_M T$ were done for the complexes, and plotted against $T$, but neither of parameters obeyed the Curie-Weiss law.

The failure of the magnetism data of **[1]** and **[2]** to fit the Curie-Weiss law prompted the search for a fit to other models. Attempts were made to fit the magnetic susceptibility data to four other models. Initially, the Bleaney-Bower[146] model for dimers was applied. Three other models namely Fisher's[147], Bonner-Fisher[148], and

Rueff[149] which are solutions to Heisenberg's 1D infinite chain of S=½ spins were later applied. The data could not be satisfactorily fit to any of these models. The suggestion in the ESR test that the presence of signal was due to paramagnetic impurities was investigated. A model was then developed on the basis that the impurities were non-ferrous and were oxidation states of the $[(F_{64}Pc)_2M]$ produced during the synthesis and/or purification processes. The amount of impurities was expected to be small, probably no more than about 5%. This meant that the impurities would be diluted in the sample. However, since the nature of the dispersion was unknown, one could not rule out the existence of the impurities in aggregations (such as large crystallites). These impurities may therefore obey the Curie-Weiss law. While there may be more than one impurity, in this first instance, only one was considered.

The molar magnetic susceptibility $\chi_M$ is independent of mass of the sample; therefore values obtained from it are a measure of the magnetization of the magnetic species. In the case of the $[(F_{64}Pc)_2M]^{n\pm}$ (M=Lu and Y) and n = 0,1,2 series, their magnitude should depend on concentration of species with $\pi$-radical electrons. Since the $\chi_M$ vs. $T$ plot could not fit the Curie-Weiss model, it was fitted to model which included Curie-Weiss plus a term which is independent of temperature. The equation for the model was:

$$\chi_M = \frac{C}{T - \theta} + \chi_0 \tag{3.39}$$

where $\chi_0$ is a term which is independent of temperature and represents the difference between measured and the Curie-Weiss contribution to $\chi_M$. The data fitted this model appropriately and the results are shown in Table 3.7

**Table 3.7** Results of the Non Linear Fit on the $\chi_M$ Data Using Equation 3.39

| Complex | Curie Const., C | Weiss Const., $\theta$ (K) | $\chi_0$ | R-Value |
|---------|-----------------|----------------------------|----------|---------|
| $(F_{64}Pc)_2YH$ | 0.0031 | −0.28 | 0.000613 | 0.99677 |
| $(F_{64}Pc)_2LuH$ | 0.0039 | 0.65 | 0.001016 | 0.99851 |

The $\chi_M$ vs. $T$ data shows Curie constants that are more than two orders smaller than 0.37 cm$^3$•K/mol, the value calculated for spin only system with an S = ½. This translates to a 0.8% of the paramagnetic impurity in **[2]** and 1.1% of paramagnetic impurity in **[1]** based on the reduced $\chi_M$. An approximate 100% increase in the $\chi_M$ would result in an effective magnetic moment of 1.73 BM. The relative values of $\chi_M$ vs. $T$ for experimental **[1]** and **[2]** and simulated Pc$_2$Y, and 2% of a $[(F_{64}Pc)_2M]^0$ are shown in Figure 3.14.
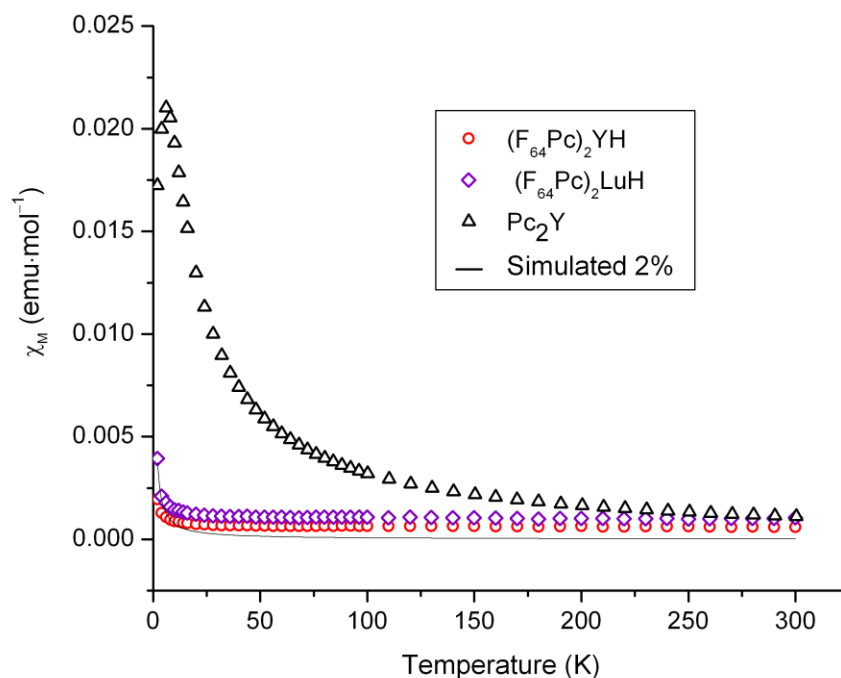


**Figure 3.14** Plots of experimental $\chi_M$ vs. $T$ of $(F_{64}Pc)_2YH$ and $(F_{64}Pc)_2LuH$ and simulated Pc$_2$Y and 2% $[(F_{64}Pc)_2M(III)]^0$ samples.

A re-arrangement of the equation 3.37 gives the equation:

$$\chi'_M = \chi_M - \chi_0 = \frac{C}{T - \theta} \tag{3.38}$$

where $\chi'_M$ is the susceptibility of the paramagnetic impurity without the temperature independent term. A plot of $\chi'_M$ vs. $T$ has a near perfect non-linear fit of the Curie-Weiss law. It is known that the product $\chi'_M T$ vs. $T$ can reveal whether a sample has simple paramagnetic, ferromagnetic or anti-ferromagnetic behavior. Figure 3.15 shows the nature of the plots in each case.
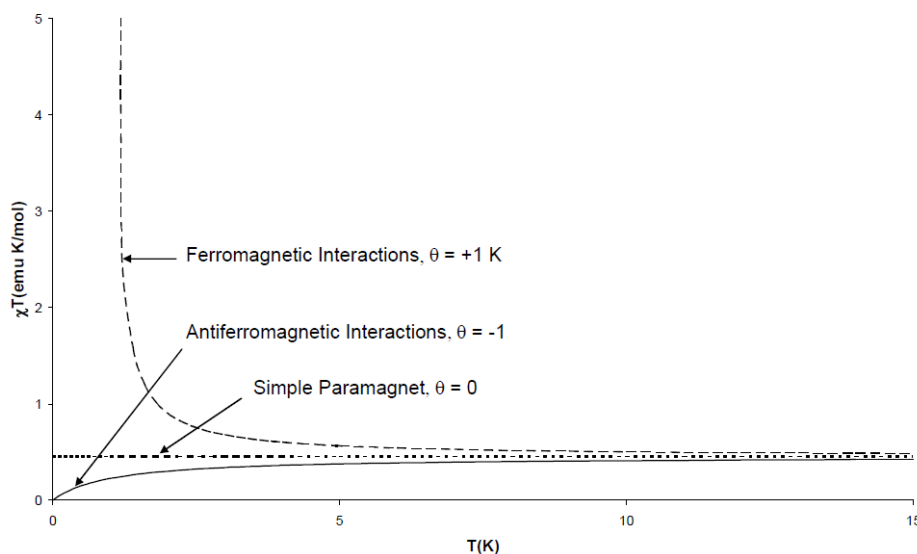


**Figure 3.15** Shapes of the $\chi_M T$ vs. $T$ curves for various kinds of magnetic interactions.[150]

Results from Table 3.7 showed the Weiss constant to be negative for **[2]** but positive for **[1]**. This would suggest that the presence of anti-ferromagnetic interactions in the impurities in **[2]** and ferromagnetic interaction for the **[1]** impurities. This finding was further assessed by plotting two sets of curves. They are the $\chi_M'T$ vs. $T$ and the $\chi_M'^{-1}$ vs. $T$ curves. The plots are shown in Figure 3.16.
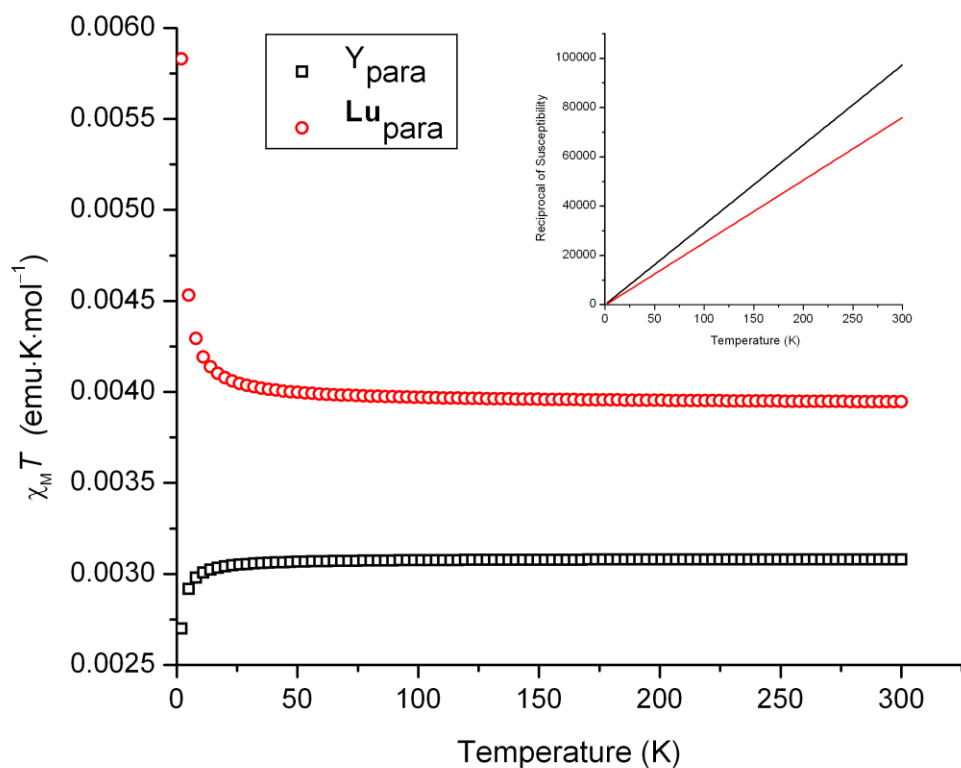
**Figure 3.16** Plots of $\chi_M{'}T$ vs. $T$ and $\chi_M{'}^{-1}$ vs. $T$ showing the weak ferromagnetic interaction for the paramagnetic impurity, $^{Lu}$**para** in $(F_{64}Pc)_2LuH$ and the weak antiferromagnetic interaction of the paramagnetic impurity, $^{Y}$**para** for $(F_{64}Pc)_2YH$ at low temperature.

The plot of $\chi_M{'}T$ vs. $T$ shows an anti-ferromagnetic interaction for the $^{Y}$**para** and ferromagnetic interaction for the $^{Lu}$**para.** In the plot of $\chi_M{'}^{-1}$ vs. $T$, linear regression of the data resulted in a Weiss constants $\theta = -0.27$ K for $^{Y}$**para** and $\theta = 0.78$ K for $^{Lu}$**para** respectively. The existence of neutral sandwich phthalocyanine Y and Lu complexes with similar magnetic behavior has been documented:[151] the anti-ferromagnetic neutral $Pc_2Y$[152] and the ferromagnetic $Pc_2Lu$.[153] However, while these results point to the possibility of $\pi$-radical electron(s), the oxidation states of these paramagnetic impurities have not yet been verified.

The small temperature independent term was introduced to account for possible errors in the use of the calculated diamagnetic correction value and measurement errors due to the low magnetism of the samples. In fact, Vogt et al.[154] reported that increasing the quality of the samples in their measurement of the van Vleck's temperature independent paramagnetism (TIP) led to a reduction in the value of $\chi_0$. TIP is the phenomenon where materials with closed shell ground states still exhibit a $\chi_M$ which is paramagnetic and independent of temperature.[155] This TIP or van Vleck paramagnetism is said to originate from the coupling of ground states and excited states through a magnetic field if there is spin-orbital coupling.[156] The use of Equation 3.39 therefore assists in accounting for errors in measurement process. Furthermore, non zero values of $\chi_0$ were obtained for both $(F_{64}Pc)_2YH$ and $(F_{64}Pc)_2LuH$ while it has been reported that TIP values for the heavier lanthanide compounds are negligible,[137, 154] or zero in the case of $Lu^{3+}$ compounds.[137] This makes it unlikely that $\chi_0$ observed in the cases of **[1]** and **[2]** was due to van Vleck's paramagnetism alone. Further comment on the value of $\chi_0$ should await higher precision testing of pure samples of **[1]** and **[2]**.

This small value of the paramagnetism in samples of **[1]** and **[2]** would explain why there is an ESR signal in the solid state. The nature of these impurities will be further examined in Chapter 6 where the redox properties of the $(F_{64}Pc)_2MH$ will be studied.

## 3.8 Electronic Spectra

The electronic spectra of the lanthanide bispthalocyanines have been the subject of several investigations. [53, 55-57, 82, 95, 151, 157] They have been known to exist in three distinct colored species; blue, green and red, both for those produced chemically and for those electro-generated. The potential applications of these materials have resulted in a several theoretical electronic spectra studies. In this thesis, both the UV-visible and NIR regions are of interest due to the possible presence of the $F_{64}Pc^{\bullet-}$ $\pi$ radical species. The $F_{64}Pc^{\bullet-}$ $\pi$-radical species produces several marker bands in these regions.

### 3.8.1 UV-Visible Spectra

UV-Visible spectrum was done on a Cary 50 Bio UV-visible Spectrophotometer interfaced to a Dell Dimension XPS T450 computer and collected using the Cary Win-UV software. Samples for UV-visible spectroscopy were tested in 1.0 and 0.1 cm quartz cuvettes. UV-visible spectra of the both the **[1]** and **[2]** complexes was carried out in several polar solvents, typically between 300 and 1000 nm. The solvents included acetone, chloroform, pyridine and methanol. Their solution color depends on the concentration. When the concentration is dilute (ca. 4 mg/L), the solution is purple. As the concentration increased, the color appeared blue. The spectra were essentially similar in all the solvents with small changes in position of the peak wavelength, $\lambda_{max}$ in the observed bands. No aggregation was observed as the concentrated solutions gave identically shaped curves. The aggregation studies typical of the $(F_{64}Pc)_2MH$ is shown in Figure 3.17. Verification of the lack of aggregation was probed via the Lambert-Beer law using the six observed peaks in the spectrum. Straight lines were observed for the plots of absorbance vs. concentration for concentrations up to 149 $\mu$mol/L, the maximum

concentration allowed before the onset of peak distortion by the measuring apparatus. A plot of the Lambert-Beer aggregation is probe is shown in Figure E.3   The UV-visible spectra of the complexes are shown in Appendix E.   The list of peaks and their corresponding extinction coefficients as recorded in the experimental spectra are shown in Table 3.8.
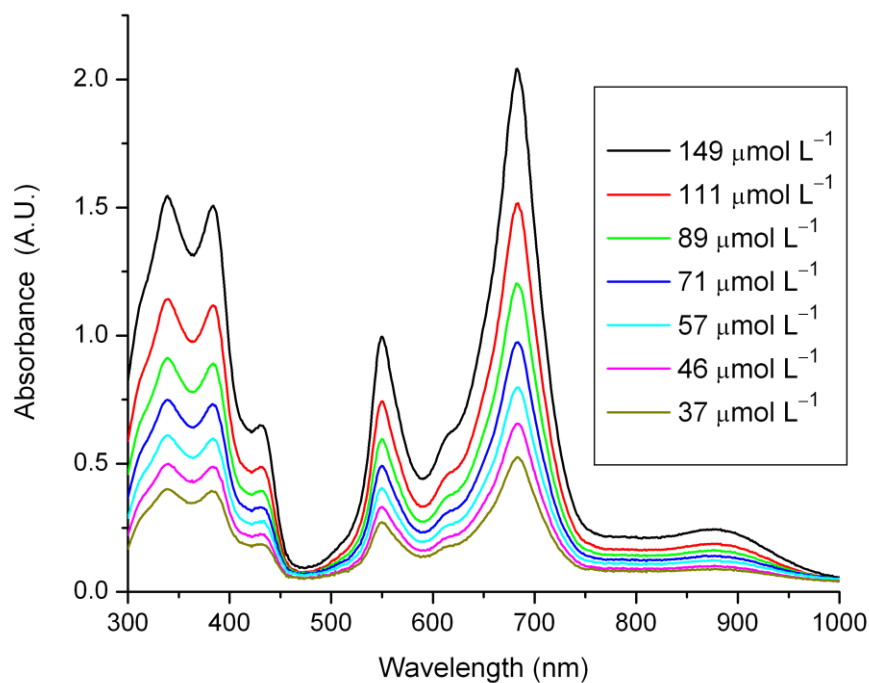


**Figure 3.17** Aggregation studies of $(F_{64}Pc)_2YH$ in methanol showing lack of aggregation. The spectra is typical of the $(F_{64}Pc)_2MH$.

The bisphthalocyanines have a $\pi$ conjugated system of about 18 electrons, the amount depending on the charge of the complex.   This system leads to intense absorptions in the UV-Visible region.   The UV-visible region is characterized by two main absorption bands.   They are the called the Q and B (Soret) bands.   Both bands are assigned to $\pi \rightarrow \pi^*$ allowed transitions arising from the $\pi$ conjugated system.   The Q band

transitions are centered in the 640 - 690 nm region, while the B band is centered in the 320 – 350 nm region.[12, 53, 95, 104]  While these two bands are generally found in all the bisphthalocyanines, there are two transitions that have been historically considered as marker bands for the neutral bisphthalocyanine species.   These bands occur at 460-500 nm and 880 – 900 nm due to intramolecular charge transfer between the two rings.[158] These bands will be referred to as the blue vibronic (BV) and red vibronic (RV), respectively.[10]

**Table 3.8** Peaks in the UV-Visible Spectra of $(F_{64}Pc)_2LuH$ and $(F_{64}Pc)_2YH$ in Methanol

| Complex | $\lambda_{max}$ (nm) and Extinction Coefficient [log$\varepsilon$] (L•mol$^{-1}$•cm) | | | | | |
|---|---|---|---|---|---|---|
| $(F_{64}Pc)_2YH$ | 877,[4.13] | 682,[5.07] | 549,[4.78] | 431,[4.58] | 383,[4.95] | 338,[4.97] |
| $(F_{64}Pc)_2LuH$ | 918,[4.00] | 687,[5.15] | 546,[4.73] | 433,[4.58] | 385,[4.94] | 340,[5.01] |

The number, intensities and position of the various bands are influenced by factors such as the size of the central metal ion, the number and nature of the substituents and the redox state of the complexes.[52]  There is general blue shifting of the Q band with a decrease in the ionic radii of the central lanthanide cation.

Complexes **[1]** and **[2]** share some of the flagship bands found in the spectra of the neutral molecules.   This was surprising because the current literature did not reveal any $[Pc_2Ln(III)]^-$ complexes with any of the two $[Pc_2Ln]^0$ marker bands located around 450 nm and 900 nm.   The similarities and differences are shown on the comparative UV-visible spectra which included the NIR region of 800-1000 nm for $Pc_2Y$ and $(F_{64}Pc)_2YH$ in Figure 3.18.   The $(F_{64}Pc)_2MH$ is a one electron reduced  complex from the neutral molecule.  This reduction should cause a split in the Q-band which should be replaced by two weaker bands, one which is blue shifted and the other red shifted relative to the

neutral complex.[56, 57, 68, 159].  The BV and RV bands were reported absent from the UV-visible spectra of reduced species and explained by the absence of the $\pi$ radical $Pc^{\bullet-}$ in the one electron reduced complex.[52]  The presence of minute quantities of impurities of the neutral species (~1%) cannot have extinction coefficient necessary to be observed with such large absorbance in the experimental UV-visible results.
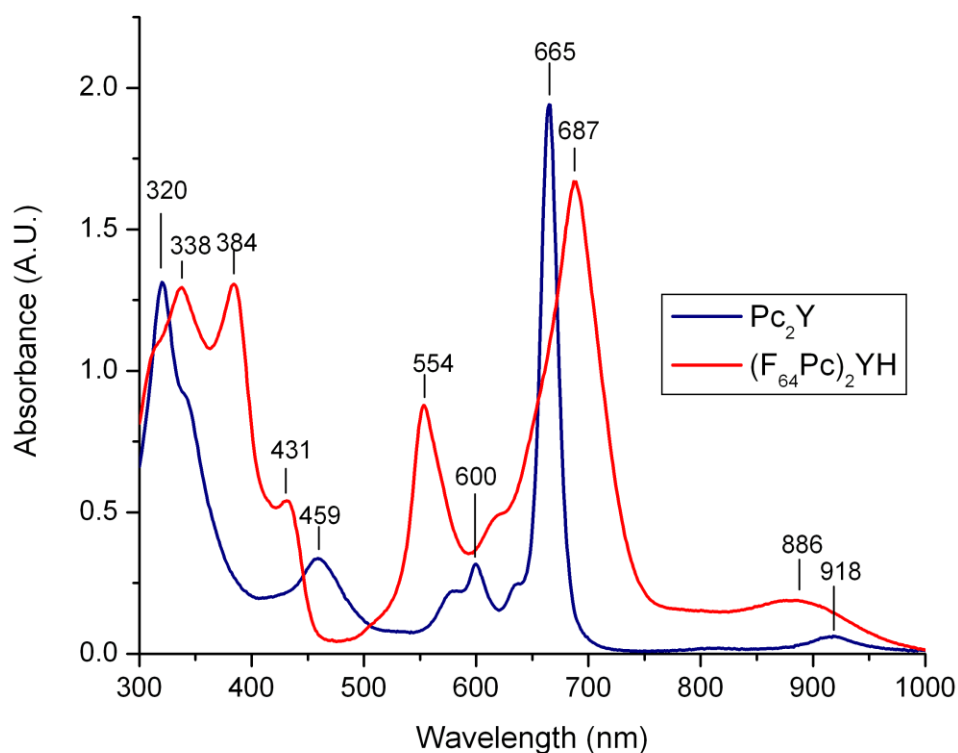


**Figure 3.18**  UV-visible spectra of $Pc_2Y$ and $(F_{64}Pc)_2YH$ in chloroform.  Both the Q and B bands are red shifted in $(F_{64}Pc)_2YH$ relative to $Pc_2Y$.

### 3.8.2 Deconvolution and TDDFT Analysis of Electronic Spectra of $(F_{64}Pc)_2LuH$ and $(F_{64}Pc)_2YH$

The experimental UV-visible spectra contain peak ($\lambda_{max}$) positions which are a linear combination of more than one band (overlapping) and will also contain errors due to machine noise. In order to further analyze the spectra, deconvolution was carried out using the open source deconvolution software Fityk®[160]. The Levenberg-Marquardt least squares method was utilized and data was fit to the Gaussian model in the cases of [1] and [2] and to a Voigt model in the case of $Pc_2Y$. The $Pc_2Y$ spectrum was best fitted to the Voigt model and this supported a suggestion that Voigt curves may have more success modeling deeper, narrower absorption bands.[161]

The deconvolution process itself is not perfect. Analysis of the experimental spectra depends on several initial guesses as to which peaks (or bands) are present and also on the mathematical model is used. The experimental electronic spectra have a wavelength precision of 2 nm. The deconvolution process will also result in shifts in some previously overlapped peak positions. Furthermore, it was found that both the absorbance intensities of the experimental spectra and sequencing of the tasks in the deconvolution process seem to affect the final result.

The results of deconvolutions presented represent many trials, and as such, there were some peaks which appear in all deconvolution trials (common bands) for all the complexes and they are highlighted on the deconvoluted spectra. There is a high probability that these common bands make up the final shape of the experimental spectra. The other bands show too many variations or they appear at the edge of the spectrum so their existence and/or $\lambda_{max}$ has a lower probability. The deconvoluted spectrum of [2] is shown in Figure 3.19, while that of [1] and the details of both are shown in Appendix E.
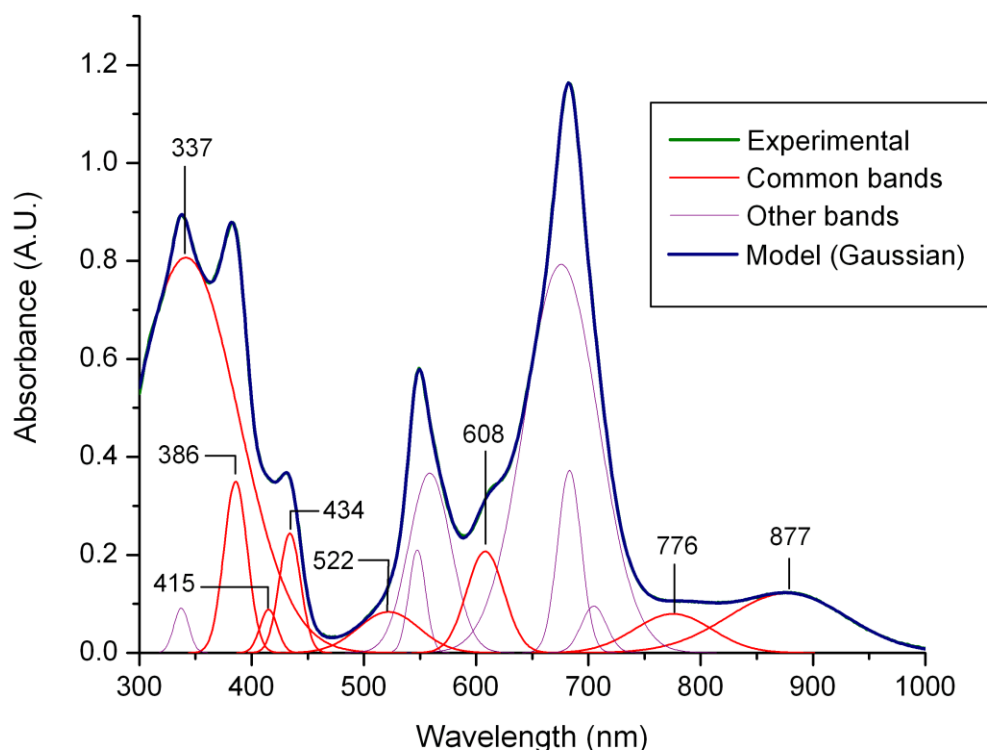
**Figure 3.19** Deconvoluted UV-Visible (and NIR 800-1000 nm) spectrum of $(F_{64}Pc)_2YH$ in methanol.

Support for the spectra deconvolution was sought from the TDDFT calculations carried out by Liao et al.[109] In the electronic spectra1 analysis, excitation energies in eV and oscillator strengths, *f*, were calculated from electronic transitions between atomic orbitals in several probable electronic energy states. The corresponding wavelengths of the excitation energies were calculated and compared with the bands obtained from the deconvoluted experimental electronic spectra. An attempt was also made to assign the spectral bands as named in VanCott et al.[162] and is customarily used. The tabulated comparison is presented on Table 3.9

**Table 3.9** Comparison of the Calculated Excitation Energies ($E^{exc}$) and Oscillator Strengths (*f*) of $(F_{32}Pc)_2MH$ (M=Y, Lu) with the Deconvoluted Experimental Electronic Spectra of $(F_{64}Pc)_2YH$ and $(F_{64}Pc)_2LuH$

| State | Contribution (%) | $E^{exc}$, (eV) | | *f* | $E^{exc}$, (nm) | | Band* | Expt. Spectra | |
|-------|-----------------|-----------------|----|-----|-----------------|----|-------|-----------|-----|
| | | $Y^{F32}$ | $Lu^{F32}$ | | $Y^{F32}$ | $Lu^{F32}$ | | [2] (nm) | [1] (nm) |
| $1^1E$ | 92 ($48a_2 \rightarrow 108e$) | 0.97 | 0.95 | 0.0004 | 1281 | 1308 | IV | - | - |
| $2^1E$ | 50 ($47a_2 \rightarrow 108e$); 38 ($48a_2 \rightarrow 109e$) | 1.35 | 1.33 | 0.007 | 921 | 935 | RV | 877 | 915 |
| $3^1E$ | 39 ($47a_2 \rightarrow 108e$); 38 ($48a_2 \rightarrow 109e$); 12 ($47a_2 \rightarrow 109e$) | 1.74 | 1.73 | 0.654 | 714 | 718 | $Q_1$ | 776 | 801 |
| $4^1E$ | 75 ($47a_2 \rightarrow 109e$); 14 ($48a_2 \rightarrow 109e$) | 1.82 | 1.84 | 0.1158 | 683 | 676 | $Q_2$ | 684 | 688 |
| $5^1E$ | 97 ($53b_1 \rightarrow 108e$) | 1.93 | 1.95 | 0.0164 | 644 | 637 | $Q_3$ | 676 | 664 |
| $6^1E$ | 93 ($52b_1 \rightarrow 108e$) | 2.06 | 2.06 | 0.0966 | 603 | 603 | $Q_4$ | 608 | - |
| $7^1E$ | 72 ($53b_2 \rightarrow 108e$); 26 ($52b_2 \rightarrow 108e$) | 2.22 | 2.13 | 0.0746 | 560 | 584 | $Q_5$ | 559 | - |
| $8^1E$ | 73 ($52b_2 \rightarrow 108e$); 22 ($53b_2 \rightarrow 108e$) | 2.27 | 2.28 | 0.1208 | 548 | 545 | $Q_6$ | 548 | 548 |
| $10^1E$ | 97 ($53b_1 \rightarrow 109e$) | 2.38 | 2.4 | 0.0158 | 522 | 518 | $Q_7$ | 522 | - |
| $13^1E$ | 69 ($52b_1 \rightarrow 109e$); 22 ($46a_2 \rightarrow 108e$) | 2.51 | 2.51 | 0.1438 | 495 | 495 | $Q_8$ | - | 495 |
| $16^1E$ | 88 ($53b_2 \rightarrow 109e$) | 2.59 | 2.59 | 0.043 | 480 | 480 | BV | - | - |
| $17^1E$ | 84 ($61a_1 \rightarrow 108e$) | 2.63 | 2.61 | 0.0208 | 473 | 476 | BV | - | - |
| $20^1E$ | 86 ($51b_1 \rightarrow 108e$) | 2.74 | 2.73 | 0.022 | 454 | 455 | BV | - | - |
| $23^1E$ | 48 ($51b_2 \rightarrow 109e$); 34 ($45a_2 \rightarrow 108e$) | 2.93 | 2.94 | 0.0378 | 424 | 423 | $B_1$ | 434 | 438 |
| $26^1E$ | 34 ($46a_2 \rightarrow 109e$); 34 ($61a_2 \rightarrow 109e$) | 3.03 | 3.04 | 0.0324 | 410 | 409 | $B_2$ | 415 | 421 |
| $31^1E$ | 76 ($102e \rightarrow 63a_1$) | 3.20 | 3.21 | 0.0604 | 388 | 387 | $B_3$ | 386 | 388 |
| $41^1E$ | 56 ($59a_1 \rightarrow 109e$) | 3.53 | 3.51 | 0.408 | 352 | 354 | - | - | - |
| $45^1E$ | 41 ($58a_1 \rightarrow 109e$); 24 ($106e \rightarrow 54b_2$) | 3.66 | 3.67 | 0.2074 | 340 | 339 | N | 337 | 346 |

$Y^{F32}$, $(F_{32}Pc)_2YH$;  $Lu^{F32}$,$(F_{32}Pc)_2MH$

* Spectral band assigned.

Table 3.9 shows some excitation transitions with strong *f* values which are not observed in the deconvoluted spectra of **[1]** and **[2]** and alternatively some with low *f* values which that are undoubtedly observed experimentally and contained in the deconvoluted spectra. The most prominent of these being the transitions in the RV band, which is normally absent from the one electron reduced species, but showed up prominently in both the experimental and its deconvoluted spectra. In fact, the intensity of its absorbance is greater than that of $Pc_2Y$. In addition, it is some 20 nm blue shifted

compared to the RV band in $Pc_2Y$ in contrast to a general red shifting of the other bands in the $(F_{64}Pc)_2MH$ electronic spectra.

Both methods indicated the absence of transitions in the BV band and general red shifting of the B, Q and N bands relative to $Pc_2Y$. The B and N bands were shifted approximately 60 nm and the main Q band approximately 20 nm. Of the eight common bands shown on Figure 3.20, the band at around 610 nm is missing from [1], but it appears to be obscured in main Q band. It appears in the TDDFT electronic spectral model.

A small broad band which occurs at around 780 nm in the deconvoluted spectra appears to be the small satellite peak expected from the split of the main of the main Q band on the one electron reduction of the neutral species. Kasuga et al.[68], called this band the X-band and reported that it shifted to longer wavelengths on reduction of the size of the central metal ion. This shift observed and reported in Table 3.11 where it shifted from 776 nm in [2] to 801 nm in [1]. They also reported that this band was absent from the neutral species and it was also not seen in the deconvoluted spectrum of the neutral $Pc_2Y$, shown in Figure 3.20. The deconvolution also revealed the structure of the broadened main Q band in [1] and [2].

The narrow, sharp main Q band of $Pc_2Y$ contrasts with the broad one on the $(F_{64}Pc)_2MH$. Non equivalent macrocycles due to the presence of the proton appears to be responsible for the difference in the shape.
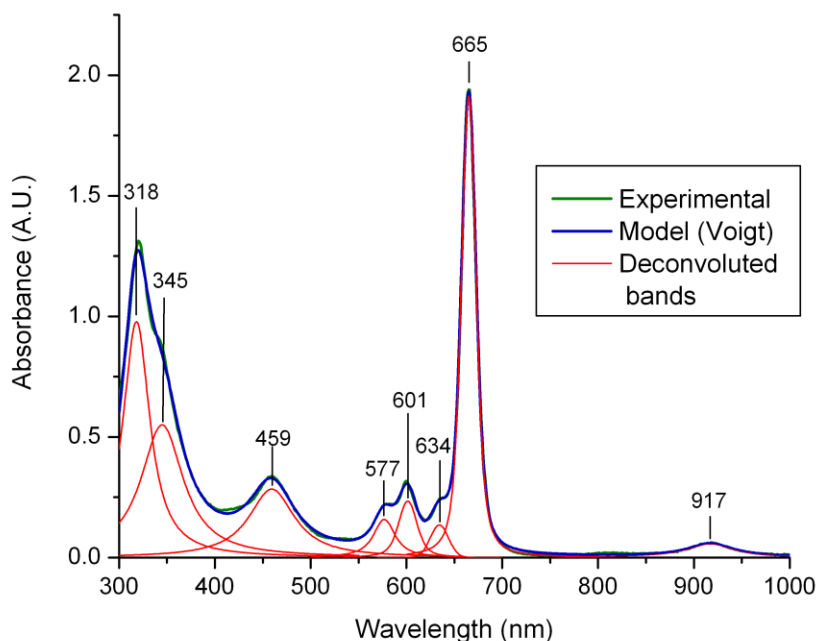
**Figure 3.20** Deconvoluted UV-Visible spectrum of $Pc_2Y$ in chloroform.

The argument for the non equivalence of the macrocycles in the $(F_{64}Pc)_2MH$ is weakly supported by the experiment structure calculations and strongly supported by the DFT structure optimization calculations. Previous studies to locate the proton was done on the protonated bisporphyrin complexes with the conclusion that the proton was thought to be ligated to the four pyrolle nitrogens on one of the macrocycles,[117] and this is supported by the present calculations by Liao et al.[109] It could well be the case for the $(F_{64}Pc)_2MH$ otherwise the two macrocycles on these homoleptic complexes should be equivalent leading to a sharp main Q band, similar to the case of the $F_{64}PcZn$[110] or the $Pc_2Y$.

The red shifting of the main Q and B bands of the $(F_{64}Pc)_2MH$ complexes relative to their un-substituted $Pc_2Y$ counterpart is being attributed to the F and $i\text{-}C_3F_7$

substituents.  Electron withdrawing groups are known to cause this effect.[95, 163, 164]  This contrasts with RV band that is blue shifted relative to $Pc_2Y$.  Again, this appears anomalous because the shifting of these bands usually follows the trends in the Q and B bands.  Of note, however, band $Q_6$ of **[1]** and **[2]** in Table 3.11 which is a vibronic component of the main Q band ($Q_2$) appears to blue shift as the main Q band red shifts relative to $Pc_2Y$.

The presence of the UV-visible bands related to both the neutral and anionic complexes in the $(F_{64}Pc)_2MH$ are probably due to the low symmetry  of these bispthalocyanines.  The complexes are neither of true $D_{4d}$, or $C_{4v}$ symmetry point groups. Rather the point symmetry is $C_1$.  This symmetry group along with the distortions of the $F_{64}Pc^{2-}$ ring from planarity has apparently resulted in several transitions that are not normally allowed in higher symmetries being allowed. DFT/TDDFT studies have indeed indicated that this may be the case.[10, 109] Kahlal et al.[10]  report that although there is general agreement between the experiment and calculations, the case of the oxidized and reduced species is not as good as the neutral molecule.  They attribute this to solvent and counter-ion effects, and indicate that the experimental peak wavelength ($\lambda_{max}$) values of complexes such as the $[Pc_2Lu]^+$ and $[Pc_2Lu]^-$  could be easily indexed to calculated transitions. They are associated with the same excitations as the neutral form.  The calculated values of their $[LuPc_2]^{+/0/-1}$ do show peaks similar to the BV and RV values obtained from our $(F_{64}Pc)_2MH$.  Several of the excitations are forbidden but are vibronically allowed.

### 3.8.3 NIR Spectra

The NIR of spectra of the $(F_{64}Pc)_2MH$ complexes were conducted on a Cary 500 UV-vis/NIR spectrophotometer machine in the wavelength range 800-2400 nm in chloroform and methanol.  The machine is located at Rutgers University, Newark, NJ.  NIR spectra of **[1]** and **[2]** are shown in Figure 3.21 along with that of $Pc_2Y$.   The one electron reduced species are not expected to have any bands in NIR region because of the perceived absence of the π-radical phthalocyanine ligand.    Whereas the neutral $Pc_2Y$ shows the band at 917 nm (RV) and bands at around 1260, 1410 and 1540 nm,  the so called intervalence (IV) bands, the  $(F_{64}Pc)_2MH$ only exhibited  one peak  which has already been  assigned to the RV band.  The absence of the IV band is predicted for the reduced $[Pc_2Ln]^-$ species.[9]  Its presence in the neutral species in the 1100-1600 nm region is attributed to the HOMO-SOMO transition and sometimes with charge transfer between macrocycles.  In $C_{4v}$ symmetry, the proposed transition is $1a_2 \rightarrow 2a_2$, ( π→π*) lies around 1300 nm and agrees with experiment.  This fully supports delocalized nature of unpaired electron.

To assist in the interpretation of these spectra, the NIR spectrum of the $PC_2Y$ was de-convoluted to help identify specific transitions.  The de-convoluted spectrum shown in Figure 3.22 (b) exhibited all the peaks previously observed, albeit with slight deviations.  Tests were also conducted up to wavelengths of 2400 nm in ethanol and methanol but no peaks were observed for **[1]** and **[2]**.

The TDDFT calculations done by Liao et al., Table 3.12, indicate very low oscillator strength for **[1]** and **[2]** which also supports its absence in the experimental spectra.
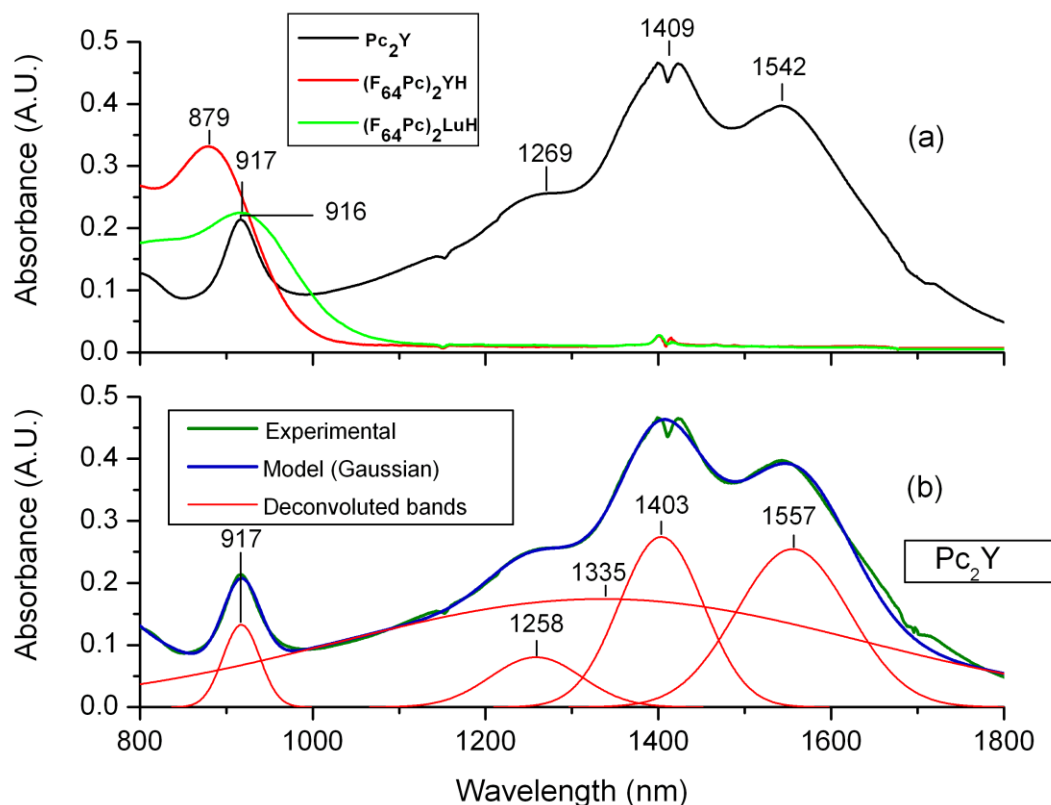
**Figure 3.21** (a) NIR spectra of $(F_{64}Pc)_2YH$, $(F_{64}Pc)_2LuH$ and $Pc_2Y$ in chloroform. The split in the spectra at ca. 1400 nm is due to instrument error in background subtraction. (b) Deconvoluted spectrum of $Pc_2Y$.

## 3.9 Thermal Analysis

Thermal analysis encompasses a group of techniques that are used to analyze the impact of temperature changes on a material. They are generally based upon the detection of changes in the enthalpy or the specific heat of a sample with temperature. The supply of heat to a sample in a specific physical state normally results in a predictable change in temperature and enthalpy governed by its specific heat capacity. Although a constant value is often reported for the specific heat capacity of a substance, it often changes slowly with temperature. Abrupt changes are usually the result of phenomena such as

changes in state (melting, boiling etc.), crystallization, glass transition, chemical reactions or decomposition.   Techniques included in thermal analysis are:

- ➢ Differential Scanning Calorimetry, DSC
- ➢ Dynamic Adiabatic Calorimetry,
- ➢ Differential Thermal Analysis, DTA
- ➢ Thermogravimetric Analysis, TG
- ➢ Thermomechanical Analysis, TMA
- ➢ Dynamic Mechanical Thermal Analysis, DMTA
- ➢ Dielectric Thermal Analysis.

### 3.9.1  Thermogravimetric Analysis (TGA)

TGA is a measure of the quantity and the rate of change of mass of a substance as a function of temperature or time in a controlled environment.  The test is usually conducted as one of several procedures to determine the thermal stability of the substance, typically up to a temperature of 1000ºC.  TGA is a versatile characterization tool and can be used to provide information about materials that exhibit a mass loss during testing.  The information includes thermal stability, oxidative stability, effects of corrosive or reactive environments, moisture and volatiles content and composition of multi-component systems.

Thermo-gravimetric analysis (TGA) was done at NJIT on a Perkin Elmer Pyris 1 TGA machine equipped with The Thermal Analysis Gas Station (TAGS) which allows control of the gas flow and switching through Pyris software.  Both a nitrogen and air atmospheres were available during the test.  Tests were conducted on [1] and [2] both in

atmospheres of air and nitrogen gas.  The rate of heating was 5ºC/minute from 30ºC up to

500ºC.  Figure 3.22 shows thermal analysis.
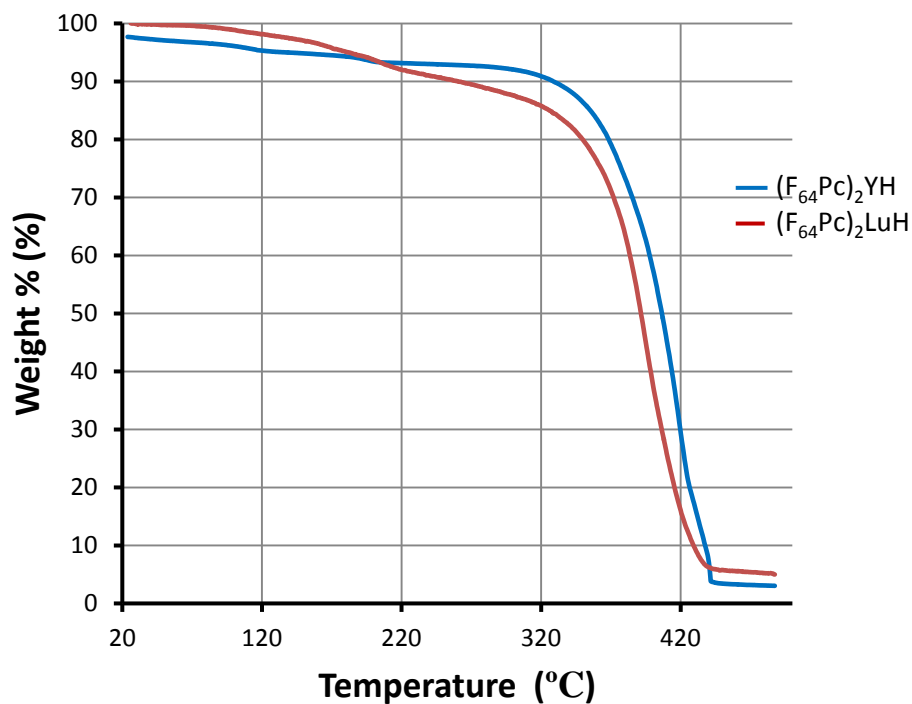


**Figure 3.22** TGA of $(F_{64}Pc)_2YH$ and $(F_{64}Pc)_2LuH$ in air.

The samples began to show large weight loss at about 330ºC.   Separate heating

under a vacuum up to 285ºC confirmed that the samples actually began to sublime slowly

at this temperature.  The absence of burnt residue at the end of the test in both air and

nitrogen gas atmospheres indicate resistance of the samples to thermal breakdown.

### 3.9.2 Differential Scanning Calorimetry

DSC measures the difference in the quantity of heat required to raise the temperature of a sample and a reference as a function of temperature. The sample and reference are placed in identical environments such that they are maintained at the same programmed temperature throughout the experiment. The temperatures are measured by temperature measuring transducers, such as a platinum resistant thermocouple. A feedback control system is programmed so that the temperatures of both thermometers are compared and the electrical energy supplied to each heater adjusted so that they maintain the same programmed temperature. Differences in heat flow between the sample and reference are measured. Under these conditions, the rate of change of temperature is dependent on the rate of heat absorption and the sample's specific heat. A smooth change in the rate of heat absorbed by the sample is obtained unless there is some thermal event that occurs during the heating (or cooling) cycle which causes a significant change in the specific heat of the sample and an abrupt change in heat absorption rate. Events such as changes in state, (melting, sublimation), crystallization, decomposition and glass transition are examples of such events. The results are usually plot on a DSC curve which is plot of heat flow versus temperature. A typical DSC curve is shown in Figure 3.24. DSC has applications area such as purity analysis, characterization of substances, quality control in the polymers, determination of oxidative stability and drug analysis.
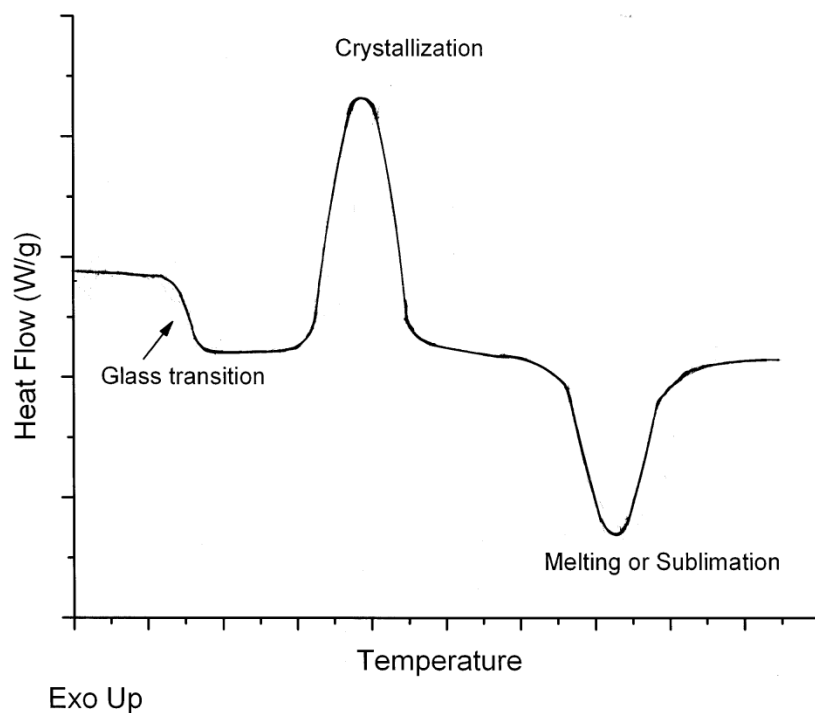
**Figure 3.23** Typical DSC curve showing features. The graph shows exothermic thermal transitions as a positive peak, referred to in DSC graphs as "Exo Up".

DSC tests were carried out on a TA Instruments Q100 V9.8 Build 296 DSC machine located at the University of Medicine and Dentistry of New Jersey, Newark, NJ. Samples of **[1]** and **[2]** were heated in non-hermetically sealed aluminum cans in an atmosphere of nitrogen up to a temperature of 500ºC. The heating ramped at 10.00 ºC/min. The thermograms of the results of the DSC tests in Figures 3.25 and 3.26 show two main thermal events in the region 300-340ºC and around 490ºC. In the 140-300ºC region, **[1]** shows two first order thermal transitions while **[2]** to shows one. Since the experiments were done with the DSC machine set at "Exothermic up", the valleys in the

curves are endothermic transitions suggesting a possible onset of changes in state. The heating of $(F_{64}Pc)_2MH$ up to 300ºC in order to determine their melting points in previous experiments did not result in their melting. Attempts to sublime them under vacuum up to 285ºC did not result in melting either. The complexes are not expected to show two sublimation points so the 1st order endothermic thermal transition occurring at 241ºC in **[2]** is likely due to changes in the crystal structure of the complex. This could be in the form of a change of the space group or even a change in the twist angle of the macrocycles to a higher energy arrangement. It is unlikely that they are due to the presence of impurities from substances such as **[2-2]** or **[2-3]** due to their predicted low concentrations. This may also be the case for **[1]** that has two similar 1st order thermal transitions at 170ºC and 221ºC.
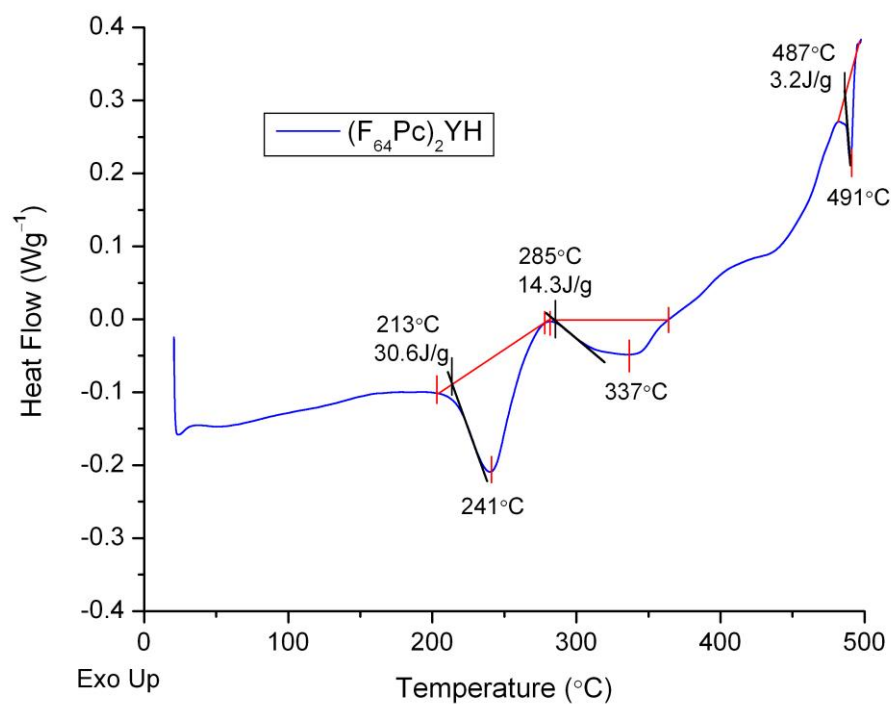


**Figure 3.24** DSC thermogram of $(F_{64}Pc)_2YH$.

Both **[1]** and **[2]** show 1st order endothermic thermal transitions at 300ºC and 337ºC which show some consistency with the TGA tests. Despite the different rates of heating between the two tests, TGA exhibits large mass loss at around 330ºC and DSC data shows an endothermic 1st order transition in the region 300ºC-370ºC. It is therefore likely that these DSC thermal transitions represent sublimation.

The thermal event at ~490ºC is sharp and is another 1st order endothermic thermal transition. It is not a sublimation of **[1]** and **[2]** because it has been established that sublimation occurred before. The UV-visible spectra in methanol of the materials remaining after the DSC test show changes (Figure 3.27) which suggest a change in the composition of the materials.
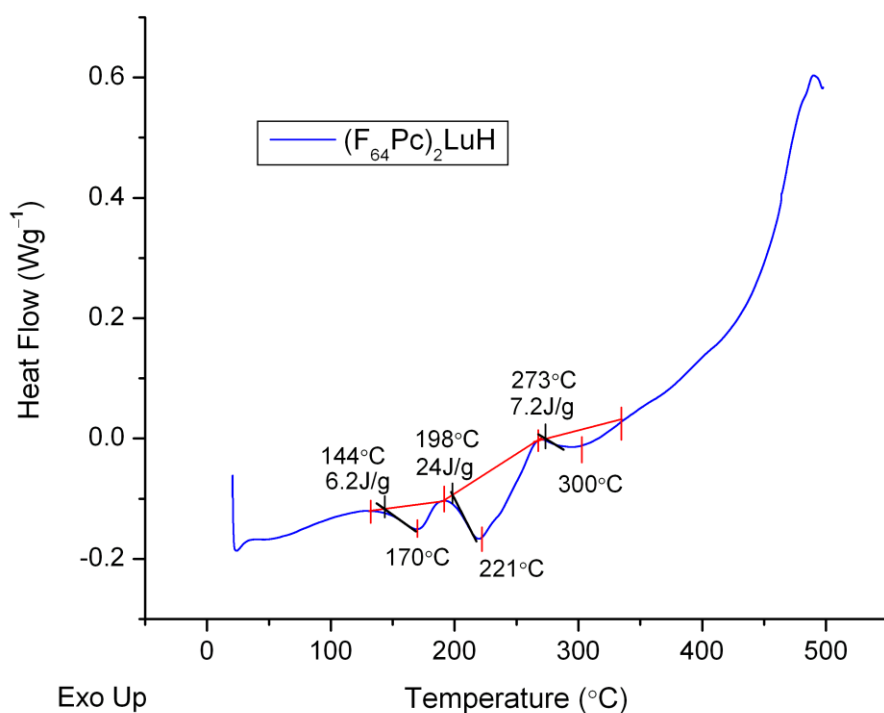


**Figure 3.25** DSC thermogram of $(F_{64}Pc)_2LuH$.

Examination of the DSC graph of **[1]** shows that the highest temperature event occurs at a slightly higher temperature than **[2]** and while the remains of **[2]** formed a green solution, that of **[1]** was predominantly blue.   The origin of the other features on the DSC graphs has not been elucidated.

Interestingly, complex **[2]** that apparently completed its event centered at 491°C gave a spectrum with a split Q-band similar to that of the triple decker $Pc_3M_2$ complexes.[70, 94, 165]   The blue remains of **[1]** have produced UV-visible spectrum which appears to be a mixture of the sample compound and its thermally transformed state.  An analysis of the spectra shown on Figure 3.26 will reveal the absence of the BV and RV bands in the new product(s).
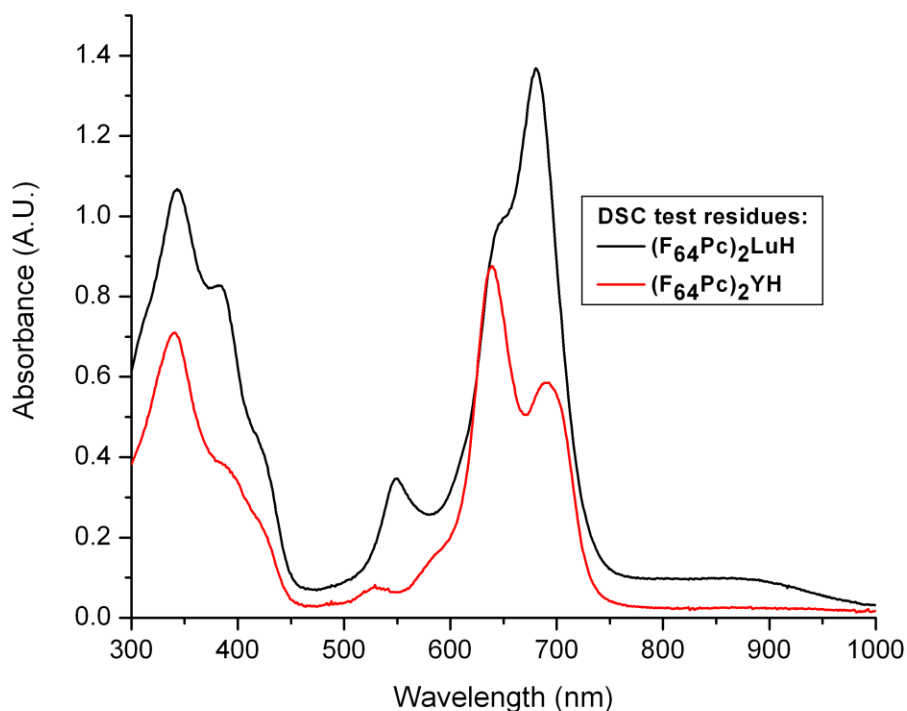


**Figure 3.26** UV-visible spectra of remains of the $(F_{64}Pc)_2MH$ samples in the DSC test dissolved in methanol.

Further, the band occurring at about 550 nm has been blue shifted to 535 nm and the B band is no longer split. It is unlikely that the products formed are the monophthalocyanines, $F_{64}PcM$ or the free base $F_{64}PcH_2$ exclusively, because their UV-visible spectra are different.

The conditions in the non-hermetically sealed aluminum can in the DSC test probably mirrored the solid state conditions under which the triple deckers can be formed from the double decker. The first triple deckers were synthesized under solid state conditions at high temperature ~ 300°C by Kirin et al.[94] If the $(F_{64}Pc)_3M_2$ species are present, then a way may have finally been found to synthesize the these compounds. Their synthesis have been elusive for quite some time as it was attempted based on the metalation of the double decker complex using the $Ln(OAc)_3 \cdot nH_2O$ in the presence of the free base and 1,1,1 trichlorobenzene.

### 3.10 Summary

The characterization of the closed shell $(F_{64}Pc)_2MH$ complexes, M=Y, Lu revealed that the first representatives of this new class of bis[octakis(perfluoro $i$-$C_3F_7$) octakis(perfluoro)phthalocyninato]M(III) complexes, can be formulated as $[(F_{64}Pc^{2-})]_2[M^{3+}][H^+]$. Although single crystal X-ray diffraction did not reveal the presence of the proton due to the complexes' large mass, it was partially confirmed via mass spectroscopy. DFT analysis done elsewhere via geometric structure optimization of the said X-ray structures has revealed asymmetry in the structure supporting the differences in experimental atomic bond lengths which could not be confirmed because most of them

were within the limits of experimental error. The weak magnetism observed in DC magnetometry of the microcrystalline solids was shown to be due to an approximate 1% impurity of paramagnetic species present in the sample. The complexes are otherwise diamagnetic in keeping with fact that the central M[III] ions in **[1]** and **[2]** have closed shells and the ligands having no unpaired electrons. This small paramagnetic impurity was confirmed by the observance of a symmetrical ESR signal of the microcrystalline solid with g = 2.004. The absence of the ESR signal in solution also supports the presence of the impurity which probably disappears on protonation or counter-effects in solution. Fluorine-19 NMR in acetone $D_6$ exhibited an approximate 6:1:1 ratio of primary aliphatic, to aromatic to tertiary aliphatic flourines. They had the same approximate chemical shifts of the diamagnetic $F_{64}PcZn$ occurring at  −71 (6F, $CF_3$), −104 (1F, Ar-F) and −165 (1F, CF). This further supported the diamagnetism of the complexes. The axial proton proposed to be attached to a pyrrole N was not observed in $^1H$ NMR spectroscopy. IR spectroscopy revealed the presence of the $CF_3$ groups and vibrations typical of the phthalocyanine ring. The marker transmission of the π-radical electron of the neutral species, expected as a strong, sharp peak in the region 1314-1322 $cm^{-1}$ was absent. There were no peaks in the IV band (1000-1600 nm) of the NIR spectra in keeping with their observed absence in the one electron reduced lanthanide bisphthalocyanine complexes. Thermal analysis confirmed the robustness of the complexes through resistance to thermal decomposition up to at least 450ºC. UV-visible spectroscopy exhibited a split B band at *ca.* 340 and 387 nm  and a relatively broad Q band at *ca.* 684 nm, both of which are red shifted relative to their un-substituted analogues. In addition, vibronic components of the Q-band appear at around 780 nm,

610 nm, 550 and 500 nm. The presence of bands in the RV region of the electronic spectra (~ 880 nm) which are reported characteristic of the neutral species of the bisphthalocyanines, is anomalous because it has not been reported in the literature. However, this band in RV region was found to be blue shifted, while the B and Q bands red shifted. This is also uncharacteristic of the general trend in the shifts in the electronic spectroscopy of Pc complexes on substitution with electron withdrawing groups. Literature theoretical electron spectroscopy and TDDFT studies have shown that this band may belong to vibronically allowed transitions, therefore it may be observed as well in the one electron reduced complexes. Herein it is that reported that the first set of fluorine substituted $[(F_{64}Pc)_2M]^-$ complexes exhibiting peaks in the RV region of the electronic spectra of Y and lanthanide bisphthalocyanines.

# CHAPTER 4

## STRUCTURE AND SPECTROSCOPIC PROPERTIES
## OF $(F_{64}Pc)_2LnH$ COMPLEXES (Ln = Tb, Dy)

### 4.1 Overview

A primary objective of this dissertation is to synthesize and characterize perfluoro substituted bisphthalocyanines which have potential applications as multifunctional single molecular magnets. The best known lanthanide metals which are candidates for this application are terbium, dysprosium and holmium and erbium because of the presence of large numbers of unpaired electrons in the ground state of their free ions. The presence of spin orbit coupling inthese metals is also important as it increases the values of their effective magnetic moments.

Terbium and dysprosium bisphthalocyanines were reported as having single molecular magnetic behavior and the decision was therefore made to use these metals for a first evaluation of the effect of electron withdrawing groups on the magnetism and other properties of the complexes.

This chapter covers the structure and the spectroscopic properties of the $(F_{64}Pc)_2TbH$, **[3]** and the $(F_{64}Pc)_2DyH$, **[4]** complexes. It also examines similarities and differences between these and the properties of the closed shell Y and Lu analogues.

### 4.2 Mass Spectroscopy

The challenges in accurately determining the empirical formula and the oxidation state of the complexes necessitated the conduct of the mass spectroscopy of **[3]** and **[4]** in both the positive and negative modes, using different matrixes and calibration methods. The

MALDI-TOF was the ionization method utilized for these samples. In general the internal calibration methods give a better accuracy than the external calibration method in this mode. This was also observed in Table 5.1 where alpha-cyano-4-hydrocinnamic acid (CCA) was used in the positive mode with PEG4000 as the internal standard. A mass accuracy of 17 and 6 ppm for $(F_{64}Pc)_2TbH$ and $(F_{64}Pc)_2DyH$, respectively were obtained. The matrix 2-[(2*E*)-3-(4-*tert*-butylphenyl)-2-methylprop-2-enylidene]malononitrile (DCTB) has been purported to be a relatively soft aprotic matrix compared to other polar matrices and this is evidenced by a highly unlikely protonation of the analytes.[166] When DCTB was used in the positive mode for the $(F_{64}Pc)_2DyH$ complex, two Na+ ions were adducted with the apparent loss of a proton. Both modes appear to support the present protonated form of the complexes in forming the $[M-H]^-$ species in the negative mode and the $[M+H]^+$ species in the positive mode in the MALDI-TOF test method.

**Table 4.1** Mass Spectroscopy Data for $(F_{64}Pc)_2TbH$ and $(F_{64}Pc)_2DyH$ Using the MALDI-TOF Method

| Complex (empirical formula) | Mode, and Matrix | Calculated Peak (m/z) | Observed Peak (m/z) | Mass[a] Accuracy (ppm) | Comment |
|---|---|---|---|---|---|
| $C_{112}F_{128}N_{16}TbH$ | Neg, DCTB | 4159.7732 | 4159.56 | 51 | $[M-H]^-$ |
| $C_{112}F_{128}N_{16}TbH$ | Pos, CCA | 4161.7888 | 4161.86 | 17 | $[M+H]^+$ |
| $C_{112}F_{128}N_{16}DyH$ | Neg, DCTB | 4163.7763 | 4163.74 | 9 | $[M-H]^-$ |
| $C_{112}F_{128}N_{16}DyH$ | Pos, CCA | 4165.7920 | 4165.82 | 6 | $[M+H]^+$ |
| $C_{112}F_{128}N_{16}DyH$ | Pos, DCTB | 4209.7559 | 4209.36 | 95 | $[M-H+2Na]^+$ |

Key: Neg = Negative, Pos = Positive.

Challenges were reportedly experienced in trying to generate positively charged ions for this procedure. In fact, no structurally valuable result was obtained for the closed shell $(F_{64}Pc)_2MH$ (M=Y, Lu) using the CCA matrix in the positive mode. The ability of

the $(F_{64}Pc)_2LnH$ complexes to form the positively charged (adducted) species during the MALDI-TOF method is probably linked to some interaction with 4f electrons of the lanthanide. This was also supported by the reduction of their effective magnetic moment from that of the free ion in the DC magnetometry test (Chapter 5). In general the calculated isotopic patterns of complexes were similar to the experimentally observed values. The differences were attributable to the large size of the complexes and the lower accuracy of the TOF mass analyzer compared to the FT-ICR. The observed and calculated patterns are compared for the negative modes in Appendix A.

## 4.3 X-ray Diffraction

Single crystal X-ray diffraction was also carried out on the $(F_{64}Pc)_2LnH$ complexes. The crystals were obtained from the slow evaporation of mixture of acetone/chloroform (35%/65%) at room temperature. The crystals grew as dark bronze cuboids. Table 4.2 summarizes the crystal data for $(F_{64}Pc)_2TbH$ and $(F_{64}Pc)_2DyH$. Details can be found in Appendix B.

The X-ray crystallographic data did not fully support the empirical formula. For these molecules, the assumed the ionic formula $([F_{64}Pc]^{2-})_2[Ln^{3+}]H^+$ could not be supported by the structure due to the missing proton. It was again assumed that the difficulty in locating this proton was due to the large size of the macromolecule and the test procedure. The $(F_{64}Pc)_2TbH$ complex is polymorphic. It was found to crystallize in two different space groups. It crystallizes into the same P4/ncc space group as [1] and [2], but it also forms the $P2_1/c$ space group which will be designated as [3′]. It formed the two different space groups in the same solvent system. Different solvent systems

were tried such as acetone/toluene, acetone, methyl ethyl ketone, methyl ethyl ketone/toluene but the other complexes did not form the P2$_1$/c group. The different crystal system is thought to be due to the amount of solvent left in the crystal the conditions under which the crystallization process took place.

**Table 4.2** X-ray Crystallography Data for $(F_{64}Pc)_2TbH$ and $(F_{64}Pc)_2DyH$

| Empirical Formula | $C_{112}F_{128}N_{16}Dy$ | $C_{112}F_{128}N_{16}Tb$ | $C_{112}F_{128}N_{16}Tb$ |
|---|---|---|---|
| Formula weight | 4163.60 | 4160.20 | 4160.20 |
| Temperature, K | 300 | 100(2) | 100(2) |
| Wavelength, Å | 1.54178 | 1.54178 | 1.54178 |
| Crystal system | Tetragonal | Tetragonal | Monoclinic |
| Space group | P4/ncc | P4/ncc | P2$_1$/c |
| Unit cell dimensions | | | |
| a, Å | 27.1967(12) | 27.5107(4) | 20.6911(6) |
| b, Å | 27.1967(12) | 27.5107(4) | 20.9584(7) |
| c, Å | 23.553(2) | 23.6687(9) | 36.6961(12) |
| α | 90° | 90° | 90° |
| β | 90° | 90° | 95.539(2) |
| γ | 90° | 90° | 90° |
| Volume, Å$^3$ | 17421.596 | 17913.4(8) | 15839.0(9) |
| Z | 4 | 4 | 2 |
| Density (calc.), g/cm$^3$ | 1.594 | 1.543 | 1.763 |
| F(000) | 8040.0 | 8004 | 8097.0 |
| R$_1$ | 0.0945 | 0.1128 | 0.0752 |
| wR$_2$ | 0.2855 | 0.3120 | 0.2096 |
| Crystal size, mm$^3$ | 0.12 x 0.13 x 0.16 | 0.20 x 0.20 x 0.15 | 0.25 x 0.23 x 0.14 |
| θ range for data collection | 4.60 to 54.96° | 3.22 to 67.58º | 3.01 to 67.63° |
| Refinement method | Full-matrix least-squares on F$^2$ | Full-matrix least-squares on F$^2$ | Full-matrix least-squares on F$^2$ |
| Goodness-of-fit on F$^2$ | 1.311 | 1.140 | 1.093 |

Several geometric parameters were also calculated for **[3]**, **[3′]** and **[4]** from their X-ray structures. They are summarized on Table 4.3. The two complexes with the P4/ncc space group will be considered first. The reduction of Ct(4N)--Ct(4N) distance with the smaller Ln$^{3+}$ ion was observed as expected because the smaller dysprosium ion formed a complex with a smaller Ct(4N)--Ct(4N). An analysis of the Metal--N bond lengths

revealed two different set of values, one set being longer than the other, representing the asymmetry caused by non-equivalent $F_{64}PcH$ and $F_{64}Pc$ ligands. This asymmetry was also observed in the radius of curvature of the $F_{64}Pc$ rings. The curvature was measured as the convexity of the $F_{64}Pc$ rings and defined as the sphere of radii, $R_i$, in the model presented in Figure 3.3. The data shows a non equivalence of the rings. The $F_{64}PcH$ ring is expected to have less curvature due to its longer metal to pyrrole nitrogen bonds.

**Table 4.3** Some Geometrical Parameters of $(F_{64}Pc)_2LnH$

| | **[3]** | **[3′]** | | **[4]** |
|---|---|---|---|---|
| Ct(4N)--Ct(4N), Å | 2.81 | 2.83 | | 2.79 |
| Metal--N, Å | 2.426(6), 2.433(6). Average: 2.430 (6) | 2.436(4), 2.436(4). Average: 2.436(4) | | 2.417(6), 2.421(6). Average: 2.419(6) |
| $R_i$ Å | 19.5, 19.9. Average: 19.7 | 19.5, 14.4 Ave.: 16.9 | 29.4, 18.4 Ave.: 23.9 | 20.2, 20.4 Average: 20.3 |
| φ ° | 32 | 29 | | 32 |
| γ ° | 4.5, 7.8 | 5.2, 7.5 | | 3.9, 7.6 |

Ct(4N)--Ct(4N); Distance between the planes formed by the 4 coordinating pyrolle nitrogens.
Metal--N; Distance between central metal ion and the 4 coordinating pyrolle nitrogens.
$R_i$ ; Sphere of radii for each Pc face.
φ °; Twist angle between opposing phthalocyanine rings, measured from eclipsed position.
γ °; Angle made by the bond that links the two benzene ring C atoms that bear the $i$-$C_3F_7$ groups with the 4N plane.

The monoclinic **[3′]** is unlike the tetragonal phase in that the molecules are no longer parallel but almost perpendicular, occurring in pairs whose 4N planes makes an 87.6° angle, Figure 4.1(b). Peripheral $i$-$C_3F_7$ groups of one molecule penetrate the fluorine-lined NCIS of the other molecule, up to the van der Waals contacts not only with other F, but also with C and N atoms of the macrocycle. This architecture leads to a more compact packing, the solvent-accessible volume being 22%, ~2/3 of that of tetragonal phases. The arrows of Figure 4.1(c) mark the reduced symmetry of the monoclinic **[3']** compared with the tetragonal **[3]**, Figure 4.1(d), for which a 4-fold axis is present. Interestingly, the cogwheel-type alignment of the two rings is in opposite directions, each

coordinating $F_{64}Pc(2-)$ ring being chiral. Constructing fluorinated, chiral spintronics devices is an intriguing possibility.
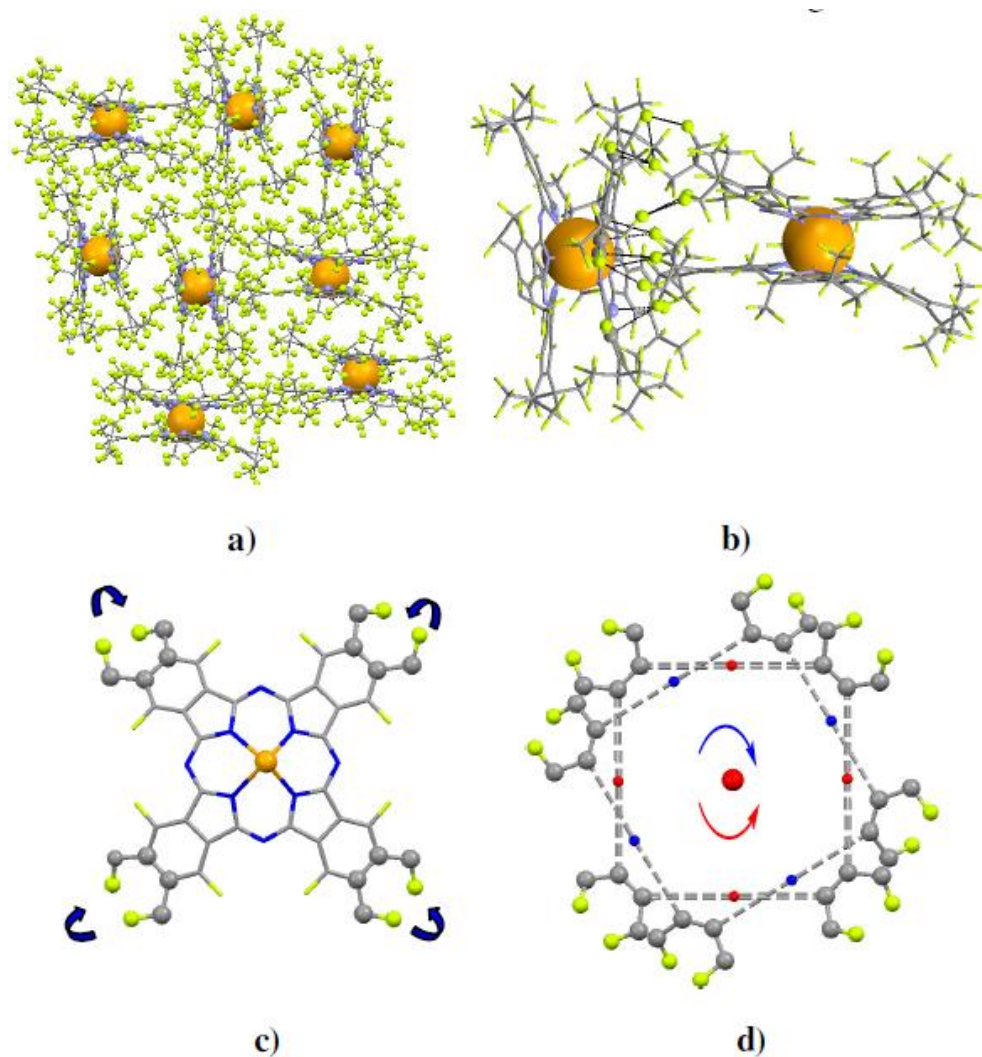


**Figure 4.1** Single-crystal X-ray structural characterizations of **[3']** a monoclinic $F_{64}Pc$-based double-decker metal complex. a) Packing diagram. b) Partial packing diagram showing the van der Waals contacts as black dashed lines and the atoms involved as ball-and-stick representations. c) Half of the molecular structure (one Pc ring) viewed along the $C_4$ axis. The arrows connect the tertiary F atoms that are above the plane of the ring with those that are below it. d) Schematic representation of the tetragonal phase viewed along the 4-fold axis. The arrows indicate the alignment direction of the tertiary F atoms for the two Pc rings, color-coded in blue and red.

At molecular-level, **[3']** adopts an even more eclipsed configuration, $\phi = 29°$ vs. 32° for the tetragonal **[3]**. The curvature radii are now non-equivalent within each Pc ring of **[3']**: 19.5, 14.4 and 29.4, 18.4 Å, respectively.  The averages, 16.9 and 23.9 Å reflect the greater intramolecular distortions in **[3']** relative to **[3],** undoubtedly due to intermolecular interactions.  It was noted that most sandwich complexes do not form columnar stacks, this architecture requiring long-chain substituents that induce liquid crystalline mesophases.[167] It thus appeared that the $i$-$C_3F_7$ groups could simulate to a certain extent, the effects of longer alkyl groups. However, the establishment of a trend must await a larger $i$-$C_3F_7$ database.

### 4.4 Nuclear Magnetic Resonance (NMR) Spectroscopy

NMR spectroscopy was carried out on the $(F_{64}Pc)_2LnH$ complexes in several polar solvents including, acetone $D_6$, acetonitrile $D_3$,  pyridine $D_5$ and chloroform D.  $^{19}F$ NMR was done in order to confirm the presence of the $CF_3$, aromatic F and the primary aliphatic F groups.  $^1H$ NMR was carried out to try to confirm the presence of the proton on the complex.  Neither of these techniques was successful in presenting any new data except the chemical shifts of the complexes.   The high paramagnetism of the central lanthanide ion interfered with the tests.  The chemical shifts associated with the three fluorine groups were observed but an integration of the peaks to confirm the 6:1:1 ratio of primary aliphatic F to aromatic F to tertiary aliphatic F failed.  The results of the NMR shifts are presented on Table 4.4.

**Table 4.4** $^{19}$F NMR of $(F_{64}Pc)_2LnH$ Complexes in Acetone $D_6$

| Complex | Primary Aliphatic CF$_3$ shifts, (ppm) and J (Hz) | Aromatic F shifts, ppm | Tertiary Aliphatic CF shifts, ppm |
|---|---|---|---|
| $(F_{64}Pc)_2TbH$ | −82.1 | −119.3 | −193.0 |
| $(F_{64}Pc)_2$ DyH | −77.4 | −97.3 | −180.3 |

All the respective chemical shifts of **[3]** were observed further upfield from those of the **[4]** by −4.7, −22.0 and −12.7 ppm for the CF$_3$, Ar-F and aliphatic CF signals respectively, signifying their slightly different chemical environment in solution. The $^{19}$F NMR spectra of $(F_{64}Pc)_2LnH$ also exhibited the broad "hump" feature on which the tertiary aliphatic fluorine signal sits. Plots of the $^{19}$F spectra of **[3]** and **[4]** are shown in Appendix C.

No proton peaks were observed in any of the solvents used for 1H NMR. This was anticipated because the proton shifts were not observed in the diamagnetic analogues **[1]** and **[2]**.

### 4.5 IR Spectroscopy

The IR spectroscopy of **[3]** and **[4]** was carried out using solid state KBR discs. The KBR disks were made up of approximately a 2% weight of sample. As with **[1]** and **[2]** complexes the spectra obtained revealed frequencies that could be assigned to pyrrole stretching, isoindole breathing, isoindole stretching vibrations, aza (C-N) stretching vibrations, and coupling of pyrrole and aza stretching vibrations. There is still uncertainty regarding the locations of vibrations of the proton on the ring. However, signals should be obtained from the stretching, bending and wagging of the C-F bonds

on the benzene rings and on the $i$-C$_3$F$_7$ moiety. The initial assignments based on literature[5, 120-123] are set out in Table 4.5:

**Table 4.5** Infrared Peaks and Initial Assignments for (F$_{64}$Pc)$_2$TbH and (F$_{64}$Pc)$_2$ DyH

| Complex and Some Absorptions in cm$^{-1}$. | | Assignments |
|---|---|---|
| (F$_{64}$Pc)$_2$ TbH | (F$_{64}$Pc)$_2$ DyH | |
| 730m, 717m, | 730m,717m | |
| 753m | 753m | |
| 967s, 982s, | 967s, 982s | |
| 1094s, 1056w | 1094s, 1056w | Coupling of isoindoline deformation and |
| 1170 s | 1170s | Symmetric CF stretch |
| 1248vs | 1249vs | Anti-symmetric CF stretch |
| | 1385w, 1340w | |
| 1375w | 1399w | |
| 1454w | 1454w | |
| 1487w | 1490w | Isoindole stretching |
| 1638m | 1651w | Benzene ring stretch |
| 1749w | 1749w | Benzene ring stretch |

*Legend: vs = strongest absorption, s = strong, m = medium, w = weak, b = broad*
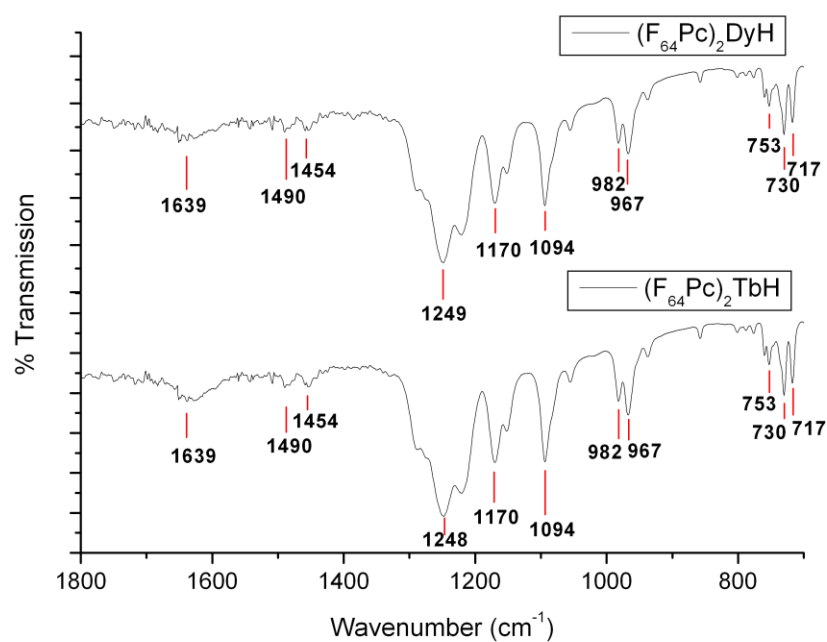


**Figure 4.2** IR spectra of (F$_{64}$Pc)$_2$TbH, (F$_{64}$Pc)$_2$DyH from KBR discs.

An examination of Table 4.4 and Figure 4.2 shows the absence of the very intense band in the range 1314-1322 $cm^{-1}$ that is characteristic of the radical species and which is due to pyrolle stretching.[120]

## 4.6 Electron Spin Resonance

ESR was conducted on the dry microcrystalline solids of the [3] and [4]. No signal was obtained from [3]. It was assumed that a small, approximate 1% paramagnetic species was present in the samples, similar to the cases of [1] and [2] and thus signal should be observed. A very noisy signal was observed in the case of [4] with a g value of 2.003.

Trojan et al.[86] noted that no signal was observed from $Pc_2Tb$ at room temperature and attributed this to interactions between the unpaired 4f electrons of the metal core and the radical electron. In the case of the $Pc_2Tb$, the interaction was anti-ferromagnetic leading to no observed signal. In the case of the Dy, complex it was found that there was an anti-ferromagnetic interaction at low temperature (ca. 2-60 K) and a ferromagnetic interaction at high (room) temperature. The ESR was carried out at high temperature and thus a signal was observed.

## 4.7 UV-Visible Electronic Spectra

The UV-Visible spectra of the both the [3] and [4] were carried out in several solvents, typically between 300 nm and 1000 nm. The solvents included acetone, chloroform, methanol and ethanol. Technically, wavelengths above 800 nm are considered to be in the NIR region. The spectra are essentially similar in all the solvents with slight changes

in the positions of $\lambda_{max}$ in the observed bands as was the case for **[1]** and **[2]**. The observed spectra of **[3]** and **[4]** complexes are shown in Figure 4.4.

The peak positions as read from observed spectra and their respective extinction coefficients are set out in Table 4.6.  Shoulders have been omitted from the spectra as they will be examined in the deconvoluted spectra using FityK® software.  The B and Q bands were red shifted relative to their un-substituted analogues while the  RV band is blue shifted. As it was with **[1]** and **[2],** it was anomalous because there is a general trend in the red shifting of the UV-Vis peaks when substitutents are placed on the Pc ring. That is, these main bands tend to shift the same way.   The excitations responsible for the bands in the UV-visible spectra are expected to be the same as for **[1]** and **[2]** except for minor shifts due to instrument error and size of the central metal ion.   The largest deviations in the peak wavelength ($\lambda_{max}$) occurs in the RV band with $\lambda_{max}$ of **[3]** being the shortest and **[1]** the longest; a difference of approximately 58 nm.  In general, $\lambda_{max}$ of the bands for **[1]** occurs at longer  $\lambda_{max}$ relative to **[2]**-**[4].**   ($F_{64}Pc)_2$LuH, **[1],** has the smallest central metal ion.  The differences between the other bands are too close to call because the readings are only accurate to 2 nm.

**Table 4.6** UV-Visible Spectra of $(F_{64}Pc)_2$TbH and $(F_{64}Pc)_2$DyH in Methanol

| Complex | Peaks (nm) and Extinction Coefficient [log $\varepsilon$] (L•mol$^{-1}$•cm) | | | | | |
|---|---|---|---|---|---|---|
| $(F_{64}Pc)_2$TbH | 860 [4.13] | 681,[5.01] | 552,[4.79] | 429,[4.58] | 383,[4.96] | 339,[4.96] |
| $(F_{64}Pc)_2$DyH | 869,[4.11] | 680 [5.00] | 549,[4.78] | 428,[4.54] | 384,[4.90] | 339,[4.92] |

The deconvoluted spectra of [**3**] and **[4]** contain similar peaks to **[1]** and **[2]** .  The presence of the band in the RV region which is characteristic of the neutral $Pc_2$Ln species was again surprising.   The presence of the both the neutral and reduced species in

solution is unlikely because of the expectation that the peaks responsible for the IV bands would also be present. In fact, the reduction of the $(F_{64}Pc)_2LnH$ in methanol using hydrazine hydrate produces peaks in the IVB region. That is, the $[F_{64}Pc^{2-}]Ln^{3+}[F_{64}Pc^{3-}]$ species appeared to be formed and the $\pi$ radical $[F_{64}Pc^{3-}]$ apparently being responsible for the peaks appearing in the IV band.
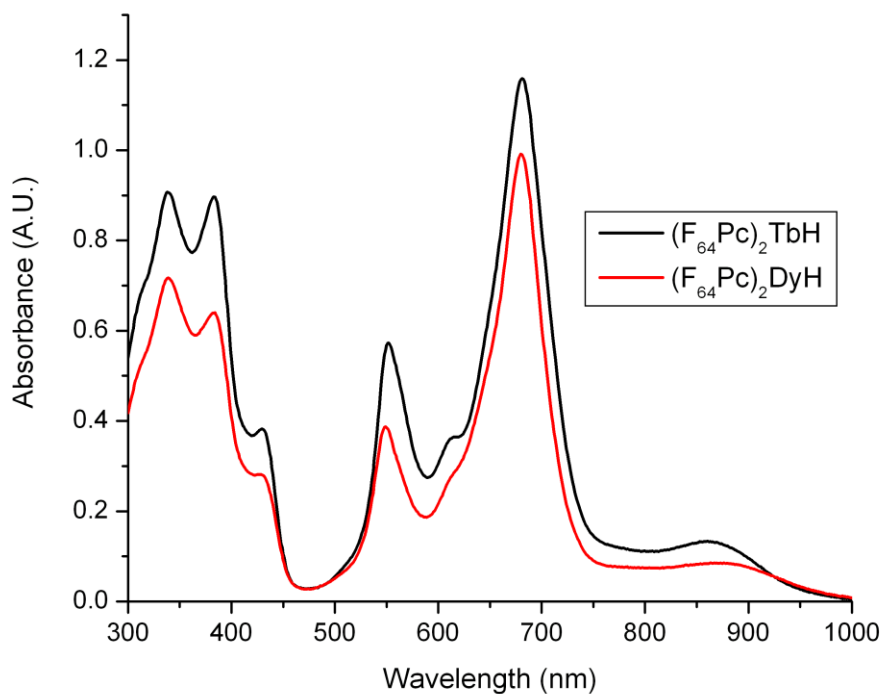


**Figure 4.3** UV-visible spectra of $(F_{64}Pc)_2TbH$ and $(F_{64}Pc)_2DyH$ in methanol.

Furthermore, neither the protonation nor the deprotonation of **[1]**-**[4]** was found to be solvent dependent since polar protonated solvents such as methanol did not give a radically different UV-visible spectra from weakly basic solvents such as pyridine. That is, no evidence a reaction such as in Equation 4.1was observed.

$$(F_{64}Pc)_2 Ln(III)H \xleftrightarrow{\ Pyridine(-H+)\ } (F_{64}Pc)_2 Ln(III)^- \qquad (4.1)$$
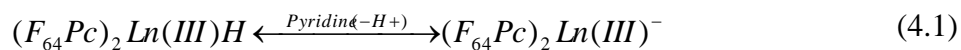
It appears, therefore,  that only the protonated form exists in solution and not both forms as suggested by Spyrolias et al.[117]  for **[1]**-**[4].**
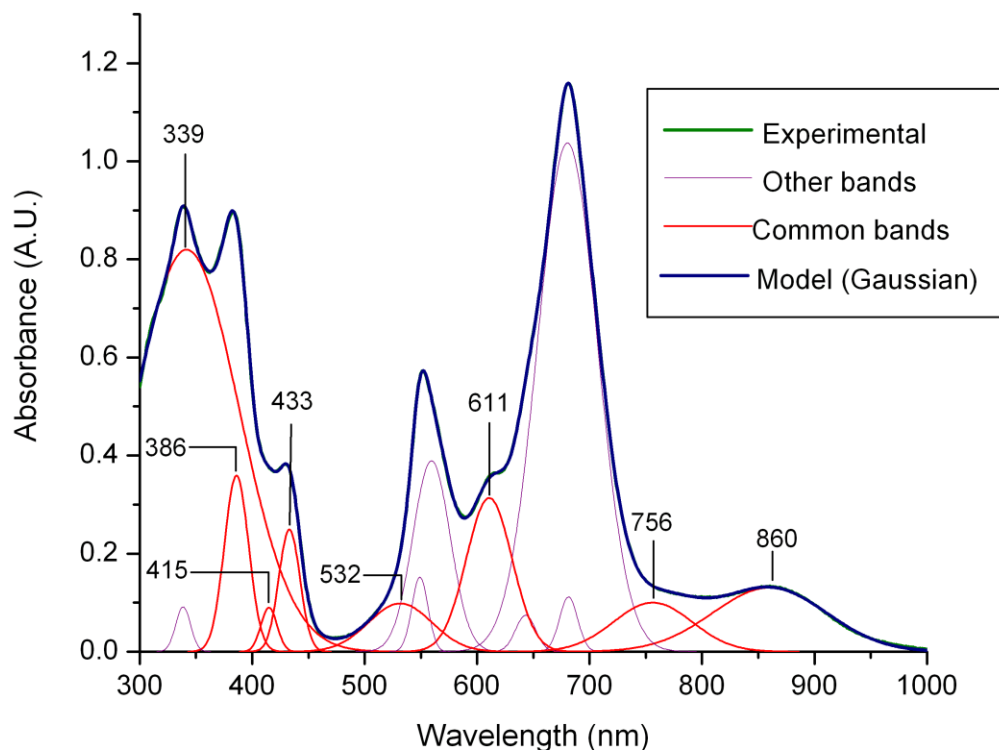


**Figure 4.4**  Deconvoluted electronic  spectrum of $(F_{64}Pc)_2TbH$ in  methanol.

As was found with **[1]** and **[2]** the common bands identified were similar, and the BV band was still absent.  The common bands were at approximate $\lambda_{max}$ of 880, 760, 610, 520, 433, 415, 386 and 339 nm.  The specific values are listed on Table 4.7.   It appears that most of the excitations identified in the TDDFT calculations of Liao et al.[109]   can be applied to **[3]** and **[4]**.

**Table 4.7** Comparison of the Deconvoluted UV-Visible Spectra of $(F_{64}Pc)_2TbH$ and $(F_{64}Pc)_2DyH$ and Proposed Band Assignments

| $(F_{64}Pc)_2TbH$ $\lambda_{max}$ (nm) | $(F_{64}Pc)_2DyH$ $\lambda_{max}$ (nm) | Proposed Band Assignment |
|---|---|---|
| 860 | 871 | RV |
| 756 | 764 | $Q_1$ |
| 681 | 682 | $Q_2$ |
| 680 | 682 | $Q_2$ |
| 643 | 644 | $Q_3$ |
| 611 | 608 | $Q_4$ |
| 559 | 554 | $Q_5$ |
| 549 | 547 | $Q_6$ |
| 532 | 515 | $Q_7$ |
| 433 | 434 | $B_1$ |
| 415 | 415 | $B_2$ |
| 386 | 387 | $B_3$ |
| 342 | 342 | N |
| 339 | 340 | N |

There was striking consistency in the location of the B bands in all four complexes suggesting that these may not be metal dependent but rather depend mainly on the $F_{64}Pc^{2-}$ ring. The shortcomings of the deconvolution method were again evident in variations shown especially in the region of the $Q_2$ band. While it agrees in principle with some of the results of the TDDFT calculations, there were several peaks in the Q Band region where it was challenging to know their exact locations. That is, repeated deconvolution of the same data shifted bands in this $Q_2$ region to different absorbances and $\lambda_{max}$.

No bands were observed in the IV region of the electronic spectrum of **[3]** and **[4]**.

## 4.8 Thermal Analysis

Thermal analysis of **[3]** and **[4]** included TGA and DSC. TGA was carried out in atmospheres of both air and nitrogen gas. The rate of heating was 10ºC/minute from 20ºC up to 500ºC and then sample was held at 500ºC for 30 minutes. The complexes began to show weight loss at about 270ºC. Separate heating under a vacuum up to 285ºC confirmed that the samples began to sublime at this temperature. The absence of burnt residue at the end of the test in both air and nitrogen gas atmospheres suggests the absence of their thermal breakdown. Figure 4.5 shows the TGA graph of weight % vs. temperature for **[3]** and **[4]**. The examination of the samples using DSC provided further information as to their stability.
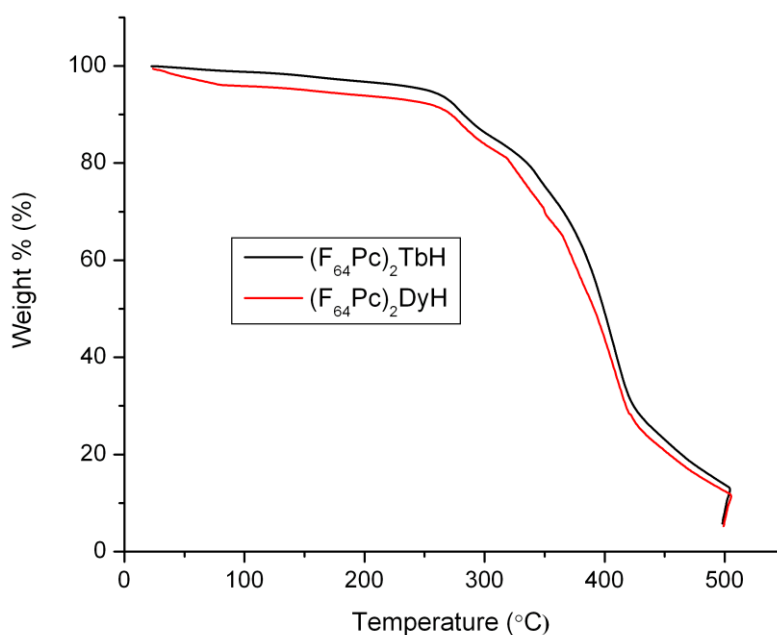


**Figure 4.5** TGA plots of $(F_{64}Pc)_2TbH$ and $(F_{64}Pc)_2DyH$ in air.

DSC was carried out on **[3]** and **[4]** in an atmosphere of nitrogen gas and heated to a temperature of 500ºC. The heat flow vs. temperature graphs show four main events. The 1st order thermal transition commencing at about 273°C and peaking at 312ºC for **[3]** was interpreted to represent the onset of sublimation. Similarly for **[4]**, this 1st order thermal transition commenced at 276ºC and peaked at 323ºC. This is supported by the TGA graphs and other sublimation tests. The two thermal events occurring at lower temperatures may be due to events such changes in the crystalline structure or intramolecular conformation. The origin of the 1st order thermal endothermic event at ca. 490°C appears to be related to the breakdown of the double layer structure (i.e loss of a ring) and or the formation of the triple layer structure based on split Q in the Q-Band seen in the UV-Vis of the residue of the material used for the test.
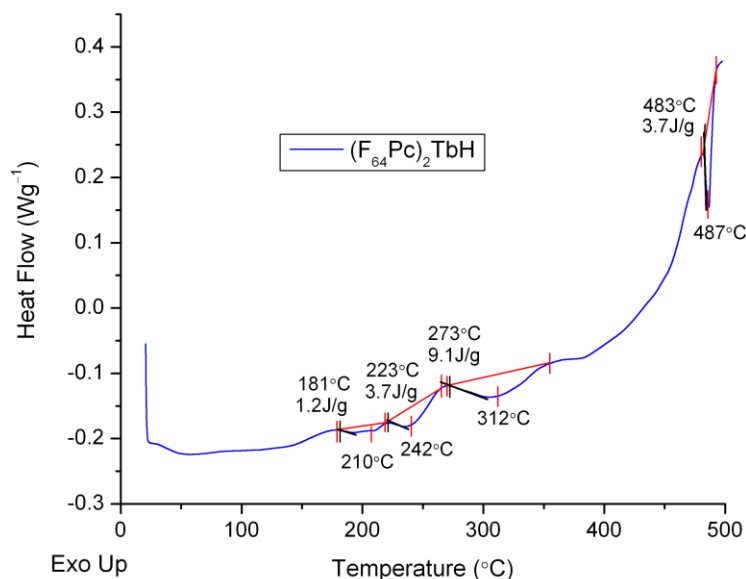


**Figure 4.6** DSC of $(F_{64}Pc)_2TbH$ in $N_2$ gas between 20ºC and 500ºC.
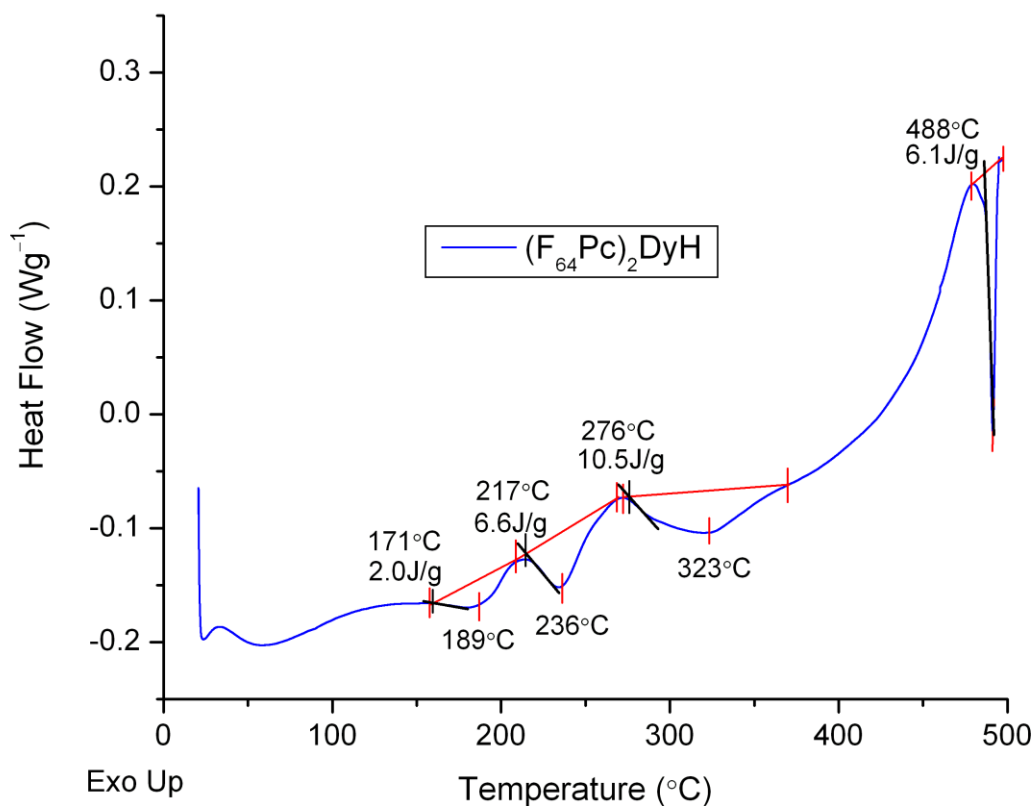
**Figure 4.7** DSC of $(F_{64}Pc)_2DyH$ in $N_2$ gas between 20ºC and 500ºC

The color of the methanol solution made from the recovered residue of the DSC test was green. The split Q-band of this type along with the absence of the BV and RV bands is known to be associated with the triple layer form i.e the trisphthalocyanines.[68, 94] The UV-visible spectrum of the DSC residue of $(F_{64}Pc)_2DyH$ is shown in Figure 4.8. The Q band normally found at 682 nm on the unheated material appears to split into two peaks, one red shifted to 692 and the other blue shifted to 637 nm. In addition, the peak previously appearing at 550 nm either disappeared or was blue shifted to 529 nm with

lower intensity. The band normally occurring at about 340 nm appeared to be undisturbed.
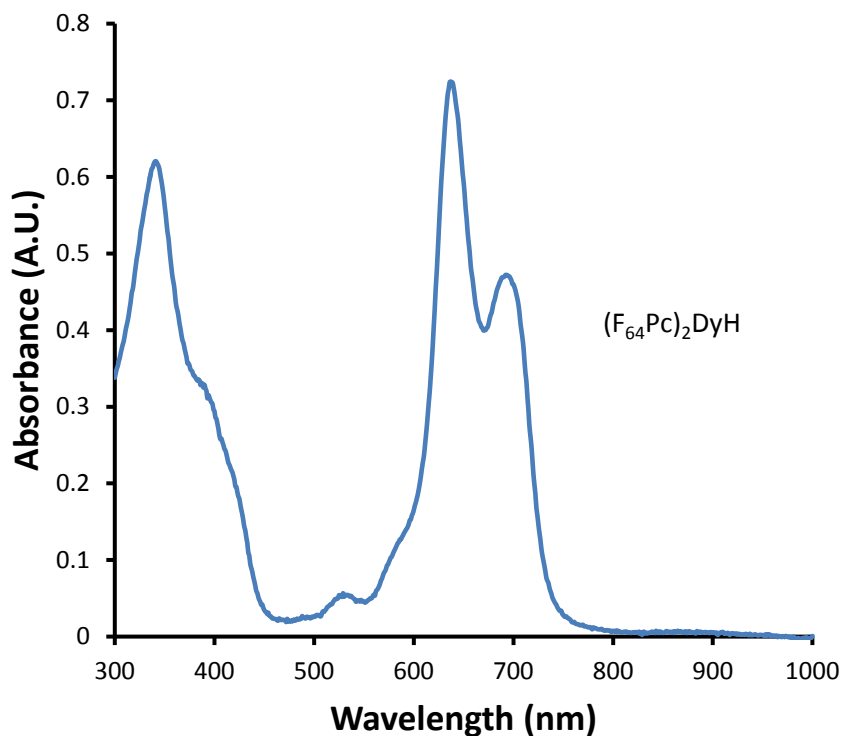


**Figure 4.8** UV-visible spectra of remains of the $(F_{64}Pc)_2DyH$ sample in the DSC test dissolved in methanol.

## 4.9 Summary

As in the case of the $(F_{64}Pc)_2LuH$ and $(F_{64}Pc)_2YH$, the properties of the $(F_{64}Pc)_2LnH$ (Ln = Tb, Dy) are strongly influenced by the F atoms and the $i$-$C_3F_7$ groups attached to the Pc ring and less so the central metal ion. The non-magnetic properties are similar to [1] and [2] and small variations can be attributed to the lanthanide contraction. The paramagnetic core of the $(F_{64}Pc)_2LnH$ appears to affect both the ESR and the NMR results. $^{19}$F NMR signals were obtained, but only the chemical shifts could be used to confirm the presence

of the primary aliphatic ($CF_3$), aromatic (Ar-F) and the tertiary aliphatic (C-F) fluorines. Peak integrals appeared to be distorted by the paramagnetic metal core, and that limited the structural information could be gleaned from the values. The chemical shifts of all fluorines in the $CF_3$, Ar-F and C-F moieties were shifted further upfield compared to shifts for **[1]** and **[2]**, with complex **[3]** had the more negative values compared to **[4]**.

The absence of an ESR signal in **[3]** is consistent with literature findings[168] but their explanation may not be the same as in this case. In the cases of **[1]** and **[2]**, the explanation forwarded is that the signal came from an approximate 1% paramagnetic impurity of the radical species, suggesting that the ligand carries the unpaired electron responsible for the signal. In the case of **[3]**, if a similar quantity of paramagnetic impurity is present, then it appears that its unpaired electron is coupling anti-ferromagnetically with the unpaired electrons in the $Tb^{3+}$ core of the paramagnetic impurity at room temperature. An ESR signal is obtained for **[4]** and here it is assumed that the interaction in the paramagnetic impurity between the $Dy^{3+}$ unpaired 4f electrons and the radical ligand is ferromagnetic at high temperature as indicated by Trojan et al.[86]

The protonated form, $(F_{64}Pc)_2LnH$ of the complexes as the stable form is supported by the UV-Vis data, NMR, IR and X-ray spectroscopy.

# CHAPTER 5

## MAGNETOMETRY
## of $(F_{64}Pc)_2LnH$ COMPLEXES (Ln = Tb, Dy)


### 5.1 Overview

The magnetic properties of materials can be probed by several techniques. These include

NMR, EPR, Neutron Diffraction,[169, 170] MCD[171, 172], Muon Spin Relaxation (µSR)[173, 174], Magnetic Force Microscopy,[175, 176] and DC and AC magnetometry. Investigation of

the structural and magnetic properties of large molecular clusters is complex and requires

the use of many different techniques. Calculations of the energy levels of large clusters

include techniques of elastic neutron scattering and polarized neutron scattering. They

often provide both magnetic and structural information on the specimen. NMR, EPR and

µSR are referred to as resonance techniques and their use depend on many factors

relating to the nature of the sample and which magneto, energy, or spin dynamics data is

required.[177]

DC magnetism is a popular method of carrying out the initial magnetic

characterization, as was done for **[1]** and **[2]**. The so called Zero Field Cooled-Field

Cooled (ZFC-FC) test when carried out at relatively low magnetic field may detect

certain magnetic effects due to irreversibility such as ferromagnetism.[178] The ZFC-FC

test involves a cooling of the sample in to a low temperature, typically 2-5 K in a zero

magnetic field. At this lowest temperature, a single value of the DC magnetic field is

then applied to the sample as its temperature is raised to the highest temperature,

typically 300-400 K during which the magnetization is measured, (the ZFC portion). The

temperature is the again lowered to the previous low temperature at the same DC

magnetic field and the sample's magnetization is then measured either on cooling, or when it is being warmed up to the high temperature, (the FC part of the procedure). In DC magnetism measurements, the sample's magnetization can be measured as a function of the magnetic field, *M(H)* at constant temperature to also detect hysteresis. During DC magnetic testing, the equilibrium value of the magnetization is measured.

While DC magnetism may produce important information on a sample's magnetic properties such as its ferromagnetism, anti-ferromagnetism, and the presence or absence of a Curie-Weiss behavior, it is still very limited. Other important magnetic characteristics such as spin glass phenomena, superparamagnetism, magnetic phase transitions and superconductivity may not be detected. Such phenomena may be detected in AC magnetometry. In AC magnetometry, a time varying field, *H(t)* is usually superimposed on a small DC magnetic field. This results in the induction of a time dependent magnetic moment, $M_{ac}(H)$ in the sample. This *H(t)* is the driving frequency, $\omega$ and it can be shown that:

$$M_{ac} = \frac{dM}{dH}H \ \sin \omega t \tag{5.1}$$

where dM/dH is the susceptibility, $\chi$. Under conditions where $\omega$ is small, the DC moment will follow (approximately), the AC moment of the sample. However, for certain samples, there may be a lag of the sample's magnetization behind that of the driving magnetic field. The sample is then said to exhibit a dynamic response. The magnetization response is often described as the $\chi$ and the phase lag angle $\varphi$. These two parameters are used to then describe an in-phase susceptibility $\chi'$, and an imaginary, or out-of-phase susceptibility, $\chi''$. They are related to the $\chi$ and $\varphi$ by the expressions;

$$\chi' = \chi \cos \varphi \tag{5.2}$$

$$\chi'' = \chi \sin \varphi \tag{5.3}$$

$\chi_{ac}$ can therefore be expressed as:

$$\chi_{ac}(\omega) = \chi'(\omega) - i \chi''(\omega) \tag{5.4}$$

The magnitude of $\chi$ is then $\chi = \sqrt{\chi'^2 + \chi''^2}$ and $\varphi = \arctan(\chi''/\chi')$. $\chi'$, is called the magnetic dispersion. As the limit of low AC frequency approaches that of DC magnetometry, $\chi'$ is the slope of $M(H)$.[178]

Dissipative processes in the sample are represented by the imaginary component $\chi''$. Many interesting phenomena can be probed by AC magnetometry. Manipulation of parameters, $\chi'$, $\chi''$, $\omega$, temperature $(T)$, $H$ in plots such as $\chi'T$ vs. $T$, $\chi''/\chi'$ vs $T$, $\chi$ vs. $H$ and $\chi''$ vs. $T$ can reveal information about a sample's magnetic properties. For example, a nonzero imaginary susceptibility in ferromagnetic materials can indicate irreversible domain wall movement or absorption due to a permanent moment. Additionally, both $\chi'$ and $\chi''$ are very sensitive to thermodynamic phase changes, and are often used to measure transition temperatures.[178] A plot of a series of $\chi''$ *vs.* $\chi'$ referred to as a Cole-Cole diagram, is an Argand diagram[179] and it forms a semicircle if only one relaxation process occurs.[180] A Cole-Cole (or Nyquist) diagram may be described as a plot of imaginary vs. real components (Argand diagram) of the response of frequency dependent devices/materials. The Cole-Cole model is relaxation model and is based on the original generic equations developed by the Coles.[181, 182]

## 5.2 Molecular Magnetism

Molecular magnetism is generally regarded as the phenomenon whereby the magnetism in a substance is attributed to single molecules or ions, each behaving as a magnet in contrast to traditional bulk magnets such as ferromagnets where the magnetism is produced by cooperating molecular/atomic units. Single Molecular Magnets (SMMs) represent a "bottoms up" approach to nanomagnetism.[183] Molecular magnets exhibit many properties of bulk magnets but they also exhibit new phenomena some of which are quantum related such as Quantum Tunneling of Magnetization (QTM),[91, 184-186] quantum coherence/decoherence,[2, 187] quantum phase interference,[188] staircase hysteresis loops[186, 188] and temperature independent relaxation.[189, 190]

The criteria for molecules to exhibit SMM behavior varies, but in general they should be macro or supra-macromolecules, have a total high spin and have high magnetic anisotropy. Magnetic anisotropy may be caused by Zero Field Splitting (ZFS) and is said to have profound effects on magnetic properties. ZFS is the removal of spin microstate degeneracy for systems with $S > \frac{1}{2}$ in the absence of an applied field. The removal of this degeneracy is a consequence of molecular electronic structure and/or spin density distribution.[191] The "D" parameter is associated with axial ZFS and for odd electron systems, removes the microstate degeneracy and produces Kramer's doublets. Understanding ZFS is essential for the rational design of SMMs because the energy barrier separating the $+m_s$ and $-m_s$ microstates is equal to $|S^2D|$.[191] A high magnetic anisotropy implies an easy axis of magnetization (usually referred to a longitudinal or z-axis). An application of a magnetic field along z, $B_z$, causes a shift in the potential

wells.[192] Figure 5.1 shows the potential wells, microstates and the shift in the one of the wells.

Magnetic relaxation is a process which involves a system at an equilibrium state going to new equilibrium state after perturbation. The time between the two equilibrium states is called relaxation time.[193] The application of a time varying magnetic field as in AC susceptibility provides this perturbation. For bulk magnets, the hysteresis is associated with alignment of, and growth of domains with the AC magnetic field and results from long range order.
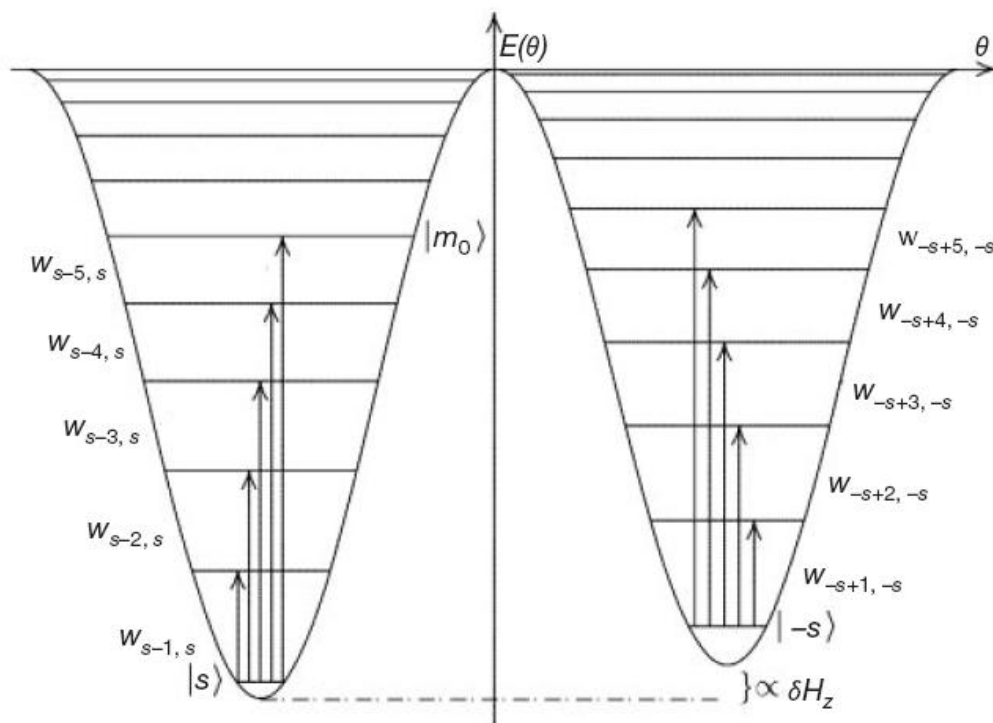


**Figure 5.1** Double-well potential of a uniaxial spin, tilted on the application of a magnetic field. One of the wells represents a spin up and the other a spin down. The different levels $|m\rangle$ corresponds to the magnetic quantum numbers, the eigenvalues for the $S_z$.[194] Differences between the energy levels is approximately $10$ cm$^{-1}$.

SMMs can be considered as super paramagnetic particles approaching nano-sized particles whose spins are so strongly bound by exchange interaction energy that they act as single spin. For classical bulk magnets, the relaxation is thermal in nature. Classical magnetic behavior is observed in SMM at sufficiently low temperatures where they exhibit hysteresis. The presence of steps in the hysteresis loops at certain values of the magnetic field is evidence of QTM.[185] An example of an SMM is the $M_{12}$ class of compounds formulated with a core of $[Mn^{III}_{10}Mn^{II}_2O_{16}Cl_2]$ of which $[Mn_{12}O_8C_{14}(O_2CPh)_8(hmp)_6]$ (hmp is from 2-(hydroxymethyl) pyridine) is a member.[195] This class of high spin transition metal compounds with S=10 are famous for exhibiting the phase lag and QTM in a time varying magnetic field. In some SMMs, the relaxation may be a hybrid of both thermal and quantum processes. This was unexpected because according to semi-classical theoretical work, at some temperature called the crossover temperature, $T_c$ the system was expected to relax strictly by thermal dynamics. The result is the occurrence of tunneling at temperatures into the regime that semi-classical theories would predict purely thermal dynamics.

The semi classical concept of tunneling often involves a particle escaping from a metastable potential well as shown in Figure 5.2, with inadequate energy to overcome the potential barrier. The particle therefore tunnels through the barrier instead of climbing over it.
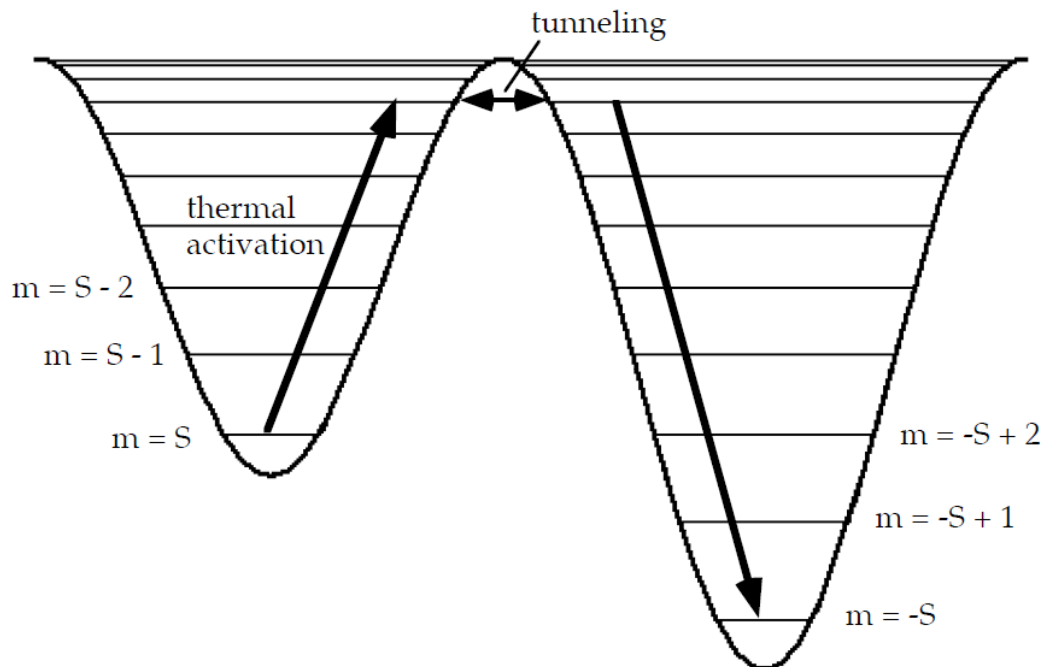
**Figure 5.2** Thermally assisted resonant tunneling process for $Mn_{12}$ type molecules under the action of an applied magnetic field along the easy axis. The different $|m\rangle$ levels for an S = 10 system are shown.[185]

A SMM with anisotropy gives the magnetization vector a preferred direction, known as the easy axis. The Hamiltonian which may have the most relevance to this molecule is:[185]

$$\mathcal{H} = -DS_z^2 - AS_z^4 - g\mu_B S_z H_z + \mathcal{H}' \qquad (5.5)$$

where $D$ and $A$ are anisotropy constants originating primarily from crystal and molecular fields, $\mathcal{H}'$ contains the terms that do not commute with $S_z$ and is thus responsible for tunneling. In zero external magnetic field, the magnetization minima and maxima are aligned parallel and anti-parallel with the $z-$ axis and flipping between these extremes requires overcoming a barrier of, $U = DS_z^2 + AS_z^4$. The height of the barrier can be reduced by the applied field. As the temperature is raised, the system attains the thermal

energy to activate the magnetization over the potential barrier and due to the much shortened relaxation time, paramagnetic behavior is observed.

The SMM behavior discovered in bis(phthalocyaninato) complexes of Tb, Dy, and Ho[91, 184] has been reported to have a fundamentally different mechanism from that of the transition metal SMM such as $Mn_{12}$. Whereas molecules such as $Mn_{12}$ exhibit QTM between different substates $|S_z|$, these $[Pc_2Ln]$ molecules manifest QTM between the entangled states $|J_z\rangle |I_z\rangle$ of the electron and nuclear systems.[196] This is coupling of the moments of electron spin, orbital angular and nuclear spins by the perturbation of hyperfine and nuclear quadrupole interactions. Takamatsu et al.[197] indicated that the ligand field splitting itself is insufficient to explain the staircase structures at $\mu_0 H = 0$. They found it necessary to include the interaction of the $4f^8$ electrons and the I = 3/2 nuclear spin of the nucleus of the Tb(III) central ion. They carried out a numerical analysis which included the ligand field, LF term, the hyperfine interaction term, $A_{hf}J \cdot I$ and the nuclear quadrupole interaction term $P\{I_z^2 - 1/3I(I+1)\}$. The inclusion of the nuclear quadrupole term was necessary to explain the occurrence of steps that were not equidistant in the $[Pc_2Tb]^-$ ion. The case of the Dy complex exhibited greater complications with the presence of seven naturally occurring isotopes with only the $^{161}Dy$ and $^{163}Dy$ having I = 5/2, while all the others have I = 0.
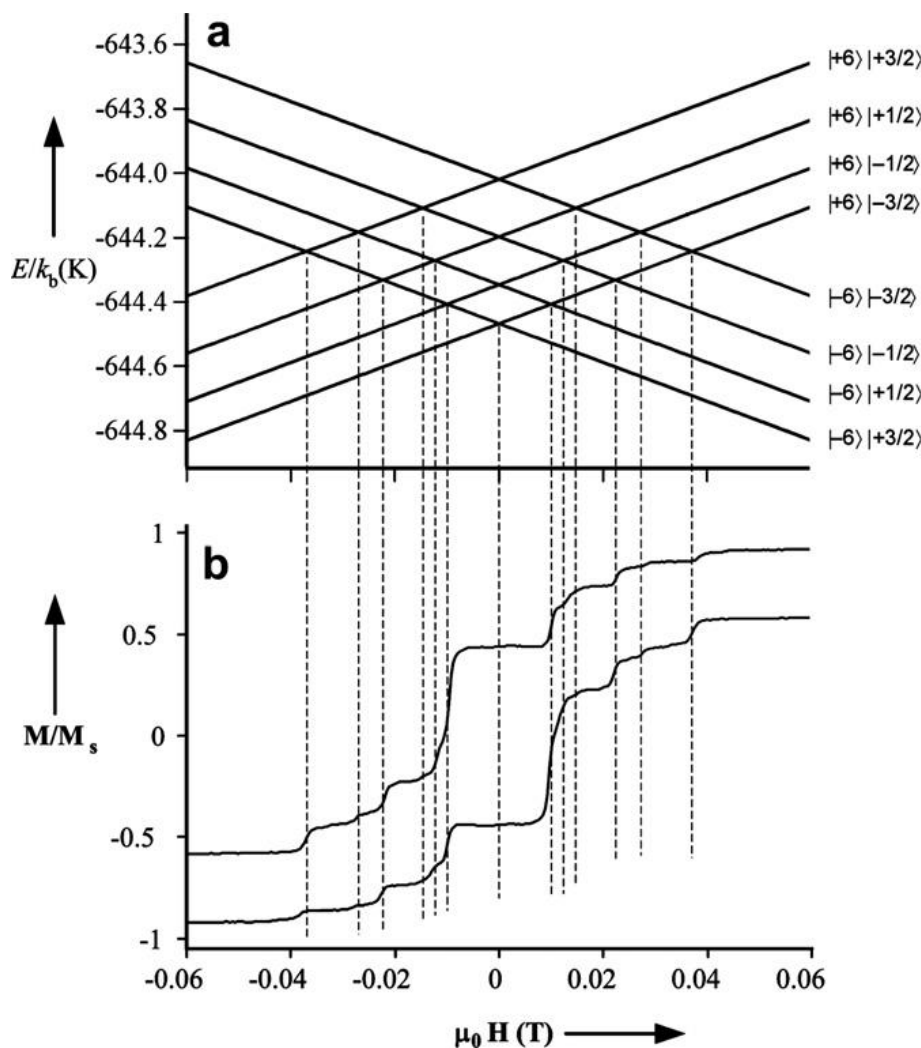
**Figure 5.3** (a) Nuclear quadrupole interactions and hyperfine interactions represented by Zeeman energy diagrams calculated with terms, $A_{hf} = 0.0173$ cm$^{-1}$ and P =0.010 cm$^{-1}$. (b) QTM shown by steps in the hysteresis loop at 0.04 K for a single crystal of $[(Pc_2Tb_{0.02}Y_{0.98}]^- \cdot TBA^+$ measured at 0.001 T/s.[88]

According to Kramer's theorem of spin parity, no tunneling should occur for the isotopes with I = 0 and they should not contribute to the step structure. Ishikawa[88] also reported that in the tunnel splitting, the gaps for the Tb complex are two orders of magnitude larger than for the Dy complex and it may explain why no clear steps are seen where $\mu_0 H \neq 0$. The coupling of the half integer spins of the nuclei (I = 5/2) and 4f$^9$

electronic (J =13/2) to generate integer spins produce the necessary avoided crossings and lead to the main step seen at $\mu_0 H = 0$ for the Dy complex.

## 5.3 DC Magnetism in $(F_{64}Pc)_2LnH$ (Ln = Tb, Dy)

Magnetism of **[3]** and **[4]** was first confirmed by conducting DC magnetometry tests on the oven dried powdered samples using the SQUID MPMS-XL magnetometer at Argonne National Laboratory. The ZFC-FC test at static magnetic field of 10 Oe was conducted between 2 and 300 K. The samples were also subject to hysteresis testing by reversing the DC magnetizing field between −50,000 Oe and 50 000 Oe at temperatures of 2, 5, 50, 100, 200 and 300 K. Repeat DC magnetometry testing was carried out at Rowan University, New Jersey on their SQUID MPMS-VSM magnetometer. The ZFC-FC was done at 100 Oe and 5000 Oe between the temperatures 5 and 300 K. Similarly, the samples were subjected to hysteresis testing by reversing the DC magnetic field between 50,000 Oe and −50,000 Oe at a temperature of 5 K.

Results of both tests revealed a Curie-Weiss paramagnetic behavior of the samples. No special magnetic features were revealed either at DC magnetic fields of 10 Oe, 100 Oe or 5000 Oe for the ZFC-FC tests. No hysteresis was observed during DC magnetic hysteresis testing, suggesting the absence of long range order such as would be observed in ferromagnetism or ferrimagnetism. Saturation was observed at low temperature hysteresis testing (5 K) but no remanence point or coercive field was observed. Plots of the hysteresis tests are shown in Figure 5.4.
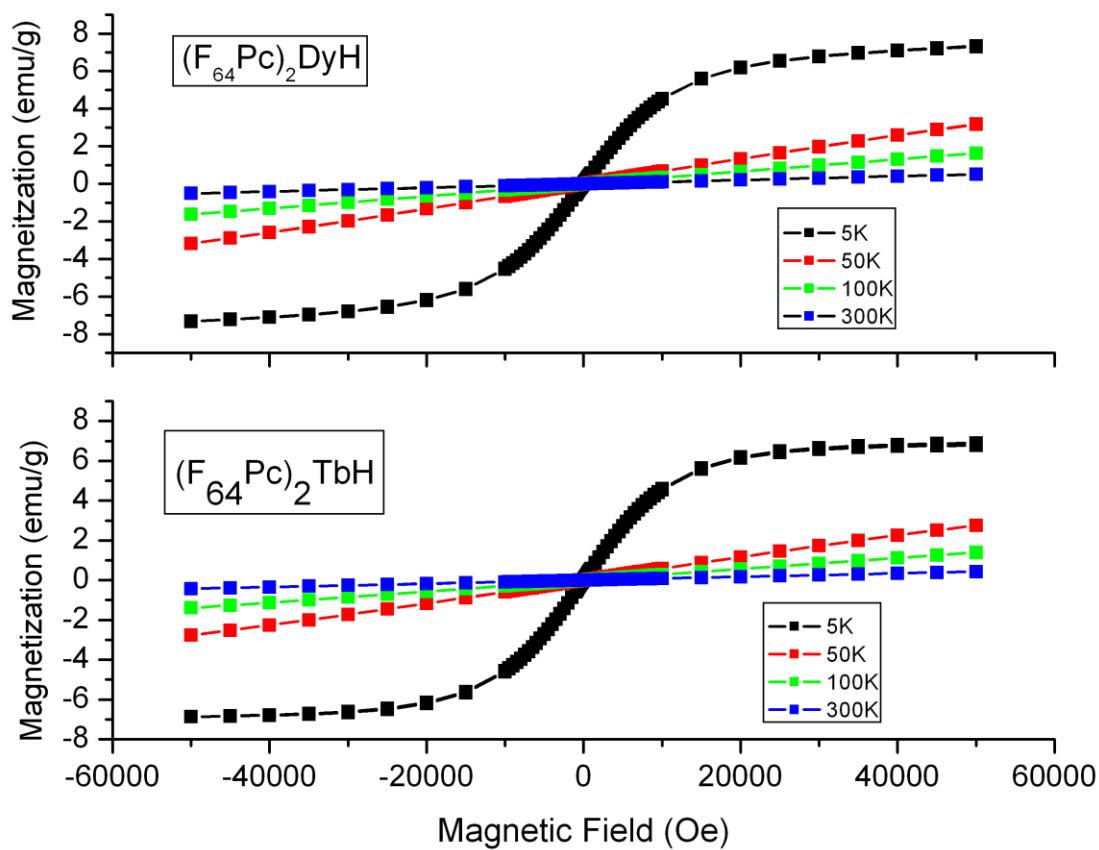
**Figure 5.4** Hysteresis testing of $(F_{64}Pc)_2TbH$ and $(F_{64}Pc)_2DyH$ in DC magnetic field.

The $1/\chi_M$ vs. $T$ and $\mu_{eff}$ vs. $T$ was plotted for DC magnetism at 10 Oe and 5000 Oe for both complexes and are shown in Figures 5.5 and 5.6.
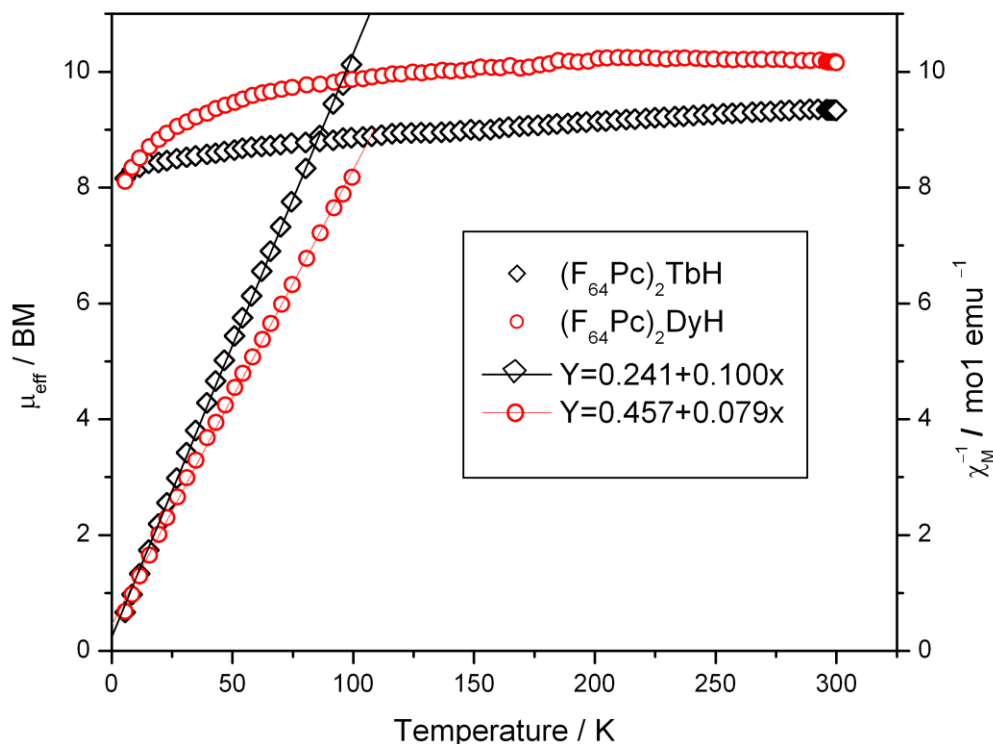
**Figure 5.5** Plot of $\mu_{eff}$ and $\chi_M^{-1}$ vs. *T* for $(F_{64}Pc)_2TbH$ and $(F_{64}Pc)_2DyH$ at DC magnetic field of 5000 Oe.

Both curves exhibit anti-ferromagnetic behavior at low temperature manifested by a negative Weiss temperature. The $\mu_{eff}$ and $\theta$ are 8.9 BM and −2.4 K and 10.1 BM and −5.8 K respectively for **[3]** and **[4]** at DC magnetic field of 5000 Oe. The results of testing in the 10 Oe DC magnetic field are 8.9 BM and −1.6 K and 10.7 BM and −2.7 observed for **[3]** and **[4]**. Overall, $\mu_{eff}$ lie within range of 9.1-9.7 and 9.0-10.7 BM, respectively, observed for $Tb^{3+}$ and $Dy^{3+}$ sandwich complexes.[193, 198]
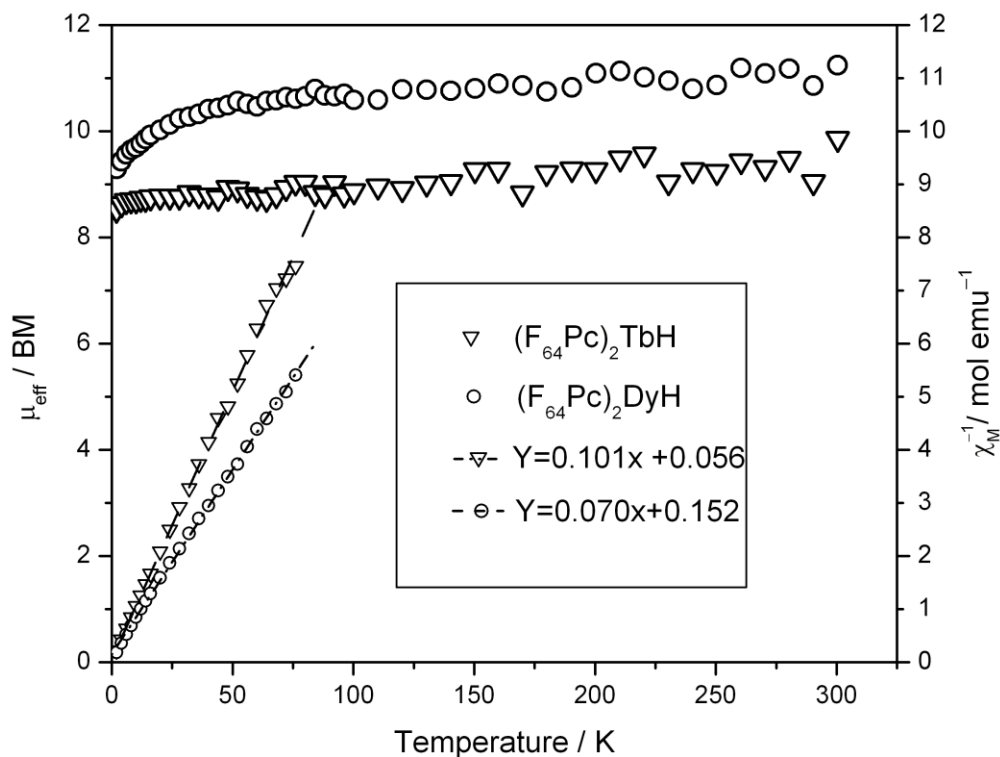
**Figure 5.6** Plot of $\mu_{eff}$ and $\chi_M^{-1}$ vs. *T* for $(F_{64}Pc)_2TbH$ and $(F_{64}Pc)_2DyH$ at dc magnetic field of 10 Oe.

## 5.4 Sub-Kevin Hysteresis Magnetic Testing.

In order to further assess the magnetism of **[3]** and **[4]**, samples were subjected to hysteresis testing at low temperature. The magnetic tests were carried out on the undiluted samples at sub-kelvin temperatures (0.04 K – 1.1 K) on the micro-SQUID magnetometer at Institut Néel, CNRS, France by Dr. Wolfgang Wernsdorfer and co-workers and the data provided. This was the first test of SMM behavior of **[3]** and **[4]**. Clear evidence of hysteresis was observed for both samples. Results of these tests are shown on Figures 5.7 and 5.8.
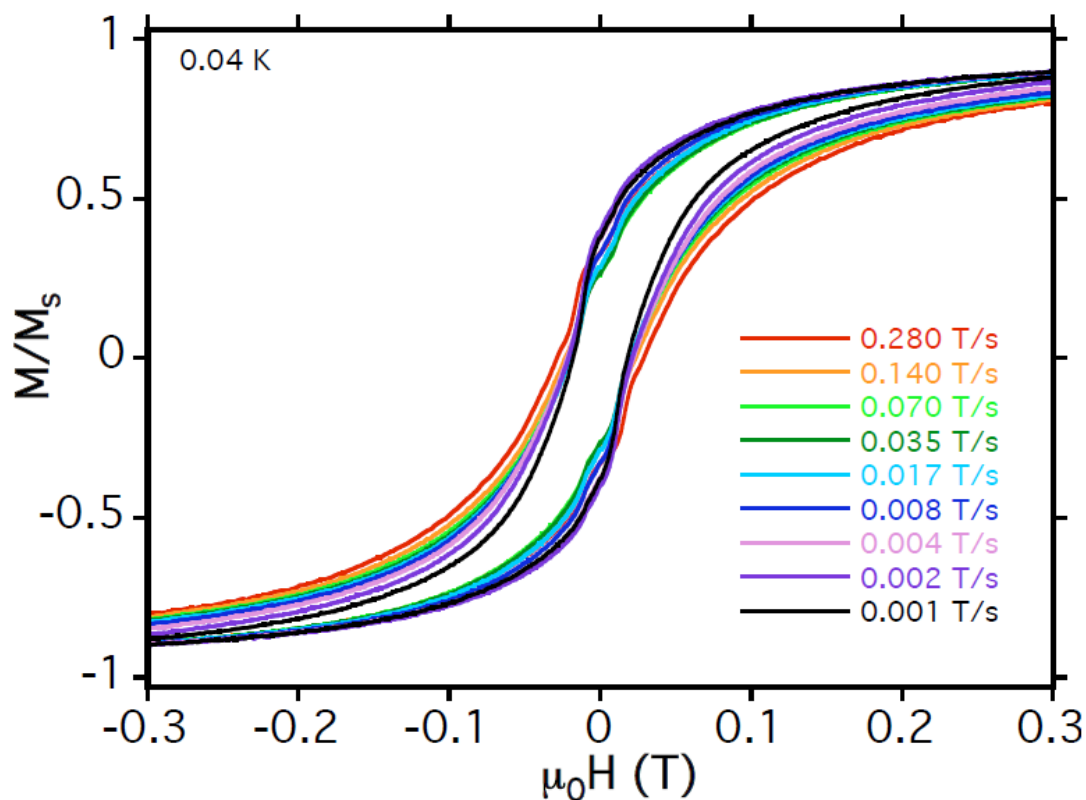
**Figure 5.7** Enlargement of hysteresis loops of $(F_{64}Pc)_2TbH$ at 0.04 K. M = magnetization, $M_s$ = saturated magnetization and $\mu_0H$ is the magnetic field.

Analysis of the data from Figures 5.7 and 5.8 shows the larger hysteresis curves indicating slower response as the frequency was increased. The steep fall in the magnetization at field $\mu_0H = 0$, in the case of **[4]**, was due to the smaller energy gaps of the multiplets and the presence of seven isotopes of Dy and is in keeping with previous observations. [88, 91] It showed a lower remenance response than in **[3]**, which does not fall as sharply at $\mu_0H = 0$. No evidence of quantum tunneling of magnetization was observed for either of the complexes. This was probably due to the use of undiluted samples. Analyses of the X-ray structures of the complexes show columnar stacking in which the

molecular units are effectively isolated from each other within each stack. However, the separation between the stacks is within the the van der Waals radii of the atoms and interactions are therefore possible as was also observed by the presence of a non-zero Curie- Weiss value in the DC magnetism of the complexes.
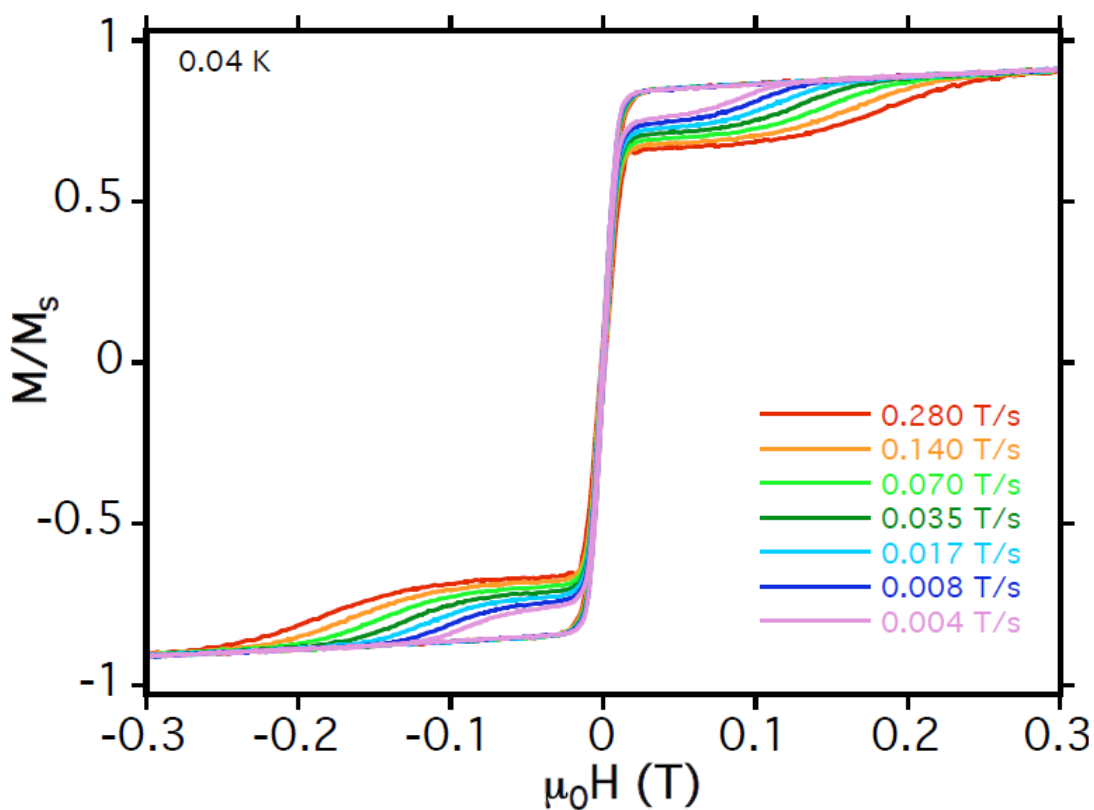


**Figure 5.8** Enlargement of hysteresis loops of $(F_{64}Pc)_2DyH$ at 0.04 K. M = magnetization, $M_s$ = saturated magnetization and $\mu_0H$ is the magnetic field.

Ishikawa et al.[7] has shown that the slowed response to the time varying magnetic field for the unsubstituted $[Pc_2Ln]^0$ and $[Pc_2Ln]^-$ complexes is not due to range order, but is a response of the SMM behavior brought on by uniaxial anisotropy. The AC

magnetic results obtained for **[3]** and **[4]** are similar to the response of the unsubstituted analogues and this is strong evidence for SMM behavior in these complexes.

## 5.5 AC Magnetism

After SMM behavior has been observed in magnetic materials, an important measure is the relaxation time, $\tau$, of the material. This can be measured directly or indirectly. Direct measurements include $\mu$SR and indirect measurements include the use of AC magnetism. The time varying applied magnetic field can be specified by its angular driving frequency, $\omega$ or in cycles per second, Hz. When $\omega \ll \tau^{-1}$, the magnetization is always in equilibrium over the time scale of the experiment. The measured susceptibility is the same as the static susceptibility and is called the isothermal susceptibility, $\chi_T$. If $\omega \gg \tau^{-1}$ then the magnetic system is effectively isolated from the surroundings and an adiabatic susceptibility, $\chi_S$ is measured, which is smaller than $\chi_T$.[199] A dynamic susceptibility can be expressed as:

$$\chi' = \chi_S + \frac{\chi_T - \chi_S}{1 + \omega^2 \tau^2}; \quad \chi'' = \frac{(\chi_T - \chi_S)\omega\tau}{1 + \omega^2 \tau^2} \tag{5.6}$$

The real part of the susceptibility is dispersion and the imaginary part is absorption. The Bloch's equation for magnetization along a longitudinal axis for these complexes may be expressed as:[7]

$$\frac{dM(t)}{dt} = \frac{1}{\tau}[\chi_M H(t)] - M(t) \tag{5.7}$$

where $H$(t) is the time varying magnetic field. This equation gives the result for $\chi''$ which can be used experimentally to obtain peak values at which a blocking temperature, $T_b$ may occur. It is given by:

$$\chi_M'' = \frac{\omega\tau\chi_M}{1 + \omega^2\tau^2} \tag{5.8}$$

A plot of $\chi_M''/\chi_M$ versus temperature, $T$ gives a graph in which $\tau$ coincides with $1/\omega$ at a peak temperature of which corresponds to $d\,(\chi_M''/\chi_M)/dT = 0$, yielding the relaxation time. A plot of relaxation time against the temperature within a specified range will yield the exponential dependence of the Arrhenius law given by:

$$\tau^{-1} = \tau_0{}^{-1}e^{-\frac{\Delta}{kT}} \tag{5.9}$$

where $\tau_0$ is the attempt time and $\Delta$ is the energy barrier for reorientation to the magnetic field. The equation can be manipulated in several ways, but it was made into a linear equation as natural logarithms and given by:

$$\ln(\tau^{-1}) = \ln(\tau_0^{-1}) - \frac{\Delta}{kT} \tag{5.10}$$

The actual plot in this case was $\ln(\tau^{-1})$ versus 1/T with a slope of $\Delta$/k.

## 5.6 AC Magnetism of (F$_{64}$Pc)$_2$TbH Above 2 K

AC magnetism data was collected on a sample of **[3]** using the SQUID-XL magnetometer by collaborators Ishikawa and co-workers at Osaka University, Japan. The sample was subjected to a driving AC field, ($H$(t)) of amplitude 3.9 Oe, under as much as three different DC static magnetic fields, ($H$dc) of 0, 1000 and 3000 Oe. Temperature dependence and frequency dependence data was generated from these tests.

The $\chi_M'$ and $\chi_M''$ response of to changes in temperature at driving frequencies of 1 kHz, 100 Hz, 10 Hz and 1Hz for $H$dc of 1000 Oe is shown in Figure 5.9. Slowed relaxation response to the oscillating magnetic field was observed and exhibited by the

peaks in $\chi'_M$ and $\chi''_M$. These AC susceptibility peak positions showed a general increase in temperature with increase in $H(t)$ and fell within the range 7 to 43 K. There was an approximate increase of 4 K for each peak position in $\chi'_M$ when moving from $H$dc of 1000 Oe to 3000 Oe. Increases in the peak positions of $\chi''_M$ were also observed between these said $H$dc, but they were less consistent and varied between 1 and 5 K. No clear AC susceptibility peaks were observed for $H$dc = 0. This was probably due to the sample not being diluted and suggests that interactions with neighboring $(F_{64}Pc)_2TbH$ molecules has some impacts on the phase lag.
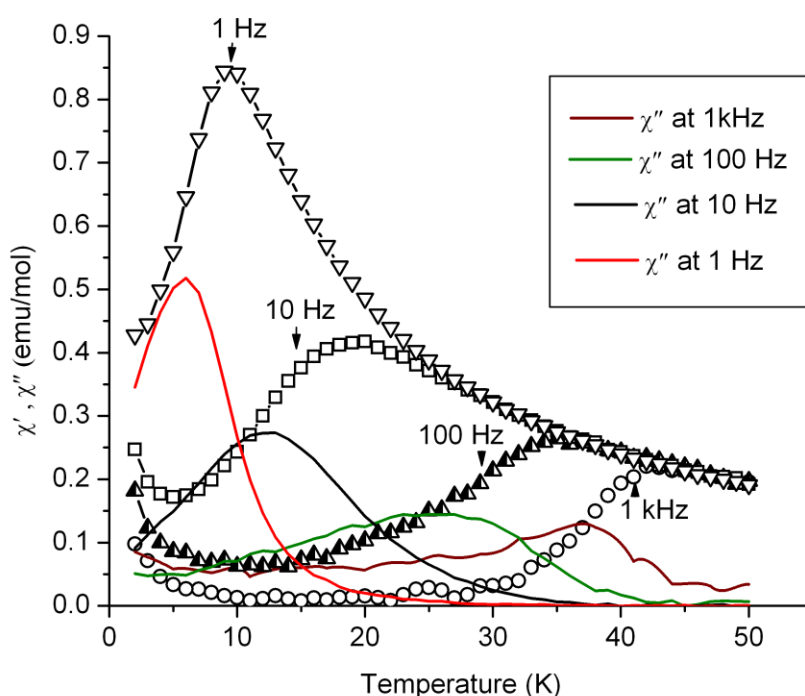


**Figure 5.9** Plot of the temperature response of $\chi''$ (solid lines) and $\chi'$ (line + symbol) to the AC magnetism of $(F_{64}Pc)_2TbH$ at static bias magnetic field of 1000 Oe.

Figure 5.10 shows a plot of $\chi''_M/\chi_M$ vs. $T$. The positions of $\chi''_M/\chi_M = 0$ representing the peak out-of-phase component of the AC susceptibility, occurring at 40,

33, 19 and 8 K for ac frequencies of $10^3$, $10^2$, 10 and 1 Hz, respectively. These values are within the range of 40, 32 and 15 K for AC frequencies of $10^3$, $10^2$, 10 Hz obtained from the anionic $[Pc_2Tb]^-[TBA]^+$.[88] An estimate of the pre-exponential factor ($1/\tau_0$) and the phenomenological barrier height to magnetic moment reversal were done for both the tests, where $H$dc of 3000 and 1000 Oe were applied. Ishikawa et al.[7, 89] carried out similar testing on both the diluted and undiluted samples and reported that the $\chi_M''/\chi_M$ peaks for 10, 100 and 997 Hz shifted to higher temperatures or remained unchanged on dilution.
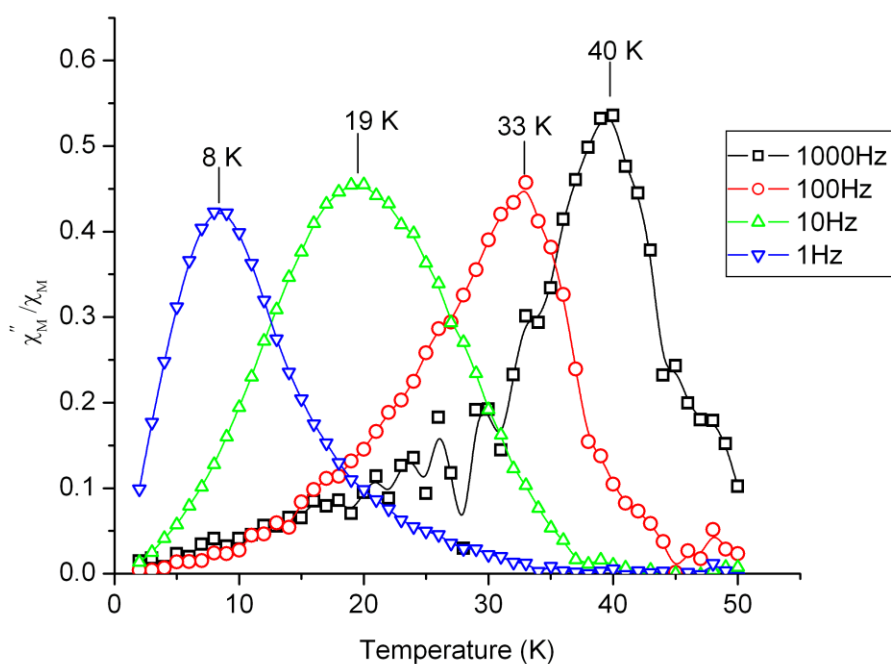


**Figure 5.10** Plot of $\chi_M''/\chi_M$ vs temperature for $(F_{64}Pc)_2Tb$ for DC field bias of 3000 Oe showing the peak out-of-phase components at 40, 33, 19 and 8 K for AC frequencies of $10^3$, $10^2$, 10 and 1 Hz, respectively.

For the undiluted samples, they obtained values of 28, 34, and 40 K respectively compared to those of the undiluted sample of 16, 32 and 40 K. This compares with both

the sets of results obtained from **[3]** which were 15, 29 and 37 K and 19, 34 and 40 K for

$H$dc fields of 1000 and 3000 Oe, respectively. The difference between the results for

diluted and undiluted samples was attributed to the presence of intermolecular

interactions between $[Pc_2Tb]^-$ which shorten the relaxation time in the lower temperature

range. This appears to be the case with **[3]** and as was shown with the $[Pc_2Tb]^-$ species,

the slowed magnetization relaxation of the $[(F_{64}Pc)_2Ln]^-$ is an intrinsic SMM property

rather than the result of intermolecular interactions and long range order.[200]
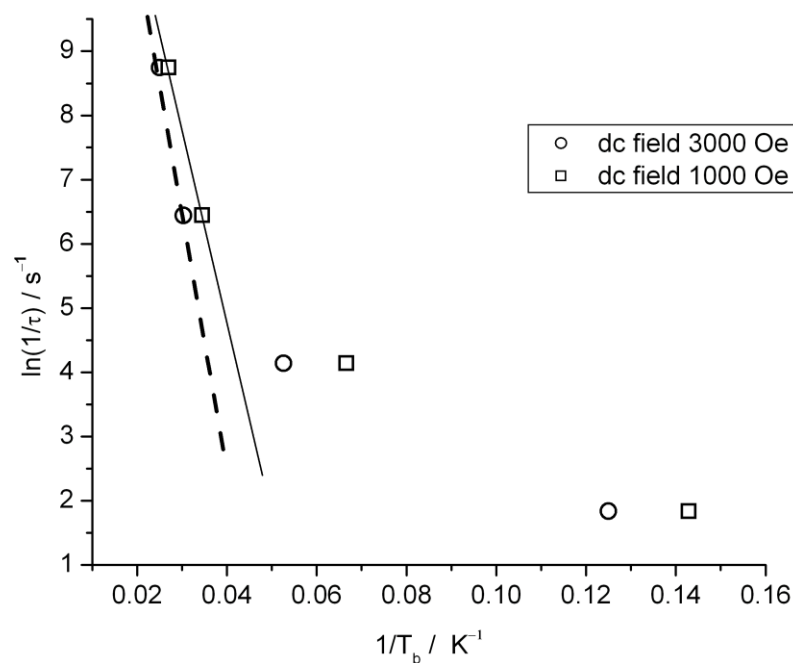


**Figure 5.11** Plots of the natural logarithm of the relaxation times $\ln(1/\tau)$ for the driving frequencies $10^3$, $10^2$, 10 and 1 Hz versus the reciprocal of the temperature, $T_b$, occurring at peak $\chi_M''/\chi_M$ values. Straight lines are drawn to represent the two points on each plot which represent temperatures above 25 K where the two phonon Orbach process occurs.

Ishikawa et al.[200] also explained the relaxation process of the lanthanide ions.

The relaxation mechanism was perceived in a different manner from that of $Mn_{12}$ or $Fe_8$

molecules. They formulated it as the exchange energy processes between the

paramagnetic ions and phonon radiation which are induced by the modulation of the crystal or ligand field under the action of lattice vibrations. Three major processes were considered between the two lowest substates: (1) a direct process which involves the absorption or emission of a phonon with the same energy separation between the spin up and spin down states generated by either Zeeman interaction, ligand field potential or both; (2) the Raman process where a phonon is scattered by the spin system based on the rules of Raman scattering and; (3) the two phonon Orbach (spin-lattice relaxation) process involving excited states of the relaxation ion. Of the three processes, the presence of a dominant Orbach process meant that the energy barrier to magnetization relaxation, $\Delta$, can be estimated via an Arrhenius type analysis as shown in Equation 5.10. Plots of $\ln(1/\tau)$ versus $1/T_b$ should yield a straight line. Ishikawa et al.[200] found that the plot was not an exact straight line. The high temperature data obtained with frequencies 997 to 10 Hz for the diluted sample of [Pc$_2$Tb]$^-$ formed a straight line and corresponded to temperatures above 25 K. The two-phonon Orbach process is dominant in range $25 \leq T \leq 40$ K and was thus determined to be the dominant process in this temperature range. The data below this temperature range was not found to fit this regime and was assigned the direct or Raman process.

An Arrhenius analysis carried out on the AC magnetometry data of (F$_{64}$Pc$_2$)TbH is plotted in Figure 5.11. Due to the use of undiluted sample, only two points remained in the temperature range $25 \leq T \leq 40$ K. Nevertheless, the two points were used to plot graphs of AC data with $H$dc of 1000 and 3000 Oe. The results of the Arrhenius analysis from Figure 5.11 for $H$dc of 3000 Oe, are $1/\tau_0 = 3.3 \times 10^8$ s$^{-1}$, with the energy barrier, $\Delta = 300$ cm$^{-1}$, while for $H$dc of 1000 Oe, the results are $1/\tau_0 = 2.7 \times 10^7$ s$^{-1}$ and the energy

barrier, $\Delta = 215$ cm$^{-1}$. These results span some earlier literature values ($\Delta = 230$ cm$^{-1}$ and $1/\tau_0 = 5.0 \times 10^7$ s$^{-1}$).[7, 88] for the [Pc$_2$Tb]$^-$ complex.

Figure 5.12 shows the ground state multiplets of some [Pc$_2$Ln]− complexes. In addition, the large energy difference between the two lowest substates of the Tb complex is indicative of a strong uniaxial anisotropy along the C$_4$ axis. This anisotropy is one of the requirements of SMM behavior.
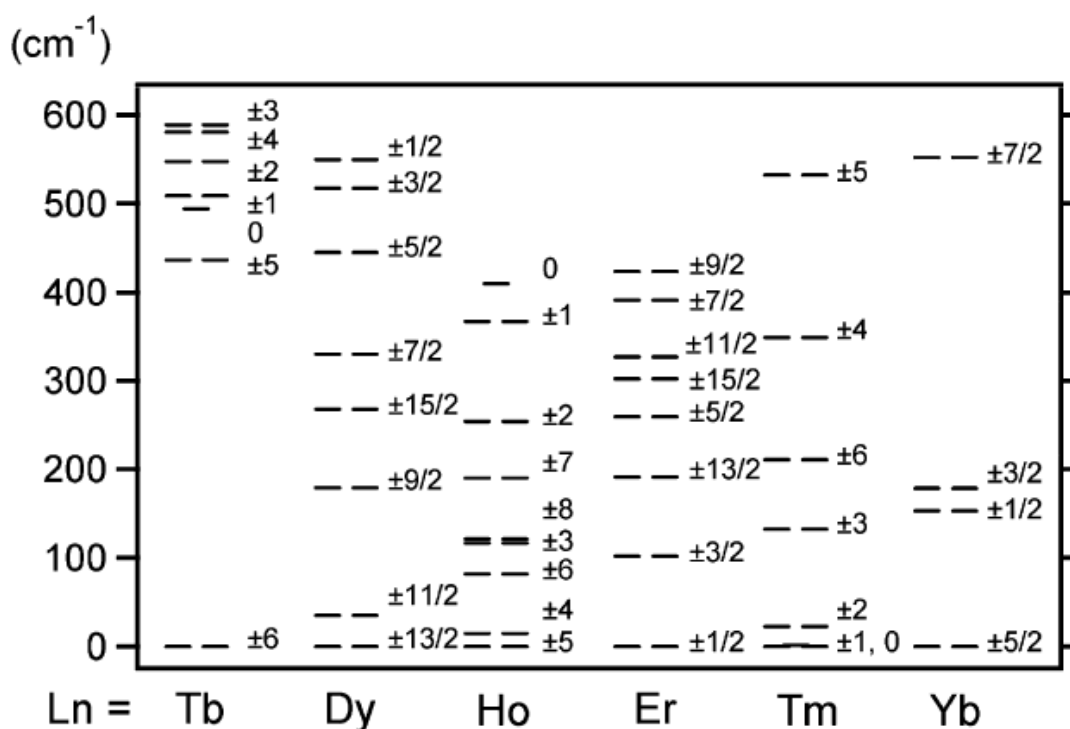


**Figure 5.12** The ground state multiplets of [Pc$_2$Ln]−TBA$^+$. (Ln = Tb, Dy, Ho, Er, Tm, Yb).[88]

The value of $\Delta$ was revised by Ishikawa et al.[198] in their paper in which they used solution $^1$H NMR and AC magnetometry to determine the ligand-field parameters of the some [Pc$_2$Ln]TBA ( Ln = Tb$^{3+}$, Ho$^{3+}$, Er$^{3+}$, Tm$^{3+}$ and Yb$^{3+}$) complexes. Based on the

energy difference between the two lowest sub-levels of about 400 cm$^{-1}$, $\Delta$ should be closer to this value.

In a study of the spin dynamics of the [Pc$_2$Tb]$^-$ through solid state $^1$H NMR, Branzoli et al.[201] confirmed the high temperature phonon assisted transitions among the crystal field levels, in general agreement with previous literature results.  The activation barriers in the processes were, however, found to be higher, with values ranging from 640 cm$^{-1}$ for diamagnetically diluted samples to 584 cm$^{-1}$ for the undiluted.  The said authors found that at cryogenic temperatures, the barrier to magnetization reversal and tunneling rates changed from sample to sample.  The diamagnetically diluted [Pc$_2$Tb]$^-$ molecules appeared to be affected by the samples magneto/thermal history.  This finding has implications for the matrix arrangements around [Pc$_2$Tb]$^-$ which can alter the splitting of the crystal field levels, its symmetry and hence its spin dynamics.   The higher temperature Orbach processes were also found to be present in neutral [Pc$_2$Tb]$^0$ molecules when probed with μSR and $^1$H NMR.  The barrier between the ground and the first excited states was similar to that of  [Pc$_2$Tb]$^-$  diluted in a TBA matrix (640 cm$^{-1}$) and the relaxation time was close to  0.1 ms at temperatures under 50 K.[174]  The increase in the temperature of about 10 K at which the neutral species showed slowed relaxation to AC magnetometry for the neutral [Pc$_2$Tb]$^0$  above the  [Pc$_2$Tb]$^-$  was earlier established.[7]

## 5.7 AC Magnetic Testing of $(F_{64}Pc)_2DyH$

Temperature dependent magnetism data was collected for $H$dc of 0, 1000, 2000 and 3000 Oe at $H$(t) of 1, 10, 100 and 1000 Hz. The amplitude of the AC driving frequency was 3.9 Oe. Temperature dependent plots of $\chi'_M$ vs. $T$ and for $\chi''_M$ vs. $T$ at these frequencies were done. The delayed relaxation (hysteresis) was observed by peaks in the curves of the four frequencies occurring at lower temperatures compared to [3]. No peaks were observed at $H$dc = 0 Oe and this was attributed to the use of the undiluted samples and the amplitude of the driving frequency. These AC susceptibility peak positions showed a general increase in temperature with increase in $H$dc and fell within the range 2 to 9 K. The higher frequencies of 1 kHz and 100Hz exhibited little change with increased $H$dc while the lower frequencies showed an approximate 2 K decrease in each peak position in $\chi'_M$ when moving from the $H$dc of 1000 Oe through to 3000 Oe. Changes in the peak positions of $\chi''_M$ for the higher frequencies were similar and only an approximate 1 K temperature change was observed for the two lower frequencies when moving from the $H$dc of 1000 Oe through to 3000 Oe. More detailed AC magnetic data on [4] is shown in Appendix D.

A more detailed analysis of the frequency dependent plots, $\chi'_M$ vs. $f$ and $\chi''_M$ vs. $f$ was carried out. The frequency range was 0.1 Hz to 10 kHz at temperatures of 2, 3, 4, 5, 6, and 7 K. Hdc was 0, 500, 1000, 2000 and 3000 Oe. Within the temperature range, there was a general shifting to higher frequencies for the lower temperature $\chi''_M$ peaks with increase of $H$dc from 500 to 3000 Oe. The effect was divergence of the temperatures towards the range of frequencies 20<$f$<300 Hz.

The frequency dependency data was used to carry out an Arrhenius analysis with peaks $T_b$, at 2, 3, 4, 5, 6, and 7 K. As with data from [3], an undiluted sample was used and peaks for the four $H$dc were plotted. The graph of $\ln(1/\tau)$ vs. $1/T_b$ was plotted and is shown in Figure 5.13. The graph showed that as the $H$dc was reduced the relationship shifted from being convex towards being linear, as was expected in the Arrhenius analysis. An approximation based on the predicted diluted sample and an $H$dc = 0 Oe was made by plotting the three points on the graph at $H$dc = 500 Oe. This approximation gave a $\tau_0^{-1}$ of 1.6 x $10^5$ $s^{-1}$ and a $\Delta$ = 31 $cm^{-1}$. It compares to the literature value of $\Delta$ = 30 $cm^{-1}$ and $\tau_0^{-1}$ = 3.0 x $10^5$ $s^{-1}$ for $[Pc_2Dy]^-$.[200]
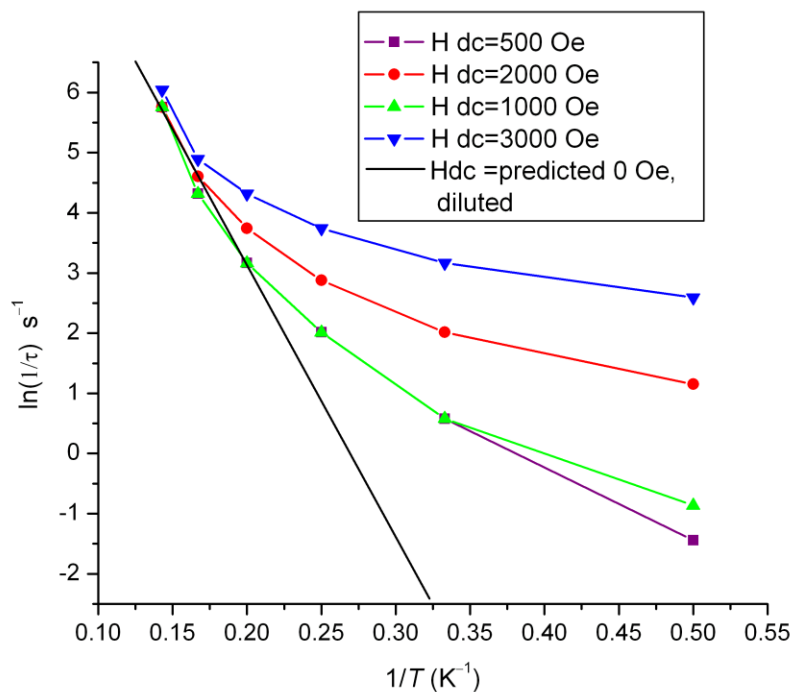


**Figure 5.13** Plots of the natural logarithm of the relaxation times $\ln(1/\tau)$ for the frequencies associated with temperatures 2, 3, 4, 5, 6, and 7 K and versus the reciprocal of the temperature, occurring at peak $\chi_M''/\chi_M$ values. The straight line (black) was drawn to approximate the diluted sample with $H$dc = 0 Oe, from which $\Delta$ and $\tau_0^{-1}$ were estimated.

Despite not having AC magnetic data on the diluted sample, the properties of the [4] showed several other properties in common with the $[Pc_2Dy]^-$. It was reported that the $\chi_M''/\chi_M$ peaks shifted to slightly higher temperatures on dilution, but to a lesser extent than in the case of the $[Pc_2Tb]^-$.[200] The peaks for the undiluted sample were located at 4.5, 7, and 11.5 K while for the diluted sample, they shifted to 5.5, 7.5 and 12 K for AC frequencies of 10, 100 and 997 Hz, respectively. The Arrhenius analysis result of $\Delta = 31$ cm$^{-1}$ is general agreement with the energy difference between lowest and second lowest sublevels of $Pc_2Dy$. Furthermore, the approximation of the straight line on all the points on the $\ln\tau^{-1}$ vs. $1/T_b$ graph appears reasonable because previously, all points were found to lie on a straight line indicating that the Orbach process was again dominant but in the entire temperature range, 12 to 3 K.[200] The reduction in the value of $\Delta$ for $[Pc_2Dy]^-$ relative to the Tb complex was reported as due to the lower energy of the substate through which the two phonon relaxation process takes place.[200]

Special frequency dependence tests of $H$dc were carried out at 2 K. $H$dc was varied in steps of 50 Oe from 0 to 200 Oe and in steps of 100 Oe up to 2000 Oe. The plots examined the frequency dependence of both $\chi_M'$ and $\chi_M''$ peaks. The graphs on Figure 5.14 showed that between $H$dc of 0 Oe and 100 Oe peak position of $\chi_M''$ shifted from 1000 Hz to about 7 Hz. There was then a slower shift of the peak $\chi_M''$ position to a minimum of about 0.3 Hz at at $H$dc = 800 Hz. The $\chi_M''$ position then converged within the frequency band 0.4 Hz to 4 Hz for a further increase in $H$dc up to 2000 Oe.

The $\chi_M'$ curves exhibited a general falling off in magnitude as the frequency was increased. Increasing $H$dc resulted in curves starting to fall at lower frequencies with a convergence in a frequency band approximately between 0.1 and 10 Hz. Professor

Ishikawa (email communication)[202] noted that he had never observed this phenomenon before.



(a)                                                                 (b)

(c)                                                                 (d)
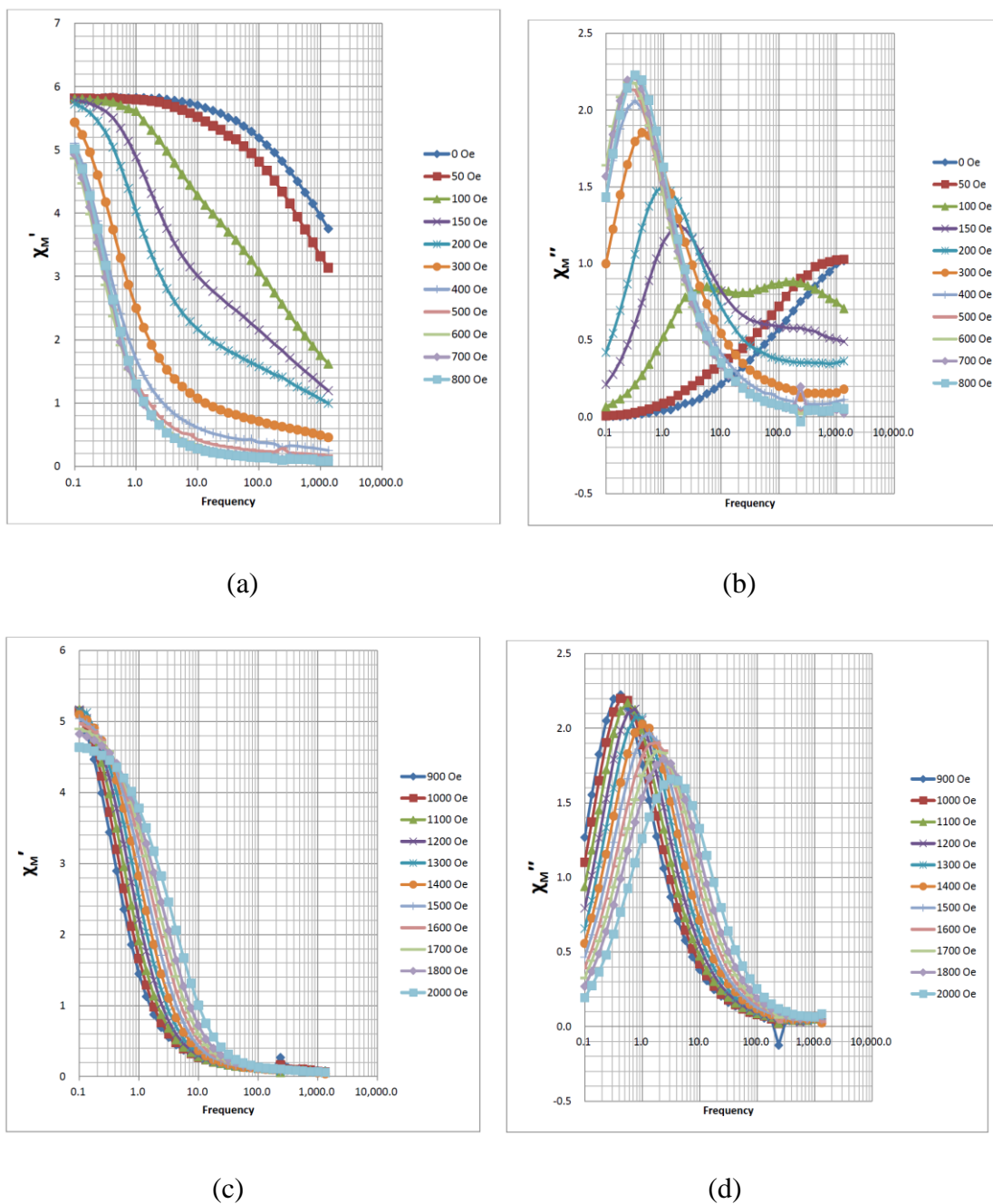
**Figure 5.14** The frequency dependence at both $\chi'_M$ and $\chi''_M$ peaks of $(F_{64}Pc)_2DyH$ at varied $H$dc at a temperature of 2 K.

**5.8  DC Magnetism of $(F_{64}Pc)_2TbH$ and $(F_{64}Pc)_2DyH$ at 5% Dilution in Eicosane**

The DC magnetism of **[3]** and **[4]** was measured in a dilute 5% (mol/mol) frozen solution of eicosane, $C_{20}H_{42}$. A DC magnetic field of 500 Oe was applied between the temperatures of 1.8 and 300 K.   Plots of $\chi_M$ vs. $T$, $\chi_M^{-1}$ vs. $T$ and the effective magnetic moment, $\mu_{eff}$ vs. $T$ were done for both complexes and are shown on Figure 5.15.

**Table 5.1** Curie-Weiss Constants and Magnetic Test Results

| **Complex** | **C (emu·K/mol)** | **θ (K)** | **$\mu_{eff}$ (BM)** | **R** |
|---|---|---|---|---|
| $(F_{64}Pc)_2TbH$ | 10.88 | −2.29 | 9.33 | 0.9997 |
| $(F_{64}Pc)_2DyH$ | 13.03 | −0.53 | 10.2 | 0.9999 |

A *Levenberg-Marquardt (LMA)* non-linear least squares algorithm was used to fit the Curie-Weiss (C-W) law on the plot $\chi_M$ vs. $T$, while a linear regression was done on the $\chi_M^{-1}$ vs. $T$.  While the LMA minimizes this function, experience with it in this context, is that it tends to underestimate the values of constants C and θ in the C-W law relative to the linear regression.  This happens because the linear regression model has a goal of adjusting the values of slope and intercept to find the line that best predicts y from x in a sample of  x,y  data.  More precisely, the goal of linear regression is to minimize the sum of the squares of the vertical distances of the points from the line.[203] Alternatively, the *LMA* algorithm is an iterative technique that locates the minimum of a function that is expressed as the sum of squares of nonlinear functions.  That is, it is a numerical solution to the problem of minimizing a function.[204, 205]   This highlights the differences in how each algorithm treats the data.  Additionally, LMA treats the raw data herein, while the linear regression operates on the reciprocal of the susceptibility vs. temperature.

The results of the linear regression on $\chi_M^{-1}$ vs. $T$ are, therefore, presented on Table 5.1.
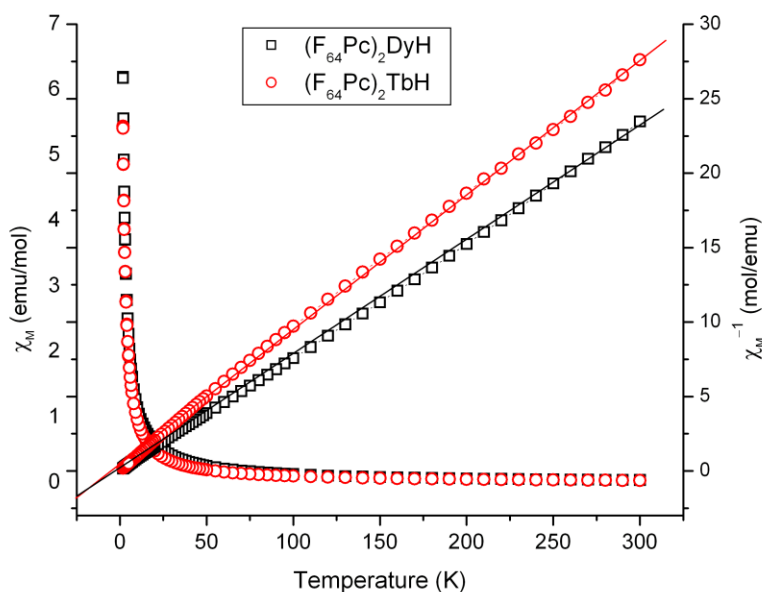


**Figure 5.15** Plots of DC magnetic testing of a 5% (mol/mol) dilution of $(F_{64}Pc)_2TbH$ and $(F_{64}Pc)_2DyH$ in eicosane. The left scale represents $\chi_M$ vs. $T$ while the right scale represents $\chi_M^{-1}$ vs. $T$.

The values C, $\theta$ and $\mu_{eff}$ lie within the range previously obtained. Examination of the plot of $\mu_{eff}$ vs. $T$., Figure 5.16, reveals that curve for **[3]** follows a regular path with $\chi_M T$ increasing with an increase in temperature and then approaches a limiting value. However, the curve for **[4]** increases more rapidly with temperature, reaches a maximum and then begins to decrease. This observed $\mu_{eff}$ vs. $T$ behavior of **[4]** is being interpreted as an initial anti-ferromagnetic behavior at low temperature (up to about 30 K) which then changes to ferromagnetic behavior at higher temperature and at >150 K, the thermal action begins to reduce the ferromagnetic behavior as it approaches 300 K, hence the reduction in $\mu_{eff.}$ A similar behavior of $Pc_2Dy$ was reported by Trojan et al.[86]
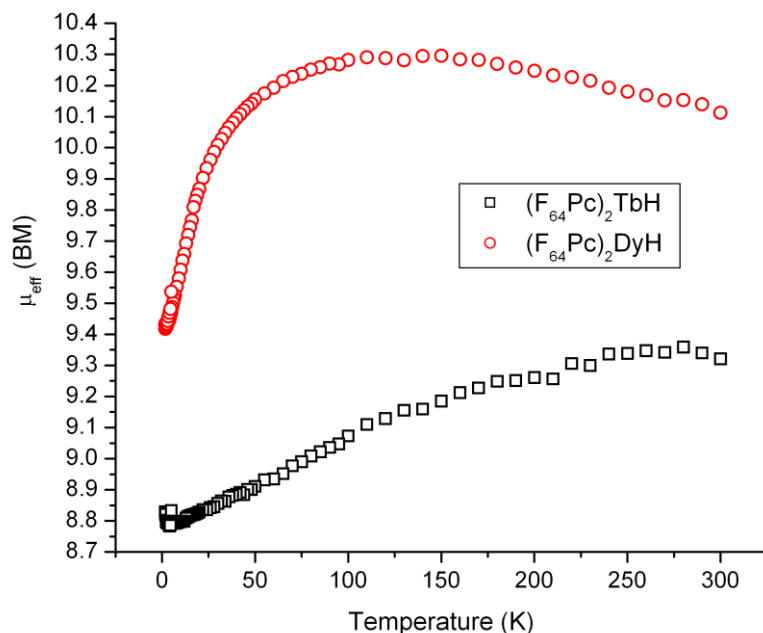
**Figure 5.16** Plots of DC magnetic tests of a 5% (mol/mol) dilution of $(F_{64}Pc)_2TbH$ and $(F_{64}Pc)_2DyH$ in eicosane showing the effective magnetic moment, $\mu_{eff}$ vs. temperate.

### 5.9 Summary

DC magnetization studies revealed that both $(F_{64}Pc)_2TbH$, **[3]** and $(F_{64}Pc)_2DyH$, **[4]** exhibited an antiferromagnetic Curie-Weiss behavior with no special observed features such as spin-glass behavior. The ZFC-FC test carried at low DC magnetic field (10 Oe) and higher field (5000 Oe) within the temperature range 2-300 K produced similar results. On an average, the $\mu_{eff}$ and Weiss constants, $\theta$ were found to be 8.9 BM and −2.0 K and 10.4 BM and −4 K for **[3]** and **[4]**, respectively. DC magnetism results of tests carried out on the diluted samples of **[3]** and **[4]** supported these results except for the $\theta$ value of **[4]** which was only −0.53. These values are within the range reported for one electron reduced Tb and Dy sandwich lanthanide complexes reported elsewhere.[86, 198]

Results of the AC magnetization studies in the range 2-50 K revealed $\chi_M''/\chi_M$ peak temperatures of 19, 33 and 40 K similar to literature values. The energy barrier to magnetization relaxation was consistent with literature values within the temperature range $25 \leq T \leq 40$ K. The source of slow magnetization relaxation of these classes of molecules has been reported to be influenced by the ligand field. The complexes' ligand field induces a splitting of the electronic sub-structures making an Orbach relaxation process possible. Sub-states formed from this splitting gives rise to a series of "spin up" and "spin down" states. The ground multiplet of the Tb complex is J = 6 and splitting and the lowest $J_z$ sub-states are $J_z = \pm 6$ corresponding to the maximum and minimum states. The energy barrier, and the pre-exponential factors obtained for **[3]** was in the range $\Delta = 200$-$300$ cm$^{-1}$ and $\tau_0^{-1} = 3.0 \times 10^8$-$2.8 \times 10^7$ s$^{-1}$ and for **[4]**, $\tau_0^{-1} = 1.6 \times 10^5$ s$^{-1}$ and a $\Delta = 31$ cm$^{-1}$. These values are in the range obtained for the respective unsubstituted $^{[}Pc_2Tb]^-$ and $[Pc_2Dy]^-$ analogues using similar test methods.

Magnetization studies carried out on these complexes in the sub-kelvin temperature range (0.04 – 1.1 K) on the micro-SQUID machine, revealed hysteresis with AC magnetic field rates between 0.001 T/s and 0.280 T/s. Both **[3]** and **[4]** exhibited slowed response to the changing magnetic fields, characteristic of the behavior of the SMMs previously studied in this class of materials

Close examination of the sub-kelvin temperature magnetic hysteresis of **[3]** and **[4]** did not reveal the staircase hysteresis loops which are known to accompany (QTM). This is believed to be due to the use of the undiluted samples in the test. Dispersing these molecules in the appropriate matrix to increase the distance between the molecular units should allow the observance of QTM.

The AC magnetic testing of **[4]** exhibited some anomalous results. The $\chi_M{}''$ vs. $f$ plot peaked at a frequency which shifts to lower value as temperature was raised. Interestingly, with $H$dc = 0, the shift of the peak of $\chi_M{}''$ vs. $f$ appeared as if was almost temperature independent at around 100 Hz.  More detailed AC magnetic testing at 2.0 K, with $H$dc varying between 50-100 Oe, revealed that the $\chi_M{}''$ peaks seemed to converge within a small frequency range of about 0.4 Hz to 4 Hz at $H$dc ~ 2000 Oe.

# CHAPTER 6

## MCD AND REDOX PROPERTIES
### of $(F_{64}Pc)_2LnH$ COMPLEXES (Ln = Tb, Dy)

### 6.1 Overview

Electroanalytical methods are a subset of techniques in analytical chemistry. The techniques include potentiometry, voltammetry and coulometry. Common to all of these methods is the setting up of an electrochemical cell in which current or potential difference of an analyte contained in the cell is measured.[206, 207] In potentiometry, the difference in potential between electrodes is measured while in coulometry the amount of matter transformed during an electrolysis reaction is measured by quantifying the charge through current measurements. Voltammetry is used to obtain information about the analyte by measuring the current while the applied potential is varied.[208]

There are several variants of the voltammetric techniques. These include Cyclic Voltammetry, (CV) Linear Sweep Voltammetry, Polarography, Differential Pulse Voltammetry, (DPV) Staircase Voltammetry and Anodic or Cathodic Stripping Voltammetry. In analytical chemistry, CV and DPV are among the prominent methods for analyzing the redox properties of substances.

### 6.2 Cyclic Voltammetry

Voltammetry experiments investigate the half cell reactivity of an analyte by obtaining current information on the cell while sweeping the applied voltage. The electrochemical cell generally has a set-up which involves three electrodes called the working, auxiliary and reference electrodes. The working electrode makes contact with the analyte which is

usually in the form of an aqueous or non-aqueous solution or a solvent. The tasks of applying the controlled potential to the working electrode and then to balance the charge due to electrochemical activity at its interface are shared between the auxiliary and reference electrodes. Control and measurement of the potential on the working electrode is done by the reference electrode which does not allow the passage of a current. The reference electrode is a half cell with known reduction potential and it therefore acts as a potential reference. Electrochemical activity at the working electrode will result in an observed current. The auxiliary electrode can then vary its potential within the range to achieve this observed current which can effect oxidation or reduction of the supporting electrolyte or solvent (analyte). This three electrode system is the base system used in voltammetry for obtaining current and voltage information. A schematic of the three electrode system is shown in Figure 6.1.
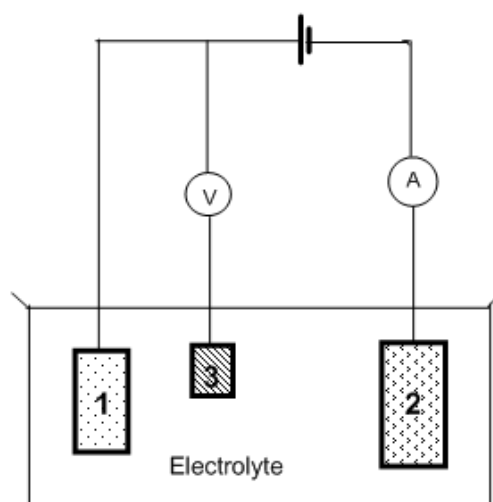
**Figure 6.1.** Three-electrode setup: (1) working electrode; (2) auxiliary electrode; (3) reference electrode.

Different electrodes can be tuned for specific systems and ranges. Working electrodes must be an electronic conductor and be electrochemically inert. Common materials used for the working electrodes in voltammetry include gold, platinum, mercury and glassy carbon. During use, materials may be adsorbed onto the surface of the working electrode and cause degradation of its performance. These electrodes should be cleaned regularly to remove the deposits.

The reference electrode is required have a constant potential. The passage of a current through this electrode or changes in temperature will cause changes in potential. Concentration of the filling electrolyte can also affect the potential of the cell. These are minimized by having high input impedance for the reference electrode and using a constant temperature apparatus during testing, and proper storage of the electrode to maintain concentration of the electrolyte as necessary. Common reference electrodes include the calomel consisting of $Hg/Hg_2Cl_2$ and the silver/silver chloride (Ag/AgCl). The Standard Hydrogen Electrode, (SHE) is considered the standard electrode from which the other electrodes are referenced.

The auxiliary electrode typically provides a surface for a redox reaction to balance the one occurring at the surface of the working electrode and normally does not need any special care, but its surface area must match or be larger than that of the working electrode. It is commonly made from platinum wire.

### 6.2.1 Theory of Cyclic Voltammetry

In cyclic voltammetry and the applied potential is swept at particular rate, $v$(t) commencing at an initial value of $E_i$. It is customary to sweep it in a negative direction initially to cause reduction, and at a predetermined value, it is switched in the positive

direction. In the electrochemical cell, a reversible reaction involving a single electron is represented by:

$$M^+ + e^- \leftrightharpoons M \tag{6.1}$$

where $M$ is the analyte. The $M^+$ has migrated to the electrode and in the case of reduction, for example, receives an electron from the electrode surface before diffusing away to the bulk solution. Electric current at the surface of the working electrode is generated by the transfer of electrons from the electrode to the redox species. In the absence of a redox couple, the electrode-solution interface acts as an electric double layer, and may be approximated to a parallel plate capacitor.

The current flow through the solution of the electrochemical cell is carried by the ions. It is known as the Faradaic current and it depends on the kinetics of electron transfer and the rate at which the redox species diffuse to the electrode surface. For the one electron transfer, (Equation 6.1) the kinetics of the electron transfer may be described by the Nernst equation on the assumption that the electron transfers are reasonably fast. The Nernst equation may be written as:

$$E = E^{0\prime} - \frac{RT}{nF} ln \frac{[M^+]}{[M]} \tag{6.2}$$

where E is the half-cell reduction-potential at the temperature of interest, $E^{0\prime}$ is the standard cell potential at the temperature of interest, $R$ is the universal gas constant: $R = 8.314\,472(15)$ J K$^{-1}$mol$^{-1}$, $F$ is the Faraday's constant: $F = 9.648\,533\,99(24){\times}10^4$ Cmol$^{-1}$, and n is the number of moles of electrons transferred in the cell reaction or half reaction. The Nernst equation can be reduced to the form in Equation 6.3 for a cell at 25°C with *RT/F* approximated to a constant 25.693 mV and the natural logarithm function changed to logarithm to the base 10. The reduced form is:

$$E = E^{0\prime} - 0.0592 log \frac{[M^+]}{[M]} \tag{6.3}$$

The rate at which the ions diffuse through to the electrodes is described by Fick's law for mass transfer by diffusion. It relates the distance from the electrode ($x$), time, ($t$) and reactant concentration, $C_M$ to the diffusion coefficient, $D_M$. That is:

$$\frac{\partial C_M}{\partial t} = D_M \frac{\partial^2 C_M}{\partial x^2} \tag{6.4}$$

### 6.3 Spectroelectrochemistry

Spectroelectrochemistry may be best described as the combination of techniques of electrochemistry and spectroscopy in the study of the redox chemistry of organic, inorganic, biochemical and biological molecules.[209, 210] It can follow changes in oxidation states of species at the electrode through spectroscopic measurements at the electrode/electrolyte interphase. In-situ spectroscopic techniques in spectro-electrochemistry are varied but in general include UV-visible, IR, X-rays, magnetic resonance methods and microwave. The electromagnetic radiations used in the techniques are detected/applied in various methods. These methods include transmission, reflection, polarized light, and scattered light.[211]

### 6.3.1 Transmission Type Experiments

These types of experiments are based on the reduction in the intensity of a beam of light after it interacts with an electrochemical cell. Application of this method depends on the transparency of the electrolyte to the range of wavelengths used. For water, UV radiation above 200 nm and all wavelengths of visible light are transmitted. The absorbance, A is usually measured in these experiments and it is given by;

$$A = -\log{(1 - \alpha)} \qquad (6.5)$$

where α is the absorptance. Light entering the interphase with intensity, $I_0$ will be reflected, transmitted, scattered and absorbed. The law of conservation of energy requires that the sum of these processes add up to unity:[211]

$$1 = \alpha + \tau + \rho + \sigma \qquad (6.6)$$

where $\alpha = I_{abs}/I_0$, $\tau = I_{tr}/I_0$, $\rho = I_{refl}/I_0$, and $\sigma = I_{scat}/I_0$. The light beam is usually applied perpendicular to the electrode surface in this case.

The heart of spectroelectrochemistry of this type lies in the use of Optically Transparent Electrodes (OTEs). Optically transparent cells suitable for use in conventional UV-visible spectrometer can be made.[209, 210, 212] In general, OTEs can be a thin metal film (such as Au or Pt) deposited on transparent substrate such as glass or quartz,[213, 214] a glass plate coated with a thin film of optically transparent conducting material (such as Indium doped Tin Oxide (ITO)),[215] micro meshes in which the mesh openings allow the passage of light, (e.g. gold mini grids) between transparent substrates,[216-218] and thicker free standing metal meshes.[211] Many new materials and assemblies have been developed for use as OTEs and Optically Transparent Thin-Layer Electrodes (OTTLEs) such as diamond and graphene based electrodes,[219, 220]hybrids,[221] colloidal materials deposited between substrates instead of mini grids,[222] and emerging materials.[223]

The OTE is set up in the electrochemical cell either as a single working electrode or as a stack of working electrodes and is combined with a reference and auxiliary electrode usually in conventional set-up as in Figure 6.1. During operations, the transmitted intensity is measured as a function of the potential. This is used with other

parameters to calculate absorbance as the wavelength is varied in a UV-visible experiment.

### 6.3.2 Reflectance Type Experiments

In reflectance type spectroelectrochemical experiments, the intensity of the reflected beam is measured as a function of potential. The reflectance is thus given by:[211]

$$\rho(E) = I_{refl}(E)/I_0 \tag{6.7}$$

where, E is potential. The reflectance is measured at two potentials. One of these is a reference potential and is ideally taken at a film free surface and the other at the potential at which a surface film is formed. The normalized differential reflectance, $\Delta\rho(E)/\rho(E)$ is the plotted versus potential or wavelength.[224]

UV-visible differential reflection spectroscopy is a suitable method for investigating multilayer films of oxides or metals or monolayers of strongly absorbing molecules, atoms or ions. It is useful for obtaining absorption spectra of molecular films as a function of the redox state of the film, which depends on electrode potential.

### 6.4 Magnetic Circular Dichroism (MCD)

### 6.4.1 Introduction to MCD

Electromagnetic waves are transverse waves in which the energy travels as oscillations of magnetic and electric fields oriented at 90° to each other. In ordinary light, there is no preferential oscillation of the field vectors. Maxwell's theory predicts that light can be polarized since it is a transverse wave. After passing through certain crystals such as tourmalines, ordinary light can emerge with oscillation of its electric field vector in one

plane. The light is then said to be plane linearly polarized. The electric vector actually remains in a plane containing the propagation direction.

In general, the polarization can be linear, circular or elliptical. The classification of the polarization depends on the orientation of the electric vector. For monochromatic light, the amplitude of the vector changes sinusoidally with time. When light is circularly polarized, the tip of the electric vector describes a circular helix about the propagation direction. The amplitude of the vector is constant. The frequency of rotation is equal to the frequency of the light. Elliptically polarized light differs from circularly polarized light in that although the vector also rotates about the propagation direction, the amplitude of the vector changes so that the projection of the vector on a plane at right angles to the propagation direction describes an ellipse. Circular polarization is a specific case of the more general elliptical polarization.

In circular polarization, the electric field vector may rotate to the right or to the left. As seen from the receiver of the light, the rotation may be termed as left-handed or right-handed and the polarization is described based on this handedness. Dichroism in certain anisotropic materials is the property of having different absorption coefficients for light polarized in different directions.[225] Circular dichroism is, therefore, the differential absorption of left- and right-circularly polarized light. It is observed in solution of enantiomers. The circular dichroism of a chiral molecule can in principle be used to determine its enantiomeric form, referred to as its absolute configuration.[226]

Faraday first showed that optical activity could be induced in matter by the application of a magnetic field in the direction of the propagation.[227] This led to the development of Magnetic Induced Circular Dichroism spectroscopy or simple Magnetic

Circular Dichroism (MCD). MCD is the differential absorption of left and right circularly polarized light induced in a sample by the application of a magnetic field oriented parallel to the direction of light propagation. MCD has currently found applications in macromolecules with metal centers such as proteins, phthalocyanines and metal porphyrins.[228]

### 6.4.2 MCD Theory

MCD spectroscopy is based on the difference in absorption, ΔA of left circular polarized light (lcp) and right circular polarized (rcp). That is:

$$\Delta A = A_{lcp} - A_{rcp} \qquad (6.8)$$

where $A_{lcp}$ = absorption of lcp and $A_{rcp}$ = absorption of rcp. In dilute solutions, Beers law is applicable and ΔA may also be given by:[226]

$$\Delta A = (\Delta \varepsilon) c l \qquad (6.9)$$

where $\Delta \varepsilon$ is the difference in the extinction coefficients of lcp and rcp, $\varepsilon_{lcp}$ - $\varepsilon_{rcp}$; c is the solute molarity; and $l$ is the sample's path length in centimeters.

Electric dipole transitions selection rules for the rcp light is a dipole moment of −1 and for +1 for lcp light.[229] The MCD dispersion can be expressed as a function that is linear in the applied magnetic field strength B.[230, 231] That is:

$$\frac{\Delta A}{E} = \gamma B \left[ A_1 \left( \frac{-\partial f(E)}{\partial E} \right) + \left( B_0 + \frac{C_0}{kT} \right) f(E) \right] \qquad (6.10)$$

where $\gamma$ is a collection of constants, k is the Boltzmann constant, $T$ is the temperature, E is the energy of the incident radiation and $f(E)$ is a band shape function.

The constants A, B, and C are characteristic parameters specific to a given molecule and to a particular transition. It is customary to refer to the contributions in

Equation 6.10 containing A, B, and C as A-, B-, and C- terms, respectively. The MCD intensity is proportional to three different contributions. The B- and C- terms both show an absorption band shape in MCD. However, the A- term corresponds to a signal with a derivative band shape. The A and B terms are temperature independent, whereas MCD C- term intensity is temperature dependent. Figure 6.2 illustrates the different origins of the A-, B- and C- term mechanisms.
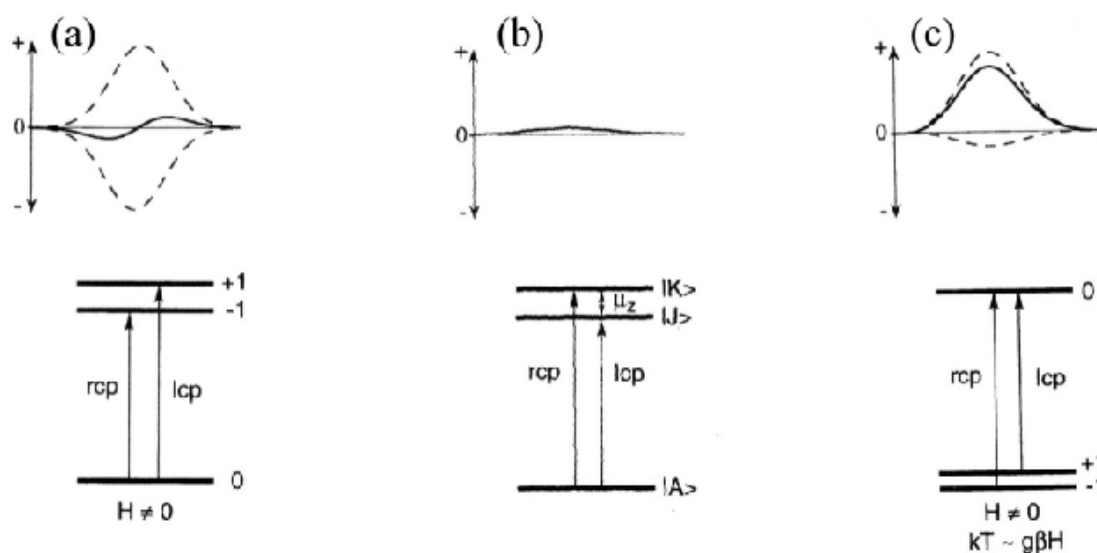


**Figure 6.2** MCD mechanisms (a) A-term, (b) B-term and (c) C-term.[232]

The intensity of the A- term arises as result of Zeeman splitting in the excited or ground degenerate states. Zeeman splitting is usually small (a few cm$^{-1}$ in energy) which results in almost a cancellation of the oppositely signed lcp and rcp light and results in a derivative band shape. The observance of the B- term occurs when magnetic field induced mixing of the excited state, |J> with an energetically close intermediate state, |K> occurs. It may also be observed in field induced mixing between the ground state, |A>

and an intermediate state, |K>.  A significant B- term intensity only arises if |K> is close in energy to either |J> or |A>.  Whereas it is necessary for the for the energy separation in |A> and |K> to be small enough to allow mixing, it should be large enough to prevent |K> from being thermally populated, otherwise this leads to C- term intensity.

The intensity of C- term arises from a degenerate ground state  which undergoes a Zeeman Effect splitting due to the applied magnetic field.  Because degenerate ground states are due to spin degeneracy, only paramagnetic compounds exhibit C- term signals. Increasing the applied magnetic field and lowering the temperature will result in increased C- term intensity up to the saturation limit.  The C- term is the most important MCD mechanism at low temperature.[233-235]

The temperature and magnetic field dependent C-term intensity contains the complete information of the properties of the ground state including g values and zero-field splitting parameters as well as the polarization of the electronic transitions. Experimentally, the C-term spectrum can be calculated from MCD raw data by subtraction of MCD spectra measured at different temperatures but with the same applied magnetic field.  A- and B- terms can be distinguished via their different band shapes.[232]

### 6.4.3 MCD Studies of SMMs

MCD has been shown to be an invaluable tool in the study of the properties of SMMs. The confirmation of SMM behavior in a molecule traditionally depends on techniques that use bulk samples in AC magnetometry.  This technique relies on the use of magnetically dilute samples in order to rule out long range order as the primary cause of magnetic hysteresis.  While these techniques can provide this information, there are

drawbacks in finding the correct diamagnetic dilution matrix, one which will not react or affect the properties of the material under test.

The potential application of SMMs in high density information storage media requires "spin up" and "spin down" states to persist in order to maintain the integrity of the stored information. The application of a magnetic field provides a means of inducing or erasing electron spin polarization. The use of optical methods of the reading the sign and extent of spin polarization and, possibly, of creating or erasing spin polarization in SMMs has been investigated.[236] Optical methods provide a highly sensitive and rapid way to read such information. MCD spectroscopy on frozen solutions is also considered a powerful tool for studying SMMs because the electronic transitions are better resolved in the absorption spectrum compared to the spectra of unpolarized light. The spin polarized ground state induced by the applied magnetic field is measured through the intensity and sign of absorption of circular polarized photons. Manipulation of the selection rules and orientation of axial polarization can result in information from an isotropic sample which is wavelength, and hence orientation dependent.[236]

## 6.5 Electrochemistry of $(F_{64}Pc)_2Ln$

Electrochemistry of the sandwich phthalocyanine compounds have been studied extensively.[237, 238] The studies included both homoleptic and heteroleptic complexes with a variety of different substituents.[72, 239] Starting from the neutral complex, they have exhibited up to five reductions and two oxidation processes. In general, the number of redox states, and their respective standard half potentials, $E^0_{1/2}$ depend on the nature of subsituents on the macrocycles.[238] During the synthesis of the $(F_{64}Pc)_2MH$ complexes,

there were some anomalies such as the presence of a weak magnetism in the formulated diamagnetic complexes $(F_{64}Pc)_2MH$, (M=Lu, Y). The presence of "magnetic impurities" was partially confirmed by an EPR signal of the microcrystalline powdered sample at room temperature. The presence of iron based impurities was ruled out as the cause, thereby implying the possibility of reduced or oxidized states of the complexes. It was, therefore, necessary to study their electrochemical behavior to help elucidate the nature of these impurities. The assessment of the bulk reversibility of the electrochemical processes in solution was necessary to perform MCD measurements on the redox states of $(F_{64}Pc)_2TbH$ in solution.

Redox measurements of the $(F_{64}Pc)_2Ln$ were done at Institut de Ciència de Materials de Barcelona, (CSIC)-CIBER-BBN Barcelona Spain, using the Princeton Applied Research VersaSTAT 3 potentiostat/galvanostat machine. The experiments were conducted by collaborators, Prof Veciana and co-workers and raw data was provided as well as some results in a draft manuscript.[240]

For the purposes of these electrochemical studies, the $[(F_{64}Pc)_2Ln]^{n\pm}$ series will be designated as $\mathbf{1_{Ln}}^{n\pm}$, with for example, the one electron reduced $[(F_{64}Pc)_2Tb]^-$ designated as $\mathbf{1_{Tb}}^-$. Unless specified otherwise, potentials given in this section are V vs. SCE. The redox properties of the complexes were studied by cyclic voltammetry for 0.5 M solutions of $F_{64}Pc_2Ln$ (Ln = Tb, Dy and Lu) in acetone containing 0.1 M [TBA][PF$_6$] as electrolyte. A total of five processes were observed for $\mathbf{1_{Tb}}$, including one oxidation process at 1.58 V and four reduction processes at 0.14, −0.21, −0.67 and −1.10 V (see Figure 6.3). The processes at 0.14 and −0.21 V were found to be reversible, and those at

1.58, −0.67 and −1.10 were quasi-reversible. Redox potentials for $1_{Lu}$ and $1_{Dy}$ are shown in Appendix G.
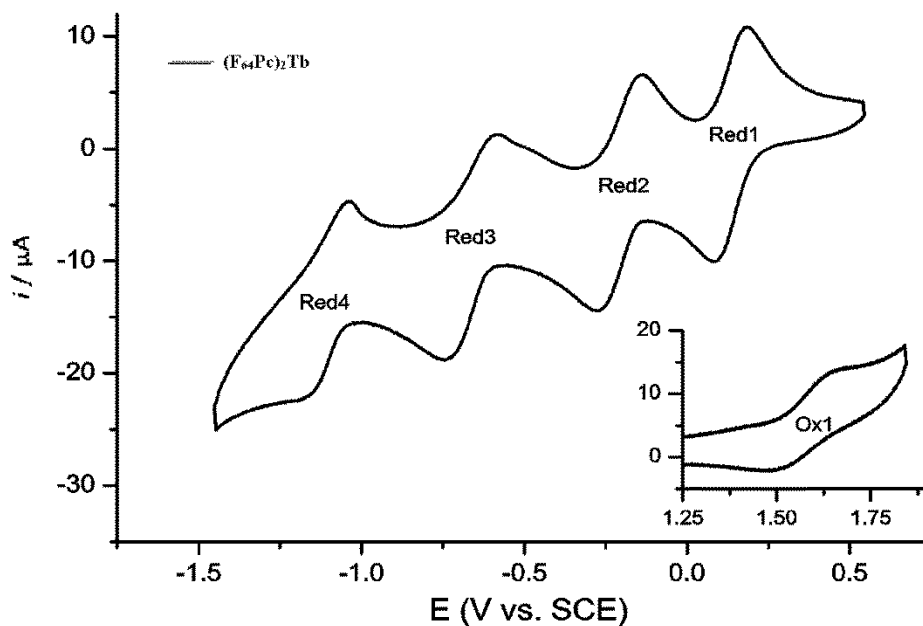


**Figure 6.3** Cyclic voltammograms at 100 mV s$^{-1}$ of solutions of $1_{Tb}$ in a 0.1 M electrolyte solution of tetrabutylammonium hexafluorophosphate in acetone.

The F atoms and the $i$-C$_3$F$_7$ moiety connected directly to the Pc macrocyles exhibit strongly electron withdrawing characteristics and have been shown to affect the redox behavior of monophthalocyanine F$_{64}$PcZn[241] relative to the unsubstituted PcZn. This has been confirmed by TDDFT studies[109] in which Ionization Potential (IP) of the (F$_{64}$Pc)$_2$M are lower than respective IPs of F$_{64}$PcZn. The inductive effect of the fluorine moieties has made the anionic redox states of the $1_{Ln}$ series the more stable species.

$$[(F_{64}Pc)_2Ln]^0 \xrightleftharpoons[\text{Ox1}]{1e\text{-}} [(F_{64}Pc)_2Ln]^- \xrightleftharpoons[\text{Red1}]{1e\text{-}} [(F_{64}Pc)_2Ln]^{2-}$$

$$1e\text{-} \updownarrow \text{Red2}$$

$$[(F_{64}Pc)_2Ln]^{5-} \xrightleftharpoons[\text{Red4}]{1e\text{-}} [(F_{64}Pc)_2Ln]^{4-} \xrightleftharpoons[\text{Red3}]{1e\text{-}} [(F_{64}Pc)_2Ln]^{3-}$$
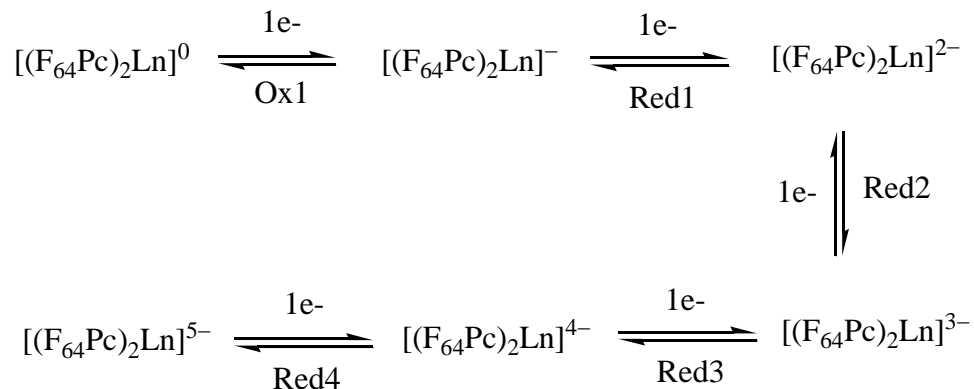
**Figure 6.4** The one electron redox processes of $(F_{64}Pc)_2Ln$. Ox1 = 1st oxidation process and Red*n* represents the nth reduction process.

Starting from the neutral complex, the first oxidation potential, Ox1shown in Figure 6.4, is 1.5 V and the first reduction potential, Red1 is 0.14V. These values of the redox potentials are between 1.2 and 1.5 V higher than those of the unsubstituted or alkoxy substituted analogues.[238]

The establishment of the redox potentials opened the possibility of electrogenerating the reduced species. This was done, and the reduced/anionic species were probed by spectroelectrochemistry at an optical transparent electrode. Spectral changes of some $\mathbf{1_{Tb}}^{n-}$ are shown in Figure 6.5. Similar spectral changes for $\mathbf{1_{Dy}}^{n-}$ and $\mathbf{1_{Lu}}^{n-}$ are shown in Appendix G.

On starting with ionic compound $\mathbf{1_{Tb}}^{-}$, the application of a potential of −0.25 V vs. Ag/AgCl the dianionic analogue $\mathbf{1_{Tb}}^{2-}$ could be electrogenerated. The observed electronic spectrum of $\mathbf{1_{Tb}}^{2-}$ exhibited four main spectral features. There was a gradual disappearance of the band at 682 nm in the Q-band region of the anionic species giving rise to a new band at 645 nm with a shoulder at 694 nm. In the region between 440 and 500 nm usually referred as the BV region, two new bands appeared at 452 and 495 nm. The BV region contains one of the "finger print" transitions due to the presence of the π-

radical electron. The split B-band of $\mathbf{1_{Tb}}^-$ joins in a single broad band at 360 nm. The fourth feature occurred in the NIR region where the band around 860 nm assigned to a vibronic transition of the split Q-band disappeared and a new band appeared at 920 nm, while an intervalence, (IV) band appeared around 1200 nm, consistent with a mixed valence state.

A one electron reduction of the $\mathbf{1_{Tb}}^{2-}$ was obtained by the application of a potential of −0.70 V vs. Ag/AgCl to form the trianionic $\mathbf{1_{Tb}}^{3-}$. In the BV region of the observed electronic spectra of the $\mathbf{1_{Tb}}^{3-}$, the intensity of the band at 452 nm experienced a strong increase in intensity while the band at 495 appeared unchanged. In addition, the split in the Q-band widened and deepened with new peaks occurring at 620 and 697 nm. The BV region exhibited a diminishing of a single peak but with a general increase of broad intensity. In addition, in the NIR region, the IV band at around 1200 nm disappeared while a new band appeared at 1500 nm.

An assessment of the clean electrogeneration of the reduced species was carried out by regenerating $\mathbf{1_{Tb}}^{2-}$ and $\mathbf{1_{Tb}}^-$ through the successive application of potentials −0.2 and −0.33 V vs. Ag/AgCl, respectively. The bulk reversibility of the process was demonstrated by the identity of the spectra of the starting material and regenerated samples. The isolated spectra of the three redox states are shown in Figure 6.6
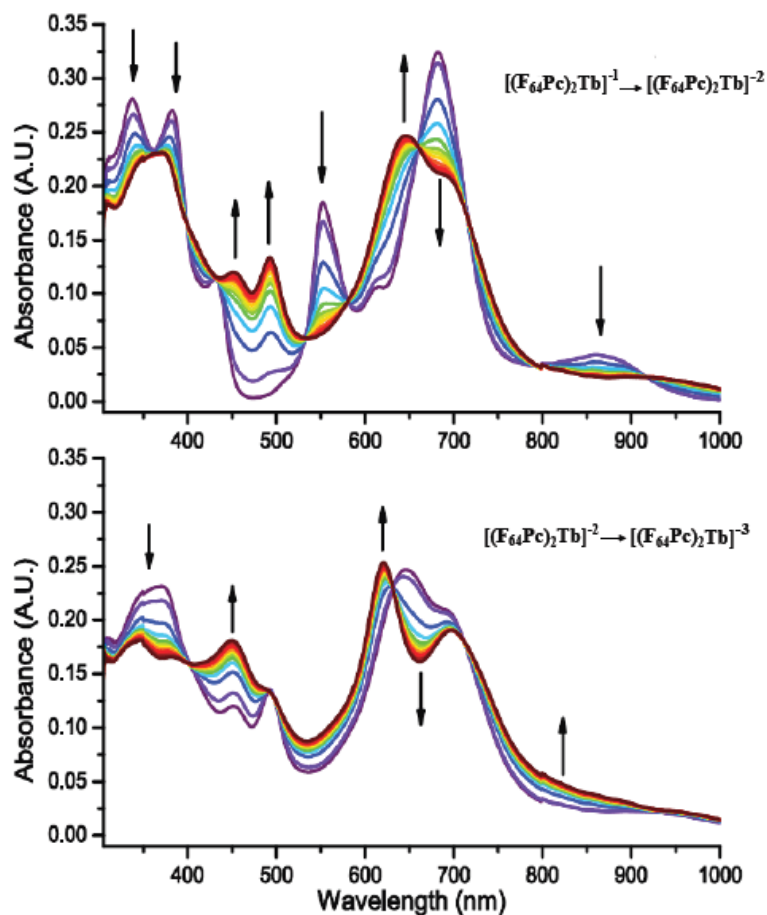
**Figure 6.5** Successive UV-visible spectra during the electrochemical conversions of a solution of $1_{Tb}^-$ to $1_{Tb}^{2-}$ applying a potential of -0.25 V vs. Ag/AgCl (top) and of $1_{Tb}^{2-}$ to $1_{Tb}^{3-}$ applying a potential of -0.70 V vs. Ag/AgCl (bottom) in acetone with 0.1 M tetrabutylammonium hexafluorophosphate.

Chemical reduction of $1_{Tb}^-$ to $1_{Tb}^{2-}$ by the use of the strong bases, hydrazine hydrate in methanol and KOH in methanol/acetone was carried out at NJIT. The addition of any of these bases to the $1_{Ln}^-$ results in a change in color from the blue to green. UV-visible spectra of this green product were similar to the ones produced by electrogeneration. The spectrum of the $1_{Tb}^{2-}$ is shown in Figure 6.7. This further supports the results of the spectroelectrochemical tests on the $1_{Tb}$.
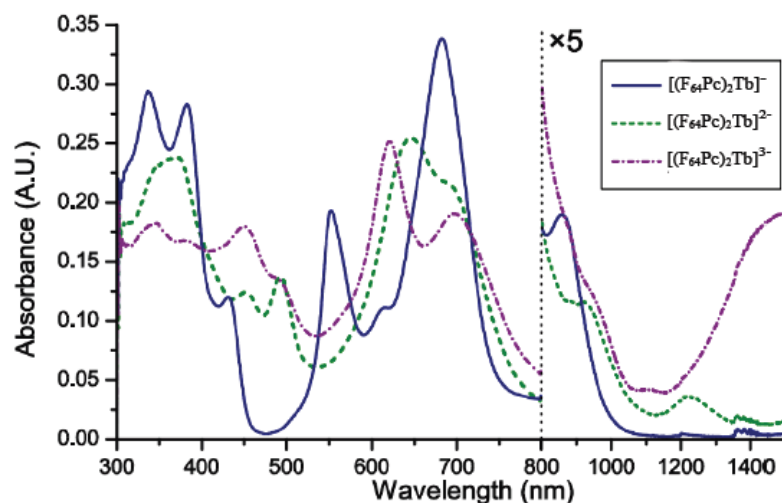
**Figure 6.6 UV.** UV-visible absorption spectra of a solution of $[(F_{64}Pc)_2Tb]^-$ in 0.1 M electrolyte solutions of tetrabutylammonium hexafluorophosphate in acetone, and of solutions of $[(F_{64}Pc)_2Tb]^{2-}$ and $[(F_{64}Pc)_2Tb]^{3-}$ generated electrochemically from it.
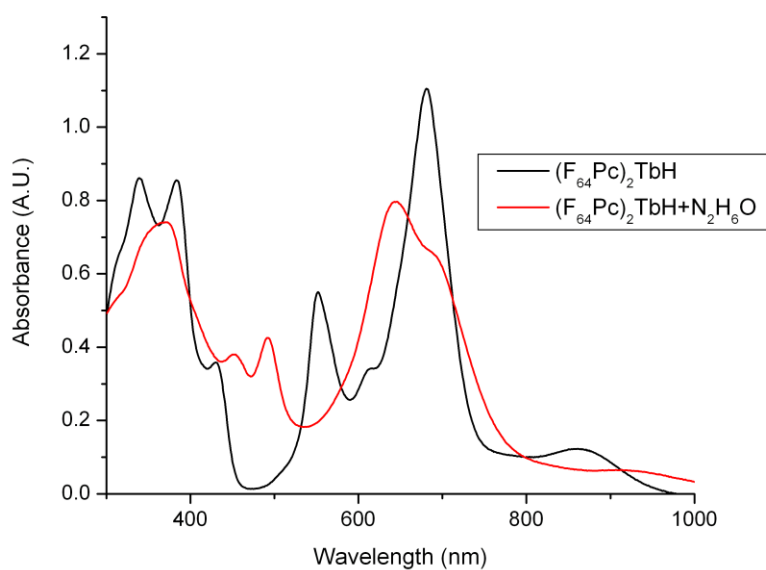


**Figure 6.7** Electronic spectra of $1_{Tb}{}^-$ and $1_{Tb}{}^{2-}$ in methanol. The reduction of was achieved by two drops of hydrazine hydrate (100%) placed in the 1.0 cm standard UV-visible cuvette.

All four compounds, **[1]**-**[4]** were able to be reduced in this way, producing essentially similar spectra with small differences due to the nature of the central metal ion.

## 6.6 Electron Paramagnetic Resonance of $(F_{64}Pc)_2LnH$

The anomalous results of the ESR obtained earlier at CUNY, particularly the presence of a signal from the solid state ESR spectra of **[1]** and **[2]** prompted further EPR studies in an environment where the possibility of electrogeneration could remove other oxidation states of the complexes. These were also carried out at Institut de Ciència de Materials de at Institut de Ciència de Materials de Barcelona. For the $\mathbf{1_{Lu}}^-$ and $\mathbf{1_Y}^-$ complexes, the diamagnetic metal core meant that an EPR signal must be generated by an unpaired electron in the phthalocyanine ring, meaning one of these rings must contain a $\pi$-radical electron. A repeat of the EPR test with **[1]** in acetone did not produce a signal at room temperature. A frozen solution at 150 K consisting of a mixture of acetone and 0.2 M TBAPF$_6$ exhibited a weak disonian signal at g = 2.0021, with a line width of *ca.* 9 G.
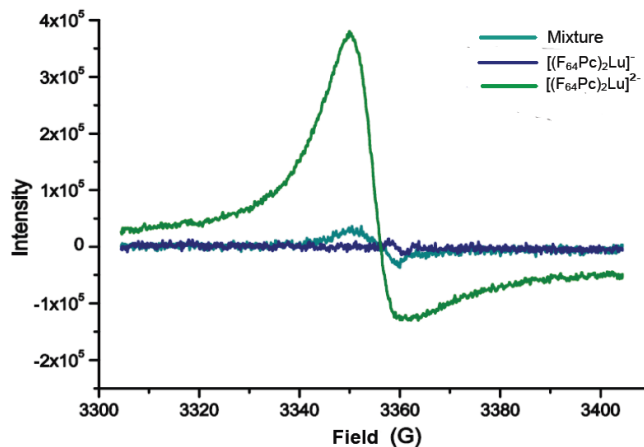


**Figure 6.8** EPR spectra of $[(F_{64}Pc)_2Lu]^-$ and $[(F_{64}Pc)_2Lu]^{2-}$ and the non electrolyzed sample containing a mixture of the two redox states.

The EPR signal in the initial mixture could be correlated to the presence of traces of $\mathbf{1_{Lu}}^{2-}$ in the sample and could be checked by UV-visible spectroscopy. A subsequent electrolyzing of the sample at 0.6 V vs. Ag/AgCl for about 30 minutes ensured that a pure $\mathbf{1_{Lu}}^-$ state was obtained which was EPR silent. A sample solution of $\mathbf{1_{Lu}}^{2-}$ was then prepared by bulk electrolysis at 0.3 V vs. Ag/AgCl for one hour and a strong EPR signal with g = 2.0021 was obtained, with a disonian line shape and a line width of approximately 12 G.

These results confirm the initial assessment that the ESR signal from the powdered samples of **[1]** and **[2]** was due to small amount of non-ferrous paramagnetic impurities. The strong disonian signal obtained previously at CUNY can probably be attributed to a larger concentration of the impurities in the solid state and the larger sample size.

## 6.7 MCD of $(F_{64}Pc)_2TbH$

The presence of slow relaxation to magnetization reversal in magnets during AC magnetism testing provides one piece of evidence of SMM behavior but it may also be the result of long range order. Conducting the test on dilute samples can effectively separate the sample's molecules/ions from each other. Solids can be co-crystallized in compatible diamagnetic matrixes or frozen in solution. MCD spectroscopy has been shown to be a powerful tool in the study of SMMs in dilute solutions.[171, 236, 242] The $\mathbf{1_{Tb}}$ sample was chosen for testing because of its enhanced SMM properties. A solvent glass with good optical properties was prepared from a dilute solution of $\mathbf{1_{Tb}}$ in acetone containing 0.8 M TBAPF$_6$. Solutions of $\mathbf{1_{Tb}}^-$, $\mathbf{1_{Tb}}^{2-}$ and $\mathbf{1_{Tb}}^{3-}$ were electrogenerated

from it at potentials of 0.37 V (to ensure electrolysis of the trace amounts of $\mathbf{1_{Tb}}^{2-}$), $-0.03$ and $-0.47$ V vs. SCE, respectively. The electrogenerated samples were then injected into the MCD cell and frozen in liquid $N_2$ prior to insertion into the spectrometer. A comparison of the absorption spectra of the electrogenerated samples with that of the in-situ at room temperature was used as the basis for a quality assessment. The in-situ absorption spectra of the dilute frozen samples of $\mathbf{1_{Tb}}$ were found to correspond essentially to their room temperature spectra. The only important difference observed was a splitting of the broad Q-band at 682 nm into two bands at 703 and 660 nm for $\mathbf{1_{Tb}}^{-}$ which was attributed to a better resolution of the bands at low temperatures.
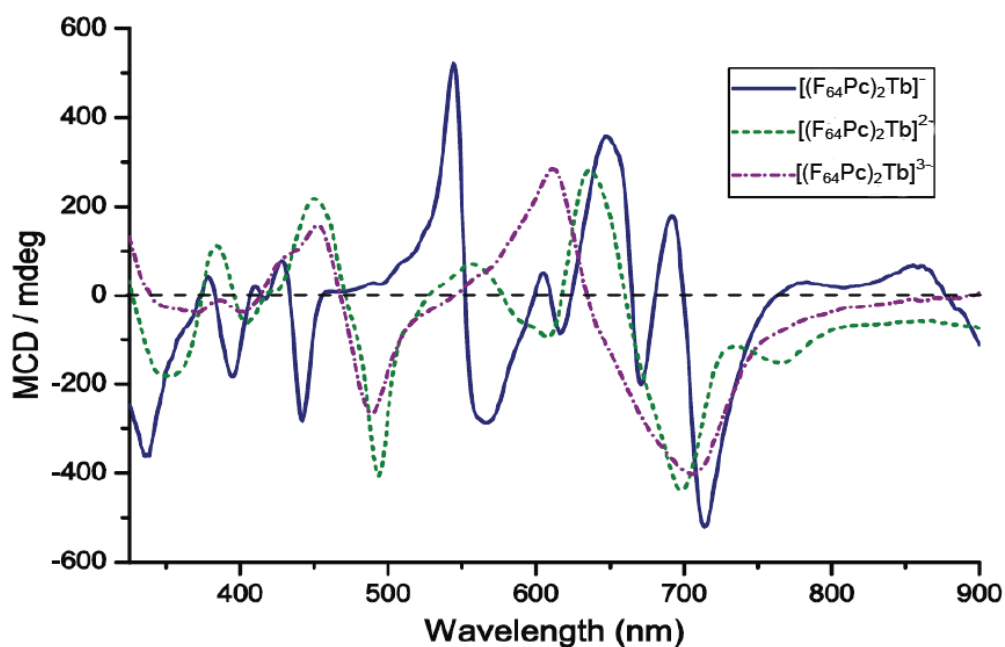


**Figure 6.9** MCD spectra of solutions of $[(F_{64}Pc)_2Tb]^{-}$, $[(F_{64}Pc)_2Tb]^{2-}$ and $[(F_{64}Pc)_2Tb]^{3-}$ at 3 K and 7 T in acetone with 0.8 M tetrabutylammonium hexafluorophosphate.

The three electrogenerated samples were characterized by low temperature MCD and complex spectra were obtained as shown previously in Figure 5.9. The MCD spectrum of $\mathbf{1_{Tb}}^-$ was dominated by two pseudo A-terms corresponding to the split Q-band at 700 and 661 nm, and another pseudo-A term at 552 nm. In $\mathbf{1_{Tb}}^{2-}$, the band at 700 nm gave rise to an absorption shaped MCD term while the band at 621 nm appeared as a pseudo-A term. The Q-band of $\mathbf{1_{Tb}}^{3-}$ yielded two absorption-shaped terms of opposite sign at 705 and 610 nm. In the BV region of the electronic spectra, the π-radical band of both $\mathbf{1_{Tb}}^{2-}$ and $\mathbf{1_{Tb}}^{3-}$ exhibited temperature dependent negative MCD terms at 494 and 488 nm respectively.

MCD was also used to probe the magnetism of the three samples, $\mathbf{1_{Tb}}^-$, $\mathbf{1_{Tb}}^{2-}$ and $\mathbf{1_{Tb}}^{3-}$ through magnetization experiments in solution at 1.8 K by monitoring their MCD terms. In order to avoid errors due to significant distortion arising from the overlap of the different terms, reasonably well isolated terms were selected to record the magnetization hysteresis curves. The MCD intensity was measured at 562, 494 and 705 nm for $\mathbf{1_{Tb}}^-$, $\mathbf{1_{Tb}}^{2-}$ and $\mathbf{1_{Tb}}^{3-}$ respectively, while sweeping the applied magnetic field between $\pm 2$ T at a sweep rate of 1 T/min. Hysteresis was observed in all three substances and the curves are shown in Figure 6.10. The MCD hysteresis curves of both $\mathbf{1_{Tb}}^-$ and $\mathbf{1_{Tb}}^{3-}$ which were measured at 562 and 705 nm respectively, showed a "butterfly" hysteresis which is commonly observed for the sandwich species. A narrowing of the hysteresis loops observed for $\mu_0 H < 0.1$ T could be attributed to the occurrence of quantum tunneling of magnetization at small field values between the different $|J_Z\rangle$ $|I_Z\rangle$ states in sandwich lanthanide complexes.[91] This contrasted with the field dependent MCD intensity of the Q-band of $\mathbf{1_{Tb}}^{2-}$ which exhibits an open loop without any notable narrowing close to

zero-field. This tends to indicate a lower efficiency in the tunneling regime for $\mathbf{1_{Tb}}^{2-}$ when compared to the other redox states.
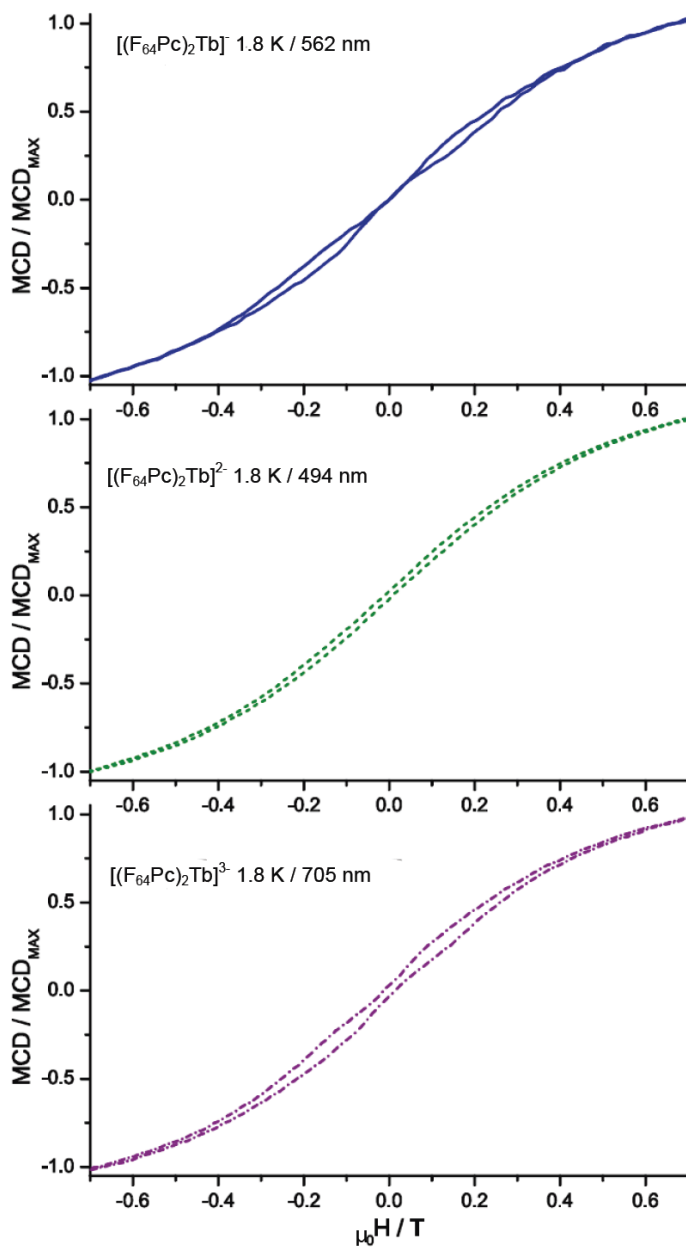


**Figure 6.10** Hysteresis curves of the normalized MCD intensity recorded at 1.8-1.9 K and at a sweep rate of 1 T.min$^{-1}$ for $[(F_{64}Pc)_2Tb]^-$ (top), $[(F_{64}Pc)_2Tb]^{2-}$ (middle) and $[(F_{64}Pc)_2Tb]^{3-}$ (bottom).

The field dependent MCD intensity shares some similarities with earlier studies carried out on different redox forms of a lanthanide sandwich compound.[171]  In that case, where the MCD were recorded under similar conditions, the anionic and cationic sandwich complexes exhibited "butterfly" hysteresis while the neutral complex did not. Although different compounds were used in both sets of experiments, a trend seemed to emerge in which the odd electron states (i.e., +1, −1, and −3) exhibited butterfly-shaped hysteresis while the odd redox states such as 0 and −2 exhibited an open loop hysteresis. This coincided with the EPR-active species, which are those having unpaired electrons in Pc macrocycles.  It is suggesting that the radical nature of the ligands in the neutral and dianionic states of the sandwich compounds deactivates the tunneling regime during field MCD testing.

## 6.8 Summary

Electrochemical studies identified five redox processes for the $(F_{64}Pc)_2M$ (M= Lu, Tb, Dy) complexes of which one is oxidation and other four are reduction starting from the neutral $[(F_{64}Pc)_2M]^0$ complex.  The two first reduction processes are reversible while the others are quasi-reversible. Mass spectroscopy (MS) done earlier on the blue compounds obtained from the synthesis procedure formulated them as $[(F_{64}Pc)_2MH]$, that is the one electron reduced state $[(F_{64}Pc)_2M]^-$. Spectroelectrochemistry, showed that the electronic spectra of the $[(F_{64}Pc)_2M]^-$ is similar to that of the $(F_{64}Pc)_2MH$ complexes, thereby supporting the results of the MS.  The chemically generated reduction of $(F_{64}Pc)_2MH$ by the use of hydrazine hydrate to the $[(F_{64}Pc)_2M]^{2-}$ was supported by spectroelectrochemistry through the electronic spectra of the electrogenerated species.

The anomaly of the ESR signal from the diamagnetic complexes $(F_{64}Pc)_2YH$ and

($F_{64}Pc)_2LuH$ can be reasonably explained by the presence of a reduced species, most likely $[(F_{64}Pc)_2M]^{2-}$, due to its ease formation by reduction. The $[(F_{64}Pc)_2M]^{2-}$ may have also been formed in the synthesis process, with small amounts remaining after fractionation.

MCD spectroscopy showed that the broadened Q-band of the $(F_{64}Pc)_2MH$ compared to the $Pc_2M$ complexes was due to the overlap of two peaks as shown by two pseudo-A terms. The presence of the $\pi$-radical electrons of the $F_{64}Pc^{3-}$ has been confirmed through temperature dependent negative MCD terms at 494 and 498 nm, respectively.

The use of dilute frozen samples of the first three reduced species of $(F_{64}Pc)_2Tb$ for MCD magnetization studies confirmed that the hysteresis and the slowed relaxation to magnetization reversal as was observed through SQUID AC magnetization studies was not due to long range order. This could also be extended to the $(F_{64}Pc)_2Dy$ complex and was further evidence of SMM behavior in this class of complexes. Furthermore, QTM which was not observed in the SQUID magnetometry of undiluted solid samples was observed in MCD and presents additional evidence of SMM behavior. The observed phenomenon of the lack of butterfly-shaped hysteresis in the EPR active species requires further study.

# CHAPTER 7

## DISCUSSION AND FUTURE DIRECTIONS

### 7.1 Overview

The principles behind the application of single molecular magnets will be presented in the context of qubits for very fast quantum computers and high capacity magnetic devices. Some of the other possible applications of the complexes **[1]**-**[4]** will then be discussed.

### 7.2 Quantum Computers

The development of a new class of computational algorithm based on the rules of quantum mechanics[243] [244, 245]rather than classical physics led to the proposal of the storage of information as quantum phase. Whereas classical computers use the binary bit as the smallest size for information storage, quantum computers use a two level quantum system or the qubit. A quantum parallelism in which quantum mechanical systems can be in a superposition of computational states and simultaneously carry out multiple computations in the same computer is an underlying principle.[246] Quantum mechanical phenomena include superposition, entanglement and coherence.

In a quantum computer, the logic circuitry and time steps are essentially classical, only the memory bits that hold the variables are in quantum superpositions - these are called qubits.[246] Generally, a quantum computer having n qubits can be in an arbitrary superposition of $2^n$ different states simultaneously. On the other hand, a classical computer can be in only one of these $2^n$ states at any one time. The operation of the quantum computer is achieved by manipulating those qubits with a fixed sequence of

quantum logic gates. The sequence of gates to be applied is known as quantum algorithm.[247]

A number of physical implementations of the quantum computer based on certain principles and systems have been pursued. The use of flawed diamonds involve the creation of a qubit made possible by the electronic or nuclear spin of nitrogen-vacancy centers in diamond;[248, 249] quantum computers based on large-area current-biased Josephson junction whose two lowest energy quantum levels are used to implement a solid-state qubit;[250] nuclear magnetic resonance in solution where the qubit is provided by nuclear spins within the dissolved molecule[251, 252] provide a few examples. The demonstrations of quantum computers are based on the quantum computational algorithms such as Grover's[245, 246, 253], Shor's[244, 254] and Deutsch-Jozsa.[255]

A major of objective of this research was to develop molecular magnets which could be candidates for qubits to be used in quantum computers. In fact, a proposal for the implementation of Grover's algorithm was developed for the high spin 3d class of molecular magnets such as $Mn_{12}$ and $Fe_8$.[194] These SMMs use spin eigenstates as qubits. Each eigenstate represents a different binary unit, i.e., $2^0$, $2^1$, $2^2$ … . They act as storage units of a dynamic random access memory device, thereby allowing information storage and retrieval. The decoding of read-out, stored information was to be achieved by using fast ESR pulses, accessing stored numbers of up to $10^5$ with access time as short as $10^{-5}$ s.[194]

The establishment of SMM behavior in **[3]** and the observance of QTM through MCD testing puts it among those candidates which can act as qubits in quantum computers. The mechanism for QTM in $Pc_2Tb$ complex was reported as different from

the 3d, high spin SMMs. In this complex the ground state multiplets are split by the ligand field from the two Pc ligands giving rise to strong magnetic anisotropy. [88] In the Tb complex, the lowest substates are assigned to $J_z = \pm 6$, which are the maximum and minimum values and correspond to the "spin-up" and "spin-down" states in the $J_z = 6$ ground multiplet. In the Dy complex, the lowest substates are characterized as $J_z = \pm 13/2$, the second largest in the $J = 15/2$ ground state.[8]

The exploitation of the substate multiplets  of the lanthanide bisphthalocyanines for use as qubits in the implementation of quantum computing is still in its infancy.  It is perceived that its operation would be based on similar principles used for the 3$d$ based magnets.  However, recent developments have seen electric control of the angle between the two ligands of $Pc_2Tb$ adsorbed to a Au(III) surface.[256] The upper Pc ligand in $Pc_2Tb$ was rotated by applying a controlled electric current, leading to the disappearance and reappearance of Kondo peaks.  Reversible switching between two stable ligand orientations by applying a current pulse should make it possible to code information at a single-molecule level.   Despite being neutral molecules, **[3]** and **[4]** may still be potentially applicable because their behavior may be similar to $Pc_2Tb$ when attached to certain conducting surfaces.

Complexes **[3]** and **[4]** should remain as candidates for qubits because of their other related properties.  The fact that they are also soluble, air stable, resistant to oxidation, form crystals easily and are redox active also makes them even more attractive.  Their multifunctional nature may not be limited to these stated properties because their ability to form thin films, electrical, photonic, biochemical or catalytic properties have not been studied.   There are current drawbacks to their use as qubits,

chief among them being the low temperature at which SMM and hence qubit activity will be realized.

In general, the qubits in a quantum computer must be able to retain the quantum information they are given long enough to perform quantum logic operations across them. That is, the system must be isolated from interactions in the environment which will cause premature quantum decoherence. However, it must also interact in a controllable fashion to enable easy reading of the qubits.

### 7.3 Some Potential Applications in Electronic Semiconductor Devices

The development of ambipolar field-effect transistor based on organic-inorganic hybrid structure[257] opened the possibilities for similar devices using $Pc_2Ln$ as the organic film in the device. Organic Thin-Film Field Effect Transistors (OTFTs) are emerging as attractive candidates for low-price, large-area, and flexible circuit applications.[51] An important property of these devices is the mobility of semi-conducting organic material. Li et al.[51] reported that incorporation of the electron withdrawing groups such as F and CN on the on the Pc ring improved this mobility by converting the Pcs from p-type to n-type semiconductors. The mechanism was via the lowering of the Lowest Unoccupied Molecular Orbital (LUMO) energy level and thus facilitated the injection of an electron.

One of the challenges to the development of quantum computing and high density magnetic storage devices is the effective deposition and adsorption of the organic molecules to surfaces without modification of the SMM properties of the organic molecule. The other common techniques used to deposit molecules such vapor deposition and Langmuir-Blodgett techniques did not result in a demonstration of

magnetic properties of the adsorbed molecules.[4] Using a special technique, Vitali et al.[258] deposited $Pc_2Tb$ crystals on Cu(111) surface as SMM. Their studies revealed that the interaction with the metal surface preserved both the molecular structure and the large spin magnetic moment of the metal center. The 4f electron states were not perturbed by the adsorption, while a strong molecular/metal interaction could induce the suppression of the minor spin contribution delocalized over the molecular ligands.

A study of SMMs, $Pc_2Tb$, $Pc_2Dy$ and $Pc_2Y$ deposited on Au(111) by Katoh et al.[9] using Scanning Tunneling Microscopy (STM) and Scanning Tunneling Spectroscopy (STS) revealed the occurrence of the Kondo effect in the TbPc molecules at 4.8 K, but neither the DyPc, YPc nor any of the sandwich complexes exhibited this effect. The Kondo temperature, $T_k$ was ca. 250 K. In addition, these authors investigated the electronic transport properties of PcLn molecules as the active layer in top- and bottom-contact thin-film organic field effect transistor devices. PcTb molecule devices exhibit *p*-type semiconducting properties and the PcDy based devices exhibited ambipolar semiconducting properties. The electronic application of not only sandwich $(F_{64}Pc)_2MH$ complexes, but also their monophthalocyanines counterparts present exciting possibilities.

### 7.4 Future Work

1. Determine the conditions under which $(F_{64}Pc)_2TbH$ forms the two pseudo-morphs **[3]** and **[3′]**, having the space groups P4/ncc and the P2/$_1$c respectively. Furthermore, investigate whether complexes **[1]**, **[2]** and **[4]** are also polymorphic and will form crystal structures in both space groups under similar conditions.

2. Improve the purity of the products **[1]**-**[4]** by applying other separation techniques such as High Performance Liquid Chromatography (HPLC) or vacuum sublimation. A three stage process in the case of vacuum sublimation is suggested. This begins with heating the >95% pure product in a closed glass ampoule at ca 300ºC for about two hours, with the intention of causing a breakdown or reaction of impurities. The resulting material could then be subjected to liquid chromatography in an attempt to remove most of the impurities or undesired substances formed. Finally, use vacuum sublimation to extract the products and leaving impurities in the bulk sample.

3. Purification and full characterization of the byproducts **[2-1]**, **[2-2]** and **[2-3]** from the synthesis reactions. The initial electronic and mass spectroscopy characterization data is suggesting that **[2-1]** and **[2-3]** may be sandwich compounds while **[2-2]** may be a monophthalocyanine. (See Appendix H).

4. The ability of the compounds to form homogenous and strongly adhering thin films using the various coating techniques such as Langmuir Blodgett, physical vapor deposition and electrophoretic should be pursued. Substance **[2-2]** appears to be very surface active. Furthermore, the potential applications of complexes [**2**] and **[3]** as photovoltaics, semiconductor devices, qubits and high capacity storage devices may depend to some extent on their ability to form good films.

5. The electrical conductivity of films of **[1]**-**[4]** for potential applications.

6. Investigate the possibility of chemical synthesis of a stable $H^+[F_{64}Pc^{2-}]Ln^{3+}[F_{64}Pc^{3-}]M^+$ complex where M is a cation. This is essentially the $[(F_{64}Pc)_2Ln]^{2-}$ species and since the $[(F_{64}Pc)_2Ln]^-$ is the stable species then it

may be possible to find a cation or cations which can stabilize the dianionic complex.

7. Perform additional DSC tests on purer **[1]**-**[4]** to determine if the first order thermal transitions occurring at ~180°C and ~240°C are due to changes in crystalline structure. Testing could be performed in the reverse (while cooling) or the use of the Modulated DSC (MDSC).[259, 260] patented by TA Instruments.

8. Separate and characterize the material that was formed in the DSC experiment at the point where the first order thermal event occurring at around 490°C, resulted in a change in the color and electronic spectra of the residue of **[1]**-**[4]**. The thermal event was endothermic; therefore, there is a real possibility that there was a reaction because the electronic spectra were differed from the spectra obtained from the synthesis products and byproducts. While it has been speculated that this green substance may be a three layer sandwich compound, it may also be a phthalocyanine formed by the replacement of the existing metal by Al from the metal can.

9. Include the $[(F_{64}Pc)_2M]^{2-}$ (M = Lu, Y) species in the DFT and TDDFT studies of the of the complexes due to the real possibility of isolating a stable form of this complex and the fact that its electronic spectra has been measured.

10. Neutron scattering or Muon Spin Relaxation (µSR) studies should be carried out to further probe the magnetic properties of the complexes, in particular to more accurately measure their energy barrier to magnetic reversal, $\Delta$ and their attempt time.

11.  ESR studies of the single crystals to detect anisotropy and measure the $g_\perp$ and $g_\parallel$ values.

12. Further, investigate whether the $\pi$-radical nature of the Pc ligand deactivates the tunneling regime in the sandwich compounds during the MCD experiments.

13. Complete the AC magnetometry testing of dilute samples of **[3]** and **[4]**.

14. Continuation of the investigation of the anomalous results of $\chi_M''$ vs. $f$ in the AC magnetic testing of **[4]**.

# CHAPTER 8

## SUMMARY AND CONCLUSIONS

### 8.1 Synthesis and Structure

This research reports the synthesis, single-crystal X-ray structures and electronic and magnetic properties of the first examples of a new class of sandwich complexes of H-free ligands, stabilized in their closed-shell electronic configurations. Before this work, sandwich complexes of any metal that did not contain C-H bonds were unknown. Bis[octakis($i$-$C_3F_7$) octakis(perfluoro)phthalocyaninatoM(III)H], (M = Lu **[1]**; Y, **[2]**; Tb, **[3];** and Dy, **[4]**) abbreviated $(F_{64}Pc)_2MH$, were synthesized in 5-12% yields from perfluoro-(4,5 di-isopropyl) phthalonitrile and a metal salt using a microwave-assisted procedure. MALDI-TOF mass spectra confirmed the results. The formation of sandwich complexes was somewhat surprising given the reduced basicity of the ligand due to the presence of F and perfluoroalkyl $i$-$C_3F_7$ groups.

The identity of the $F_{64}Pc$ ligands was confirmed spectroscopically. The high solubility of the complexes in organic solvents facilitated the use of $^{19}F$ NMR for the elucidation their structure and spin states. Complexes **[1]** and **[2]** exhibit three NMR signals at −71.4, −103.7, −165.0 and −71.6, −103.3, −165.0 ppm, respectively, in 6:1:1 ratio, assigned to the primary aliphatic, aromatic and tertiary aliphatic fluorine atoms, respectively, the conformation was by analogy with the spectrum of diamagnetic $F_{64}PcZn$ , which exhibited signals at −71.3 (6 F), −103.9 (1 F) and −164.6 (1 F) ppm.[261] The similar chemical shifts and peak widths indicated magnetically equivalent $F_{64}Pc^{2-}$ ligands in **[1]** and **[2]** and virtually eliminated the possibility of a $F_{64}Pc^{\bullet-}$ ligand. The paramagnetic $Tb^{3+}$ and $Dy^{3+}$ in **[3]** and **[4]** broaden and shift the $^{19}F$ signals up-field by

10.7 and 6.0 for primary aliphatic F, 15.6 and −6.4 ppm for aromatic F and 28.0 and 15.3 ppm for tertiary aliphatic F, respectively. An accurate integration of the $^{19}$F NMR peaks was not possible.

The characteristic IR bands in the 1300 - 1350 cm$^{-1}$ range, diagnostic of π radical anions,[125] were absent in all complexes. Deconvoluted UV-visible spectra revealed red-shifted N, B and Q bands relative to unsubstituted complexes, an effect of the F and the $i$-C$_3$F$_7$ electron withdrawing groups. The proton, unobserved at the NMR time-scale, apparently rendered the Pc rings of [1]-[4] slightly non-equivalent resulting in split Q bands. This split being relatively small, was obscured by a broadened Q-band, but was revealed by deconvolution of the UV-visible spectra and confirmed by MCD spectroscopy. The gaps between the peaks of the split Q-band of [1]-[4] was ca. 40 nm which was less than the 67-100 nm gaps observed for reduced, non-fluorinated complexes.[52, 57, 68, 82, 159, 163] Spectroelectrochemistry of [1], [3] and [4] revealed a widening of this gap on reduction of the complexes.

The bands observed for [1]-[4] beyond 800 nm in the RV region of the electronic spectra were ascribed to vibronic transitions of the Q-band of the anionic complexes and not to the bands that characterize the F$_{64}$Pc$^{\bullet-}$ radical anions electron neutral species.[9] The absence of NIR absorptions in the 1000-2200 nm region, attributed to F$_{64}$Pc$^{\bullet-}$/F$_{64}$Pc$^{2-}$ pair further supports the above assignments.[72, 262] The electronic spectra of [1]-[4] were concentration independent indicating the ability of $i$-C$_3$F$_7$ groups to promote site isolation in solution and, possibly, magnetic dilution in the solid-state.

The solid-state architectures and the effects of the fluorine atoms and $i$-C$_3$F$_7$ groups upon the structure of double-deckers were revealed via single crystal X-ray

studies. The formation of stable X-ray quality crystals was somewhat unexpected given the enhanced peripheral $i$-$C_3F_7$ group's steric congestion and their anticipated impact upon convex ring distortions. Long-range ordering was also in doubt. Nevertheless, single-crystals, albeit of medium quality were obtained by the room-temperature evaporation of acetone/chloroform (35%/65%) solutions. The four complexes are isomorphous, tetragonal space group P4/ncc. $(F_{64}Pc)_2TbH$ exhibits polymorphism through the crystallization into a monoclinic space group $P2_1/c$ as well and is denoted by **[3′]**. The molecular structures confirm the double-decker architecture. The X-ray structures also showed convexity of the $F_{64}Pc$ rings and analysis of several geometrical parameters such as Metal--N distances and the radius of the sphere of curvature, $R_{sf}$ revealed asymmetry in the complexes. This asymmetry was manifested by differences in values of the geometrical parameters between the two $F_{64}Pc^{2-}$ rings. It was generally found that one ring had longer Metal--N distances and greater $R_i$, providing additional evidence of presence of the proton on that $F_{64}Pc^{2-}$ ring. The evidence provided by the medium quality X-ray structures was somewhat weak due to small differences between the values of the geometrical parameters; in some cases within the limits of one standard deviation. However, initial DFT calculations provided support for this asymmetry showing statistically significant differences between defined bond distances of the $F_{64}Pc^{2-}$ and $F_{64}Pc^{2-}H^+$ rings.

Although differences in $R_i$ were noted for the $F_{64}Pc^{2-}$ rings, the convexity was not symmetrical. This type of asymmetry was assessed by measuring the degree of rotation of the eight benzene rings around their centers, as measured by the angle, $\gamma$ made by the bond that links the two benzene ring C atoms that bears the $i$-$C_3F_7$ groups with the 4N

plane. Results of this assessment revealed differences in $\gamma$ among the benzene rings. This non-equivalency provided a weak yet notable support for the presence of a proton; a well reported difficult identification via X-ray diffraction, exacerbated by the 4-fold disorder.[53, 107, 108]

The $\phi$ twist angles between the $F_{64}Pc^{2-}$ rings, 32.0 ± 0.5°, however, indicated a 10° shift toward the eclipsed configuration in comparison with the unsubstituted sandwich complexes, for which the twist angles are 42° (45° for a perfectly staggered complex). The presence of the bulky $i$-$C_3F_7$ groups, similarity of the Metal--N and 4N inter planar distances between the $Pc_2Ln$ and $(F_{64}Pc)_2MH$ sandwich complexes should make $\phi$ closer to the 45° angle. It appears that the stable orientations of the $i$-$C_3F_7$ groups conform to the 32° twist angle. The 29° twist angle of the **[3′]** polymorph of $(F_{64}Pc)_2TbH$ is, perhaps, due to greater intermolecular interactions in the more compact re-arrangement of the molecules in the monoclinic space group.

The magnetic properties, including intermolecular coupling could be affected by the above molecular distortions, but are more likely to be determined by long-range ordering. The common packing diagrams for [**1**]-[**4**], reveal a columnar stacking architecture and F-lined channels, an uncommon mode of packing for anionic sandwich complexes, and somewhat unexpected due to the high content of fluorinated isoalkyl groups and a high percentage, 34 ± 1% of solvent accessible volume. Columnar stack architecture was also unexpected, due to requirement for long chain substituents that induce liquid crystalline mesophases.[167] The potential of the $i$-$C_3F_7$ groups to simulate, to some extent, the longer to alkyl groups appears to be a possibility.

Unlike the tetragonal phase, the molecules of **[3′]** are no longer parallel but almost perpendicular, occurring in pairs whose 4N planes makes an 87.6° angle. Peripheral $i$-C$_3$F$_7$ groups of one molecule penetrate the fluorine-lined Non-Covalent Interaction Space (NCIS) of the other molecule, up to the van der Waals contacts not only with other F, but also with C and N atoms of the macrocycle. This architecture leads to a more compact packing, the solvent-accessible volume being 22%, ~2/3 of that of tetragonal phases. The monoclinic [**3'**] has reduced symmetry compared with the tetragonal [**3**], for which a 4-fold axis is present. A cogwheel alignment of the two rings is in opposite directions, each coordinating F$_{64}$Pc$^{2-}$ ring being chiral.

In addition to structural effects, the replacement of all H atoms with F atoms and $i$-C$_3$F$_7$ groups was anticipated to impart thermo-chemical robustness, for high stability in technologically viable applications. Thermogravimetric analysis (TGA) and Differential Scanning Calorimetry (DSC) revealed that all complexes are stable in air, sublimation starting at ca. 285°C at 1 atm. In non-hermetically containers, DSC detects first order endothermic thermal events occurring below this temperature, these being attributed to possible rearrangements in the crystal structures. The first order endothermic thermal events occurring at ~490°C for the Y, Dy and Tb complexes and at 500°C for Lu appeared to be the result of a chemical reaction based on the UV-visible spectra of the residues at the end of the test.

Initial cyclic voltammetry revealed that [(F$_{64}$Pc$^{2-}$)(F$_{64}$Pc$^{2-}$)HM(III)] resisted oxidization to [(F$_{64}$Pc$^{2-}$)(F$_{64}$Pc$^{•-}$)M(III)] in ethanol which was consistent with the lack of aerobic oxidation. The electronic deficiency of these new sandwich complexes on the other hand, facilitates the addition of an electron; for example, for [**3**] E$_{1/2}$ = 0.04V (vs

Ag/AgCl). Additional electrochemical tests done in acetone, identified five redox processes for the $(F_{64}Pc)_2M$ (M= Lu, Tb, Dy) complexes, of which one was oxidation and other four were reductions starting from the neutral $[(F_{64}Pc)_2M]^0$. The values of the redox potentials were 1.2 to 1.5 V higher than those of the unsubstituted or alkoxy substituted analogues. Since the metals are redox inactive, the redox chemistry is ligand centered. While these results showed some consistency with the known sandwich complexes of Y, Lu, Tb and Dy in that they could be also be reduced and oxidized, several of them exhibited two or more oxidations.[62, 238] The relative difficulty in oxidizing was suggesting that bulky cations such as TBA were unnecessary in [1]-[4] to stabilize diamagnetic ligand electronic configurations.

Complexes [1] and [2] were ESR silent in solution and the solid-state, as expected for closed-shell ligands. Paramagnetic impurities, g = 2.004, less than 5% were detected in solid-state. Spectroelectrochemical studies partially confirmed the nature of the paramagnetic impurities as reduced species of the form $[(F_{64}Pc)_2M]^{2-}$ due to their ease of formation. No ESR signal was observed for [3] and this was consistent with the absence of ESR signals for $Tb^{3+}$ sandwich complexes noted previously.[168] The $Dy^{3+}$ complex [4] exhibited complex ESR spectra, consistent with the literature.[86] The detailed interpretation of the $Dy^{3+}$ complex's ESR results is beyond the scope of this research project.

MCD spectroscopy of solutions of $[(F_{64}Pc)_2Tb]^-$, $[(F_{64}Pc)_2Tb]^{2-}$ and $[(F_{64}Pc)_2Tb]^{3-}$ of acetone with 0.8 M of tetrabutylammonium hexafluorophosphate were carried at 3 K. The split Q-band of the $[(F_{64}Pc)_2Tb]^-$ was confirmed by the presence of two pseudo A-terms at 700 and 661 nm. The MCD terms in $[(F_{64}Pc)_2Tb]^{2-}$ exhibited

close correspondence to absorbencies in the UV-visible spectrum of $(F_{64}Pc)_2TbH$ that was reduced with hydrazine hydrate. The presence of the $\pi$-radical band of $[(F_{64}Pc)_2Tb]^{2-}$ and $[(F_{64}Pc)_2Tb]^{3-}$ was exhibited by two temperature dependent MCD terms at 494 and 498 nm respectively.

## 8.2 Magnetism

Further insights into the influence of the $i$-$C_3F_7$ group upon the magnetic properties of this class of sandwich compounds were obtained via magnetometry and MCD studies. Variable temperature magnetic susceptibility measurements, AC and DC magnetization studies between 2 and 300 K showed ferromagnetic impurities were absent as indicated by magnetization curves. To begin with, the weak paramagnetism exhibited by **[1]** and **[2]** during DC magnetic measurements was determined to be due to small amounts (~1%) of paramagnetic impurities. The source of these paramagnetic impurities was found to be other redox states of the $[(F_{64}Pc)_2M]$ complexes containing unpaired electrons, their presence confirmed by cyclic voltammetry and spectroelectrochemistry. Approximately the same small amounts of this class of paramagnetic impurities were also believed to be present in **[3]** and **[4]**. Both **[3]** and **[4]** are paramagnetic in keeping with their central $Tb^{3+}$ and $Dy^{3+}$ ions having six and five unpaired electrons respectively. On an average, the effective magnetic moment, $\mu_{eff}$ and Weiss constant, $\theta$ were found to be 8.9 BM and $-2.0$ K and 10.4 BM and $-4$ K for **[3]** and **[4]**, respectively. DC magnetism results of tests carried out on the diluted samples of **[3]** and **[4]** supported these results except for the $\theta$ value of **[4]** which was only $-0.53$. These values are within the range reported for

one electron reduced Tb and Dy sandwich lanthanide complexes reported elsewhere.[86, 198]

Results of the AC magnetization studies on **[3]** in the range 2-50 K, revealed $\chi''_M/\chi_M$ peak at temperatures of 19, 33 and 40 K which are similar to literature values.[7] The energy barrier to magnetization relaxation was consistent with literature values within the temperature range $25 \leq T \leq 40$ K. The source of slow magnetization relaxation of these classes of molecules has been reported to be influenced by the ligand field. The complexes' ligand field induces a splitting of the electronic sub-structures making an Orbach relaxation process possible. Sub-states formed from this splitting, gives rise to a series of "spin up" and "spin down" states. The ground multiplet of the Tb complex is J = 6 and splitting and the lowest $J_z$ sub-states are $J_z = \pm 6$ corresponding to the maximum and minimum states. The energy barrier, and the pre-exponential factors obtained for **[3]** was in the range $\Delta = 200\text{-}300$ cm$^{-1}$ and $\tau_0^{-1} = 3.0$ x $10^8$-$2.8$x$10^7$ s$^{-1}$ and for **[4]**, $\tau_0^{-1} = 1.6$ x $10^5$ s$^{-1}$ and $\Delta = 31$ cm$^{-1}$. These values are in the range obtained for the respective unsubstituted [Pc$_2$Tb]$^-$ and [Pc$_2$Dy]$^-$ analogues using similar test methods. This means that the impact of the electron withdrawing peripheral groups on $\Delta$ and $\tau_0^{-1}$ is at least similar to these unsubstituted analogues and their exact impact may have to be determined using more accurate probing methods such as neutron scattering and μSR.

Magnetization studies carried out on **[3]** and **[4]** in the sub-kelvin temperature range (0.04-1.1 K) on the micro-SQUID machine revealed hysteresis with the AC magnetic field swept at rates between 0.001 T/s and 0.280 T/s. Both **[3]** and **[4]** exhibited slowed response to the changing magnetic fields, characteristic of the behavior of the SMMs previously studied in this class of materials.

Close examination of the sub-kelvin temperature magnetic hysteresis of **[3]** and **[4]** did not reveal the staircase hysteresis loops which are known to accompany (QTM). This is believed to be due to the use of the undiluted samples in the test. Dispersing these molecules in the appropriate matrix to increase the distance between the molecular units should allow for the observance of QTM.

The AC magnetic testing of **[4]** exhibited some anomalous results. The $\chi_M''$ vs. $f$, ($f$ = frequency) plot shows peaks at frequencies which shift to a lower value as temperature is raised. Interestingly, with $H$dc = 0, the shift of the peak of $\chi_M''$ vs. $f$ appeared as if it as almost temperature independent, remaining at around 100 Hz. More detailed AC magnetic testing at 2.0 K with $H$dc varying between 0 and 2000 Oe, revealed that the $\chi_M''$ peaks seemed to converge within a small frequency range of about 0.4 Hz to 4 Hz at $H$dc of ~ 2000 Oe.

The use of dilute frozen samples of the first three reduced species of $(F_{64}Pc)_2Tb$ for MCD magnetization studies, confirmed that the hysteresis and the slowed relaxation to magnetization reversal as was observed through SQUID AC magnetization studies was not due to long range order. This could also be extended to the $(F_{64}Pc)_2Dy$ complex and is further evidence of SMM behavior in this class of complex. Furthermore, QTM which was not observed in the SQUID magnetometry of undiluted solid samples was observed in MCD and presents additional evidence of SMM behavior. The observed phenomenon of the lack of the "butterfly-shaped hysteresis" in the EPR active species requires further study.

# APPENDIX A

## MASS SPECTROSCOPY ISOTOPIC PATTERNS

This appendix contains the experimental and isotopic patterns of the mass spectroscopy of the $(F_{64}Pc)_2MH$, with M=Lu(III) Y(III), Tb(III) and Dy(III), $^{BG}Y$ and of $Pc_2Y$.
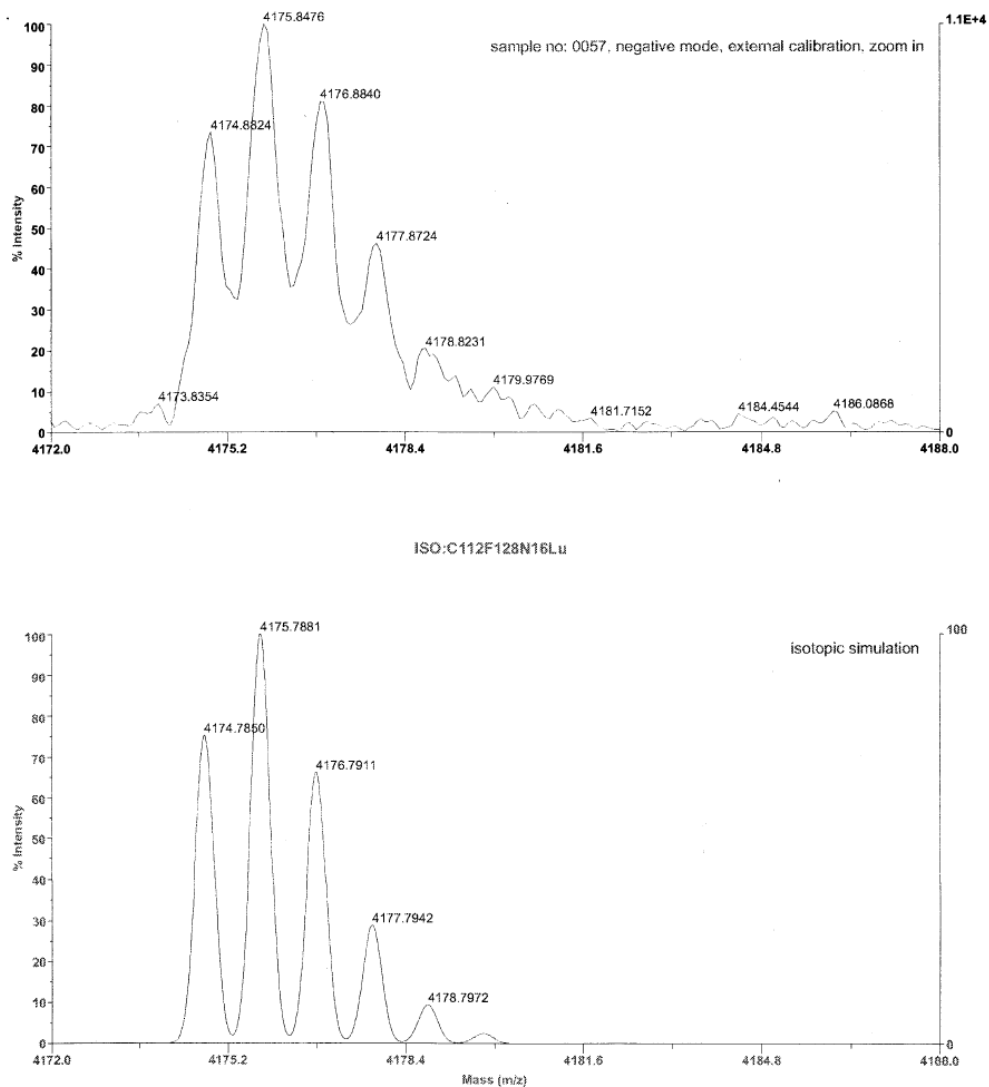


**Figure A.1** Observed MS MALDI-TOF isotopic pattern of $(F_{64}Pc)_2LuH$ (top) and calculated isotopic pattern of $(F_{64}Pc)_2Lu$ (below). In the negative mode, H is lost ($[M-H]^-$) and the pattern resembles that of the non-protonated form.
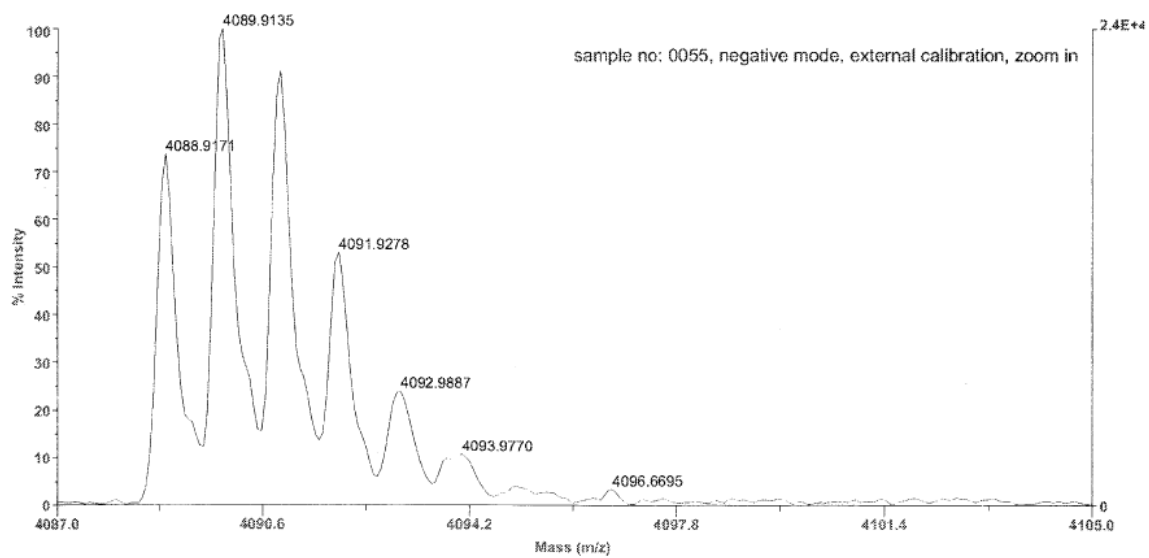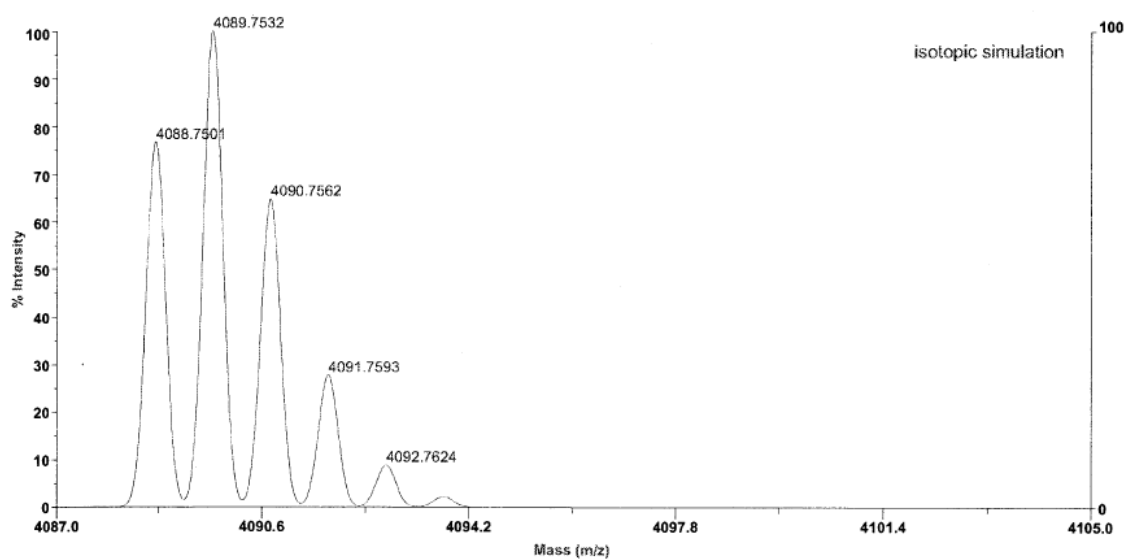
**Figure A.2** Observed MS MALDI-TOF isotopic pattern of $(F_{64}Pc)_2YH$ (top) and calculated isotopic pattern of $(F_{64}Pc)_2Y$ (below). In the negative mode, H is lost ($[M-H]^-$) and the pattern resembles that of the non-protonated form.
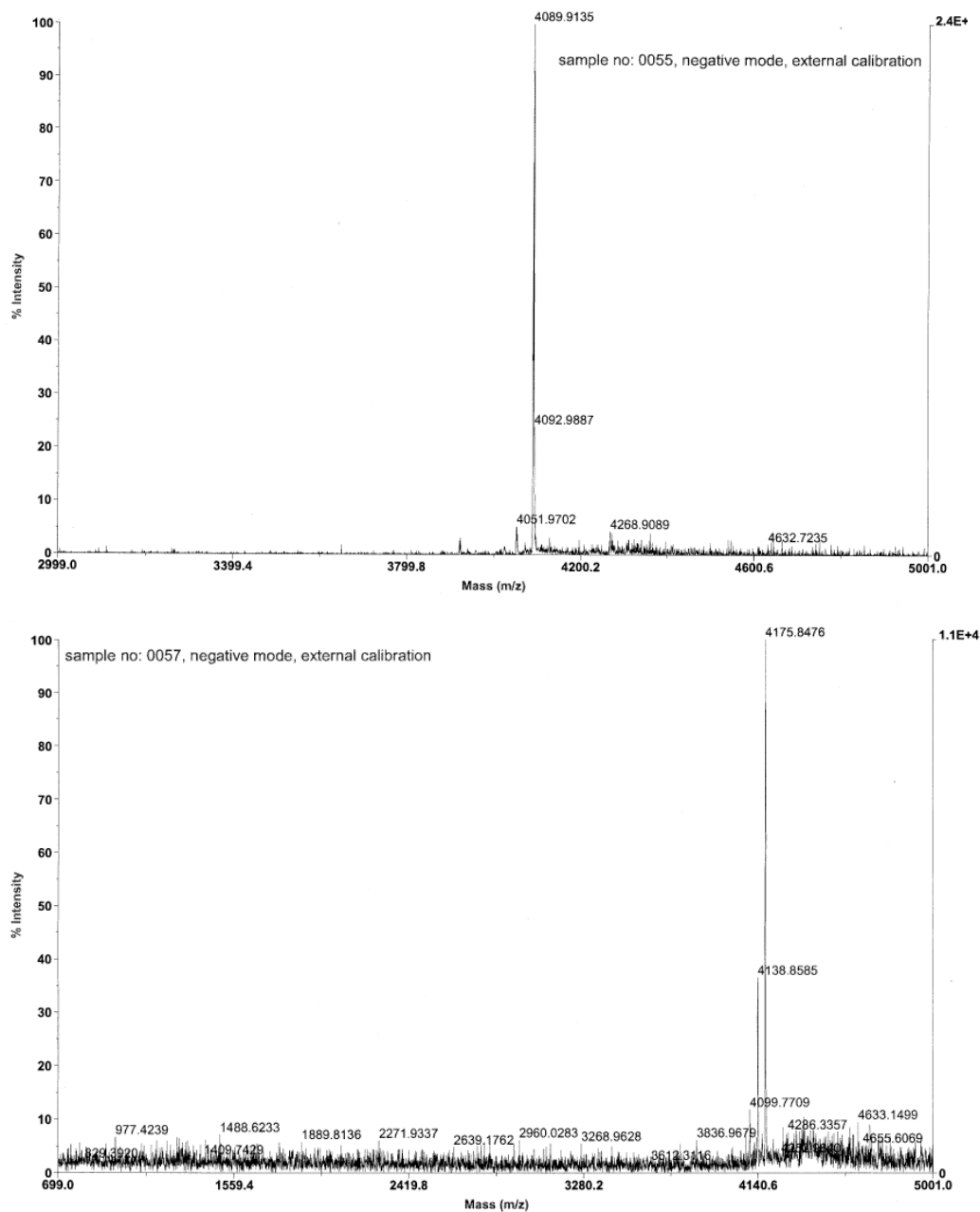
**Figure A.3** Observed MS MALDI-TOF of the $(F_{64}Pc)_2YH$ complex (top) and the $(F_{64}Pc)_2LuH$ complex bottom.

ISO:C112F128N16Tb



ISO:C112F128N16Tb + (H)1
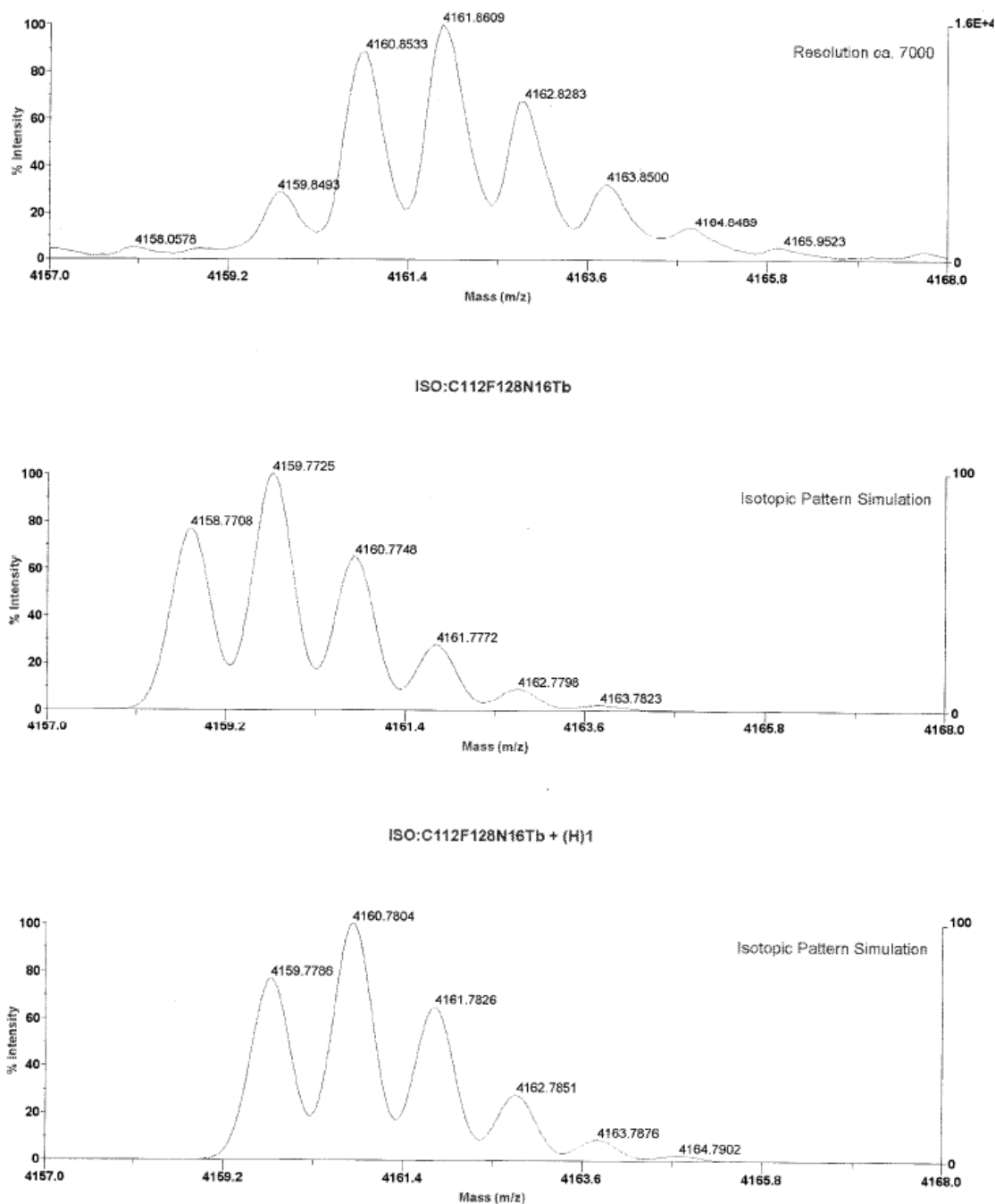


**Figure A.4** Observed MALDI-TOF MS isotopic pattern of $(F_{64}Pc)_2TbH$ in the positive mode (top) with PEG4000 internal calibrant in a CCA matrix. Simulated isotopic patterns of $(F_{64}Pc)_2Tb$ (middle) and $(F_{64}Pc)_2TbH$ (bottom) are shown for comparison. The observed spectrum reflects $(F_{64}Pc)_2TbH+H^+$ providing evidence for the protonated form of the complex.
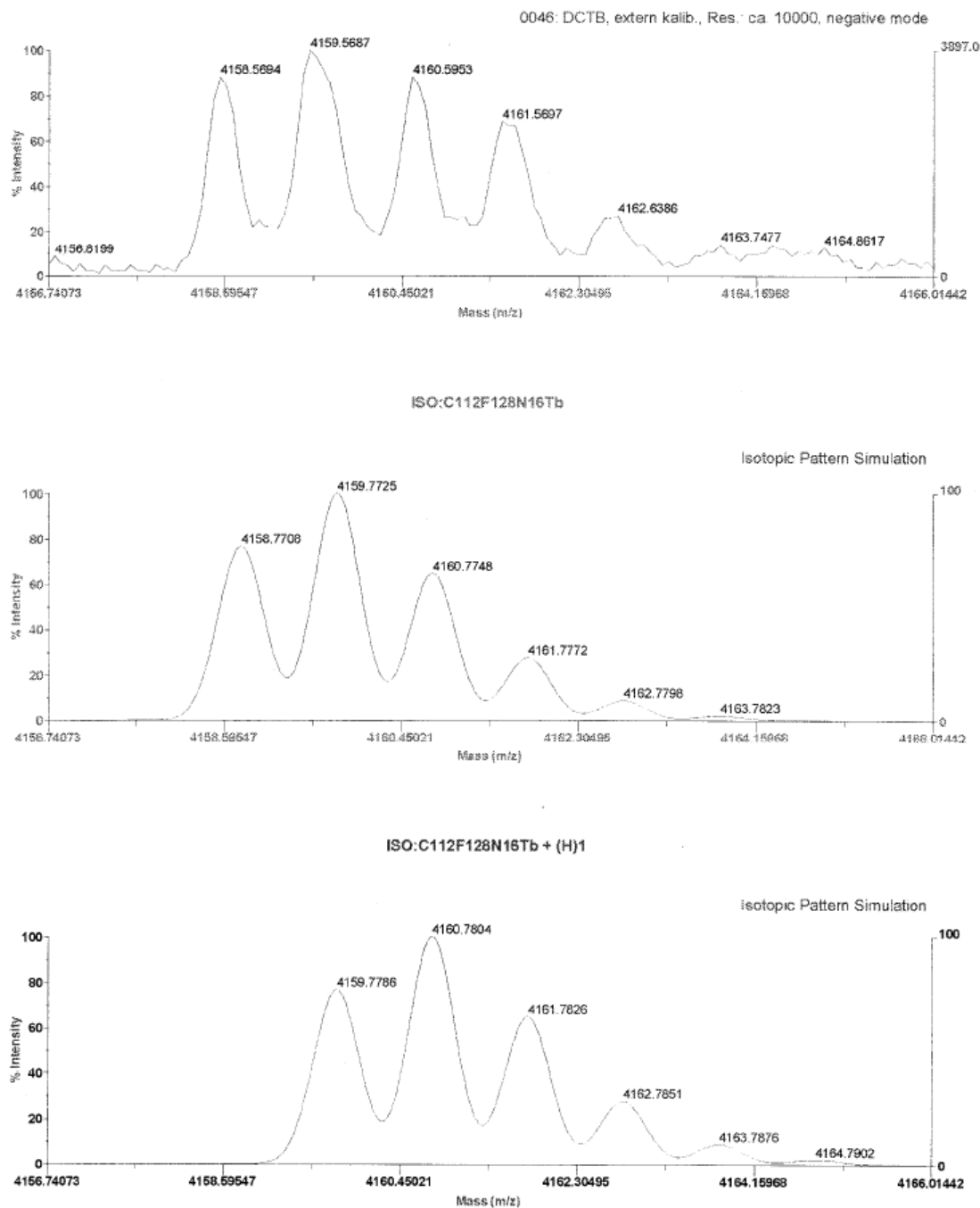
**Figure A.5**  Observed MALDI-TOF MS isotopic pattern of $(F_{64}Pc)_2TbH$ in the negative mode (top) with external calibration and DCTB as the matrix .  Simulations of the isotopic pattern for $(F_{64}Pc)_2Tb$ (middle) and $(F_{64}Pc)_2TbH$ (bottom) are shown.
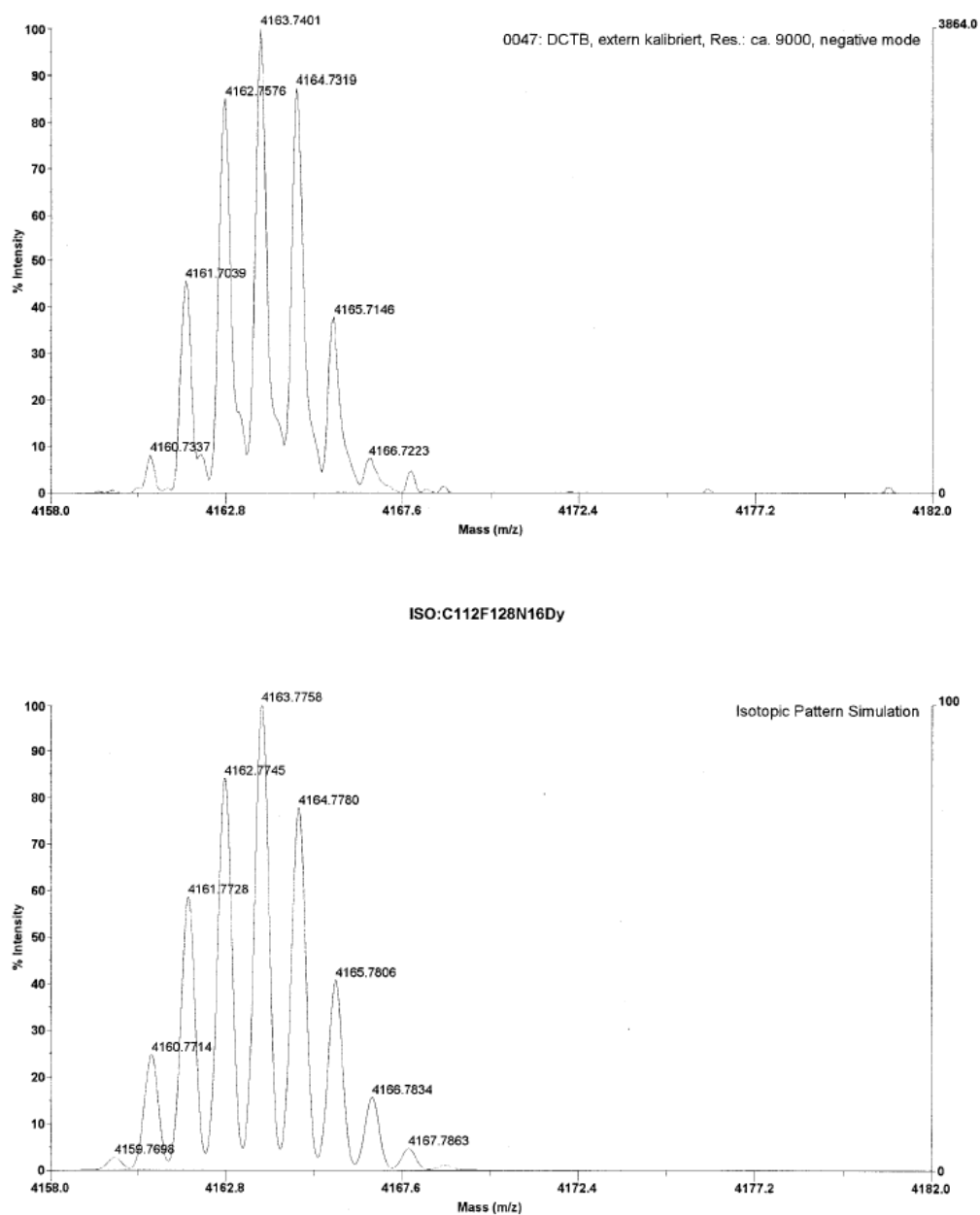
**Figure A.6** Observed MALDI-TOF MS isotopic pattern of $(F_{64}Pc)_2DyH$ in the negative mode (top) with external calibration and DCTB as the matrix. A simulation of the isotopic pattern for $(F_{64}Pc)_2Dy$ (bottom) is shown.
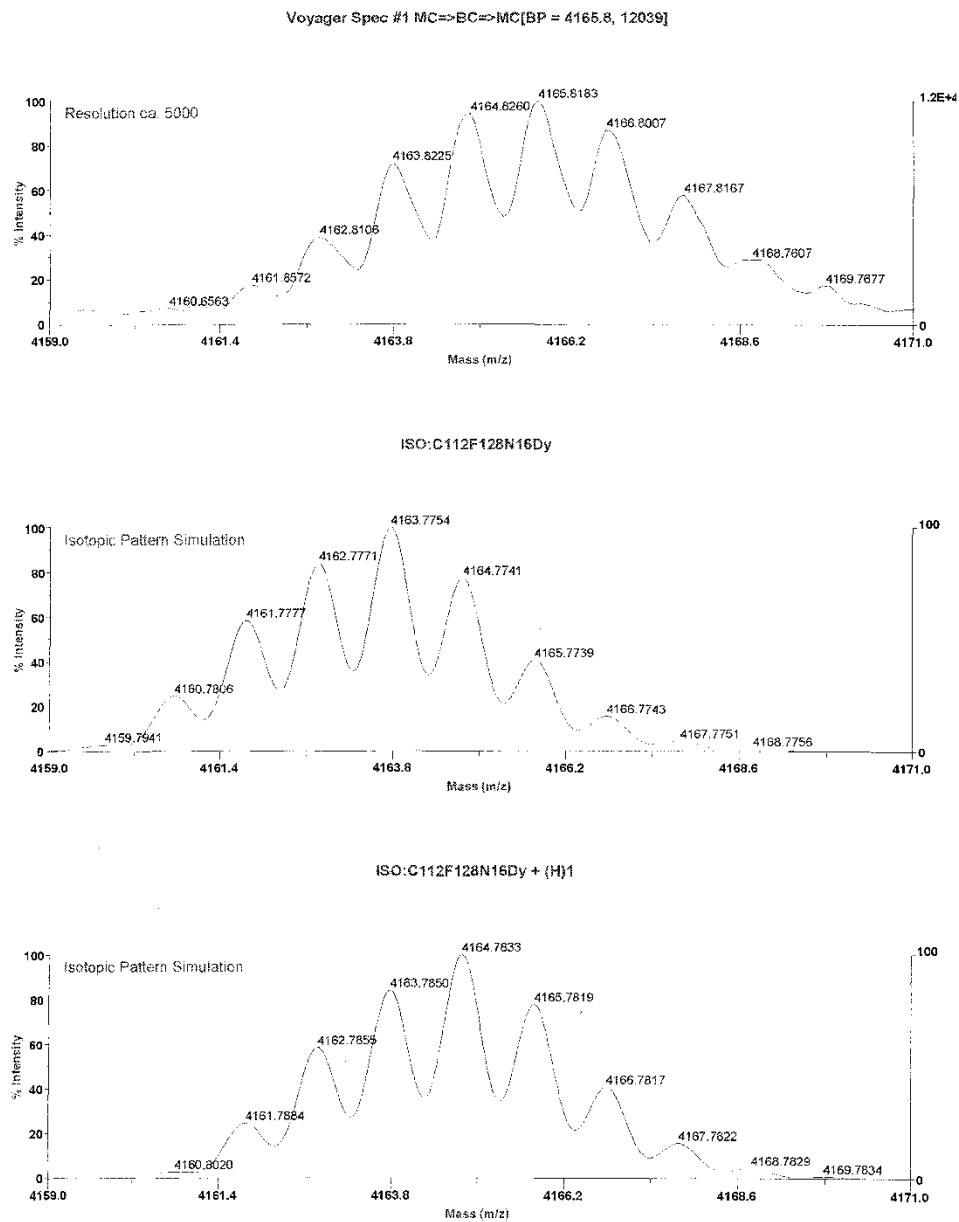
**Figure A.7** Observed MALDI-TOF MS isotopic pattern of (F$_{64}$Pc)$_2$DyH in the positive mode (top) with PEG4000 internal calibrant in a CCA matrix. Simulated isotopic patterns of (F$_{64}$Pc)$_2$Tb (middle) and (F$_{64}$Pc)$_2$DyH (bottom) are shown for comparison.
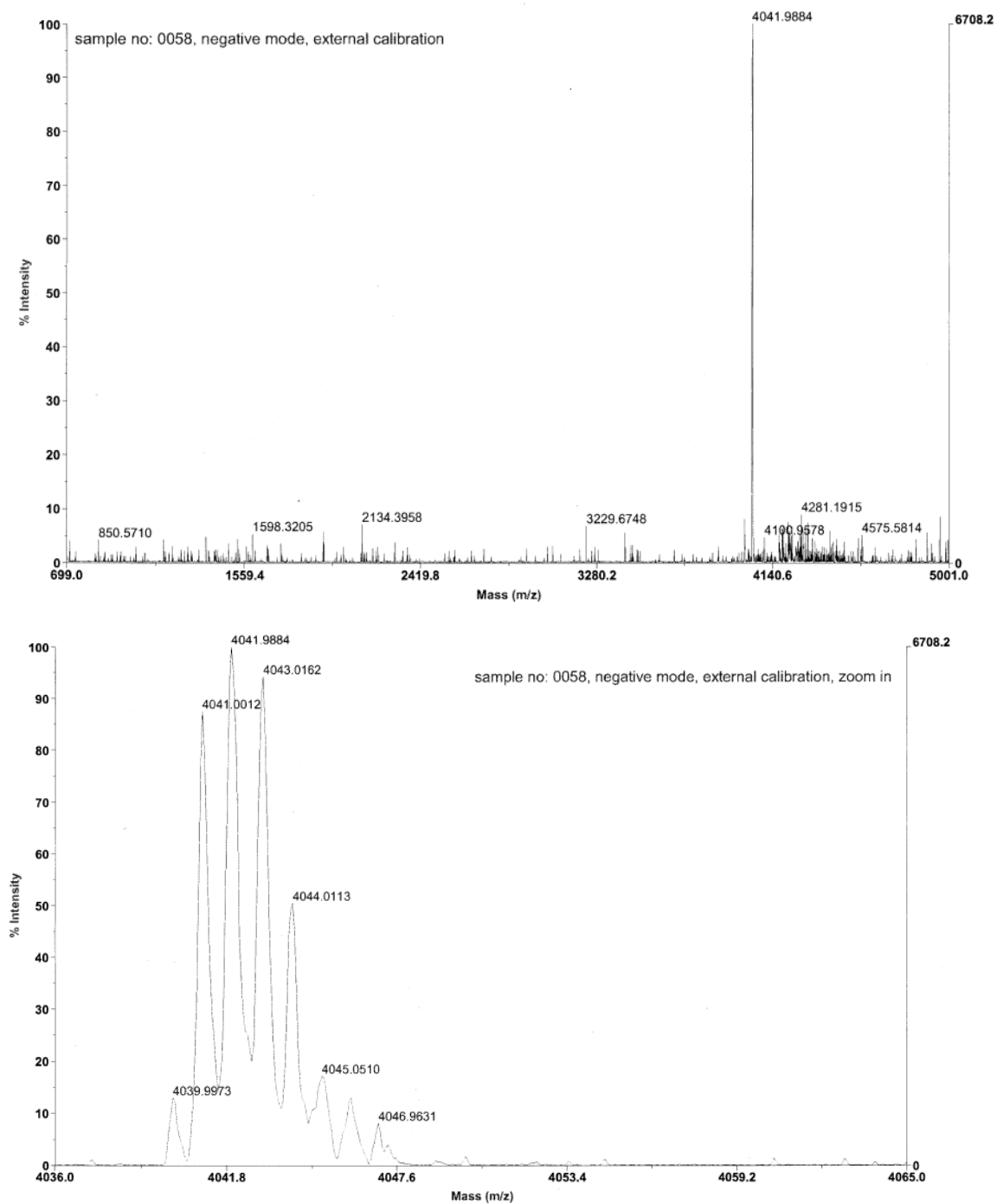
**Figure A.8** Observed MALDI-TOF MS isotopic pattern of $^{BG}$Y in the negative mode in CCA matrix (top). The expanded observed isotopic pattern is shown (bottom).

**(a)**                                                        **(b)**
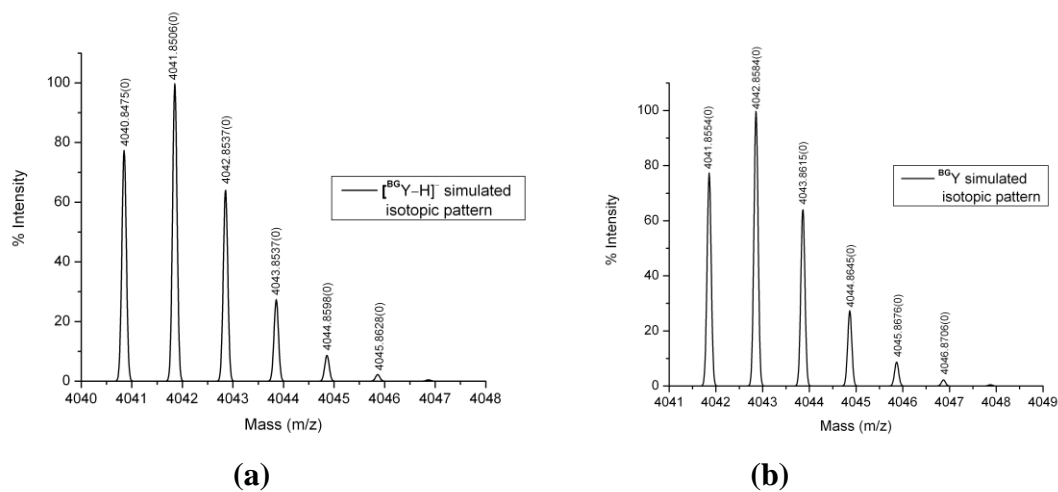
**Figure A.9** (a) Simulated MS spectrum of [$^{BG}$Y−H]$^-$ representing the observed spectrum and (b) simulated MS spectrum of $^{BG}$Y.
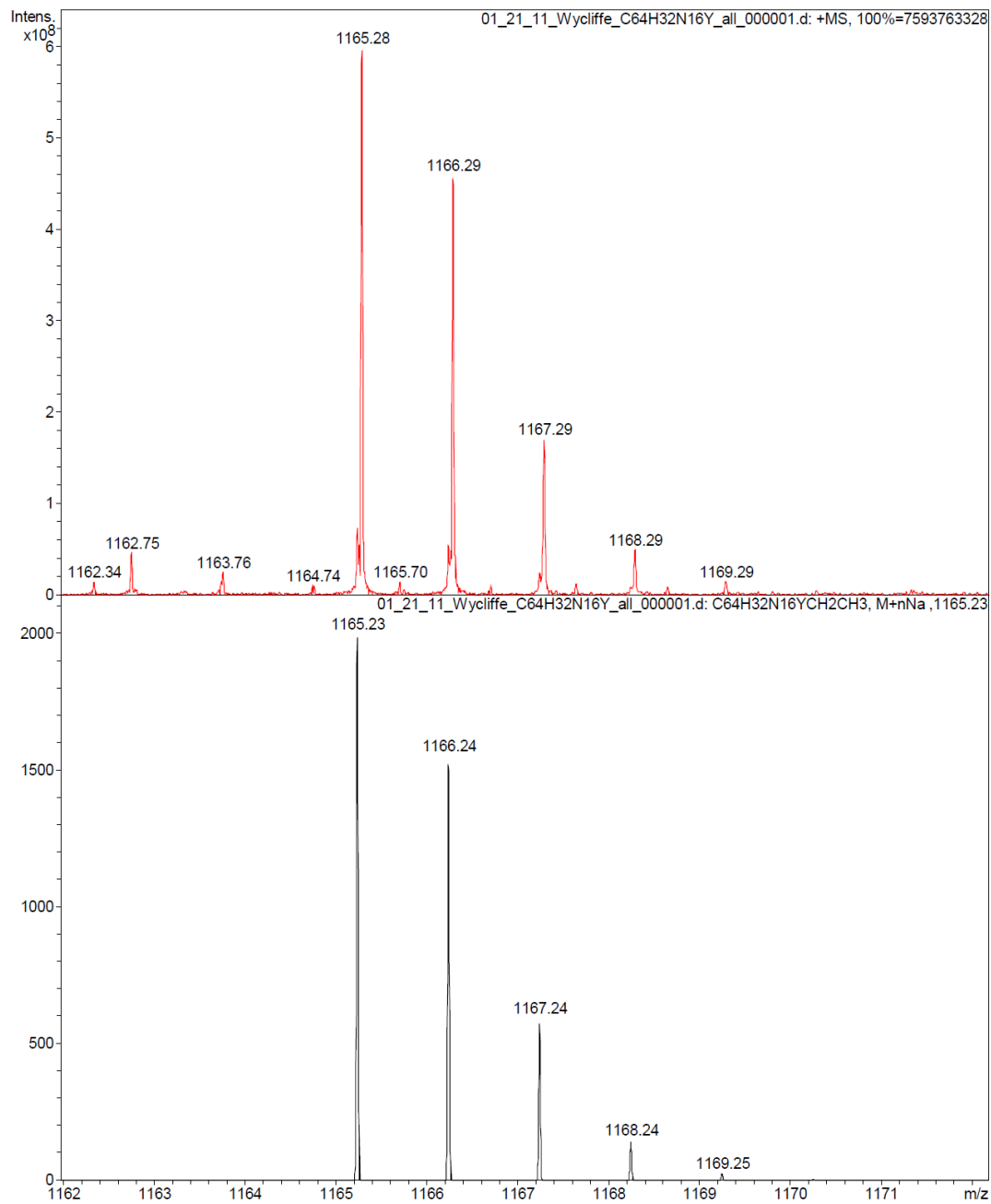
**Figure A.10** Mass spectroscopy of pattern of Pc$_2$Y in the positive mode. The patterns are shown with a C$_2$H$_5$Na adducted. It has empirical formula C$_{64}$H$_{32}$N$_{16}$Y with an isotopic molecular mass of 1113.205 Da.

# APPENDIX B

## RESULTS OF SINGLE CRYSTAL X-RAY DIFFRACTION

This appendix contains definitions and the tables of the crystal refinement results for the

five X-ray structures of complexes **[1]**, **[2]**, **[3]**, **[3′]** and **[4]**.

### B.1 X-ray Diffraction and Refinement Definitions

When a particular model is used in the solution and refinement of a molecular structure

obtained from X-ray or Neutron scattering data, the results contain information from

parameters defined by the particular discipline. Structure refinements were carried out

using the SHELXL-97 and SHELXTL 6.14[263, 264] packages and some specific

definitions have been included.

### B.1.1 The Structure Factor[265]

The structure factor $F_{hkl}$ is a mathematical function describing the amplitude and phase of

a wave diffracted from crystal lattice planes characterized by Miller indices $h,k,l$. It may

be given by the equation;

$$F_{(h,k,l)} = \sum_j f_j \exp[\, 2\pi \cdot i(hx_{(j)} + ky_{(j)} + lz_{(j)}]$$

(B.1)

where the sum is over all atoms in the unit cell, $x_j, y_j, z_j$ are the positional coordinates of

the $j$th atom, $f_j$ is the scattering factor of the $j$th atom.

## B.1.2 Zeroth Order Structure Factor

The evaluation of the structure factor in zeroth order case, where h = 0, k = 0, l = 0, may

be described by the expression;

$$F(000) = \left[\left(\sum f_r\right)^2 + \left(\sum f_i\right)^2\right]^{\frac{1}{2}} \tag{B.2}$$

where where $f_r$ is the real part of the scattering factors at, $f_i$ is the imaginary part of the

scattering factors at, $\theta$ is the Bragg angle, and the sum is taken over each atom in the unit

cell. F(000) is essentially a count of electrons in the cell.

## B.2 Residual or R-Factors[266]

The quality of a model can be judged with various residual or R- factors.   These factors

should converge to a minimum during the refinement and are quoted when the structure

is published.  Three of the common R-factors used are;

(1) The R1 factor in SHELXTL is based on structure factor F and is the unweighted

residual factor. It is defined as;

$$R1 = \frac{\sum ||F_o| - |F_c||}{\sum |F_o|} \tag{B.3}$$

where  $F_o$ is observed structure factor, $F_c$ is the calculated structure factor amplitudes.

(2) The weighted R factor, (wR2 in SHELXL) is defined as;

$$wR2 = \left[\frac{\sum w(F_o^2 - F_c^2)^2}{\sum wF_o^2}\right]^{\frac{1}{2}} \tag{B.4}$$

where w is the weighting factor. It is related to the refinement of the structure against the square of the structure factors.

(3) The Goodness of Fit, GooF or simply *S,* is defined as:

$$S = \left[\frac{\sum w(F_o^2 - F_c^2)^2}{(N_R - N_P)}\right]^{\frac{1}{2}} \tag{B.5}$$

where $N_R$ is the number of independent reflections and $N_P$ is the number of refined parameters.

**Table B.1** Experimental Parameters and Structure Refinement for $(F_{64}Pc)_2Lu$

| | |
|---|---|
| Empirical formula | C112 F128 Lu N16 |
| Formula weight | 4176.25 |
| Temperature | 100(2) K |
| Wavelength | 1.54178 Å |
| Crystal system | Tetragonal |
| Space group | P4/ncc |
| Unit cell dimensions | a = 27.1399(4) Å |
| α= 90°. | |
| | b = 27.1399(4) Å |
| β= 90°. | |
| | c = 23.7987(10) Å |
| γ = 90°. | |
| Volume | 17529.5(8) Å$^3$ |
| Z | 4 |
| Density (calculated) | 1.582 g/cm$^3$ |
| Absorption coefficient | 2.774 mm$^{-1}$ |
| F(000) | 8028 |
| Crystal size | 0.47 x 0.41 x 0.20 mm$^3$ |
| Theta range for data collection | 4.61 to 57.39°. |
| Index ranges | -28<=h<=29, -29<=k<=29, -26<=l<=25 |
| Reflections collected | 124883 |
| Independent reflections | 5997 [R(int) = 0.0889] |
| Completeness to theta = 57.39° | 99.9 % |
| Max. and min. transmission | 0.6015 and 0.3537 |
| Refinement method | Full-matrix least-squares on F$^2$ |
| Data / restraints / parameters | 5997 / 277 / 617 |
| Goodness-of-fit on F$^2$ | 1.115 |
| Final R indices [I>2sigma(I)] | R1 = 0.0783, wR2 = 0.2288 |
| R indices (all data) | R1 = 0.0837, wR2 = 0.2351 |
| Largest diff. peak and hole | 2.337 and -4.668 e.Å$^{-3}$ |

**Table B.2** Atomic Coordinates (x $10^4$) and Equivalent Isotropic Displacement Parameters ($A^2$ x $10^3$) for $(F_{64}Pc)_2Lu$.  U(eq) is Defined as One Third of the Trace of the Orthogonalized $U^{ij}$ Tensor

|         | x         | y         | z         | U(eq)    |
|---------|-----------|-----------|-----------|----------|
| **Lu**  | 2500      | 2500      | 8012(1)   | 27(1)    |
| **N(1)**| 2900(2)   | 3101(2)   | 8579(2)   | 35(1)    |
| **N(2)**| 2477(1)   | 1772(2)   | 7445(2)   | 29(1)    |
| **N(3)**| 3345(2)   | 1596(2)   | 7343(2)   | 34(1)    |
| **N(4)**| 3711(2)   | 2746(2)   | 8686(2)   | 40(1)    |
| **C(1)**| 3551(2)   | 3630(2)   | 8765(3)   | 43(2)    |
| **C(2)**| 3120(2)   | 3902(2)   | 8795(3)   | 44(1)    |
| **C(3)**| 3139(2)   | 4389(2)   | 8955(3)   | 48(2)    |
| **C(4)**| 3583(3)   | 4637(2)   | 9046(3)   | 59(2)    |
| **C(5)**| 4029(3)   | 4356(3)   | 9001(3)   | 63(2)    |
| **C(6)**| 3993(2)   | 3855(3)   | 8849(3)   | 52(2)    |
| **C(7)**| 4557(3)   | 4537(3)   | 9116(5)   | 82(3)    |
| **C(8)**| 4894(4)   | 4189(5)   | 9438(5)   | 140(6)   |
| **C(9)**| 4830(9)   | 4662(12)  | 8571(14)  | 120(20)  |
| **C(9')**| 4784(9)  | 4709(8)   | 8562(11)  | 180(30)  |
| **C(10)**| 3427(4)  | 5274(3)   | 9815(5)   | 116(4)   |
| **C(11)**| 3123(3)  | 5487(2)   | 8810(4)   | 84(3)    |
| **C(12)**| 3537(3)  | 5193(3)   | 9186(4)   | 77(3)    |
| **C(13)**| 4417(2)  | 1926(2)   | 7095(3)   | 39(1)    |
| **C(14)**| 4008(2)  | 2196(2)   | 7245(2)   | 37(1)    |
| **C(15)**| 4031(2)  | 2701(2)   | 7265(2)   | 35(1)    |
| **C(16)**| 4481(2)  | 2928(2)   | 7180(3)   | 39(1)    |
| **C(17)**| 4908(2)  | 2675(2)   | 7051(2)   | 42(1)    |
| **C(18)**| 5395(2)  | 2970(3)   | 7068(3)   | 50(2)    |
| **C(19)**| 5489(2)  | 3269(3)   | 6543(3)   | 65(2)    |
| **C(20)**| 5450(2)  | 3282(3)   | 7622(3)   | 68(2)    |
| **C(21)**| 5246(2)  | 1805(2)   | 6694(3)   | 50(2)    |
| **C(22)**| 5550(2)  | 1469(3)   | 7098(3)   | 63(2)    |
| **C(23)**| 5029(2)  | 1466(3)   | 6202(3)   | 69(2)    |
| **C(24)**| 4873(2)  | 2147(2)   | 6967(2)   | 43(2)    |
| **C(25)**| 3492(2)  | 2057(2)   | 7360(2)   | 33(1)    |
| **C(26)**| 2713(2)  | 3571(2)   | 8683(2)   | 39(1)    |
| **C(27)**| 3405(2)  | 3117(2)   | 8656(2)   | 38(1)    |
| **C(28)**| 2876(2)  | 1472(2)   | 7367(2)   | 32(1)    |
| **F(1)** | 2721(1)  | 4629(1)   | 9014(2)   | 55(1)    |
| **F(2)** | 4396(1)  | 3590(1)   | 8783(2)   | 65(1)    |
| **F(3)** | 4553(2)  | 4957(2)   | 9418(3)   | 118(2)   |
| **F(4)** | 4660(3)  | 3879(3)   | 9790(3)   | 142(3)   |
| **F(5)** | 5221(3)  | 4449(3)   | 9749(4)   | 186(4)   |
| **F(6)** | 5186(2)  | 3902(3)   | 9073(4)   | 165(4)   |
| **F(7)** | 4890(20) | 4260(18)  | 8260(30)  | 160(20)  |
| **F(7')**| 4767(11) | 4368(8)   | 8149(13)  | 99(7)    |
| **F(8)** | 5259(15) | 4822(16)  | 8760(30)  | 159(17)  |
| **F(8')**| 5256(8)  | 4862(9)   | 8550(20)  | 149(12)  |
| **F(9)** | 4604(13) | 5009(17)  | 8280(19)  | 190(20)  |
| **F(9')**| 4543(7)  | 5096(6)   | 8333(9)   | 91(6)    |
| **F(10)**| 3055(2)  | 5271(2)   | 8326(3)   | 110(2)   |
| **F(11)**| 3290(2)  | 5941(2)   | 8737(4)   | 145(3)   |
| **F(12)**| 2695(2)  | 5525(2)   | 9081(3)   | 107(2)   |

**Table B.2** Atomic Coordinates (x $10^4$) and Equivalent Isotropic Displacement Parameters ($A^2$ x $10^3$) for $(F_{64}Pc)_2Lu$. U(eq) is Defined as One Third of the Trace of the Orthogonalized $U^{ij}$ Tensor, Continued

|  | x | y | x | U(eq) |
|---|---|---|---|---|
| F(13) | 2695(2) | 5525(2) | 9081(3) | 107(2) |
| F(14) | 3384(3) | 5749(2) | 9924(3) | 159(4) |
| F(15) | 3806(3) | 5104(3) | 10097(3) | 130(3) |
| F(16) | 4377(1) | 1438(1) | 7048(2) | 55(1) |
| F(17) | 4503(1) | 3418(1) | 7244(2) | 50(1) |
| F(18) | 5179(2) | 3128(2) | 8027(2) | 72(1) |
| F(19) | 5329(2) | 3761(2) | 7519(2) | 80(1) |
| F(20) | 5917(1) | 3295(2) | 7772(2) | 86(2) |
| F(21) | 5118(2) | 3574(2) | 6420(2) | 77(1) |
| F(22) | 5890(2) | 3538(2) | 6600(2) | 94(2) |
| F(23) | 5548(2) | 2977(2) | 6097(2) | 84(1) |
| F(24) | 5783(1) | 2651(2) | 7118(2) | 65(1) |
| F(25) | 5259(2) | 1222(2) | 7436(2) | 75(1) |
| F(26) | 5828(2) | 1163(2) | 6816(3) | 96(2) |
| F(27) | 5845(2) | 1748(2) | 7405(2) | 81(1) |
| F(28) | 5589(1) | 2077(2) | 6405(2) | 70(1) |
| F(29) | 5368(2) | 1414(2) | 5803(2) | 89(2) |
| F(30) | 4907(2) | 1021(2) | 6367(2) | 87(2) |
| F(31) | 4639(2) | 1681(2) | 5972(2) | 79(1) |
| F(32) | 3951(2) | 5448(2) | 9052(3) | 108(2) |

**Table B.3**  Bond Lengths [Å] and Angles [°] for $(F_{64}Pc)_2Lu$

| | | | |
|---|---|---|---|
| Lu-N(1)#1 | 2.380(4) | Lu-N(2) | 2.394(4) |
| Lu-N(1)#2 | 2.380(4) | Lu-N(2)#3 | 2.394(4) |
| Lu-N(1) | 2.380(4) | Lu-N(2)#2 | 2.394(4) |
| Lu-N(1)#3 | 2.380(4) | Lu-N(2)#1 | 2.394(4) |
| | | | |
| N(1)-C(27) | 1.383(7) | C(4)-C(12) | 1.548(10) |
| N(1)-C(26) | 1.396(7) | C(5)-C(6) | 1.410(10) |
| N(2)-C(25)#1 | 1.361(7) | C(5)-C(7) | 1.537(11) |
| N(2)-C(28) | 1.368(7) | C(6)-F(2) | 1.318(7) |
| N(3)-C(25) | 1.316(7) | C(7)-F(3) | 1.348(10) |
| N(3)-C(28) | 1.316(7) | C(7)-C(9) | 1.53(3) |
| N(4)-C(26)#1 | 1.302(8) | C(7)-C(9') | 1.53(3) |
| N(4)-C(27) | 1.307(7) | C(7)-C(8) | 1.523(17) |
| C(1)-C(6) | 1.363(9) | C(8)-F(4) | 1.347(12) |
| C(1)-C(2) | 1.383(8) | C(8)-F(5) | 1.353(9) |
| C(1)-C(27) | 1.470(8) | C(8)-F(6) | 1.410(11) |
| C(2)-C(3) | 1.378(8) | C(9)-F(9) | 1.32(3) |
| C(2)-C(26) | 1.447(8) | C(9)-F(7) | 1.32(3) |
| C(3)-F(1) | 1.316(7) | C(9)-F(8) | 1.32(3) |
| C(3)-C(4) | 1.398(9) | C(9')-F(8') | 1.35(2) |
| C(4)-C(5) | 1.435(11) | C(9')-F(9') | 1.35(2) |

**Table B.3**   Bond Lengths [Å] and Angles [°] for (F$_{64}$Pc)$_2$Lu, Continued

| | | | |
|---|---|---|---|
| C(9')-F(7') | 1.35(2) | C(18)-C(19) | 1.511(11) |
| C(10)-F(13) | 1.302(9) | C(18)-C(20) | 1.576(10) |
| C(10)-F(15) | 1.313(11) | C(19)-F(22) | 1.318(7) |
| C(10)-F(14) | 1.318(9) | C(19)-F(23) | 1.333(8) |
| C(10)-C(12) | 1.541(14) | C(19)-F(21) | 1.337(8) |
| C(11)-F(10) | 1.306(9) | C(20)-F(18) | 1.285(8) |
| C(11)-F(11) | 1.325(8) | C(20)-F(20) | 1.316(7) |
| C(11)-F(12) | 1.331(9) | C(20)-F(19) | 1.361(8) |
| C(11)-C(12) | 1.644(14) | C(21)-F(28) | 1.372(7) |
| C(12)-F(32) | 1.358(8) | C(21)-C(24) | 1.519(9) |
| C(13)-F(16) | 1.335(7) | C(21)-C(22) | 1.562(10) |
| C(13)-C(14) | 1.378(8) | C(21)-C(23) | 1.601(11) |
| C(13)-C(24) | 1.408(9) | C(22)-F(26) | 1.307(7) |
| C(14)-C(15) | 1.371(8) | C(22)-F(25) | 1.311(8) |
| C(14)-C(25) | 1.477(8) | C(22)-F(27) | 1.324(8) |
| C(15)-C(16) | 1.382(8) | C(23)-F(30) | 1.313(8) |
| C(15)-C(28)#3 | 1.467(8) | C(23)-F(31) | 1.326(8) |
| C(16)-F(17) | 1.338(6) | C(23)-F(29) | 1.331(8) |
| C(16)-C(17) | 1.382(8) | C(25)-N(2)#3 | 1.361(7) |
| C(17)-C(24) | 1.451(9) | C(26)-N(4)#3 | 1.302(8) |
| C(17)-C(18) | 1.544(9) | C(28)-C(15)#1 | 1.467(8) |
| C(18)-F(24) | 1.367(8) | F(7')-F(9) | 1.82(5) |
| | | | |
| N(1)#1-Lu-N(1)#2 | 71.25(11) | N(2)-Lu-N(2)#3 | 71.43(11) |
| N(1)#1-Lu-N(1) | 71.25(11) | N(1)#1-Lu-N(2)#2 | 132.77(14) |
| N(1)#2-Lu-N(1) | 110.9(2) | N(1)#2-Lu-N(2)#2 | 153.82(14) |
| N(1)#1-Lu-N(1)#3 | 110.9(2) | N(1)-Lu-N(2)#2 | 75.07(16) |
| N(1)#2-Lu-N(1)#3 | 71.25(11) | N(1)#3-Lu-N(2)#2 | 87.76(15) |
| N(1)-Lu-N(1)#3 | 71.25(11) | N(2)-Lu-N(2)#2 | 111.3(2) |
| N(1)#1-Lu-N(2) | 87.76(15) | N(2)#3-Lu-N(2)#2 | 71.43(11) |
| N(1)#2-Lu-N(2) | 75.07(16) | N(1)#1-Lu-N(2)#1 | 153.83(14) |
| N(1)-Lu-N(2) | 153.83(14) | N(1)#2-Lu-N(2)#1 | 87.76(15) |
| N(1)#3-Lu-N(2) | 132.76(14) | N(1)-Lu-N(2)#1 | 132.76(14) |
| N(1)#1-Lu-N(2)#3 | 75.08(16) | N(1)#3-Lu-N(2)#1 | 75.07(16) |
| N(1)#2-Lu-N(2)#3 | 132.77(14) | N(2)-Lu-N(2)#1 | 71.43(11) |
| N(1)-Lu-N(2)#3 | 87.76(15) | N(2)#3-Lu-N(2)#1 | 111.3(2) |
| N(1)#3-Lu-N(2)#3 | 153.83(14) | N(2)#2-Lu-N(2)#1 | 71.42(11) |
| C(27)-N(1)-C(26) | 108.0(4) | C(2)-C(1)-C(27) | 106.7(5) |
| C(27)-N(1)-Lu | 123.3(4) | C(3)-C(2)-C(1) | 119.6(6) |
| C(26)-N(1)-Lu | 124.1(3) | C(3)-C(2)-C(26) | 132.4(6) |
| C(25)#1-N(2)-C(28) | 109.3(5) | C(1)-C(2)-C(26) | 107.8(5) |
| C(25)#1-N(2)-Lu | 122.6(3) | F(1)-C(3)-C(2) | 118.2(5) |
| C(28)-N(2)-Lu | 123.1(3) | F(1)-C(3)-C(4) | 119.2(5) |
| C(25)-N(3)-C(28) | 122.3(5) | C(2)-C(3)-C(4) | 122.5(6) |
| C(26)#1-N(4)-C(27) | 123.6(5) | C(3)-C(4)-C(5) | 117.4(6) |
| C(6)-C(1)-C(2) | 119.9(6) | C(3)-C(4)-C(12) | 115.7(6) |
| C(6)-C(1)-C(27) | 133.4(6) | C(5)-C(4)-C(12) | 127.0(6) |

**Table B.3**  Bond Lengths [Å] and Angles [°] for (F₆₄Pc)₂Lu, Continued

| | | | |
|---|---|---|---|
| C(6)-C(5)-C(4) | 118.2(6) | C(10)-C(12)-C(4) | 111.4(7) |
| C(6)-C(5)-C(7) | 114.7(6) | F(32)-C(12)-C(11) | 100.9(7) |
| C(4)-C(5)-C(7) | 127.1(6) | C(10)-C(12)-C(11) | 109.0(7) |
| F(2)-C(6)-C(1) | 118.0(6) | C(4)-C(12)-C(11) | 114.3(6) |
| F(2)-C(6)-C(5) | 119.9(6) | F(16)-C(13)-C(14) | 118.9(5) |
| C(1)-C(6)-C(5) | 122.1(6) | F(16)-C(13)-C(24) | 118.4(5) |
| F(3)-C(7)-C(9) | 105.5(14) | C(14)-C(13)-C(24) | 122.6(5) |
| F(3)-C(7)-C(9') | 101.8(11) | C(15)-C(14)-C(13) | 120.2(5) |
| C(9)-C(7)-C(9') | 6.7(15) | C(15)-C(14)-C(25) | 107.0(4) |
| F(3)-C(7)-C(8) | 105.2(8) | C(13)-C(14)-C(25) | 132.7(5) |
| C(9')-C(7)-C(8) | 112.4(11) | C(14)-C(15)-C(16) | 118.8(5) |
| F(3)-C(7)-C(5) | 111.0(7) | C(14)-C(15)-C(28)#3 | 106.7(4) |
| C(9)-C(7)-C(5) | 111.7(14) | C(16)-C(15)-C(28)#3 | 134.5(5) |
| C(9')-C(7)-C(5) | 108.6(12) | F(17)-C(16)-C(17) | 118.7(5) |
| C(8)-C(7)-C(5) | 116.9(9) | F(17)-C(16)-C(15) | 117.8(5) |
| F(4)-C(8)-F(5) | 107.3(10) | C(17)-C(16)-C(15) | 123.4(5) |
| F(4)-C(8)-F(6) | 107.6(11) | C(16)-C(17)-C(24) | 117.8(5) |
| F(5)-C(8)-F(6) | 104.9(8) | C(16)-C(17)-C(18) | 117.1(5) |
| F(4)-C(8)-C(7) | 114.5(9) | C(24)-C(17)-C(18) | 124.8(5) |
| F(5)-C(8)-C(7) | 110.2(10) | F(24)-C(18)-C(19) | 106.3(5) |
| F(6)-C(8)-C(7) | 111.7(10) | F(24)-C(18)-C(17) | 109.5(5) |
| F(9)-C(9)-F(7) | 111(2) | C(19)-C(18)-C(17) | 113.7(5) |
| F(9)-C(9)-F(8) | 111(2) | F(24)-C(18)-C(20) | 101.1(5) |
| F(7)-C(9)-F(8) | 111.0(19) | C(19)-C(18)-C(20) | 112.8(6) |
| F(9)-C(9)-C(7) | 112(2) | C(17)-C(18)-C(20) | 112.4(5) |
| F(7)-C(9)-C(7) | 110(3) | F(22)-C(19)-F(23) | 108.3(6) |
| F(8)-C(9)-C(7) | 102(4) | F(22)-C(19)-F(21) | 107.6(6) |
| F(8')-C(9')-F(9') | 102.2(18) | F(23)-C(19)-F(21) | 106.5(6) |
| F(8')-C(9')-F(7') | 103.2(19) | F(22)-C(19)-C(18) | 110.6(6) |
| F(9')-C(9')-F(7') | 103.0(17) | F(23)-C(19)-C(18) | 111.0(6) |
| F(8')-C(9')-C(7) | 120(3) | F(21)-C(19)-C(18) | 112.6(5) |
| F(9')-C(9')-C(7) | 112.9(17) | F(18)-C(20)-F(20) | 111.0(6) |
| F(7')-C(9')-C(7) | 114(2) | F(18)-C(20)-F(19) | 107.9(6) |
| F(13)-C(10)-F(15) | 109.1(9) | F(20)-C(20)-F(19) | 104.8(5) |
| F(13)-C(10)-F(14) | 109.6(8) | F(18)-C(20)-C(18) | 113.4(5) |
| F(15)-C(10)-F(14) | 108.2(8) | F(20)-C(20)-C(18) | 109.5(6) |
| F(13)-C(10)-C(12) | 112.2(7) | F(19)-C(20)-C(18) | 109.9(6) |
| F(15)-C(10)-C(12) | 107.1(8) | F(28)-C(21)-C(24) | 109.7(5) |
| F(14)-C(10)-C(12) | 110.5(9) | F(28)-C(21)-C(22) | 105.4(5) |
| F(10)-C(11)-F(11) | 110.4(8) | C(24)-C(21)-C(22) | 116.4(5) |
| F(10)-C(11)-F(12) | 109.9(8) | F(28)-C(21)-C(23) | 101.1(5) |
| F(11)-C(11)-F(12) | 106.8(6) | C(24)-C(21)-C(23) | 114.7(5) |
| F(10)-C(11)-C(12) | 111.0(6) | C(22)-C(21)-C(23) | 108.1(5) |
| F(11)-C(11)-(12) | 106.8(8) | F(32)-C(12)-C(10) | 108.3(6) |
| F(12)-C(11)-C(12) | 111.8(7) | F(32)-C(12)-C(4) | 112.3(6) |
| F(27)-C(22)-C(21) | 109.0(6) | F(30)-C(23)-F(29) | 106.8(6) |
| F(30)-C(23)-F(31) | 109.0(6) | F(31)-C(23)-F(29) | 107.9(7) |

**Table B.3** Bond Lengths [Å] and Angles [°] for (F$_{64}$Pc)$_2$Lu, Continued

| | | | |
|---|---|---|---|
| F(30)-C(23)-C(21) | 113.7(6) | | |
| F(31)-C(23)-C(21) | 110.1(5) | N(4)-C(27)-C(1) | 123.3(5) |
| F(29)-C(23)-C(21) | 109.1(5) | N(1)-C(27)-C(1) | 108.6(5) |
| C(13)-C(24)-C(17) | 116.6(5) | N(3)-C(28)-N(2) | 128.2(5) |
| C(13)-C(24)-C(21) | 114.7(5) | N(3)-C(28)-C(15)#1 | 123.0(5) |
| C(17)-C(24)-C(21) | 128.3(5) | N(2)-C(28)-C(15)#1 | 108.6(4) |
| N(3)-C(25)-N(2)#3 | 130.0(5) | C(9')-F(7')-F(9) | 39.6(18) |
| N(3)-C(25)-C(14) | 121.7(5) | C(9)-F(9)-F(7') | 45(3) |
| N(2)#3-C(25)-C(14) | 108.2(4) | F(26)-C(22)-F(25) | 109.8(6) |
| N(4)#3-C(26)-N(1) | 128.0(5) | F(26)-C(22)-F(27) | 107.2(5) |
| N(4)#3-C(26)-C(2) | 123.3(5) | F(25)-C(22)-F(27) | 108.6(6) |
| N(1)-C(26)-C(2) | 108.7(5) | F(26)-C(22)-C(21) | 111.1(6) |
| N(4)-C(27)-N(1) | 127.7(5) | | |

Symmetry transformations used to generate equivalent atoms:
 #1 y,-x+1/2,z   #2 – x+1/2,-y+1/2,z   #3 -y+1/2,x,z

**Table B.4** Experimental Parameters and Structure Refinement for $(F_{64}Pc)_2Y$

| | |
|---|---|
| Empirical formula | C112 F128 N16 Y |
| Formula weight | 4090.19 |
| Temperature | 253(2) K |
| Wavelength | 1.54178 Å |
| Crystal system | Tetragonal |
| Space group | P4/ncc |
| Unit cell dimensions | a = 27.4142(4) Å |
| α= 90°. | |
| | b = 27.4142(4) Å |
| β= 90°. | |
| | c = 24.3774(10) Å |
| γ = 90°. | |
| Volume | 18320.6(8) Å$^3$ |
| Z | 4 |
| Density (calculated) | 1.483 g/cm$^3$ |
| Absorption coefficient | 2.072 mm$^{-1}$ |
| F(000) | 7900 |
| Crystal size | 0.42 x 0.41 x 0.23 mm$^3$ |
| Theta range for data collection | 3.22 to 67.58°. |
| Index ranges | -32<=h<=31, -32<=k<=29, -28<=l<=28 |
| Reflections collected | 145759 |
| Independent reflections | 8172 [R(int) = 0.0338] |
| Completeness to theta = 67.58° | 98.7 % |
| Max. and min. transmission | 0.6473 and 0.4766 |
| Refinement method | Full-matrix least-squares on F$^2$ |
| Data / restraints / parameters | 8172 / 198 / 580 |
| Goodness-of-fit on F$^2$ | 1.058 |
| Final R indices [I>2sigma(I)] | R1 = 0.0732, wR2 = 0.2226 |
| R indices (all data) | R1 = 0.0820, wR2 = 0.2319 |
| Largest diff. peak and hole | 0.679 and -0.342 e.Å$^{-3}$ |

**Table B.5** Atomic Coordinates (x $10^4$) and Equivalent Isotropic Displacement Parameters (A$^2$ x $10^3$) for $(F_{64}Pc)_2Y$. U(eq) is Defined as One Third of the Trace of the Orthogonalized U$^{ij}$ Tensor

| | x | y | z | U(eq) |
|---|---|---|---|---|
| Y | 2500 | 2500 | 8029(1) | 41(1) |
| N(1) | 3101(1) | 2098(1) | 8599(1) | 49(1) |
| N(2) | 2742(1) | 1297(1) | 8698(1) | 56(1) |
| N(3) | 2472(1) | 1779(1) | 7463(1) | 48(1) |
| N(4) | 3332(1) | 1598(1) | 7364(1) | 54(1) |
| C(1) | 3112(1) | 1606(1) | 8676(1) | 51(1) |
| C(2) | 3617(1) | 1455(1) | 8785(2) | 56(1) |
| C(3) | 3885(1) | 1876(1) | 8810(2) | 57(1) |
| C(4) | 3555(1) | 2279(1) | 8696(1) | 51(1) |
| C(5) | 3838(1) | 1013(1) | 8887(2) | 67(1) |
| C(6) | 4326(2) | 976(2) | 9037(2) | 76(1) |
| C(7) | 4604(1) | 1416(2) | 9073(2) | 72(1) |
| C(8) | 4372(1) | 1850(2) | 8969(2) | 65(1) |

**Table B.5** Atomic Coordinates (x $10^4$) and Equivalent Isotropic Displacement Parameters ($A^2$ x $10^3$) for $(F_{64}Pc)_2Y$. U(eq) is Defined as One Third of the Trace of the Orthogonalized $U^{ij}$ Tensor, Continued

|  | x | y | z | U(eq) |
|---|---|---|---|---|
| C(9) | 5158(2) | 1460(2) | 9213(3) | 97(2) |
| C(10) | 5237(3) | 1540(5) | 9817(4) | 168(4) |
| C(11) | 5462(2) | 1840(3) | 8815(4) | 117(2) |
| C(12) | 4496(2) | 449(2) | 9163(4) | 116(2) |
| C(13) | 4627(4) | 171(3) | 8646(8) | 228(8) |
| C(14) | 4149(4) | 114(3) | 9475(4) | 218(7) |
| C(15) | 2866(1) | 1478(1) | 7386(1) | 51(1) |
| C(16) | 2692(1) | 982(1) | 7281(2) | 56(1) |
| C(17) | 2189(1) | 1006(1) | 7261(1) | 55(1) |
| C(18) | 2058(1) | 1515(1) | 7374(1) | 51(1) |
| C(19) | 1926(1) | 602(1) | 7109(2) | 64(1) |
| C(20) | 2143(2) | 157(1) | 6973(2) | 68(1) |
| C(21) | 2663(2) | 119(1) | 7056(2) | 66(1) |
| C(22) | 2920(1) | 537(1) | 7182(2) | 61(1) |
| C(23) | 2957(2) | -363(2) | 7065(2) | 86(1) |
| C(24) | 3257(2) | -428(2) | 7610(3) | 114(2) |
| C(25) | 3260(3) | -457(3) | 6568(4) | 141(3) |
| C(26) | 1803(2) | -227(2) | 6709(2) | 84(1) |
| C(27) | 1493(3) | -1(3) | 6206(4) | 132(3) |
| C(28) | 1457(3) | -494(3) | 7070(4) | 129(2) |
| F(1) | 4617(1) | 2268(1) | 9006(1) | 82(1) |
| F(2) | 3568(1) | 615(1) | 8823(1) | 89(1) |
| F(3) | 5405(1) | 1042(1) | 9057(2) | 156(2) |
| F(4) | 5257(2) | 1898(2) | 8372(2) | 162(2) |
| F(5) | 5907(1) | 1659(2) | 8789(3) | 228(3) |
| F(6) | 5504(1) | 2264(2) | 9067(2) | 155(2) |
| F(7) | 5031(2) | 1972(2) | 9950(2) | 157(2) |
| F(8) | 5080(3) | 1184(2) | 10076(3) | 207(3) |
| F(9) | 5708(2) | 1622(2) | 9925(3) | 223(3) |
| F(10) | 4910(2) | 450(2) | 9453(2) | 171(2) |
| F(11) | 4411(2) | -187(2) | 9798(4) | 277(5) |
| F(12) | 3857(2) | 372(3) | 9811(2) | 200(3) |
| F(13) | 3871(2) | -159(2) | 9114(4) | 280(6) |
| F(14) | 4802(2) | -252(2) | 8727(4) | 264(5) |
| F(15) | 4301(2) | 176(2) | 8281(3) | 219(4) |
| F(16) | 5021(2) | 406(2) | 8395(4) | 220(3) |
| F(17) | 3401(1) | 520(1) | 7243(1) | 82(1) |
| F(18) | 1443(1) | 642(1) | 7072(1) | 91(1) |
| F(19) | 2653(1) | -752(1) | 7111(2) | 119(1) |
| F(20) | 3303(2) | -891(1) | 7728(2) | 161(2) |
| F(21) | 3121(2) | -172(2) | 8004(2) | 141(2) |
| F(22) | 3746(2) | -290(1) | 7492(3) | 176(2) |
| F(23) | 3557(2) | -88(2) | 6431(2) | 172(2) |
| F(24) | 3519(2) | -847(2) | 6590(3) | 202(3) |
| F(25) | 2960(2) | -516(2) | 6138(2) | 185(2) |
| F(26) | 2071(1) | -561(1) | 6438(2) | 127(1) |
| F(27) | 1410(2) | -351(2) | 5852(2) | 178(2) |
| F(28) | 1669(2) | 372(2) | 6003(2) | 166(2) |

**Table B.5** Atomic Coordinates (x $10^4$) and Equivalent Isotropic Displacement Parameters ($A^2$ x $10^3$) for $(F_{64}Pc)_2Y$.  U(eq) is Defined as One Third of the Trace of the Orthogonalized $U^{ij}$ Tensor, Continued

|        | x        | y        | z        | U(eq)   |
|--------|----------|----------|----------|---------|
| F(29)  | 1033(2)  | 125(2)   | 6396(3)  | 189(3)  |
| F(30)  | 1747(2)  | -802(2)  | 7400(2)  | 160(2)  |
| F(31)  | 1216(2)  | -236(2)  | 7427(2)  | 155(2)  |
| F(32)  | 1192(2)  | -811(2)  | 6824(3)  | 194(2)  |

**Table B.6**  Bond Lengths [Å] and angles [°] for (F$_{64}$Pc)$_2$Y

| | | | |
|---|---|---|---|
| Y-N(1) | 2.421(3) | Y-N(1)#2 | 2.421(3) |
| Y-N(1)#1 | 2.421(3) | Y-N(1)#3 | 2.421(2) |
| Y-N(3) | 2.411(3) | Y-N(3)#2 | 2.411(3) |
| Y-N(3)#1 | 2.411(3) | Y-N(3)#3 | 2.411(3) |
| | | | |
| N(1)-C(4) | 1.360(4) | C(13)-F(16) | 1.397(16) |
| N(1)-C(1) | 1.363(4) | C(14)-F(12) | 1.345(8) |
| N(2)-C(1) | 1.322(4) | C(14)-F(11) | 1.349(6) |
| N(2)-C(4)#1 | 1.331(4) | C(14)-F(13) | 1.384(7) |
| N(3)-C(18) | 1.365(4) | C(15)-C(16) | 1.463(4) |
| N(3)-C(15) | 1.374(4) | C(16)-C(17) | 1.382(5) |
| N(4)-C(15) | 1.321(4) | C(16)-C(22) | 1.390(5) |
| N(4)-C(18)#2 | 1.329(4) | C(17)-C(19) | 1.370(5) |
| C(1)-C(2) | 1.470(4) | C(17)-C(18) | 1.467(4) |
| C(2)-C(3) | 1.371(5) | C(18)-N(4)#1 | 1.329(4) |
| C(2)-C(5) | 1.377(5) | C(19)-F(18) | 1.331(4) |
| C(3)-C(8) | 1.393(5) | C(19)-C(20) | 1.399(5) |
| C(3)-C(4) | 1.454(4) | C(20)-C(21) | 1.444(6) |
| C(4)-N(2)#2 | 1.332(4) | C(20)-C(26) | 1.545(5) |
| C(5)-F(2) | 1.327(5) | C(21)-C(22) | 1.380(5) |
| C(5)-C(6) | 1.391(5) | C(21)-C(23) | 1.547(6) |
| C(6)-C(7) | 1.428(6) | C(22)-F(17) | 1.330(4) |
| C(6)-C(12) | 1.550(6) | C(23)-F(19) | 1.359(6) |
| C(7)-C(8) | 1.374(6) | C(23)-C(25) | 1.491(10) |
| C(7)-C(9) | 1.561(6) | C(23)-C(24) | 1.574(9) |
| C(8)-F(1) | 1.331(4) | C(24)-F(21) | 1.245(8) |
| C(9)-F(3) | 1.386(6) | C(24)-F(20) | 1.308(7) |
| C(9)-C(10) | 1.503(11) | C(24)-F(22) | 1.422(8) |
| C(9)-C(11) | 1.650(10) | C(25)-F(24) | 1.282(8) |
| C(10)-F(8) | 1.239(15) | C(25)-F(23) | 1.342(10) |
| C(10)-F(9) | 1.337(10) | C(25)-F(25) | 1.343(10) |
| C(10)-F(7) | 1.352(10) | C(26)-F(26) | 1.347(6) |
| C(11)-F(4) | 1.230(8) | C(26)-C(28) | 1.486(9) |
| C(11)-F(5) | 1.318(7) | C(26)-C(27) | 1.616(9) |
| C(11)-F(6) | 1.318(8) | C(27)-F(28) | 1.235(9) |
| C(12)-F(10) | 1.337(6) | C(27)-F(27) | 1.311(7) |
| C(12)-C(13) | 1.516(17) | C(27)-F(29) | 1.387(10) |
| C(12)-C(14) | 1.526(14) | C(28)-F(32) | 1.280(7) |
| C(13)-F(15) | 1.262(15) | C(28)-F(31) | 1.302(9) |
| C(13)-F(14) | 1.271(11) | C(28)-F(30) | 1.411(9) |
| N(3)-Y-N(3)#1 | 70.89(7) | N(3)#3-Y-N(1)#1 | 154.28(8) |
| N(3)-Y-N(3)#2 | 70.89(7) | N(3)-Y-N(1)#3 | 132.79(8) |
| N(3)#1-Y-N(3)#2 | 110.19(14) | N(3)#1-Y-N(1)#3 | 75.86(9) |
| N(3)-Y-N(3)#3 | 110.19(14) | N(3)#2-Y-N(1)#3 | 154.28(8) |
| N(3)#1-Y-N(3)#3 | 70.89(7) | N(3)#3-Y-N(1)#3 | 88.69(9) |
| N(3)#2-Y-N(3)#3 | 70.88(7) | N(1)#1-Y-N(1)#3 | 70.79(7) |
| N(3)-Y-N(1)#1 | 75.85(9) | N(3)-Y-N(1)#2 | 154.28(8) |

**Table B.6**   Bond Lengths [Å] and angles [°] for (F$_{64}$Pc)$_2$Y, Continued

| | | | |
|---|---|---|---|
| N(3)#1-Y-N(1)#1 | 88.69(9) | N(3)#1-Y-N(1)#2 | 132.79(8) |
| N(3)#2-Y-N(1)#1 | 132.80(8) | N(3)#2-Y-N(1)#2 | 88.69(9) |
| N(3)#3-Y-N(1)#2 | 75.85(9) | N(3)#1-Y-N(1) | 154.28(8) |
| N(1)#1-Y-N(1)#2 | 109.99(13) | N(3)#2-Y-N(1) | 75.85(9) |
| N(1)#3-Y-N(1)#2 | 70.79(7) | N(3)#3-Y-N(1) | 132.79(8) |
| N(3)-Y-N(1) | 88.69(9) | N(1)#1-Y-N(1) | 70.78(7) |
| N(1)#3-Y-N(1) | 109.99(13)) | N(1)#2-Y-N(1) | 70.79(7) |
| C(4)-N(1)-C(1) | 108.6(3) | C(10)-C(9)-C(11) | 114.3(7) |
| C(4)-N(1)-Y | 123.8(2) | C(7)-C(9)-C(11) | 114.4(4) |
| C(1)-N(1)-Y | 122.9(2) | F(8)-C(10)-F(9) | 111.6(8) |
| C(1)-N(2)-C(4)#1 | 122.3(3) | F(8)-C(10)-F(7) | 114.9(11) |
| C(18)-N(3)-C(15) | 108.2(3) | F(9)-C(10)-F(7) | 102.1(9) |
| C(18)-N(3)-Y | 123.6(2) | F(8)-C(10)-C(9) | 109.5(9) |
| C(15)-N(3)-Y | 123.10(19) | F(9)-C(10)-C(9) | 111.0(9) |
| C(15)-N(4)-C(18)#2 | 122.8(3) | F(7)-C(10)-C(9) | 107.4(7) |
| N(2)-C(1)-N(1) | 128.7(3) | F(4)-C(11)-F(5) | 115.4(8) |
| N(2)-C(1)-C(2) | 122.3(3) | F(4)-C(11)-F(6) | 109.6(7) |
| N(1)-C(1)-C(2) | 108.9(3) | F(5)-C(11)-F(6) | 105.9(5) |
| C(3)-C(2)-C(5) | 119.9(3) | F(4)-C(11)-C(9) | 111.5(5) |
| C(3)-C(2)-C(1) | 106.0(3) | F(5)-C(11)-C(9) | 105.0(7) |
| C(5)-C(2)-C(1) | 134.0(3) | F(6)-C(11)-C(9) | 109.0(6) |
| C(2)-C(3)-C(8) | 118.9(3) | F(10)-C(12)-C(13) | 103.8(7) |
| C(2)-C(3)-C(4) | 107.4(3) | F(10)-C(12)-C(14) | 105.6(6) |
| C(8)-C(3)-C(4) | 133.5(3) | C(13)-C(12)-C(14) | 105.0(7) |
| N(2)#2-C(4)-N(1) | 128.8(3) | F(10)-C(12)-C(6) | 111.1(4) |
| N(2)#2-C(4)-C(3) | 122.2(3) | C(13)-C(12)-C(6) | 112.0(8) |
| N(1)-C(4)-C(3) | 108.9(3) | C(14)-C(12)-C(6) | 118.2(5) |
| F(2)-C(5)-C(2) | 117.3(3) | F(15)-C(13)-F(14) | 112.5(10) |
| F(2)-C(5)-C(6) | 120.5(3) | F(15)-C(13)-F(16) | 103.4(15) |
| C(2)-C(5)-C(6) | 122.3(4) | F(14)-C(13)-F(16) | 101.4(9) |
| C(5)-C(6)-C(7) | 118.0(3) | F(15)-C(13)-C(12) | 114.6(8) |
| C(5)-C(6)-C(12) | 114.2(4) | F(14)-C(13)-C(12) | 114.8(15) |
| C(7)-C(6)-C(12) | 127.8(4) | F(16)-C(13)-C(12) | 108.5(8) |
| C(8)-C(7)-C(6) | 118.1(3) | F(12)-C(14)-F(11) | 106.3(8) |
| C(8)-C(7)-C(9) | 115.0(4) | F(12)-C(14)-F(13) | 110.2(9) |
| C(6)-C(7)-C(9) | 126.8(4) | F(11)-C(14)-F(13) | 109.4(7) |
| F(1)-C(8)-C(7) | 120.0(3) | F(12)-C(14)-C(12) | 111.0(7) |
| F(1)-C(8)-C(3) | 117.2(3) | F(11)-C(14)-C(12) | 109.0(8) |
| C(7)-C(8)-C(3) | 122.7(4) | F(13)-C(14)-C(12) | 110.7(8) |
| F(3)-C(9)-C(10) | 108.5(5) | N(4)-C(15)-N(3) | 128.1(3) |
| F(3)-C(9)-C(7) | 110.5(4) | N(4)-C(15)-C(16) | 122.7(3) |
| C(10)-C(9)-C(7) | 111.5(6) | N(3)-C(15)-C(16) | 109.1(3) |
| F(3)-C(9)-C(11) | 96.5(5) | C(17)-C(16)-C(22) | 118.9(3) |
| C(17)-C(16)-C(15) | 106.7(3) | F(20)-C(24)-F(22) | 102.2(5) |
| C(22)-C(16)-C(15) | 134.3(3) | F(21)-C(24)-C(23) | 115.6(5) |
| C(19)-C(17)-C(16) | 119.8(3) | F(20)-C(24)-C(23) | 110.2(5) |

**Table B.6**  Bond Lengths [Å] and angles [°] for (F$_{64}$Pc)$_2$Y, Continued

| | | | |
|---|---|---|---|
| C(19)-C(17)-C(18) | 133.6(3) | F(22)-C(24)-C(23) | 106.9(6) |
| C(16)-C(17)-C(18) | 106.4(3) | F(24)-C(25)-F(23) | 107.7(8) |
| N(4)#1-C(18)-N(3) | 128.6(3) | F(24)-C(25)-F(25) | 105.9(6) |
| N(4)#1-C(18)-C(17) | 122.0(3) | F(23)-C(25)-F(25) | 105.5(8) |
| N(3)-C(18)-C(17) | 109.4(3) | F(24)-C(25)-C(23) | 114.8(8) |
| F(18)-C(19)-C(17) | 118.4(3) | F(23)-C(25)-C(23) | 114.1(5) |
| F(18)-C(19)-C(20) | 118.6(3 | F(25)-C(25)-C(23) | 108.2(7) |
| C(17)-C(19)-C(20) | 123.0(4) | F(26)-C(26)-C(28) | 107.6(5) |
| C(19)-C(20)-C(21) | 116.8(3) | F(26)-C(26)-C(20) | 109.8(4) |
| C(19)-C(20)-C(26) | 115.8(4) | C(28)-C(26)-C(20) | 118.4(5) |
| C(21)-C(20)-C(26) | 127.2(4) | F(26)-C(26)-C(27) | 100.1(5) |
| C(22)-C(21)-C(20) | 118.3(3) | C(28)-C(26)-C(27) | 107.5(6) |
| C(22)-C(21)-C(23) | 116.2(4) | C(20)-C(26)-C(27) | 111.9(4) |
| C(20)-C(21)-C(23) | 125.3(3) | F(28)-C(27)-F(27) | 114.1(8) |
| F(17)-C(22)-C(21) | 120.0(3) | F(28)-C(27)-F(29) | 106.6(7) |
| F(17)-C(22)-C(16) | 117.3(3) | F(27)-C(27)-F(29) | 104.2(6) |
| C(21)-C(22)-C(16) | 122.6(3) | F(28)-C(27)-C(26) | 114.5(5) |
| F(19)-C(23)-C(25) | 105.9(5) | F(27)-C(27)-C(26) | 108.1(6) |
| F(19)-C(23)-C(21) | 110.6(4) | F(29)-C(27)-C(26) | 108.7(7) |
| C(25)-C(23)-C(21) | 115.3(5) | F(32)-C(28)-F(31) | 113.1(8) |
| F(19)-C(23)-C(24) | 99.3(4) | F(32)-C(28)-F(30) | 100.4(6) |
| C(25)-C(23)-C(24) | 112.1(6) | F(31)-C(28)-F(30) | 103.2(7) |
| C(21)-C(23)-C(24) | 112.3(4) | F(32)-C(28)-C(26) | 114.9(7) |
| F(21)-C(24)-F(20) | 114.0(7) | F(31)-C(28)-C(26) | 116.8(5) |
| F(21)-C(24)-F(22) | 106.8(6) | F(30)-C(28)-C(26) | 105.9(6) |

Symmetry transformations used to generate equivalent atoms:
#1 y,-x+1/2,z   #2 -y+1/2,x,z   #3 -x+1/2,-y+1/2,z

**Table B.7** Anisotropic Displacement Parameters ($\mathring{A}^2$ x $10^3$) for $(F_{64}Pc)_2Y$. The Anisotropic Displacement Factor Exponent Takes the Form: $-2\pi2[h^2\,a^{*2}\,U^{11} + \ldots +2\,h\,k\,a^*\,b^*\,U^{12}]$

| | $U^{11}$ | $U^{22}$ | $U^{33}$ | $U^{23}$ | $U^{13}$ | $U^{12}$ |
|---|---|---|---|---|---|---|
| Y | 33(1) | 33(1) | 56(1) | 0 | 0 | 0 |
| N(1) | 42(1) | 42(1) | 63(2) | 2(1) | -6(1) | 1(1) |
| N(2) | 52(2) | 43(1) | 72(2) | 13(1) | -7(1) | 0(1) |
| N(3) | 41(1) | 41(1) | 62(1) | -5(1) | -2(1) | 0(1) |
| N(4) | 46(1) | 43(1) | 73(2) | -11(1) | 2(1) | 3(1) |
| C(1) | 45(2) | 44(2) | 63(2) | 4(1) | -9(1) | 3(1) |
| C(2) | 47(2) | 49(2) | 71(2) | 5(2) | -12(2) | 3(1) |
| C(3) | 45(2) | 57(2) | 69(2) | -1(2) | -12(1) | 2(1) |
| C(4) | 42(2) | 49(2) | 62(2) | 2(1) | -9(1) | 5(1) |
| C(5) | 54(2) | 56(2) | 91(3) | 11(2) | -17(2) | 6(2) |
| C(6) | 59(2) | 63(2) | 107(3) | 10(2) | -25(2) | 13(2) |
| C(7) | 54(2) | 75(2) | 89(3) | 1(2) | -25(2) | 12(2) |
| C(8) | 46(2) | 68(2) | 81(2) | -7(2) | -15(2) | 2(2) |
| C(9) | 61(3) | 86(3) | 143(5) | -3(3) | -39(3) | 10(2) |
| C(10) | 129(6) | 200(10) | 176(8) | -39(8) | -94(6) | 65(7) |
| C(11) | 50(3) | 147(6) | 154(6) | -48(5) | -9(3) | 3(3) |
| C(12) | 78(3) | 70(3) | 199(7) | 16(4) | -54(4) | 15(3) |
| C(13) | 111(7) | 98(6) | 470(20) | -77(10) | -44(11) | 20(5) |
| C(14) | 157(9) | 131(8) | 370(20) | 138(11) | -49(11) | 39(7) |
| C(15) | 46(2) | 38(2) | 69(2) | -6(1) | -1(1) | 1(1) |
| C(16) | 52(2) | 41(2) | 76(2) | -10(1) | -2(2) | 1(1) |
| C(17) | 54(2) | 43(2) | 70(2) | -6(1) | -9(2) | 3(1) |
| C(18) | 45(2) | 39(2) | 70(2) | -7(1) | -6(1) | -1(1) |
| C(19) | 59(2) | 44(2) | 89(2) | -6(2) | -18(2) | -2(2) |
| C(20) | 77(3) | 47(2) | 80(2) | -7(2) | -13(2) | -5(2) |
| C(21) | 74(2) | 43(2) | 81(2) | -12(2) | -3(2) | 1(2) |
| C(22) | 53(2) | 47(2) | 84(2) | -12(2) | 0(2) | 2(1) |
| C(23) | 93(3) | 46(2) | 118(4) | -23(2) | -17(3) | 5(2) |
| C(24) | 105(4) | 76(3) | 163(6) | -7(4) | -33(4) | 23(3) |
| C(25) | 144(6) | 103(5) | 175(7) | -60(5) | 9(6) | 42(5) |
| C(26) | 99(3) | 49(2) | 103(3) | -22(2) | -19(3) | -8(2) |
| C(27) | 142(6) | 102(5) | 153(6) | -34(4) | -65(5) | -11(4) |
| C(28) | 122(6) | 94(4) | 171(7) | -7(5) | -23(5) | -50(4) |
| F(1) | 51(1) | 65(1) | 131(2) | -10(1) | -28(1) | -2(1) |
| F(2) | 68(1) | 50(1) | 150(2) | 22(1) | -31(1) | 2(1) |
| F(3) | 69(2) | 119(3) | 279(6) | -50(3) | -39(2) | 40(2) |
| F(4) | 157(4) | 159(4) | 171(4) | -21(3) | 54(4) | -31(3) |
| F(5) | 71(2) | 165(4) | 448(10) | -77(5) | 51(4) | 12(2) |
| F(6) | 77(2) | 121(3) | 266(6) | -26(3) | -36(3) | -8(2) |
| F(7) | 181(4) | 156(4) | 134(3) | -48(3) | -78(3) | 39(3) |
| F(8) | 232(7) | 171(5) | 218(6) | 64(4) | -88(5) | 37(5) |
| F(9) | 147(4) | 250(6) | 271(7) | -47(5) | -144(5) | 19(4) |
| F(10) | 104(3) | 112(3) | 298(6) | 31(3) | -105(3) | 29(2) |
| F(11) | 180(5) | 190(5) | 460(12) | 198(7) | -142(7) | -6(4) |
| F(12) | 156(4) | 246(7) | 197(5) | 133(5) | -36(4) | -14(5) |
| F(13) | 151(4) | 91(3) | 599(16) | 81(5) | -165(7) | -14(3) |
| F(14) | 168(5) | 88(3) | 536(14) | -67(5) | -47(7) | 55(3) |
| F(15) | 121(4) | 215(6) | 320(8) | -153(6) | -69(4) | 51(4) |
| F(16) | 141(4) | 190(6) | 328(9) | -97(6) | -9(5) | 58(4) |

**Table B.7** Anisotropic Displacement Parameters ($\AA^2$ x $10^3$) for $(F_{64}Pc)_2Y$. The Anisotropic Displacement Factor Exponent Takes the Form: $-2\pi2[h^2 a^{*2} U^{11} + ... +2 h k a^* b^* U^{12}]$, Continued

|       | $U^{11}$ | $U^{22}$ | $U^{33}$ | $U^{23}$ | $U^{13}$ | $U^{12}$ |
|-------|----------|----------|----------|----------|----------|----------|
| F(17) | 57(1)    | 49(1)    | 141(2)   | -18(1)   | 0(1)     | 10(1)    |
| F(18) | 58(1)    | 57(1)    | 158(2)   | -19(1)   | -29(1)   | -6(1)    |
| F(19) | 128(2)   | 48(1)    | 182(3)   | -11(2)   | -44(2)   | -5(2)    |
| F(20) | 161(4)   | 75(2)    | 246(5)   | 32(3)    | -68(4)   | 15(2)    |
| F(21) | 173(4)   | 124(3)   | 126(3)   | 0(2)     | -51(3)   | 16(3)    |
| F(22) | 117(3)   | 91(2)    | 320(7)   | -40(3)   | -84(4)   | 30(2)    |
| F(23) | 129(3)   | 149(4)   | 237(5)   | -82(4)   | 80(3)    | -21(3)   |
| F(24) | 195(5)   | 131(3)   | 280(7)   | -86(4)   | 8(4)     | 74(3)    |
| F(25) | 193(5)   | 205(5)   | 156(4)   | -69(4)   | 9(4)     | 0(4)     |
| F(26) | 142(3)   | 74(2)    | 164(3)   | -50(2)   | -51(2)   | 13(2)    |
| F(27) | 204(5)   | 140(3)   | 189(4)   | -68(3)   | -108(4)  | 17(3)    |
| F(28) | 232(5)   | 131(3)   | 135(3)   | 30(3)    | -75(3)   | -27(3)   |
| F(29) | 137(4)   | 131(3)   | 300(7)   | -74(4)   | -117(4)  | 20(3)    |
| F(30) | 175(4)   | 106(3)   | 198(5)   | 18(3)    | 4(4)     | -14(3)   |
| F(31) | 145(4)   | 104(3)   | 215(5)   | 3(3)     | 52(3)    | -15(2)   |
| F(32) | 171(4)   | 121(3)   | 290(6)   | -14(3)   | -52(4)   | -89(3)   |

**Table B.8** Anisotropic Displacement Parameters ($\AA^2$ x $10^3$) for $(F_{64}Pc)_2Lu$. The Anisotropic Displacement Factor Exponent Takes the Form: $-2\pi2[h^2 a^{*2} U^{11} + ... +2 h k a^* b^* U^{12}]$

|        | $U^{11}$  | $U^{22}$  | $U^{33}$  | $U^{23}$  | $U^{13}$  | $U^{12}$  |
|--------|-----------|-----------|-----------|-----------|-----------|-----------|
| Lu     | 19(1)     | 19(1)     | 41(1)     | 0         | 0         | 0         |
| N(1)   | 26(2)     | 32(2)     | 48(3)     | -5(2)     | -4(2)     | -2(2)     |
| N(2)   | 22(2)     | 19(2)     | 45(3)     | -5(2)     | -2(2)     | -2(2)     |
| N(3)   | 24(2)     | 29(2)     | 49(3)     | -6(2)     | 3(2)      | 2(2)      |
| N(4)   | 33(3)     | 36(3)     | 50(3)     | -4(2)     | -9(2)     | 0(2)      |
| C(1)   | 43(3)     | 38(3)     | 49(4)     | -13(3)    | -6(3)     | -13(3)    |
| C(2)   | 43(3)     | 41(3)     | 49(3)     | -12(3)    | -5(3)     | 0(3)      |
| C(3)   | 57(4)     | 34(3)     | 52(4)     | -16(3)    | 6(3)      | -7(3)     |
| C(4)   | 61(4)     | 46(4)     | 69(4)     | -27(3)    | 0(3)      | -17(3)    |
| C(5)   | 53(4)     | 51(4)     | 84(5)     | -27(4)    | -6(4)     | -15(3)    |
| C(6)   | 40(4)     | 48(4)     | 68(4)     | -18(3)    | -10(3)    | -6(3)     |
| C(7)   | 66(5)     | 65(5)     | 117(8)    | -42(5)    | -8(5)     | -21(5)    |
| C(8)   | 90(9)     | 127(11)   | 204(16)   | -50(11)   | -84(10)   | -19(9)    |
| C(9)   | 30(15)    | 90(30)    | 250(60)   | -30(30)   | 70(20)    | 1(17)     |
| C(9')  | 210(60)   | 100(30)   | 230(50)   | -20(30)   | -50(40)   | -30(30)   |
| C(10)  | 142(10)   | 98(8)     | 107(8)    | -54(7)    | 27(8)     | -62(8)    |
| C(11)  | 112(7)    | 29(4)     | 111(7)    | -4(4)     | 32(6)     | -6(4)     |
| C(12)  | 73(5)     | 51(4)     | 106(6)    | -33(4)    | 34(5)     | -29(4)    |
| C(13)  | 36(3)     | 27(3)     | 52(3)     | -7(2)     | 1(3)      | 2(2)      |
| C(14)  | 23(3)     | 41(3)     | 47(3)     | -4(3)     | 1(2)      | -2(2)     |
| C(15)  | 32(3)     | 22(3)     | 51(3)     | -3(2)     | 4(2)      | 1(2)      |
| C(16)  | 27(3)     | 33(3)     | 55(3)     | -6(3)     | -1(3)     | -2(2)     |
| C(17)  | 32(3)     | 41(3)     | 53(4)     | -8(3)     | 6(2)      | -1(3)     |
| C(18)  | 31(3)     | 58(4)     | 59(4)     | -11(3)    | 12(3)     | -1(3)     |

**Table B.8** Anisotropic Displacement Parameters ($\mathring{A}^2$ x $10^3$) for $(F_{64}Pc)_2Lu$. The Anisotropic Displacement Factor Exponent Takes the Form: $-2\pi2[h^2 a^{*2} U^{11} + \ldots +2 h k a^* b^* U^{12}]$, Continued

| | $U^{11}$ | $U^{22}$ | $U^{33}$ | $U^{23}$ | $U^{13}$ | $U^{12}$ |
|---|---|---|---|---|---|---|
| C(19) | 60(5) | 63(5) | 73(5) | -10(4) | 16(4) | -11(4) |
| C(20) | 45(4) | 72(5) | 85(6) | -16(4) | -2(4) | -14(4) |
| C(21) | 30(3) | 47(4) | 71(4) | 0(3) | 8(3) | 1(3) |
| C(22) | 45(4) | 59(4) | 86(5) | -4(4) | 3(4) | 17(4) |
| C(23) | 43(4) | 65(5) | 101(6) | -22(4) | 17(4) | 1(4) |
| C(24) | 28(3) | 51(4) | 51(4) | 0(3) | -1(2) | 3(3) |
| C(25) | 24(3) | 31(3) | 45(3) | -2(2) | 0(2) | 0(2) |
| C(26) | 39(3) | 32(3) | 45(3) | -7(2) | -3(2) | -1(3) |
| C(27) | 37(3) | 36(3) | 41(3) | -7(2) | -5(2) | -4(3) |
| C(28) | 29(3) | 26(3) | 42(3) | -5(2) | -1(2) | 5(2) |
| F(1) | 53(2) | 33(2) | 79(2) | -19(2) | 13(2) | -2(2) |
| F(2) | 36(2) | 55(2) | 104(3) | -27(2) | -19(2) | -7(2) |
| F(3) | 93(4) | 83(4) | 176(6) | -61(4) | -18(4) | -30(3) |
| F(4) | 168(7) | 115(5) | 143(6) | -19(4) | -85(5) | -19(5) |
| F(5) | 120(5) | 152(6) | 285(10) | -110(7) | -110(6) | -16(5) |
| F(6) | 57(3) | 108(5) | 331(12) | -81(7) | -42(5) | -3(3) |
| F(7) | 130(30) | 100(30) | 260(40) | -60(30) | 100(30) | -50(20) |
| F(7') | 110(13) | 37(7) | 151(12) | -32(7) | 54(9) | -5(7) |
| F(8) | 100(20) | 130(20) | 250(40) | -10(20) | 30(18) | -72(17) |
| F(8') | 50(9) | 79(11) | 320(30) | -73(16) | 52(11) | -27(8) |
| F(9) | 140(30) | 220(40) | 220(30) | -120(30) | 130(30) | -140(30) |
| F(9') | 98(11) | 48(8) | 127(11) | -14(7) | 43(8) | -10(7) |
| F(10) | 110(4) | 79(4) | 140(5) | 22(4) | 31(4) | 19(3) |
| F(11) | 120(5) | 53(3) | 261(9) | 0(4) | 85(5) | -20(3) |
| F(12) | 101(4) | 55(3) | 164(5) | -28(3) | 61(4) | -12(3) |
| F(13) | 113(4) | 101(4) | 86(3) | -45(3) | 39(3) | -48(3) |
| F(14) | 196(7) | 102(4) | 180(7) | -99(5) | 93(6) | -76(5) |
| F(15) | 124(5) | 153(6) | 112(5) | -43(4) | -7(4) | -60(5) |
| F(16) | 33(2) | 35(2) | 98(3) | -12(2) | 8(2) | 6(2) |
| F(17) | 32(2) | 33(2) | 84(3) | -5(2) | 12(2) | -4(1) |
| F(18) | 63(3) | 90(3) | 65(3) | -20(2) | 3(2) | -2(2) |
| F(19) | 51(2) | 56(3) | 133(4) | -28(3) | 18(2) | -10(2) |
| F(20) | 47(2) | 90(3) | 121(4) | -44(3) | -17(2) | -5(2) |
| F(21) | 70(3) | 57(2) | 104(3) | 24(2) | 30(2) | 3(2) |
| F(22) | 69(3) | 99(4) | 114(4) | -10(3) | 29(3) | -47(3) |
| F(23) | 83(3) | 81(3) | 86(3) | 1(3) | 17(2) | 0(2) |
| F(24) | 36(2) | 63(2) | 95(3) | -19(2) | 1(2) | 1(2) |
| F(25) | 57(2) | 59(2) | 110(3) | 10(2) | -7(2) | 7(2) |
| F(26) | 56(3) | 73(3) | 159(5) | -9(3) | 0(3) | 31(2) |
| F(27) | 53(2) | 83(3) | 106(4) | 0(3) | -17(2) | 2(2) |
| F(28) | 46(2) | 69(3) | 95(3) | -16(2) | 15(2) | -3(2) |
| F(29) | 79(3) | 91(3) | 96(3) | -40(3) | 26(3) | -5(3) |
| F(30) | 61(3) | 54(3) | 147(4) | -38(3) | 25(3) | -2(2) |
| F(31) | 71(3) | 84(3) | 81(3) | -25(2) | -10(2) | -5(2) |
| F(32) | 106(4) | 62(3) | 156(5) | -41(3) | 45(4) | -44(3) |
| C(25) | 24(3) | 31(3) | 45(3) | -2(2) | 0(2) | 0(2) |

**Table B.9** Experimental Parameters and Structure Refinement for
$(F_{64}Pc)_2Tb(\frac{1}{2}$ Acetone$)(\frac{1}{8}$ Chloroform$)$

| | |
|---|---|
| Empirical formula | C227.25 H6.25 Cl0.75 F256 N32 O Tb2 |
| Formula weight | 8408.32 |
| Temperature | 100(2) K |
| Wavelength | 1.54178 Å |
| Crystal system | Monoclinic |
| Space group | P 21/c |
| Unit cell dimensions | a = 20.6911(6) Å |
| α= 90°. | |
| | b = 20.9584(7) Å |
| β= 95.539(2)°. | |
| | c = 36.6961(12) Å |
| γ = 90°. | |
| Volume | 15839.0(9) Å$^3$ |
| Z | 2 |
| Density (calculated) | 1.763 g/cm$^3$ |
| Absorption coefficient | 4.140 mm$^{-1}$ |
| F(000) | 8097 |
| Crystal size | 0.25 x 0.23 x 0.14 mm$^3$ |
| Theta range for data collection | 3.08 to 67.63°. |
| Index ranges | -24<=h<=24, -24<=k<=25, -41<=l<=43 |
| Reflections collected | 120685 |
| Independent reflections | 27542 [R(int) = 0.0678] |
| Completeness to theta = 67.63° | 96.2 % |
| Absorption correction | Semi-empirical from equivalents |
| Max. and min. transmission | 0.5949 and 0.4242 |
| Refinement method | Full-matrix-block least-squares on F$^2$ |
| Data / restraints / parameters | 27542 / 9 / 2042 |
| Goodness-of-fit on F$^2$ | 1.106 |
| Final R indices [I>2sigma(I)] | R1 = 0.0780, wR2 = 0.2183 |
| R indices (all data) | R1 = 0.0919, wR2 = 0.2292 |
| Largest diff. peak and hole | 3.070 and -1.635 e.Å$^{-3}$ |

**Table B.10** Atomic Coordinates (x $10^4$) and Equivalent Isotropic Displacement Parameters ($A^2$ x $10^3$) for $(F_{64}Pc)_2Tb(\frac{1}{2}$ Acetone$)(\frac{1}{8}$ Chloroform). U(eq) is Defined as One Third of the Trace of the Orthogonalized $U^{ij}$ Tensor

| | x | y | z | U(eq) |
|---|---|---|---|---|
| Tb | 4579(1) | 3818(1) | 1285(1) | 19 |
| N(1) | 4544(2) | 4960(2) | 1408(1) | 24 |
| N(2) | 3382(2) | 5121(2) | 1373(1) | 24 |
| N(3) | 3618(2) | 4277(2) | 952(1) | 20 |
| N(4) | 3452(2) | 3548(2) | 443(1) | 23 |
| N(5) | 4605(2) | 3656(2) | 631(1) | 23 |
| N(6) | 5759(2) | 3691(2) | 569(1) | 29 |
| N(7) | 5539(2) | 4351(2) | 1089(1) | 22 |
| N(8) | 5701(2) | 5176(2) | 1544(1) | 30 |
| N(9) | 5042(2) | 3911(2) | 1918(1) | 22 |
| N(10) | 6157(2) | 3599(2) | 1877(1) | 23 |
| N(11) | 5444(2) | 3043(2) | 1418(1) | 20 |
| N(12) | 5086(2) | 2218(2) | 974(1) | 22 |
| N(13) | 4135(2) | 2747(2) | 1183(1) | 20 |
| N(14) | 3023(2) | 2866(2) | 1326(1) | 24 |
| N(15) | 3718(2) | 3626(2) | 1681(1) | 22 |
| N(16) | 4093(2) | 4266(2) | 2210(1) | 22 |
| C(1) | 3993(2) | 5252(2) | 1501(1) | 23 |
| C(2) | 4166(3) | 5761(2) | 1763(2) | 28 |
| C(3) | 3824(3) | 6169(3) | 1962(2) | 30 |
| C(4) | 4117(3) | 6614(3) | 2208(2) | 34 |
| C(5) | 4802(3) | 6684(3) | 2230(2) | 33 |
| C(6) | 5149(3) | 6244(2) | 2034(2) | 30 |
| C(7) | 4837(3) | 5775(3) | 1812(2) | 27 |
| C(8) | 5073(3) | 5278(2) | 1579(2) | 26 |
| C(9) | 3657(3) | 6931(3) | 2465(2) | 38 |
| C(10) | 3268(1) | 7494(1) | 2283(1) | 43 |
| F(7) | 2864(2) | 7735(1) | 2513(1) | 55 |
| F(8) | 2918(2) | 7328(1) | 1975(1) | 51 |
| F(9) | 3663(2) | 7956(1) | 2201(1) | 50 |
| C(11) | 3180(1) | 6438(1) | 2638(1) | 52 |
| F(4) | 3109(2) | 6610(1) | 2980(1) | 58 |
| F(5) | 2590(2) | 6421(1) | 2460(1) | 55 |
| F(6) | 3428(2) | 5851(1) | 2648(1) | 50 |
| C(12) | 5213(3) | 7222(3) | 2426(2) | 35 |
| C(13) | 5580(1) | 7021(1) | 2792(1) | 47 |
| F(14) | 5167(2) | 6982(2) | 3051(1) | 55 |
| F(15) | 6026(2) | 7447(2) | 2909(1) | 66 |
| F(16) | 5862(2) | 6461(2) | 2770(1) | 48 |
| C(14) | 5690(1) | 7558(1) | 2170(1) | 43 |
| F(11) | 5769(2) | 8171(1) | 2274(1) | 50 |
| F(12) | 6291(2) | 7306(1) | 2205(1) | 57 |
| F(13) | 5462(2) | 7540(1) | 1831(1) | 53 |
| C(15) | 3244(2) | 3927(2) | 698(1) | 23 |
| C(16) | 2560(2) | 4071(3) | 726(2) | 24 |
| C(17) | 1977(3) | 3813(3) | 570(2) | 31 |

**Table B.10** Atomic Coordinates (x $10^4$) and Equivalent Isotropic Displacement Parameters ($A^2$ x $10^3$) for $(F_{64}Pc)_2Tb$(½ Acetone)(⅛ Chloroform). U(eq) is Defined as One Third of the Trace of the Orthogonalized $U^{ij}$ Tensor, Continued

|        | x        | y        | z        | U(eq) |
|--------|----------|----------|----------|-------|
| C(18)  | 1374(3)  | 4046(3)  | 649(2)   | 34    |
| C(19)  | 1366(3)  | 4583(4)  | 894(2)   | 41    |
| C(20)  | 1963(3)  | 4822(3)  | 1047(2)  | 33    |
| C(21)  | 2549(2)  | 4561(3)  | 978(2)   | 25    |
| C(22)  | 3222(2)  | 4686(2)  | 1118(2)  | 23    |
| C(23)  | 770(3)   | 3691(4)  | 477(3)   | 72    |
| C(24)  | 594(2)   | 3081(2)  | 626(1)   | 39    |
| F(25)  | 1082(2)  | 2664(2)  | 667(1)   | 42    |
| F(24)  | 85(2)    | 2791(2)  | 449(1)   | 52    |
| F(23)  | 427(2)   | 3227(2)  | 959(1)   | 47    |
| C(24') | 801(3)   | 2984(3)  | 702(2)   | 45    |
| F(25') | 956(4)   | 2615(3)  | 423(2)   | 47    |
| F(23') | 1282(4)  | 2908(3)  | 976(2)   | 48    |
| F(24') | 270(4)   | 2784(3)  | 825(2)   | 58    |
| C(25)  | 831(2)   | 3510(2)  | 11(1)    | 30    |
| F(20)  | 240(2)   | 3530(2)  | -170(1)  | 56    |
| F(21)  | 1053(2)  | 2920(2)  | -46(1)   | 42    |
| F(22)  | 1209(2)  | 3911(2)  | -153(1)  | 48    |
| C(25') | 477(3)   | 3758(3)  | 162(2)   | 34    |
| F(20') | -72(4)   | 3419(4)  | 123(2)   | 44    |
| F(21') | 330(4)   | 4361(4)  | 88(2)    | 43    |
| F(22') | 894(4)   | 3528(4)  | -65(2)   | 44    |
| C(26)  | 761(4)   | 4855(5)  | 1040(2)  | 78    |
| C(27)  | 796(1)   | 4930(2)  | 1473(1)  | 98    |
| F(26)  | 1215(2)  | 4535(3)  | 1625(1)  | 98    |
| F(27)  | 235(2)   | 4811(3)  | 1581(1)  | 141   |
| F(28)  | 965(2)   | 5503(3)  | 1563(1)  | 94    |
| C(28)  | 533(1)   | 5439(2)  | 840(1)   | 93    |
| F(30)  | 33(2)    | 5690(2)  | 997(2)   | 191   |
| F(31)  | 343(2)   | 5290(2)  | 491(1)   | 125   |
| F(32)  | 1018(2)  | 5864(2)  | 851(1)   | 71    |
| C(29)  | 5152(2)  | 3532(2)  | 461(1)   | 23    |
| C(30)  | 4975(3)  | 3220(3)  | 112(2)   | 28    |
| C(31)  | 5318(3)  | 3008(3)  | -170(2)  | 31    |
| C(32)  | 5030(3)  | 2794(3)  | -502(2)  | 29    |
| C(33)  | 4332(3)  | 2840(3)  | -563(2)  | 30    |
| C(34)  | 3989(3)  | 2999(3)  | -263(2)  | 26    |
| C(35)  | 4304(3)  | 3189(2)  | 68(2)    | 26    |
| C(36)  | 4076(2)  | 3472(2)  | 401(1)   | 24    |
| C(37)  | 5490(3)  | 2509(3)  | -766(2)  | 36    |
| C(38)  | 5967(1)  | 1990(1)  | -586(1)  | 39    |
| F(39)  | 6107(2)  | 1574(2)  | -833(1)  | 67    |
| F(40)  | 6545(2)  | 2229(2)  | -464(1)  | 71    |
| F(41)  | 5720(2)  | 1700(2)  | -319(1)  | 77    |
| C(39)  | 5865(2)  | 3014(2)  | -963(1)  | 52    |
| F(36)  | 6249(2)  | 3368(2)  | -750(1)  | 88    |
| F(37)  | 5454(2)  | 3425(2)  | -1139(1) | 111   |
| F(38)  | 6174(2)  | 2764(2)  | -1223(1) | 82    |
| C(40)  | 3926(3)  | 2813(3)  | -940(2)  | 36    |

**Table B.10** Atomic Coordinates (x $10^4$) and Equivalent Isotropic Displacement Parameters ($A^2$ x $10^3$) for $(F_{64}Pc)_2Tb(\frac{1}{2}$ Acetone)($\frac{1}{8}$ Chloroform).  U(eq) is Defined as One Third of the Trace of the Orthogonalized  $U^{ij}$ Tensor, Continued

|         | x        | y       | z        | U(eq) |
|---------|----------|---------|----------|-------|
| F(46)   | 2822(1)  | 3223(1) | -924(1)  | 44    |
| C(41)   | 3414(1)  | 3374(1) | -1008(1) | 39    |
| F(47)   | 3371(1)  | 3533(1) | -1359(1) | 47    |
| F(48)   | 3615(1)  | 3891(1) | -816(1)  | 43    |
| C(42)   | 3584(1)  | 2166(1) | -1030(1) | 46    |
| F(43)   | 4004(2)  | 1700(1) | -1049(1) | 53    |
| F(44)   | 3226(2)  | 2211(1) | -1352(1) | 66    |
| F(45)   | 3189(2)  | 2011(1) | -775(1)  | 48    |
| C(43)   | 5904(2)  | 4768(2) | 1309(2)  | 28    |
| C(44)   | 6577(3)  | 4734(3) | 1213(2)  | 34    |
| C(45)   | 7154(3)  | 5016(3) | 1350(2)  | 43    |
| C(46)   | 7740(4)  | 4925(4) | 1175(2)  | 55    |
| C(47)   | 7704(4)  | 4561(4) | 838(2)   | 59    |
| C(48)   | 7130(4)  | 4252(3) | 733(2)   | 48    |
| C(49)   | 6576(3)  | 4333(3) | 920(2)   | 33    |
| C(50)   | 5916(2)  | 4079(3) | 846(2)   | 28    |
| C(51)   | 8361(3)  | 5146(4) | 1413(3)  | 70    |
| C(52)   | 8409(1)  | 4931(1) | 1827(1)  | 58    |
| F(52)   | 9010(2)  | 4757(2) | 1937(1)  | 70    |
| F(53)   | 8025(2)  | 4439(1) | 1875(1)  | 46    |
| F(54)   | 8256(2)  | 5399(2) | 2050(1)  | 81    |
| C(53)   | 8435(3)  | 5988(3) | 1527(2)  | 36    |
| F(57)   | 8542(4)  | 6199(3) | 1210(2)  | 61    |
| F(56)   | 7967(4)  | 6287(3) | 1655(2)  | 45    |
| F(55)   | 9004(4)  | 6067(3) | 1738(2)  | 49    |
| C(53')  | 8538(2)  | 5796(2) | 1325(1)  | 32    |
| F(56')  | 8074(2)  | 6189(2) | 1434(1)  | 36    |
| F(57')  | 8596(2)  | 5958(2) | 978(1)   | 42    |
| F(55')  | 9097(2)  | 5964(2) | 1507(1)  | 37    |
| C(54)   | 8206(4)  | 4588(8) | 552(3)   | 119   |
| C(55)   | 7851(2)  | 4650(2) | 61(1)    | 35    |
| F(63)   | 7726(2)  | 4114(2) | -70(1)   | 48    |
| F(64)   | 8374(2)  | 4893(2) | -55(1)   | 51    |
| F(62)   | 7430(2)  | 5034(3) | 132(1)   | 54    |
| C(55')  | 7874(3)  | 5148(4) | 250(2)   | 46    |
| F(63')  | 8227(4)  | 5571(4) | 122(2)   | 54    |
| F(64')  | 7303(4)  | 5423(4) | 296(2)   | 50    |
| F(62')  | 7658(5)  | 4679(5) | -30(2)   | 115   |
| C(56)   | 8504(2)  | 3816(2) | 506(1)   | 46    |
| F(58)   | 9056(2)  | 3832(2) | 810(1)   | 45    |
| F(59)   | 8250(2)  | 3342(2) | 530(1)   | 51    |
| F(60)   | 8929(2)  | 3808(2) | 230(1)   | 60    |
| C(56')  | 8639(3)  | 4198(3) | 554(2)   | 34    |
| F(60')  | 9013(4)  | 4448(4) | 293(3)   | 41    |
| F(58')  | 9033(4)  | 4209(4) | 862(2)   | 25    |
| F(59')  | 8270(5)  | 3786(4) | 428(3)   | 70    |
| C(57)   | 5694(2)  | 3901(2) | 2033(2)  | 23    |
| C(58)   | 5804(2)  | 4246(2) | 2377(2)  | 24    |
| C(59)   | 6339(2)  | 4381(2) | 2621(2)  | 26    |

**Table B.10** Atomic Coordinates (x $10^4$) and Equivalent Isotropic Displacement Parameters ($A^2$ x $10^3$) for $(F_{64}Pc)_2Tb(\frac{1}{2}$ Acetone)($\frac{1}{8}$ Chloroform). U(eq) is Defined as One Third of the Trace of the Orthogonalized $U^{ij}$ Tensor, Continued

|        | x        | y        | z        | U(eq) |
|--------|----------|----------|----------|-------|
| C(60)  | 6292(3)  | 4655(3)  | 2963(2)  | 30    |
| C(61)  | 5654(3)  | 4772(3)  | 3078(2)  | 30    |
| C(62)  | 5131(3)  | 4686(2)  | 2818(2)  | 28    |
| C(63)  | 5199(3)  | 4426(2)  | 2475(1)  | 24    |
| C(64)  | 4726(2)  | 4213(2)  | 2182(1)  | 21    |
| C(65)  | 6940(3)  | 4869(3)  | 3179(2)  | 33    |
| C(66)  | 7313(1)  | 4311(1)  | 3385(1)  | 45    |
| F(74)  | 7444(2)  | 3842(1)  | 3160(1)  | 50    |
| F(75)  | 6970(2)  | 4069(1)  | 3641(1)  | 56    |
| F(76)  | 7875(2)  | 4528(1)  | 3553(1)  | 61    |
| C(67)  | 7410(1)  | 5245(1)  | 2939(1)  | 40    |
| F(77)  | 7865(1)  | 4878(1)  | 2813(1)  | 52    |
| F(78)  | 7075(1)  | 5525(1)  | 2648(1)  | 46    |
| F(79)  | 7709(1)  | 5700(1)  | 3137(1)  | 58    |
| C(68)  | 5475(3)  | 4905(3)  | 3474(2)  | 31    |
| C(69)  | 4923(1)  | 4436(1)  | 3594(1)  | 38    |
| F(67)  | 4927(1)  | 3890(1)  | 3408(1)  | 42    |
| F(68)  | 4337(1)  | 4683(1)  | 3552(1)  | 43    |
| F(69)  | 5054(1)  | 4301(1)  | 3946(1)  | 44    |
| C(70)  | 5290(1)  | 5597(1)  | 3547(1)  | 35    |
| F(70)  | 5086(2)  | 5655(1)  | 3877(1)  | 46    |
| F(71)  | 5797(1)  | 5987(1)  | 3529(1)  | 42    |
| F(72)  | 4812(1)  | 5811(1)  | 3303(1)  | 40    |
| C(71)  | 6033(2)  | 3187(2)  | 1601(1)  | 22    |
| C(72)  | 6534(2)  | 2784(2)  | 1470(1)  | 23    |
| C(73)  | 7199(3)  | 2723(2)  | 1548(2)  | 25    |
| C(74)  | 7567(3)  | 2275(3)  | 1382(2)  | 28    |
| C(75)  | 7233(3)  | 1818(3)  | 1137(2)  | 31    |
| C(76)  | 6565(3)  | 1905(3)  | 1054(2)  | 29    |
| C(77)  | 6220(2)  | 2372(3)  | 1207(2)  | 25    |
| C(78)  | 5524(2)  | 2539(2)  | 1186(1)  | 23    |
| C(79)  | 8307(3)  | 2305(3)  | 1476(2)  | 34    |
| C(80)  | 8534(1)  | 1940(1)  | 1834(1)  | 43    |
| F(127) | 9173(2)  | 1939(2)  | 1893(1)  | 64    |
| F(128) | 8344(2)  | 1334(2)  | 1813(1)  | 57    |
| F(126) | 8293(2)  | 2199(2)  | 2118(1)  | 54    |
| C(81)  | 8614(1)  | 3002(1)  | 1504(1)  | 50    |
| F(123) | 9188(1)  | 2991(1)  | 1381(1)  | 66    |
| F(124) | 8239(2)  | 3405(1)  | 1294(1)  | 56    |
| F(125) | 8691(2)  | 3238(1)  | 1844(1)  | 60    |
| C(82)  | 7512(3)  | 1218(3)  | 973(2)   | 42    |
| C(83)  | 7107(1)  | 587(1)   | 1025(1)  | 50    |
| F(119) | 6784(2)  | 638(1)   | 1323(1)  | 55    |
| F(120) | 7512(2)  | 94(1)    | 1082(1)  | 70    |
| F(121) | 6693(2)  | 439(1)   | 746(1)   | 61    |
| C(84)  | 7618(1)  | 1297(2)  | 563(1)   | 57    |
| F(116) | 8065(2)  | 1748(2)  | 534(1)   | 76    |
| F(117) | 7851(2)  | 750(2)   | 437(1)   | 83    |
| F(118) | 7097(2)  | 1464(2)  | 355(1)   | 66    |

**Table B.10** Atomic Coordinates (x $10^4$) and Equivalent Isotropic Displacement Parameters ($A^2$ x $10^3$) for $(F_{64}Pc)_2Tb(\frac{1}{2}$ Acetone)($\frac{1}{8}$ Chloroform). U(eq) is Defined as One Third of the Trace of the Orthogonalized $U^{ij}$ Tensor, Continued

|        | x        | y        | z       | U(eq) |
|--------|----------|----------|---------|-------|
| C(85)  | 4450(2)  | 2311(2)  | 985(1)  | 22    |
| C(86)  | 3969(2)  | 1902(2)  | 783(1)  | 23    |
| C(87)  | 4005(3)  | 1404(3)  | 536(2)  | 27    |
| C(88)  | 3469(3)  | 1092(2)  | 370(2)  | 27    |
| C(89)  | 2844(3)  | 1263(3)  | 485(2)  | 28    |
| C(90)  | 2816(3)  | 1777(3)  | 728(2)  | 27    |
| C(91)  | 3363(2)  | 2093(2)  | 879(1)  | 24    |
| C(92)  | 3486(2)  | 2618(2)  | 1138(2) | 24    |
| C(93)  | 3604(3)  | 613(3)   | 68(2)   | 30    |
| C(94)  | 3820(1)  | -49(1)   | 225(1)  | 33    |
| F(100) | 3350(1)  | -319(1)  | 401(1)  | 47    |
| F(101) | 4336(1)  | 2(1)     | 466(1)  | 36    |
| F(102) | 3952(2)  | -436(1)  | -41(1)  | 43    |
| C(95)  | 4093(1)  | 853(1)   | -201(1) | 37    |
| F(103) | 4696(1)  | 649(1)   | -122(1) | 40    |
| F(104) | 3903(1)  | 650(1)   | -540(1) | 48    |
| F(105) | 4100(1)  | 1494(1)  | -215(1) | 38    |
| C(96)  | 2186(3)  | 915(3)   | 376(2)  | 38    |
| C(97)  | 1793(1)  | 1255(1)  | 55(1)   | 53    |
| F(110) | 1208(2)  | 952(2)   | -11(1)  | 74    |
| F(111) | 2083(2)  | 1231(2)  | -245(1) | 58    |
| F(112) | 1683(2)  | 1855(2)  | 131(1)  | 64    |
| C(98)  | 1752(1)  | 801(1)   | 704(1)  | 48    |
| F(107) | 2122(1)  | 760(2)   | 1022(1) | 49    |
| F(108) | 1444(1)  | 249(2)   | 650(1)  | 67    |
| F(109) | 1304(1)  | 1239(2)  | 734(1)  | 52    |
| C(99)  | 3153(2)  | 3299(2)  | 1589(1) | 23    |
| C(100) | 2687(2)  | 3447(3)  | 1850(1) | 24    |
| C(101) | 2081(3)  | 3207(3)  | 1913(2) | 31    |
| C(102) | 1770(3)  | 3363(3)  | 2219(2) | 33    |
| C(103) | 2065(3)  | 3845(3)  | 2465(2) | 33    |
| C(104) | 2671(3)  | 4068(3)  | 2395(2) | 30    |
| C(105) | 2986(3)  | 3870(2)  | 2100(2) | 24    |
| C(106) | 3645(2)  | 3965(2)  | 1994(1) | 21    |
| C(107) | 1164(4)  | 2962(4)  | 2276(2) | 60    |
| C(108) | 1253(2)  | 2221(2)  | 2209(1) | 31    |
| F(84)  | 1049(3)  | 1819(2)  | 2491(2) | 78    |
| F(85)  | 1100(3)  | 1931(2)  | 1936(2) | 69    |
| F(86)  | 1931(3)  | 2035(2)  | 2288(1) | 52    |
| C(113) | 1041(3)  | 2334(4)  | 2155(2) | 2000  |
| F(84') | 800(4)   | 1957(3)  | 2420(3) | 58    |
| F(85') | 930(3)   | 2111(3)  | 1829(2) | 48    |
| F(86') | 1624(5)  | 2070(3)  | 2228(2) | 90    |
| C(109) | 551(1)   | 3200(2)  | 2060(1) | 71    |
| F(87)  | 413(2)   | 3770(2)  | 2172(1) | 92    |
| F(88)  | 599(2)   | 3186(2)  | 1711(1) | 88    |
| F(89)  | 49(1)    | 2824(2)  | 2140(1) | 119   |
| C(110) | 1765(3)  | 4156(4)  | 2791(2) | 48    |
| C(111) | 1795(1)  | 4924(1)  | 2782(1) | 55    |

**Table B.10** Atomic Coordinates (x $10^4$) and Equivalent Isotropic Displacement Parameters ($A^2$ x $10^3$) for $(F_{64}Pc)_2Tb(\frac{1}{2}$ Acetone)($\frac{1}{8}$ Chloroform). U(eq) is Defined as One Third of the Trace of the Orthogonalized $U^{ij}$ Tensor, Continued

|        | x         | y         | z         | U(eq) |
|--------|-----------|-----------|-----------|-------|
| F(91)  | 2284(2)   | 5153(1)   | 2998(1)   | 69    |
| F(92)  | 1249(2)   | 5141(1)   | 2900(1)   | 95    |
| F(93)  | 1840(2)   | 5134(1)   | 2448(1)   | 69    |
| C(112) | 2020(2)   | 3904(2)   | 3159(1)   | 67    |
| F(94)  | 1740(2)   | 4188(2)   | 3427(1)   | 102   |
| F(95)  | 2657(2)   | 3976(2)   | 3227(1)   | 73    |
| F(96)  | 1909(2)   | 3267(2)   | 3186(1)   | 88    |
| F(1)   | 3169(2)   | 6117(2)   | 1926(1)   | 38    |
| F(2)   | 5789(2)   | 6272(2)   | 2056(1)   | 39    |
| F(3)   | 4000(2)   | 7174(2)   | 2768(1)   | 46    |
| F(10)  | 4823(2)   | 7727(2)   | 2499(1)   | 41    |
| F(17)  | 1997(2)   | 3312(2)   | 350(1)    | 41    |
| F(18)  | 1976(2)   | 5321(2)   | 1273(1)   | 44    |
| F(19)  | 269(3)    | 4087(3)   | 392(2)    | 43    |
| F(19') | 266(4)    | 3914(4)   | 775(3)    | 47    |
| F(29)  | 232(2)    | 4422(3)   | 996(2)    | 87    |
| F(33)  | 5970(2)   | 3015(2)   | -110(1)   | 44    |
| F(34)  | 3344(2)   | 2999(2)   | -305(1)   | 34    |
| F(35)  | 5146(2)   | 2169(2)   | -1037(1)  | 45    |
| F(42)  | 4328(2)   | 2921(2)   | -1207(1)  | 52    |
| F(49)  | 7092(2)   | 3902(3)   | 434(1)    | 74    |
| F(50)  | 7170(2)   | 5353(2)   | 1657(2)   | 63    |
| F(51)  | 8879(2)   | 4839(3)   | 1283(2)   | 80    |
| F(61)  | 8650(2)   | 5062(5)   | 636(2)    | 165   |
| F(65)  | 6929(1)   | 4242(2)   | 2519(1)   | 35    |
| F(66)  | 4535(2)   | 4816(2)   | 2902(1)   | 31    |
| F(73)  | 5988(2)   | 4772(2)   | 3723(1)   | 36    |
| F(80)  | 6820(2)   | 5308(2)   | 3438(1)   | 39    |
| F(81)  | 1804(2)   | 2783(2)   | 1674(1)   | 42    |
| F(82)  | 2970(2)   | 4502(2)   | 2622(1)   | 35    |
| F(83)  | 1063(2)   | 2960(3)   | 2645(1)   | 68    |
| F(90)  | 1106(2)   | 4048(3)   | 2760(1)   | 68    |
| F(97)  | 4595(2)   | 1245(1)   | 448(1)    | 28    |
| F(98)  | 2242(1)   | 1968(2)   | 826(1)    | 33    |
| F(99)  | 3052(2)   | 497(2)    | -162(1)   | 37    |
| F(106) | 2297(2)   | 311(2)    | 265(1)    | 45    |
| F(113) | 7492(1)   | 3122(2)   | 1796(1)   | 30    |
| F(114) | 6240(2)   | 1507(2)   | 818(1)    | 37    |
| F(115) | 8108(2)   | 1056(2)   | 1143(1)   | 59    |
| F(122) | 8620(2)   | 2046(2)   | 1204(1)   | 50    |
| O(1A)  | 624(10)   | 1558(10)  | 9142(5)   | 126   |
| C(1A)  | 1508(9)   | 2214(10)  | 9057(5)   | 75    |
| C(2A)  | 354(15)   | 2591(15)  | 9015(9)   | 140   |
| C(3A)  | 833(9)    | 2092(11)  | 9067(5)   | 83    |
| C(1C)  | 8560(11)  | 1862(15)  | 9458(6)   | 11    |
| Cl(1C) | 8031(9)   | 1367(9)   | 9517(5)   | 73    |
| Cl(2C) | 8931(14)  | 1534(16)  | 9168(8)   | 135   |
| Cl(3C) | 9032(15)  | 1820(20)  | 9802(8)   | 174   |

**Table B.11**   Bond Lengths [Å] and Angles [°] for $(F_{64}Pc)_2Tb(1/2$ Acetone)(1/8 Chloroform)

| | | | |
|---|---|---|---|
| Tb-N(5) | 2.429(5) | C(12)-C(13) | 1.537(6) |
| Tb-N(11) | 2.431(4) | C(12)-C(14) | 1.591(7) |
| Tb-N(3) | 2.431(4) | C(15)-C(16) | 1.461(7) |
| Tb-N(9) | 2.432(4) | C(16)-C(21) | 1.382(8) |
| Tb-N(1) | 2.438(4) | C(16)-C(17) | 1.393(7) |
| Tb-N(15) | 2.439(4) | C(17)-C(18) | 1.396(8) |
| Tb-N(13) | 2.442(4) | C(18)-C(19) | 1.443(10) |
| Tb-N(7) | 2.446(4) | C(18)-C(23) | 1.535(9) |
| N(1)-C(1) | 1.364(7) | C(19)-C(20) | 1.398(8) |
| N(1)-C(8) | 1.379(6) | C(19)-C(26) | 1.520(10) |
| N(2)-C(22) | 1.325(7) | C(20)-C(21) | 1.376(8) |
| N(2)-C(1) | 1.334(7) | C(21)-C(22) | 1.462(7) |
| N(3)-C(15) | 1.366(7) | C(23)-C(25') | 1.263(12) |
| N(3)-C(22) | 1.369(7) | C(23)-C(24) | 1.450(9) |
| N(4)-C(36) | 1.323(7) | C(23)-C(24') | 1.693(11) |
| N(4)-C(15) | 1.330(7) | C(23)-C(25) | 1.769(12) |
| N(5)-C(29) | 1.370(7) | C(26)-C(28) | 1.480(10) |
| N(5)-C(36) | 1.372(6) | C(26)-C(27) | 1.591(8) |
| N(6)-C(50) | 1.318(8) | C(29)-C(30) | 1.456(8) |
| N(6)-C(29) | 1.322(7) | C(30)-C(31) | 1.383(8) |
| N(7)-C(50) | 1.365(7) | C(30)-C(35) | 1.385(8) |
| N(7)-C(43) | 1.367(7) | C(31)-C(32) | 1.379(8) |
| N(8)-C(43) | 1.312(8) | C(32)-C(33) | 1.443(8) |
| N(8)-C(8) | 1.336(7) | C(32)-C(37) | 1.543(8) |
| N(9)-C(57) | 1.373(7) | C(33)-C(34) | 1.406(8) |
| N(9)-C(64) | 1.376(7) | C(33)-C(40) | 1.549(8) |
| N(10)-C(57) | 1.324(7) | C(34)-C(35) | 1.378(8) |
| N(10)-C(71) | 1.334(7) | C(35)-C(36) | 1.476(8) |
| N(11)-C(71) | 1.368(6) | C(37)-C(39) | 1.534(7) |
| N(11)-C(78) | 1.377(7) | C(37)-C(38) | 1.570(6) |
| N(12)-C(78) | 1.320(6) | C(40)-C(42) | 1.552(7) |
| N(12)-C(85) | 1.334(7) | C(40)-C(41) | 1.586(6) |
| N(13)-C(92) | 1.364(7) | C(43)-C(44) | 1.469(8) |
| N(13)-C(85) | 1.369(7) | C(44)-C(49) | 1.364(9) |
| N(14)-C(99) | 1.333(7) | C(44)-C(45) | 1.383(9) |
| N(14)-C(92) | 1.337(7) | C(45)-C(46) | 1.437(10) |
| N(15)-C(99) | 1.369(7) | C(46)-C(47) | 1.450(12) |
| N(15)-C(106) | 1.373(7) | C(46)-C(51) | 1.552(10) |
| N(16)-C(106) | 1.319(6) | C(47)-C(48) | 1.375(11) |
| N(16)-C(64) | 1.329(7) | C(47)-C(54) | 1.549(13) |
| C(1)-C(2) | 1.458(7) | C(48)-C(49) | 1.402(10) |
| C(2)-C(3) | 1.365(8) | C(49)-C(50) | 1.465(8) |
| C(2)-C(7) | 1.384(8) | C(51)-C(53') | 1.456(8) |
| C(3)-C(4) | 1.394(8) | C(51)-C(52) | 1.580(10) |
| C(4)-C(5) | 1.421(9) | C(51)-C(53) | 1.818(11) |
| C(4)-C(9) | 1.553(9) | C(54)-C(56') | 1.212(15) |
| C(5)-C(6) | 1.407(9) | C(54)-C(55') | 1.711(13) |
| C(5)-C(12) | 1.546(8) | C(54)-C(56) | 1.747(17) |
| C(6)-C(7) | 1.395(8) | C(54)-C(55) | 1.885(10) |
| C(7)-C(8) | 1.461(8) | C(57)-C(58) | 1.455(8) |
| C(9)-C(10) | 1.544(7) | C(3)-C(4)-C(9) | 115.3(5) |
| C(9)-C(11) | 1.603(7) | N(9)-Tb-N(13) | 109.12(14) |

**Table B.11**   Bond Lengths [Å] and Angles [°] for (F$_{64}$Pc)$_2$Tb(1/2 Acetone)(1/8 Chloroform), Continued

| | | | |
|---|---|---|---|
| C(88)-C(89) | 1.442(8) | N(1)-Tb-N(13) | 156.02(14) |
| C(88)-C(93) | 1.540(8) | N(15)-Tb-N(13) | 69.71(14) |
| C(89)-C(90) | 1.402(8) | N(5)-Tb-N(7) | 71.19(14) |
| C(89)-C(96) | 1.563(7) | N(11)-Tb-N(7) | 76.23(14) |
| C(90)-C(91) | 1.380(7) | N(3)-Tb-N(7) | 108.63(14) |
| C(91)-C(92) | 1.462(7) | N(9)-Tb-N(7) | 89.32(14) |
| C(93)-C(94) | 1.552(6) | N(1)-Tb-N(7) | 69.27(15) |
| C(93)-C(95) | 1.564(7) | N(15)-Tb-N(7) | 155.70(15) |
| C(96)-C(97) | 1.538(7) | N(13)-Tb-N(7) | 132.77(14) |
| C(96)-C(98) | 1.586(7) | C(1)-N(1)-C(8) | 108.4(4) |
| C(99)-C(100) | 1.458(8) | C(1)-N(1)-Tb | 121.7(3) |
| C(100)-C(105) | 1.379(7) | C(8)-N(1)-Tb | 121.4(3) |
| C(100)-C(101) | 1.391(8) | C(22)-N(2)-C(1) | 123.5(5) |
| C(101)-C(102) | 1.386(9) | C(15)-N(3)-C(22) | 108.5(4) |
| C(102)-C(103) | 1.451(8) | C(15)-N(3)-Tb | 120.8(3) |
| C(102)-C(107) | 1.542(9) | C(22)-N(3)-Tb | 121.3(3) |
| C(103)-C(104) | 1.384(8) | C(36)-N(4)-C(15) | 122.6(4) |
| C(103)-C(110) | 1.543(9) | (C 29)-N(5)-C(36) | 108.2(4) |
| C(104)-C(105) | 1.382(8) | C(29)-N(5)-Tb | 125.0(3) |
| C(105)-C(106) | 1.466(7) | C(36)-N(5)-Tb | 123.8(3) |
| C(107)-C(113) | 1.405(11) | C(50)-N(6)-C(29) | 122.9(5) |
| C(107)-C(109) | 1.514(10) | C(50)-N(7)-C(43) | 109.5(4) |
| C(107)-C(108) | 1.587(10) | C(50)-N(7)-Tb | 122.2(3) |
| C(108)-C(113) | 0.521(7) | C(43)-N(7)-Tb | 122.5(4) |
| C(110)-C(112) | 1.499(9) | C(43)-N(8)-C(8) | 123.0(5) |
| C(110)-C(111) | 1.612(8) | C(57)-N(9)-C(64) | 108.1(4) |
| O(1A)-C(3A) | 1.24(3) | C(57)-N(9)-Tb | 125.2(4) |
| C(1A)-C(3A) | 1.42(2) | C(64)-N(9)-Tb | 122.7(3) |
| C(2A)-C(3A) | 1.44(2) | C(57)-N(10)-C(71) | 122.8(4) |
| C(1C)-Cl(3C) | 1.52(3) | C(71)-N(11)-C(78) | 108.6(4) |
| C(1C)-Cl(2C) | 1.53(3) | C(71)-N(11)-Tb | 123.6(3) |
| C(1C)-Cl(1C) | 1.54(2) | C(78)-N(11)-Tb | 121.3(3) |
| N(5)-Tb-N(11) | 91.09(14) | C(78)-N(12)-C(85) | 122.0(5) |
| N(5)-Tb-N(3) | 69.70(14) | C(92)-N(13)-C(85) | 108.5(4) |
| N(11)-Tb-N(3) | 156.35(14) | C(92)-N(13)-Tb | 123.5(3) |
| N(5)-Tb-N(9) | 155.49(14) | C(85)-N(13)-Tb | 120.2(3) |
| N(11)-Tb-N(9) | 69.36(14) | C(99)-N(14)-C(92) | 122.1(4) |
| N(3)-Tb-N(9) | 132.57(14) | C(99)-N(15)-C(106) | 107.8(4) |
| N(5)-Tb-N(1) | 108.88(15) | C(99)-N(15)-Tb | 126.2(3) |
| N(11)-Tb-N(1) | 130.86(14) | C(106)-N(15)-Tb | 124.0(3) |
| N(3)-Tb-N(1) | 70.51(14) | C(106)-N(16)-C(64) | 123.7(5) |
| N(9)-Tb-N(1) | 76.21(14) | N(2)-C(1)-N(1) | 127.4(5) |
| N(5)-Tb-N(15) | 130.67(14) | N(2)-C(1)-C(2) | 123.1(5) |
| N(11)-Tb-N(15) | 109.64(14) | N(1)-C(1)-C(2) | 109.6(4) |
| N(3)-Tb-N(15) | 75.82(14) | C(3)-C(2)-C(7) | 118.8(5) |
| N(9)-Tb-N(15) | 71.85(14) | C(3)-C(2)-C(1) | 134.9(5) |
| N(1)-Tb-N(15) | 90.88(15) | C(7)-C(2)-C(1) | 106.3(5) |
| N(5)-Tb-N(13) | 76.33(14) | C(2)-C(3)-C(4) | 123.4(6) |
| N(11)-Tb-N(13) | 71.00(13) | C(3)-C(4)-C(5) | 118.4(6) |
| N(3)-Tb-N(13) | 90.53(13) | C(31)-C(30)-C(29) | 134.5(5) |
| C(5)-C(4)-C(9) | 125.9(5) | C(31)-C(30)-C(35) | 118.7(5) |

**Table B.11**   Bond Lengths [Å] and Angles [°] for (F$_{64}$Pc)$_2$Tb(1/2 Acetone)(1/8 Chloroform), Continued

| | | | |
|---|---|---|---|
| C(6)-C(5)-C(4) | 117.2(5) | | |
| C(6)-C(5)-C(12) | 115.6(5) | C(35)-C(30)-C(29) | 106.7(5) |
| C(4)-C(5)-C(12) | 127.1(6) | C(32)-C(31)-C(30) | 123.8(5) |
| C(7)-C(6)-C(5) | 122.1(6) | C(31)-C(32)-C(33) | 117.1(5) |
| C(2)-C(7)-C(6) | 119.5(5) | C(31)-C(32)-C(37) | 116.1(5) |
| C(2)-C(7)-C(8) | 107.2(5) | C(33)-C(32)-C(37) | 126.8(5) |
| C(6)-C(7)-C(8) | 133.1(5) | C(34)-C(33)-C(32) | 117.9(5) |
| N(8)-C(8)-N(1) | 128.0(5) | C(34)-C(33)-C(40) | 116.0(5) |
| N(8)-C(8)-C(7) | 123.6(5) | C(32)-C(33)-C(40) | 125.6(5) |
| N(1)-C(8)-C(7) | 108.4(5) | C(35)-C(34)-C(33) | 121.8(5) |
| C(10)-C(9)-C(4) | 112.8(5) | C(34)-C(35)-C(30) | 119.9(5) |
| C(10)-C(9)-C(11) | 110.4(4) | C(34)-C(35)-C(36) | 133.1(5) |
| C(4)-C(9)-C(11) | 113.6(4) | C(30)-C(35)-C(36) | 106.4(5) |
| C(13)-C(12)-C(5) | 114.1(4) | N(4)-C(36)-N(5) | 128.5(5) |
| C(13)-C(12)-C(14) | 110.8(4) | N(4)-C(36)-C(35) | 122.5(5) |
| C(5)-C(12)-C(14) | 113.1(4) | N(5)-C(36)-C(35) | 108.8(4) |
| N(4)-C(15)-N(3) | 126.9(5) | C(39)-C(37)-C(32) | 113.6(4) |
| N(4)-C(15)-C(16) | 123.7(5) | C(39)-C(37)-C(38) | 110.5(4) |
| N(3)-C(15)-C(16) | 109.2(5) | C(32)-C(37)-C(38) | 113.9(4) |
| C(21)-C(16)-C(17) | 119.5(5) | C(33)-C(40)-C(42) | 114.7(4) |
| C(21)-C(16)-C(15) | 106.3(4) | C(33)-C(40)-C(41) | 114.1(4) |
| C(17)-C(16)-C(15) | 134.2(5) | C(42)-C(40)-C(41) | 109.2(4) |
| C(16)-C(17)-C(18) | 122.4(6) | N(8)-C(43)-N(7) | 127.5(5) |
| C(17)-C(18)-C(19) | 117.7(5) | N(8)-C(43)-C(44) | 124.1(5) |
| C(17)-C(18)-C(23) | 117.0(6) | N(7)-C(43)-C(44) | 108.1(5) |
| C(19)-C(18)-C(23) | 125.3(6) | C(49)-C(44)-C(45) | 119.0(6) |
| C(20)-C(19)-C(18) | 117.9(5) | C(49)-C(44)-C(43) | 106.8(5) |
| C(20)-C(19)-C(26) | 116.7(6) | C(45)-C(44)-C(43) | 134.2(6) |
| C(18)-C(19)-C(26) | 124.8(6) | C(44)-C(45)-C(46) | 121.2(6) |
| C(21)-C(20)-C(19) | 122.9(6) | C(45)-C(46)-C(47) | 118.3(7) |
| C(20)-C(21)-C(16) | 119.4(5) | C(45)-C(46)-C(51) | 113.5(7) |
| C(20)-C(21)-C(22) | 133.6(5) | C(47)-C(46)-C(51) | 127.4(8) |
| C(16)-C(21)-C(22) | 107.0(4) | C(48)-C(47)-C(46) | 117.4(8) |
| N(2)-C(22)-N(3) | 128.8(5) | C(48)-C(47)-C(54) | 116.4(8) |
| N(2)-C(22)-C(21) | 122.5(5) | C(46)-C(47)-C(54) | 125.2(9) |
| N(3)-C(22)-C(21) | 108.7(4) | C(47)-C(48)-C(49) | 122.0(7) |
| C(25')-C(23)-C(24) | 109.1(6) | C(44)-C(49)-C(48) | 121.4(6) |
| C(25')-C(23)-C(18) | 128.5(8) | C(44)-C(49)-C(50) | 107.5(5) |
| C(24)-C(23)-C(18) | 119.8(7) | C(48)-C(49)-C(50) | 131.0(6) |
| C(25')-C(23)-C(24') | 122.4(6) | N(6)-C(50)-N(7) | 130.3(5) |
| C(24)-C(23)-C(24') | 17.2(2) | N(6)-C(50)-C(49) | 121.5(5) |
| C(18)-C(23)-C(24') | 103.5(6) | N(7)-C(50)-C(49) | 107.9(5) |
| C(25')-C(23)-C(25) | 37.7(4) | C(53')-C(51)-C(46) | 111.6(6) |
| C(24)-C(23)-C(25) | 102.7(6) | C(53')-C(51)-C(52) | 119.1(7) |
| C(18)-C(23)-C(25) | 111.7(6) | C(46)-C(51)-C(52) | 115.3(5) |
| C(24')-C(23)-C(25) | 106.4(5) | C(53')-C(51)-C(53) | 28.9(3) |
| C(28)-C(26)-C(19) | 111.6(6) | C(46)-C(51)-C(53) | 117.8(6) |
| C(28)-C(26)-C(27) | 113.4(6) | C(52)-C(51)-C(53) | 93.4(6) |
| C(19)-C(26)-C(27) | 115.4(5) | C(56')-C(54)-C(47) | 121.0(9) |
| N(6)-C(29)-N(5) | 128.3(5) | C(56')-C(54)-C(55') | 135.8(9) |
| N(6)-C(29)-C(30) | 121.8(5) | C(47)-C(54)-C(55') | 102.1(8) |
| N(5)-C(29)-C(30) | 109.7(4) | C(56')-C(54)-C(56) | 26.9(5) |

**Table B.11**  Bond Lengths [Å] and Angles [°] for (F$_{64}$Pc)$_2$Tb(1/2 Acetone)(1/8 Chloroform, Continued

| | | | |
|---|---|---|---|
| C(47)-C(54)-C(56) | 107.2(8) | C(74)-C(79)-C(81) | 115.8(4) |
| C(55')-C(54)-C(56) | 134.2(8) | C(80)-C(79)-C(81) | 108.1(4) |
| C(56')-C(54)-C(55) | 105.7(10) | C(75)-C(82)-C(84) | 112.9(5) |
| C(47)-C(54)-C(55) | 115.2(6) | C(75)-C(82)-C(83) | 114.4(5) |
| C(55')-C(54)-C(55) | 40.4(3) | C(84)-C(82)-C(83) | 109.5(4) |
| C(56)-C(54)-C(55) | 94.6(8) | N(12)-C(85)-N(13) | 129.4(5) |
| N(10)-C(57)-N(9) | 127.2(5) | N(12)-C(85)-C(86) | 121.6(5) |
| N(10)-C(57)-C(58) | 123.7(5) | N(13)-C(85)-C(86) | 108.9(4) |
| N(9)-C(57)-C(58) | 109.0(5) | C(87)-C(86)-C(91) | 119.1(5) |
| C(59)-C(58)-C(63) | 117.4(5) | C(87)-C(86)-C(85) | 134.1(5) |
| C(59)-C(58)-C(57) | 135.4(5) | C(91)-C(86)-C(85) | 106.8(4) |
| C(63)-C(58)-C(57) | 107.0(4) | C(88)-C(87)-C(86) | 123.6(5) |
| C(58)-C(59)-C(60) | 123.1(5) | C(87)-C(88)-C(89) | 117.2(5) |
| C(59)-C(60)-C(61) | 118.6(5) | C(87)-C(88)-C(93) | 115.6(5) |
| C(59)-C(60)-C(65) | 116.4(5) | C(89)-C(88)-C(93) | 127.1(5) |
| C(61)-C(60)-C(65) | 124.7(5) | C(90)-C(89)-C(88) | 118.1(5) |
| C(62)-C(61)-C(60) | 116.9(5) | C(90)-C(89)-C(96) | 115.6(5) |
| C(62)-C(61)-C(68) | 115.2(5) | C(88)-C(89)-C(96) | 126.3(5) |
| C(60)-C(61)-C(68) | 127.4(5) | C(91)-C(90)-C(89) | 122.8(5) |
| C(61)-C(62)-C(63) | 122.2(5) | C(90)-C(91)-C(86) | 118.9(5) |
| C(58)-C(63)-C(62) | 121.0(5) | C(90)-C(91)-C(92) | 135.1(5) |
| C(58)-C(63)-C(64) | 106.5(5) | C(86)-C(91)-C(92) | 106.0(4) |
| C(62)-C(63)-C(64) | 132.0(5) | N(14)-C(92)-N(13) | 127.4(5) |
| N(16)-C(64)-N(9) | 129.2(5) | N(14)-C(92)-C(91) | 122.5(5) |
| N(16)-C(64)-C(63) | 121.1(5) | N(13)-C(92)-C(91) | 109.6(5) |
| N(9)-C(64)-C(63) | 109.3(4) | C(88)-C(93)-C(94) | 112.5(4) |
| C(66)-C(65)-C(60) | 113.1(4) | C(88)-C(93)-C(95) | 114.7(4) |
| C(66)-C(65)-C(67) | 110.0(4) | C(94)-C(93)-C(95) | 110.0(4) |
| C(60)-C(65)-C(67) | 114.0(4) | C(97)-C(96)-C(89) | 111.3(5) |
| C(70)-C(68)-C(61) | 114.8(4) | C(97)-C(96)-C(98) | 110.7(4) |
| C(70)-C(68)-C(69) | 109.6(4) | C(89)-C(96)-C(98) | 114.8(5) |
| C(61)-C(68)-C(69) | 112.8(4) | N(14)-C(99)-N(15) | 128.9(5) |
| N(10)-C(71)-N(11) | 127.8(5) | N(14)-C(99)-C(100) | 121.4(5) |
| N(10)-C(71)-C(72) | 122.3(4) | N(15)-C(99)-C(100) | 109.5(4) |
| N(11)-C(71)-C(72) | 109.8(4) | C(105)-C(100)-C(101) | 118.5(5) |
| C(73)-C(72)-C(77) | 117.9(5) | C(105)-C(100)-C(99) | 107.0(4) |
| C(73)-C(72)-C(71) | 135.4(5) | C(101)-C(100)-C(99) | 134.1(5) |
| C(77)-C(72)-C(71) | 106.6(4) | C(102)-C(101)-C(100) | 123.0(5) |
| C(72)-C(73)-C(74) | 123.3(5) | C(101)-C(102)-C(103) | 118.1(5) |
| C(73)-C(74)-C(75) | 118.3(5) | C(101)-C(102)-C(107) | 115.4(5) |
| C(73)-C(74)-C(79) | 116.7(5) | C(103)-C(102)-C(107) | 126.4(6) |
| C(75)-C(74)-C(79) | 125.0(5) | C(104)-C(103)-C(102) | 116.9(5) |
| C(76)-C(75)-C(74) | 117.0(5) | C(104)-C(103)-C(110) | 116.2(5) |
| C(76)-C(75)-C(82) | 115.0(5) | C(102)-C(103)-C(110) | 126.9(5) |
| C(74)-C(75)-C(82) | 127.9(5) | C(105)-C(104)-C(103) | 123.3(5) |
| C(77)-C(76)-C(75) | 123.2(5) | C(100)-C(105)-C(104) | 120.0(5) |
| C(76)-C(77)-C(72) | 119.9(5) | C(100)-C(105)-C(106) | 106.3(5) |
| C(76)-C(77)-C(78) | 133.9(5) | C(104)-C(105)-C(106) | 133.5(5) |
| C(72)-C(77)-C(78) | 105.9(5) | N(16)-C(106)-N(15) | 128.5(5) |
| N(12)-C(78)-N(11) | 129.6(5) | N(16)-C(106)-C(105) | 121.6(5) |
| N(12)-C(78)-C(77) | 121.4(5) | N(15)-C(106)-C(105) | 109.3(4) |
| N(11)-C(78)-C(77) | 108.9(4) | C(113)-C(107)-C(109) | 91.5(5) |

**Table B.11**   Bond Lengths [Å] and Angles [°] for (F$_{64}$Pc)$_2$Tb(1/2 Acetone)(1/8 Chloroform), Continued

| | | | |
|---|---|---|---|
| C(74)-C(79)-C(80) | 112.4(4) | C(113)-C(107)-C(102) | 126.4(6) |
| C(109)-C(107)-C(102) | 113.6(7) | C(103)-C(110)-C(111) | 112.8(5) |
| C(113)-C(107)-C(108) | 18.8(3) | O(1A)-C(3A)-C(1A) | 122(2) |
| C(109)-C(107)-C(108) | 110.2(5) | O(1A)-C(3A)-C(2A) | 116(2) |
| C(102)-C(107)-C(108) | 113.9(6) | C(1A)-C(3A)-C(2A) | 122(2) |
| C(113)-C(108)-C(107) | 60.5(11) | Cl(3C)-C(1C)-Cl(2C) | 103.0(19) |
| C(108)-C(113)-C(107) | 100.7(12) | Cl(3C)-C(1C)-Cl(1C) | 104.6(19) |
| C(112)-C(110)-C(103) | 114.5(6) | Cl(2C)-C(1C)-Cl(1C) | 101.8(18) |
| C(112)-C(110)-C(111) | 111.0(5) | | |

Symmetry transformations used to generate equivalent atoms:

**Table B.12** Anisotropic Displacement Parameters ($\mathring{A}^2$ x $10^3$) for $(F_{64}Pc)_2Tb(1/2$ Acetone)(1/8 Chloroform). The Anisotropic Displacement Factor Exponent Takes the Form: $-2\pi^2[\,h^2a^{*2}U^{11} + ... + 2\,h\,k\,a^*\,b^*\,U^{12}]$

| | $U^{11}$ | $U^{22}$ | $U^{33}$ | $U^{23}$ | $U^{13}$ | $U^{12}$ |
|---|---|---|---|---|---|---|
| Tb | 16 | 20 | 19 | 0 | -1 | -1 |
| N(1) | 26 | 21 | 25 | 3 | -2 | -2 |
| N(2) | 26 | 22 | 25 | 1 | -1 | 1 |
| N(3) | 15 | 23 | 22 | 2 | 2 | 1 |
| N(4) | 23 | 23 | 21 | 1 | 0 | 3 |
| N(5) | 19 | 23 | 27 | 0 | -2 | 0 |
| N(6) | 25 | 36 | 26 | 5 | 4 | 7 |
| N(7) | 18 | 20 | 28 | 4 | 2 | -2 |
| N(8) | 28 | 21 | 39 | 2 | -8 | -1 |
| N(9) | 19 | 23 | 23 | -1 | -1 | 0 |
| N(10) | 25 | 21 | 24 | -1 | 0 | -1 |
| N(11) | 19 | 19 | 23 | -2 | 0 | 2 |
| N(12) | 24 | 20 | 22 | -2 | -2 | -2 |
| N(13) | 22 | 20 | 19 | 1 | -2 | -2 |
| N(14) | 21 | 25 | 25 | -2 | 2 | -5 |
| N(15) | 25 | 21 | 20 | 2 | 2 | 2 |
| N(16) | 22 | 18 | 25 | 3 | -1 | -1 |
| C(1) | 27 | 19 | 24 | 3 | 3 | 2 |
| C(2) | 37 | 21 | 24 | 5 | -2 | 0 |
| C(3) | 34 | 27 | 30 | 1 | 2 | -1 |
| C(4) | 46 | 25 | 31 | 3 | 5 | 3 |
| C(5) | 48 | 26 | 26 | -2 | -1 | -5 |
| C(6) | 37 | 22 | 31 | 2 | -5 | -1 |
| C(7) | 32 | 23 | 25 | 0 | -3 | 0 |
| C(8) | 27 | 20 | 30 | 1 | -7 | -2 |
| C(9) | 47 | 37 | 31 | -12 | 7 | -5 |
| C(10) | 48 | 37 | 46 | -11 | 11 | -1 |
| F(7) | 60 | 45 | 63 | -20 | 16 | 4 |
| F(8) | 63 | 39 | 48 | -8 | -4 | 8 |
| F(9) | 62 | 32 | 57 | 2 | 4 | 1 |
| C(11) | 62 | 42 | 53 | -15 | 19 | -5 |
| F(4) | 82 | 52 | 43 | -13 | 26 | -9 |
| F(5) | 55 | 53 | 60 | -17 | 19 | -8 |
| F(6) | 76 | 33 | 44 | -2 | 21 | -5 |
| C(12) | 52 | 27 | 25 | -7 | -1 | -5 |
| C(13) | 68 | 36 | 36 | 1 | -7 | -13 |
| F(14) | 88 | 52 | 25 | 0 | 1 | 5 |
| F(15) | 87 | 55 | 51 | -6 | -25 | -29 |
| F(16) | 60 | 46 | 37 | 1 | -12 | 3 |
| C(14) | 66 | 24 | 38 | -9 | 4 | -7 |
| F(11) | 77 | 28 | 46 | -9 | 12 | -18 |
| F(12) | 58 | 37 | 77 | -13 | 13 | -16 |
| F(13) | 93 | 36 | 31 | -5 | 11 | -11 |
| C(15) | 20 | 27 | 20 | 6 | -5 | -1 |
| C(16) | 19 | 28 | 25 | 6 | -1 | 0 |
| C(17) | 25 | 37 | 30 | 8 | -7 | 1 |

**Table B.12** Anisotropic Displacement Parameters ($\mathring{A}^2$ x $10^3$) for $(F_{64}Pc)_2Tb(1/2$ Acetone)(1/8 Chloroform). The Anisotropic Displacement Factor Exponent Takes the Form: $-2\pi^2[\ h^2a^{*2}U^{11} + ... + 2\ h\ k\ a^*\ b^*\ U^{12}\ ]$, Continued

|  | $U^{11}$ | $U^{22}$ | $U^{33}$ | $U^{23}$ | $U^{13}$ | $U^{12}$ |
|---|---|---|---|---|---|---|
| C(18) | 18 | 46 | 38 | 13 | -5 | -2 |
| C(19) | 26 | 66 | 31 | 3 | 0 | 4 |
| C(20) | 26 | 43 | 31 | 4 | 4 | 4 |
| C(21) | 22 | 26 | 26 | 1 | 3 | 1 |
| C(22) | 18 | 25 | 26 | 4 | 4 | 1 |
| C(23) | 25 | 45 | 141 | 7 | -18 | -5 |
| C(26) | 29 | 120 | 83 | -47 | -7 | 16 |
| C(27) | 80 | 115 | 108 | 28 | 63 | 46 |
| F(26) | 73 | 127 | 92 | 5 | 4 | 6 |
| F(27) | 34 | 170 | 222 | 85 | 24 | 4 |
| F(28) | 47 | 170 | 68 | -35 | 13 | 11 |
| C(28) | 87 | 96 | 99 | -2 | 23 | -10 |
| F(30) | 40 | 65 | 475 | -29 | 60 | 18 |
| F(31) | 56 | 143 | 171 | -99 | -15 | 24 |
| F(32) | 57 | 56 | 100 | 4 | 2 | 7 |
| C(29) | 25 | 25 | 20 | 4 | 3 | 7 |
| C(30) | 28 | 31 | 25 | 7 | 2 | 6 |
| C(31) | 32 | 34 | 28 | 6 | 8 | 9 |
| C(32) | 38 | 28 | 22 | 3 | 10 | 8 |
| C(33) | 42 | 29 | 19 | -1 | 0 | 6 |
| C(34) | 30 | 25 | 23 | 1 | 3 | 4 |
| C(35) | 32 | 24 | 21 | 3 | 4 | 3 |
| C(36) | 27 | 23 | 20 | 2 | -1 | 2 |
| C(37) | 47 | 34 | 30 | -3 | 9 | 12 |
| C(38) | 40 | 36 | 42 | -7 | 9 | 11 |
| F(39) | 69 | 62 | 67 | -28 | 1 | 35 |
| F(40) | 55 | 66 | 90 | -23 | -8 | 16 |
| F(41) | 80 | 60 | 97 | 43 | 41 | 37 |
| C(39) | 74 | 50 | 37 | 7 | 27 | 5 |
| F(36) | 126 | 79 | 63 | 0 | 34 | -40 |
| F(37) | 122 | 107 | 115 | 78 | 64 | 43 |
| F(38) | 110 | 88 | 59 | -20 | 60 | -12 |
| C(40) | 47 | 37 | 25 | 1 | 2 | 8 |
| C(41) | 48 | 40 | 28 | 2 | -6 | 8 |
| F(46) | 42 | 51 | 39 | -1 | -7 | 7 |
| F(47) | 59 | 52 | 29 | 7 | -3 | 12 |
| F(48) | 52 | 33 | 44 | 0 | -5 | 8 |
| C(42) | 65 | 45 | 26 | -5 | -10 | 15 |
| F(43) | 84 | 34 | 42 | -12 | 5 | 13 |
| F(44) | 96 | 57 | 37 | -10 | -27 | 4 |
| F(45) | 54 | 41 | 46 | -4 | -7 | -2 |
| C(43) | 18 | 23 | 42 | 10 | -8 | -3 |
| C(50) | 19 | 30 | 34 | 8 | 1 | 3 |
| C(51) | 19 | 71 | 116 | 50 | -14 | -13 |
| C(52) | 31 | 38 | 100 | 10 | -20 | -3 |
| F(52) | 29 | 76 | 99 | 23 | -20 | -1 |
| F(53) | 37 | 35 | 63 | 3 | -5 | -1 |
| F(54) | 45 | 49 | 138 | -12 | -42 | -1 |
| C(54) | 27 | 256 | 73 | 88 | -2 | -31 |

**Table B.12**   Anisotropic Displacement Parameters (Å$^2$ x 10$^3$) for (F$_{64}$Pc)$_2$Tb(1/2 Acetone)(1/8 Chloroform).  The Anisotropic Displacement Factor Exponent Takes the Form: -2π$^2$[ h$^2$a*$^2$U$^{11}$ + ... + 2 h k a* b* U$^{12}$ ], Continued

|        | U$^{11}$ | U$^{22}$ | U$^{33}$ | U$^{23}$ | U$^{13}$ | U$^{12}$ |
|--------|------|------|------|------|------|------|
| C(57)  | 23   | 20   | 24   | 3    | -1   | -2   |
| C(58)  | 23   | 21   | 26   | 1    | 0    | -1   |
| C(59)  | 21   | 24   | 32   | -2   | -5   | -4   |
| C(60)  | 38   | 26   | 24   | 2    | -9   | -4   |
| C(61)  | 38   | 23   | 26   | 1    | -6   | 0    |
| C(62)  | 34   | 22   | 27   | -1   | -4   | -3   |
| C(63)  | 30   | 23   | 19   | 4    | -2   | 0    |
| C(64)  | 24   | 18   | 22   | 5    | -1   | -3   |
| C(65)  | 34   | 35   | 27   | -7   | -7   | -1   |
| C(66)  | 39   | 50   | 43   | -4   | -16  | 1    |
| F(74)  | 47   | 46   | 52   | -8   | -20  | 10   |
| F(75)  | 56   | 58   | 50   | 12   | -10  | 13   |
| F(76)  | 44   | 68   | 63   | -13  | -34  | 3    |
| C(67)  | 35   | 44   | 40   | -8   | 2    | -10  |
| F(77)  | 33   | 65   | 56   | -14  | -5   | -10  |
| F(78)  | 51   | 46   | 41   | 1    | 0    | -14  |
| F(79)  | 56   | 61   | 54   | -20  | -2   | -32  |
| C(68)  | 44   | 27   | 21   | 0    | -4   | -5   |
| C(69)  | 45   | 39   | 28   | 2    | -5   | -6   |
| F(67)  | 58   | 32   | 34   | -3   | 1    | -13  |
| F(68)  | 42   | 54   | 33   | -2   | 5    | 0    |
| F(69)  | 61   | 46   | 25   | 4    | 0    | -10  |
| C(70)  | 49   | 31   | 23   | -4   | -4   | -3   |
| F(70)  | 69   | 39   | 30   | -11  | 6    | 0    |
| F(71)  | 54   | 31   | 38   | -5   | -2   | -5   |
| F(72)  | 53   | 35   | 32   | -1   | -4   | 5    |
| C(71)  | 21   | 22   | 23   | 1    | -3   | -1   |
| C(72)  | 23   | 23   | 23   | 0    | -3   | -1   |
| C(73)  | 27   | 25   | 23   | -2   | -3   | -1   |
| C(74)  | 23   | 31   | 31   | 6    | 1    | -3   |
| C(75)  | 27   | 31   | 35   | -1   | 1    | 2    |
| C(76)  | 24   | 33   | 30   | -6   | -4   | 1    |
| C(77)  | 23   | 29   | 23   | 1    | -5   | -1   |
| C(78)  | 26   | 23   | 18   | 2    | -3   | 0    |
| C(79)  | 25   | 37   | 41   | -5   | 7    | 2    |
| C(80)  | 25   | 49   | 52   | 2    | -7   | 5    |
| F(127) | 29   | 77   | 81   | 1    | -15  | 6    |
| F(128) | 51   | 42   | 75   | 10   | -6   | 5    |
| F(126) | 44   | 72   | 45   | 1    | -5   | 8    |
| C(81)  | 19   | 46   | 85   | 4    | 9    | 4    |
| F(123) | 33   | 56   | 113  | 2    | 29   | -5   |
| F(124) | 45   | 42   | 85   | 15   | 25   | 3    |
| F(125) | 29   | 54   | 96   | -31  | -1   | -3   |
| C(82)  | 26   | 51   | 48   | -19  | -8   | 11   |
| C(83)  | 55   | 35   | 56   | -11  | -10  | 13   |
| F(119) | 59   | 41   | 62   | -3   | -4   | -5   |
| F(120) | 64   | 42   | 99   | -18  | -24  | 20   |
| F(121) | 60   | 45   | 72   | -26  | -24  | 13   |
| C(84)  | 45   | 69   | 58   | -24  | 10   | 4    |

**Table B.12**   Anisotropic Displacement Parameters ($\mathring{A}^2$ x $10^3$) for $(F_{64}Pc)_2Tb(1/2$ Acetone)(1/8 Chloroform).  The Anisotropic Displacement Factor Exponent Takes the Form: $-2\pi^2[\,h^2a^{*2}U^{11} + ... + 2\,h\,k\,a^*\,b^*\,U^{12}]$, Continued

|        | $U^{11}$ | $U^{22}$ | $U^{33}$ | $U^{23}$ | $U^{13}$ | $U^{12}$ |
|--------|------|------|------|------|------|------|
| F(116) | 60   | 109  | 62   | -16  | 24   | -6   |
| F(117) | 68   | 104  | 78   | -50  | 14   | 28   |
| F(118) | 62   | 93   | 42   | -13  | 7    | 16   |
| C(85)  | 23   | 25   | 17   | 4    | -2   | -1   |
| C(86)  | 24   | 21   | 22   | -2   | -4   | 3    |
| C(87)  | 26   | 25   | 28   | 2    | -1   | -1   |
| C(88)  | 36   | 22   | 22   | -2   | -6   | 0    |
| C(89)  | 26   | 27   | 30   | 1    | -7   | -4   |
| C(90)  | 24   | 28   | 29   | 2    | -3   | -4   |
| C(91)  | 24   | 23   | 24   | 0    | -1   | -2   |
| C(92)  | 25   | 21   | 25   | -1   | -4   | -1   |
| C(93)  | 37   | 25   | 25   | -2   | -9   | 0    |
| C(94)  | 43   | 21   | 33   | -3   | -6   | -2   |
| F(100) | 50   | 33   | 58   | 9    | 4    | -4   |
| F(101) | 45   | 30   | 33   | -2   | -7   | 5    |
| F(102) | 61   | 26   | 39   | -10  | -8   | 10   |
| C(95)  | 55   | 29   | 26   | -4   | -5   | -5   |
| F(103) | 50   | 35   | 36   | -9   | 8    | 5    |
| F(104) | 75   | 42   | 25   | -8   | 0    | -9   |
| F(105) | 57   | 26   | 31   | 0    | 2    | 0    |
| C(96)  | 34   | 29   | 50   | -12  | -7   | -7   |
| C(97)  | 39   | 63   | 52   | -20  | -20  | 7    |
| F(110) | 38   | 98   | 81   | -26  | -26  | -7   |
| F(111) | 59   | 70   | 41   | -7   | -18  | 16   |
| F(112) | 68   | 56   | 60   | -17  | -29  | 25   |
| C(98)  | 34   | 41   | 67   | -9   | -3   | -12  |
| F(107) | 44   | 48   | 56   | 3    | 7    | -8   |
| F(108) | 47   | 55   | 102  | -20  | 17   | -24  |
| F(109) | 27   | 57   | 73   | -14  | 2    | -6   |
| C(99)  | 22   | 24   | 24   | 3    | -1   | 1    |
| C(100) | 23   | 28   | 22   | -1   | 1    | -3   |
| C(101) | 28   | 34   | 32   | -7   | 1    | -5   |
| C(102) | 29   | 37   | 33   | -3   | 4    | -6   |
| C(103) | 32   | 42   | 26   | -3   | 7    | -5   |
| C(104) | 34   | 32   | 24   | -4   | 1    | -1   |
| C(105) | 22   | 27   | 23   | 0    | 3    | 1    |
| C(106) | 22   | 22   | 19   | 2    | 1    | -1   |
| C(107) | 44   | 86   | 52   | -25  | 23   | -29  |
| C(109) | 39   | 106  | 67   | -30  | 8    | -16  |
| F(87)  | 49   | 142  | 85   | -21  | 9    | 15   |
| F(88)  | 37   | 164  | 61   | -20  | -1   | -14  |
| F(89)  | 46   | 208  | 106  | -49  | 27   | -69  |
| C(110) | 34   | 60   | 53   | -16  | 18   | -14  |
| C(111) | 45   | 65   | 56   | -23  | 12   | 8    |
| F(91)  | 55   | 67   | 89   | -39  | 26   | -18  |
| F(92)  | 52   | 77   | 162  | -59  | 35   | -7   |
| F(93)  | 58   | 45   | 104  | -4   | -1   | 6    |
| C(112) | 75   | 84   | 42   | -10  | 12   | -28  |

**Table B.12** Anisotropic Displacement Parameters ($\text{Å}^2$ x $10^3$) for $(F_{64}Pc)_2Tb(1/2$ Acetone)(1/8 Chloroform). The Anisotropic Displacement Factor Exponent Takes the Form: $-2\pi^2[\,h^2a^{*2}U^{11} + ... + 2\,h\,k\,a^*\,b^*\,U^{12}]$, Continued

|        | $U^{11}$ | $U^{22}$ | $U^{33}$ | $U^{23}$ | $U^{13}$ | $U^{12}$ |
|--------|------|------|------|------|------|------|
| F(94)  | 106 | 156 | 51  | -45 | 38  | -53 |
| F(95)  | 71  | 105 | 42  | 7   | -2  | -32 |
| F(96)  | 108 | 99  | 57  | 14  | 4   | -46 |
| F(1)   | 35  | 38  | 42  | -11 | 9   | -2  |
| F(2)   | 36  | 30  | 47  | -10 | -10 | -3  |
| F(3)   | 68  | 42  | 30  | -8  | 8   | -3  |
| F(10)  | 60  | 27  | 34  | -8  | 2   | -2  |
| F(17)  | 35  | 38  | 47  | -9  | -15 | -2  |
| F(18)  | 31  | 55  | 45  | -15 | 4   | 13  |
| F(19)  | 20  | 53  | 54  | -5  | -9  | 8   |
| F(19') | 27  | 43  | 69  | -20 | 2   | 4   |
| F(29)  | 46  | 96  | 116 | 9   | 1   | -6  |
| F(33)  | 28  | 68  | 36  | -9  | 6   | 13  |
| F(34)  | 31  | 42  | 27  | -6  | 0   | 0   |
| F(35)  | 55  | 50  | 29  | -14 | 4   | 17  |
| F(42)  | 68  | 67  | 23  | 4   | 12  | 27  |
| F(49)  | 28  | 157 | 39  | 15  | 9   | 19  |
| F(50)  | 30  | 32  | 122 | 3   | -28 | -3  |
| F(51)  | 24  | 94  | 117 | 61  | -18 | -16 |
| F(61)  | 31  | 320 | 139 | 166 | -22 | -56 |
| F(65)  | 23  | 40  | 40  | -10 | -5  | 2   |
| F(66)  | 30  | 39  | 25  | -9  | 2   | 1   |
| F(73)  | 47  | 36  | 22  | 3   | -10 | -2  |
| F(80)  | 44  | 40  | 32  | -8  | -9  | -8  |
| F(81)  | 33  | 51  | 41  | -16 | 8   | -19 |
| F(82)  | 33  | 42  | 31  | -16 | 8   | -9  |
| F(83)  | 65  | 91  | 53  | -17 | 28  | -31 |
| F(90)  | 40  | 89  | 78  | -38 | 26  | -16 |
| F(97)  | 28  | 28  | 29  | -7  | 0   | 4   |
| F(98)  | 20  | 34  | 44  | -4  | -2  | -4  |
| F(99)  | 41  | 34  | 33  | -10 | -14 | -2  |
| F(106) | 38  | 36  | 61  | -17 | -5  | -9  |
| F(113) | 19  | 35  | 36  | -8  | -2  | 0   |
| F(114) | 31  | 35  | 41  | -16 | -6  | 2   |
| F(115) | 36  | 52  | 85  | -28 | -16 | 19  |
| F(122) | 28  | 60  | 65  | -18 | 14  | 6   |

**Table B.13** Hydrogen Coordinates ( x10$^4$) and Isotropic Displacement Parameters (Å$^2$x 10$^3$) for (F$_{64}$Pc)$_2$Tb(½ Acetone)(1/8 Chloroform)

|        | x    | y    | z    | U(eq) |
|--------|------|------|------|-------|
| H(1A1) | 1756 | 1828 | 9129 | 113   |
| H(1A2) | 1641 | 2562 | 9227 | 113   |
| H(1A3) | 1592 | 2336 | 8808 | 113   |
| H(2A1) | 243  | 2661 | 8752 | 210   |
| H(2A2) | 530  | 2986 | 9128 | 210   |
| H(2A3) | -37  | 2466 | 9128 | 210   |
| H(1C)  | 8398 | 2301 | 9394 | 13    |

**Table B.14** Experimental Parameters and Structure Refinement for (F$_{64}$Pc)$_2$Tb

| | |
|---|---|
| Empirical formula | C112 F128 N16 Tb |
| Formula weight | 4160.20 |
| Temperature | 100(2) K |
| Wavelength | 1.54178 Å |
| Crystal system | Tetragonal |
| Space group | P4/ncc |
| Unit cell dimensions | a = 27.5107(4) Å |
| α= 90°. | |
| | b = 27.5107(4) Å |
| β= 90°. | |
| | c = 23.6687(9) Å |
| γ = 90°. | |
| Volume | 17913.4(8) Å$^3$ |
| Z | 4 |
| Density (calculated) | 1.543 g/cm$^3$ |
| Absorption coefficient | 3.601 mm$^{-1}$ |
| F(000) | 8004 |
| Crystal size | 0.20 x 0.20 x 0.15 mm$^3$ |
| Theta range for data collection | 2.27 to 71.07°. |
| Index ranges | -32<=h<=31, -32<=k<=29, -27<=l<=27 |
| Reflections collected | 157022 |
| Independent reflections | 8298 [R(int) = 0.1111] |
| Completeness to theta = 71.07° | 95.5 % |
| Refinement method | Full-matrix least-squares on F$^2$ |
| Data / restraints / parameters | 8298 / 457 / 617 |
| Goodness-of-fit on F$^2$ | 1.085 |
| Final R indices [I>2sigma(I)] | R1 = 0.1064, wR2 = 0.2952 |
| R indices (all data) | R1 = 0.1606, wR2 = 0.3301 |
| Largest diff. peak and hole | 1.901 and -3.813 e.Å$^{-3}$ |

**Table B.15** Atomic Coordinates (x $10^4$) and Equivalent Isotropic Displacement Parameters ($\mathring{A}^2$ x $10^3$) for ($F_{64}Pc)_2$Tb.  U(eq) is Defined as One Third of the Trace of the Orthogonalized $U^{ij}$ Tensor

| | x | y | z | U(eq) |
|---|---|---|---|---|
| Tb | 2500 | 2500 | 2020(1) | 67(1) |
| N(1) | 3098(2) | 2096(2) | 1431(3) | 79(2) |
| N(2) | 3222(2) | 2478(2) | 2613(3) | 78(2) |
| N(3) | 3388(2) | 3334(2) | 2713(3) | 88(2) |
| N(4) | 3694(2) | 2749(2) | 1308(3) | 81(2) |
| C(1) | 3486(3) | 2070(3) | 2697(4) | 84(2) |
| C(2) | 3994(3) | 2200(3) | 2820(4) | 90(2) |
| C(3) | 4402(3) | 1939(3) | 2965(4) | 103(3) |
| C(4) | 4847(3) | 2162(3) | 3075(4) | 92(2) |
| C(5) | 4883(3) | 2675(4) | 2997(4) | 99(3) |
| C(6) | 4444(3) | 2924(3) | 2861(4) | 94(2) |
| C(7) | 4011(3) | 2700(3) | 2786(4) | 86(2) |
| C(8) | 3518(3) | 2870(3) | 2697(3) | 81(2) |
| C(9) | 5237(3) | 1818(4) | 3312(4) | 116(3) |
| C(10) | 5542(2) | 1486(2) | 2899(3) | 126(6) |
| F(4) | 5805(3) | 1177(3) | 3197(3) | 193(7) |
| F(5) | 5832(3) | 1760(3) | 2589(3) | 151(4) |
| F(6) | 5244(3) | 1242(3) | 2566(4) | 142(4) |
| C(10') | 5235(6) | 1351(5) | 2916(8) | 140(20) |
| F(4') | 4997(10) | 976(7) | 3185(10) | 158(16) |
| F(5') | 5706(9) | 1214(7) | 2801(12) | 200(20) |
| F(6') | 4999(9) | 1459(6) | 2418(10) | 152(12) |
| C(11) | 5050(3) | 1463(3) | 3814(4) | 130(6) |
| F(7) | 5398(4) | 1418(5) | 4203(5) | 235(9) |
| F(8) | 4945(4) | 1027(4) | 3600(5) | 196(7) |
| F(9) | 4653(4) | 1651(4) | 4051(4) | 164(5) |
| C(11') | 5252(10) | 1718(7) | 3961(7) | 190(40) |
| F(9') | 4855(14) | 1557(12) | 4116(6) | 210(30) |
| F(8') | 5339(12) | 2100(11) | 4214(7) | 220(20) |
| F(7') | 5573(14) | 1418(10) | 4065(7) | 220(20) |
| C(12) | 5358(3) | 2976(4) | 2977(4) | 116(4) |
| C(13) | 5440(2) | 3267(2) | 3527(3) | 291(16) |
| F(14) | 5046(3) | 3535(2) | 3638(3) | 187(4) |
| F(15) | 5824(3) | 3558(3) | 3465(3) | 224(4) |
| F(16) | 5519(3) | 2960(3) | 3954(3) | 236(5) |
| C(14) | 5423(3) | 3358(4) | 2526(5) | 450(50) |
| F(12) | 5250(4) | 3816(5) | 2730(6) | 326(18) |
| F(11) | 5154(6) | 3222(5) | 2032(6) | 130(6) |
| F(13) | 5929(7) | 3399(5) | 2386(7) | 202(12) |
| C(14') | 5427(6) | 3251(5) | 2409(5) | 67(8) |
| F(11') | 5850(9) | 3240(8) | 2274(8) | 139(9) |
| F(12') | 5299(9) | 3669(10) | 2465(6) | 187(12) |
| F(13') | 5184(11) | 3059(7) | 2047(9) | 179(16) |
| C(15) | 3553(3) | 2285(3) | 1338(3) | 80(2) |
| C(16) | 3383(3) | 3116(3) | 1356(3) | 80(2) |
| C(17) | 3536(3) | 3620(3) | 1253(4) | 83(2) |

**Table B.15** Atomic Coordinates (x $10^4$) and Equivalent Isotropic Displacement Parameters ($\mathring{A}^2$ x $10^3$) for $(F_{64}Pc)_2Tb$. U(eq) is Defined as One Third of the Trace of the Orthogonalized $U^{ij}$ Tensor, Continued

|       | x        | y         | z         | U(eq)   |
|-------|----------|-----------|-----------|---------|
| C(18) | 3117(3)  | 3892(3)   | 1223(4)   | 91(2)   |
| C(19) | 3137(3)  | 4369(3)   | 1068(4)   | 91(2)   |
| C(20) | 3570(3)  | 4614(3)   | 980(4)    | 99(3)   |
| C(21) | 4016(3)  | 4339(3)   | 1021(4)   | 104(3)  |
| C(22) | 3975(3)  | 3844(3)   | 1145(4)   | 95(3)   |
| C(23) | 3524(4)  | 5176(4)   | 852(5)    | 151(5)  |
| C(24) | 3440(2)  | 5253(2)   | 225(3)    | 350(20) |
| F(20) | 3833(3)  | 5092(3)   | -68(3)    | 231(5)  |
| F(21) | 3373(4)  | 5734(3)   | 122(3)    | 329(8)  |
| F(22) | 3039(3)  | 5002(3)   | 60(3)     | 193(4)  |
| C(25) | 3140(2)  | 5468(2)   | 1192(3)   | 155(6)  |
| F(23) | 3299(2)  | 5907(2)   | 1277(4)   | 255(6)  |
| F(24) | 3065(2)  | 5257(2)   | 1675(3)   | 201(4)  |
| F(25) | 2736(2)  | 5486(2)   | 909(3)    | 233(5)  |
| C(26) | 4547(4)  | 4512(3)   | 919(4)    | 136(4)  |
| C(27) | 4904(2)  | 4181(2)   | 590(3)    | 440(30) |
| F(27) | 5209(2)  | 4456(2)   | 291(4)    | 225(4)  |
| F(28) | 4655(2)  | 3893(2)   | 241(3)    | 177(3)  |
| F(29) | 5155(2)  | 3909(3)   | 953(3)    | 280(8)  |
| C(28) | 4788(2)  | 4665(2)   | 1499(3)   | 206(9)  |
| F(30) | 5236(3)  | 4791(2)   | 1412(3)   | 226(5)  |
| F(31) | 4775(3)  | 4302(2)   | 1846(3)   | 200(4)  |
| F(32) | 4551(3)  | 5028(3)   | 1712(3)   | 251(6)  |
| F(1)  | 4361(2)  | 1459(2)   | 3024(3)   | 129(2)  |
| F(2)  | 4472(2)  | 3410(2)   | 2805(2)   | 109(2)  |
| F(3)  | 5582(3)  | 2081(3)   | 3616(6)   | 162(5)  |
| F(3') | 5673(7)  | 1975(10)  | 3042(11)  | 118(9)  |
| F(10) | 5757(2)  | 2670(3)   | 2916(4)   | 189(4)  |
| F(17) | 4373(2)  | 3575(2)   | 1214(3)   | 114(2)  |
| F(18) | 2720(2)  | 4617(2)   | 1022(2)   | 112(2)  |
| F(19) | 3937(3)  | 5420(2)   | 1055(5)   | 203(4)  |
| F(26) | 4544(3)  | 4931(3)   | 635(4)    | 184(3)  |

**Table B.16**  Bond Lengths [Å] and Angles [°] for (F$_{64}$Pc)$_2$Tb

| | | | |
|---|---|---|---|
| Tb-N(1)#1 | 2.426(6) | Tb-N(2)#1 | 2.433(6) |
| Tb-N(1) | 2.426(6) | Tb-N(2)#2 | 2.434(6) |
| Tb-N(1)#2 | 2.426(6) | Tb-N(2) | 2.434(6) |
| Tb-N(1)#3 | 2.426(6) | Tb-N(2)#3 | 2.434(6) |
| | | | |
| N(1)-C(16)#1 | 1.331(9) | C(9)-C(10) | 1.580(10) |
| N(1)-C(15) | 1.373(9) | C(9)-C(11) | 1.621(10) |
| N(2)-C(1) | 1.351(8) | C(12)-C(14) | 1.511(12) |
| N(2)-C(8) | 1.367(9) | C(12)-C(14') | 1.556(12) |
| N(3)-C(8) | 1.324(9) | C(12)-C(13) | 1.544(10) |
| N(3)-C(1)#3 | 1.329(9) | C(15)-C(18)#1 | 1.473(10) |
| N(4)-C(16) | 1.329(9) | C(16)-N(1)#3 | 1.331(9) |
| N(4)-C(15) | 1.337(10) | C(16)-C(17) | 1.471(10) |
| C(1)-N(3)#1 | 1.329(9) | C(17)-C(22) | 1.379(11) |
| C(1)-C(2) | 1.470(11) | C(17)-C(18) | 1.375(9) |
| C(2)-C(7) | 1.380(12) | C(18)-C(19) | 1.364(9) |
| C(2)-C(3) | 1.377(11) | C(18)-C(15)#3 | 1.474(10) |
| C(3)-C(4) | 1.392(12) | C(19)-C(20) | 1.384(10) |
| C(4)-C(5) | 1.428(14) | C(20)-C(21) | 1.446(12) |
| C(4)-C(9) | 1.537(12) | C(20)-C(23) | 1.580(13) |
| C(5)-C(6) | 1.425(12) | C(21)-C(22) | 1.398(12) |
| C(5)-C(12) | 1.547(13) | C(21)-C(26) | 1.554(13) |
| C(6)-C(7) | 1.353(11) | C(23)-C(24) | 1.515(11) |
| C(7)-C(8) | 1.449(11) | C(23)-C(25) | 1.552(11) |
| C(9)-C(11') | 1.560(16) | C(26)-C(27) | 1.549(10) |
| C(9)-C(10') | 1.591(15) | C(26)-C(28) | 1.582(11) |
| | | | |
| N(1)#1-Tb-N(1) | 70.70(15) | N(1)#3-Tb-N(2)#3 | 76.5(2) |
| N(1)#1-Tb-N(1)#2 | 70.70(15) | N(2)#1-Tb-N(2)#3 | 109.6(3) |
| N(1)-Tb-N(1)#2 | 109.8(3) | N(2)#2-Tb-N(2)#3 | 70.58(16) |
| N(1)#1-Tb-N(1)#3 | 109.8(3) | N(2)-Tb-N(2)#3 | 70.58(16) |
| N(1)-Tb-N(1)#3 | 70.70(15) | C(16)#1-N(1)-C(15) | 108.6(6) |
| N(1)#2-Tb-N(1)#3 | 70.70(15) | C(16)#1-N(1)-Tb | 123.7(5) |
| N(1)#1-Tb-N(2)#1 | 76.5(2) | C(15)-N(1)-Tb | 122.5(5) |
| N(1)-Tb-N(2)#1 | 88.5(2) | C(1)-N(2)-C(8) | 108.4(7) |
| N(1)#2-Tb-N(2)#1 | 133.52(19) | C(1)-N(2)-Tb | 123.0(5) |
| N(1)#3-Tb-N(2)#1 | 153.72(18) | C(8)-N(2)-Tb | 123.4(5) |
| N(1)#1-Tb-N(2)#2 | 88.5(2) | C(8)-N(3)-C(1)#3 | 124.1(7) |
| N(1)-Tb-N(2)#2 | 153.73(18) | C(16)-N(4)-C(15) | 122.2(6) |
| N(1)#2-Tb-N(2)#2 | 76.5(2) | N(3)#1-C(1)-N(2) | 128.4(7) |
| N(1)#3-Tb-N(2)#2 | 133.51(19) | N(3)#1-C(1)-C(2) | 121.6(7) |
| N(2)#1-Tb-N(2)#2 | 70.58(16) | N(2)-C(1)-C(2) | 109.8(7) |
| N(1)#1-Tb-N(2) | 133.51(19) | C(7)-C(2)-C(3) | 120.5(7) |
| N(1)-Tb-N(2) | 76.5(2) | C(7)-C(2)-C(1) | 105.2(6) |
| N(1)#2-Tb-N(2) | 153.72(18) | C(3)-C(2)-C(1) | 134.3(8) |
| N(1)#3-Tb-N(2) | 88.5(2) | C(4)-C(3)-C(2) | 122.2(8) |
| N(2)#1-Tb-N(2) | 70.58(16) | C(3)-C(4)-C(5) | 118.2(7) |
| N(2)#2-Tb-N(2) | 109.6(3) | C(3)-C(4)-C(9) | 114.2(8) |
| N(1)#1-Tb-N(2)#3 | 153.72(18) | C(5)-C(4)-C(9) | 127.4(8) |
| N(1)-Tb-N(2)#3 | 133.51(19) | C(6)-C(5)-C(4) | 116.5(8) |
| N(1)#2-Tb-N(2)#3 | 88.5(2) | C(6)-C(5)-C(12) | 116.9(8) |
| C(4)-C(5)-C(12) | 126.2(8) | N(4)-C(15)-C(18)#1 | 121.5(6) |
| C(7)-C(6)-C(5) | 123.8(8) | N(1)-C(15)-C(18)#1 | 108.9(7) |

**Table B.16** Bond Lengths [Å] and Angles [°] for $(F_{64}Pc)_2Tb$, Continued

| | | | |
|---|---|---|---|
| C(6)-C(7)-C(2) | 118.5(7) | N(4)-C(16)-N(1)#3 | 128.5(7) |
| C(6)-C(7)-C(8) | 134.0(8) | N(4)-C(16)-C(17) | 121.2(6) |
| C(2)-C(7)-C(8) | 107.5(6) | N(1)#3-C(16)-C(17) | 109.9(7) |
| N(3)-C(8)-N(2) | 127.1(7) | C(22)-C(17)-C(18) | 118.8(7) |
| N(3)-C(8)-C(7) | 124.1(7) | C(22)-C(17)-C(16) | 134.6(7) |
| N(2)-C(8)-C(7) | 108.8(6) | C(18)-C(17)-C(16) | 106.4(7) |
| C(11')-C(9)-C(10') | 116.0(12) | C(19)-C(18)-C(17) | 120.4(7) |
| C(11')-C(9)-C(4) | 119.2(10) | C(19)-C(18)-C(15)#3 | 133.5(7) |
| C(10')-C(9)-C(4) | 106.1(9) | C(17)-C(18)-C(15)#3 | 105.9(6) |
| C(11')-C(9)-C(10) | 119.5(10) | C(18)-C(19)-C(20) | 122.8(8) |
| C(10')-C(9)-C(10) | 33.9(8) | C(19)-C(20)-C(21) | 117.8(7) |
| C(4)-C(9)-C(10) | 120.0(7) | C(19)-C(20)-C(23) | 115.8(8) |
| C(11')-C(9)-C(11) | 35.1(11) | C(21)-C(20)-C(23) | 126.4(7) |
| C(10')-C(9)-C(11) | 86.8(9) | C(22)-C(21)-C(20) | 117.1(7) |
| C(4)-C(9)-C(11) | 114.7(6) | C(22)-C(21)-C(26) | 114.0(8) |
| C(10)-C(9)-C(11) | 105.8(7) | C(20)-C(21)-C(26) | 128.8(8) |
| C(14)-C(12)-C(14') | 15.0(8) | C(17)-C(22)-C(21) | 122.9(7) |
| C(14)-C(12)-C(13) | 102.6(8) | C(24)-C(23)-C(20) | 109.8(8) |
| C(14')-C(12)-C(13) | 117.3(9) | C(24)-C(23)-C(25) | 109.4(8) |
| C(14)-C(12)-C(5) | 119.6(7) | C(20)-C(23)-C(25) | 117.5(7) |
| C(14')-C(12)-C(5) | 112.9(8) | C(27)-C(26)-C(21) | 119.6(7) |
| C(13)-C(12)-C(5) | 112.0(7) | C(27)-C(26)-C(28) | 109.1(8) |
| N(4)-C(15)-N(1) | 129.4(6) | C(21)-C(26)-C(28) | 109.9(7) |

Symmetry transformations used to generate equivalent atoms:
#1 y,-x+1/2,z   #2 -x+1/2,-y+1/2,z   #3 -y+1/2,x,z

**Table B.17**   Anisotropic Displacement Parameters ($\text{Å}^2$ x $10^3$) for $(F_{64}Pc)_2Tb$.
The Anisotropic Displacement Factor Exponent Takes the Form:  $-2\pi^2[\,h^2a^{*2}U^{11} + ... + 2\,h\,k\,a^*\,b^*\,U^{12}]$

| | $U^{11}$ | $U^{22}$ | $U^{33}$ | $U^{23}$ | $U^{13}$ | $U^{12}$ |
|---|---|---|---|---|---|---|
| Tb | 48(1) | 48(1) | 105(1) | 0 | 0 | 0 |
| N(1) | 59(3) | 61(3) | 115(5) | 4(3) | 3(3) | -5(3) |
| N(2) | 62(3) | 65(4) | 108(5) | 15(3) | -6(3) | 0(3) |
| N(3) | 67(4) | 71(4) | 125(5) | 5(3) | -16(3) | -5(3) |
| N(4) | 61(3) | 53(3) | 128(5) | 9(3) | 22(3) | -1(3) |
| C(1) | 75(5) | 72(5) | 105(6) | 9(4) | -7(4) | 11(4) |
| C(2) | 76(5) | 70(5) | 125(7) | 12(4) | -14(4) | -7(4) |
| C(3) | 80(6) | 71(5) | 158(9) | 33(5) | -27(5) | 7(4) |
| C(4) | 58(5) | 104(6) | 114(6) | 11(5) | -8(4) | 12(4) |
| C(5) | 86(6) | 96(6) | 116(7) | 5(5) | -24(5) | 1(5) |
| C(6) | 80(6) | 76(6) | 127(7) | 3(4) | -21(5) | -9(4) |
| C(7) | 76(5) | 68(4) | 113(6) | 2(4) | -11(4) | -2(4) |
| C(8) | 66(4) | 73(5) | 104(6) | 7(4) | -12(4) | -7(4) |
| C(9) | 77(6) | 116(8) | 156(9) | 39(7) | 12(6) | 22(5) |
| C(10) | 92(11) | 118(13) | 168(15) | -32(11) | -48(11) | 37(10) |
| F(4) | 95(6) | 168(10) | 317(18) | 89(10) | 16(9) | 57(6) |
| F(5) | 93(5) | 150(8) | 209(10) | 39(7) | 20(6) | -12(5) |
| F(6) | 119(8) | 109(8) | 199(10) | -9(7) | 26(7) | 14(6) |
| C(10') | 60(20) | 28(17) | 320(70) | 90(30) | -20(30) | 4(15) |
| F(4') | 140(20) | 100(20) | 230(40) | -10(20) | -80(30) | 69(18) |
| F(5') | 210(40) | 90(20) | 300(50) | 30(30) | 190(40) | 60(20) |
| F(6') | 109(19) | 99(18) | 250(30) | -17(18) | 8(19) | 64(15) |
| C(11) | 123(13) | 109(13) | 158(17) | 29(11) | -48(12) | 26(10) |
| F(7) | 202(13) | 230(17) | 274(18) | 130(15) | -116(12) | 8(11) |
| F(8) | 120(7) | 134(9) | 330(20) | 123(11) | -72(10) | -12(7) |
| F(9) | 113(7) | 209(12) | 169(9) | 83(8) | 14(6) | -6(7) |
| C(11') | 240(70) | 190(60) | 140(50) | -140(50) | -90(50) | 50(50) |
| F(9') | 190(40) | 240(40) | 220(40) | -100(30) | -50(30) | 130(40) |
| F(8') | 190(30) | 350(50) | 130(20) | -130(30) | -70(20) | 70(30) |
| F(7') | 320(50) | 80(20) | 250(40) | 0(20) | -150(40) | 90(30) |
| C(12) | 58(5) | 103(7) | 187(11) | 20(6) | -51(6) | 6(5) |
| C(13) | 190(20) | 500(40) | 187(18) | 40(20) | -38(16) | -220(30) |
| F(14) | 180(7) | 141(6) | 240(9) | -70(6) | -114(7) | 30(5) |
| F(15) | 181(7) | 202(8) | 289(11) | 37(7) | -124(7) | -91(6) |
| F(16) | 187(9) | 249(11) | 272(13) | 20(9) | -75(8) | 16(8) |
| C(14) | 200(40) | 750(90) | 400(70) | 240(60) | -210(40) | -330(50) |
| F(12) | 101(9) | 94(9) | 780(50) | 175(17) | -164(18) | -47(7) |
| F(11) | 126(10) | 112(11) | 152(12) | 56(8) | 9(8) | 28(8) |
| F(13) | 93(11) | 103(12) | 410(30) | 89(15) | 52(14) | -13(8) |
| C(14') | 76(17) | 47(11) | 79(15) | -16(10) | 26(11) | -34(10) |
| F(11') | 60(11) | 81(13) | 280(20) | 32(11) | -15(12) | -14(9) |
| F(12') | 240(30) | 210(30) | 113(15) | 21(15) | 50(15) | 30(20) |
| F(13') | 170(20) | 90(14) | 280(30) | 89(17) | 50(20) | 46(15) |
| C(15) | 66(5) | 78(5) | 96(5) | -6(4) | 9(4) | 8(4) |
| C(16) | 55(4) | 70(5) | 115(6) | 7(4) | 5(4) | -8(3) |
| C(17) | 75(5) | 57(4) | 117(6) | 9(4) | 2(4) | -5(3) |
| C(18) | 81(5) | 58(4) | 133(7) | 24(4) | 7(5) | 1(3) |
| C(19) | 81(5) | 75(5) | 116(6) | 23(4) | -7(4) | -8(4) |

**Table B.17**   Anisotropic Displacement Parameters ($\text{Å}^2$ x $10^3$) for (F$_{64}$Pc)$_2$Tb.
The Anisotropic Displacement Factor Exponent Takes the    Form:  $-2\pi^2[\ h^2a^{*2}U^{11} + ...$
$+ 2\ h\ k\ a^*\ b^*\ U^{12}]$, Continued

|        | $U^{11}$ | $U^{22}$ | $U^{33}$ | $U^{23}$ | $U^{13}$ | $U^{12}$ |
|--------|----------|----------|----------|----------|----------|----------|
| C(20)  | 94(6)    | 75(5)    | 129(7)   | 19(5)    | 0(5)     | -27(4)   |
| C(21)  | 76(6)    | 92(6)    | 144(8)   | 23(5)    | 2(5)     | -22(4)   |
| C(22)  | 70(5)    | 71(5)    | 143(7)   | 37(5)    | 7(5)     | -4(4)    |
| C(23)  | 104(8)   | 107(8)   | 241(15)  | 68(9)    | -25(9)   | -26(6)   |
| C(24)  | 810(70)  | 96(12)   | 144(15)  | 4(10)    | -10(30)  | -30(20)  |
| F(20)  | 210(9)   | 169(8)   | 313(14)  | 95(9)    | -7(9)    | -73(7)   |
| F(21)  | 321(13)  | 190(9)   | 480(20)  | 230(12)  | 29(13)   | 2(9)     |
| F(22)  | 164(6)   | 229(9)   | 185(8)   | 81(7)    | -34(5)   | 18(6)    |
| C(25)  | 197(14)  | 52(5)    | 216(15)  | 30(7)    | -76(13)  | 12(7)    |
| F(23)  | 177(7)   | 117(6)   | 471(19)  | -66(8)   | -58(9)   | -14(5)   |
| F(24)  | 142(6)   | 204(9)   | 256(11)  | -86(8)   | -44(7)   | 12(6)    |
| F(25)  | 140(6)   | 122(6)   | 436(17)  | 110(8)   | -24(9)   | 5(5)     |
| C(26)  | 140(9)   | 71(6)    | 198(12)  | 36(6)    | 20(8)    | -34(6)   |
| C(27)  | 330(30)  | 340(30)  | 660(50)  | -300(40) | 380(40)  | -280(30) |
| F(27)  | 153(7)   | 184(7)   | 339(11)  | 65(8)    | 113(7)   | -30(6)   |
| F(28)  | 169(7)   | 140(6)   | 221(7)   | 17(5)    | 83(6)    | -14(5)   |
| F(29)  | 106(6)   | 167(8)   | 570(20)  | 117(12)  | 50(9)    | -28(5)   |
| C(28)  | 98(11)   | 270(30)  | 250(20)  | 48(19)   | -31(11)  | -58(14)  |
| F(30)  | 138(6)   | 125(6)   | 416(16)  | 51(7)    | -55(8)   | -26(5)   |
| F(31)  | 224(10)  | 125(6)   | 252(9)   | 50(6)    | -94(8)   | -50(6)   |
| F(32)  | 185(10)  | 203(10)  | 367(15)  | -38(10)  | -51(10)  | -78(8)   |
| F(1)   | 73(3)    | 92(4)    | 223(6)   | 55(3)    | -22(3)   | 3(2)     |
| F(2)   | 76(3)    | 82(3)    | 169(5)   | -1(3)    | -31(3)   | -8(2)    |
| F(3)   | 81(5)    | 139(7)   | 266(15)  | 56(8)    | -70(7)   | -5(4)    |
| F(10)  | 87(5)    | 160(6)   | 319(12)  | 67(7)    | -34(5)   | -17(4)   |
| F(17)  | 67(3)    | 77(3)    | 196(5)   | 31(3)    | 27(3)    | -11(2)   |
| F(18)  | 101(3)   | 61(3)    | 175(5)   | 33(3)    | -29(3)   | -3(2)    |
| F(19)  | 169(6)   | 104(5)   | 337(11)  | 76(6)    | -36(7)   | -51(4)   |
| F(26)  | 120(5)   | 114(5)   | 319(10)  | 84(6)    | 2(5)     | -44(4)   |

**Table B.18** Experimental Parameters and Structure Refinement for
(F$_{64}$Pc)$_2$Dy

| | |
|---|---|
| Identification code | 062708a |
| Empirical formula | C112 Dy F128 N16 |
| Formula weight | 4163.78 |
| Temperature | 100(2) K |
| Wavelength | 1.54178 Å |
| Crystal system | Tetragonal |
| Space group | P4/ncc |
| Unit cell dimensions | a = 27.1967(12) Å |
| α= 90°. | |
| | b = 27.1967(12) Å |
| β= 90°. | |
| | c = 23.553(2) Å |
| γ = 90°. | |
| Volume | 17422(2) Å$^3$ |
| Z | 4 |
| Density (calculated) | 1.587 g/cm$^3$ |
| Absorption coefficient | 4.001 mm$^{-1}$ |
| F(000) | 8008 |
| Crystal size | 0.12 x 0.13 x 0.16 mm$^3$ |
| Theta range for data collection | 4.60 to 54.96°. |
| Index ranges | -28<=h<=28, -28<=k<=28, -24<=l<=24 |
| Reflections collected | 98381 |
| Independent reflections | 5468 [R(int) = 0.1003] |
| Completeness to theta = 54.96° | 99.7 % |
| Refinement method | Full-matrix least-squares on F$^2$ |
| Data / restraints / parameters | 5468 / 0 / 501 |
| Goodness-of-fit on F$^2$ | 1.311 |
| Final R indices [I>2sigma(I)] | R1 = 0.0982, wR2 = 0.2855 |
| R indices (all data) | R1 = 0.1080, wR2 = 0.2971 |
| Extinction coefficient | 0.00000(2) |
| Largest diff. peak and hole | 3.152 and -6.000 e.Å$^{-3}$ |

**Table B.19** Atomic Coordinates (x $10^4$) and Equivalent Isotropic
Displacement Parameters ($Å^2$ x $10^3$) for $(F_{64}Pc)_2Dy$. U(eq) is Defined as One
Third of the Trace of the Orthogonalized $U^{ij}$ Tensor

|        | x       | y       | z       | U(eq)  |
|--------|---------|---------|---------|--------|
| Dy     | 2500    | 2500    | 2009(1) | 32(1)  |
| N(1)   | 2483(2) | 3224(2) | 2606(3) | 34(2)  |
| N(2)   | 3343(2) | 3404(2) | 2693(3) | 39(2)  |
| N(3)   | 3110(2) | 2893(2) | 1417(3) | 46(2)  |
| N(4)   | 2766(2) | 3700(2) | 1313(2) | 42(2)  |
| C(1)   | 3573(3) | 2695(3) | 1321(3) | 43(2)  |
| C(2)   | 3915(2) | 3098(1) | 1204(2) | 49(2)  |
| C(3)   | 4412(2) | 3112(1) | 1066(2) | 49(2)  |
| C(4)   | 4644(1) | 3561(2) | 978(2)  | 60(2)  |
| C(5)   | 4380(2) | 3996(1) | 1030(3) | 57(2)  |
| C(6)   | 3883(2) | 3982(1) | 1168(3) | 52(2)  |
| C(7)   | 3651(1) | 3533(2) | 1255(2) | 49(2)  |
| C(8)   | 2878(2) | 3531(3) | 2677(3) | 35(2)  |
| C(9)   | 2708(1) | 4039(1) | 2756(2) | 41(2)  |
| C(10)  | 2200(1) | 4009(1) | 2804(2) | 40(2)  |
| C(11)  | 2065(3) | 3500(2) | 2683(3) | 39(2)  |

**Table B.19** Atomic Coordinates (x $10^4$) and Equivalent Isotropic
Displacement Parameters (Å$^2$ x $10^3$) for (F$_{64}$Pc)$_2$Dy. U(eq) is Defined as One
Third of the Trace of the Orthogonalized U$^{ij}$ Tensor, Continued

|  | x | y | z | U(eq) |
|---|---|---|---|---|
| C(12) | 1929(1) | 4423(2) | 2951(2) | 46(2) |
| C(13) | 2166(2) | 4868(1) | 3049(2) | 46(2) |
| C(14) | 2675(2) | 4898(1) | 3001(2) | 45(2) |
| C(15) | 2946(1) | 4484(2) | 2854(2) | 45(2) |
| C(16) | 5213(4) | 3502(4) | 848(5) | 82(3) |
| C(17) | 5306(2) | 3398(2) | 214(2) | 125(5) |
| F(9) | 5066(2) | 2999(2) | 62(2) | 108(2) |
| F(10) | 5780(2) | 3331(2) | 130(2) | 133(3) |
| F(11) | 5153(2) | 3773(2) | -91(2) | 125(3) |
| C(18) | 5504(1) | 3075(1) | 1235(2) | 74(3) |
| F(6) | 5265(2) | 3005(2) | 1716(2) | 97(2) |
| F(7) | 5955(2) | 3224(2) | 1346(2) | 115(2) |
| F(8) | 5521(2) | 2658(2) | 949(2) | 107(2) |
| C(19) | 4574(4) | 4530(4) | 919(6) | 85(4) |
| C(20) | 4742(2) | 4770(1) | 1541(2) | 100(5) |
| F(16) | 4881(2) | 5220(2) | 1467(2) | 154(4) |
| F(17) | 5101(2) | 4516(2) | 1751(2) | 110(2) |
| F(18) | 4372(2) | 4759(2) | 1888(2) | 118(3) |
| C(21) | 4233(2) | 4900(2) | 596(3) | 144(7) |
| F(13) | 3931(2) | 4651(2) | 251(3) | 124(3) |
| F(14) | 4509(2) | 5209(2) | 290(3) | 178(5) |
| F(15) | 3967(2) | 5156(2) | 973(3) | 142(4) |
| C(22) | 3128(3) | 3396(3) | 1346(3) | 46(2) |
| C(23) | 2982(3) | 5390(3) | 2949(3) | 51(2) |
| C(24) | 1812(3) | 5259(3) | 3339(4) | 58(2) |
| C(25) | 3297(1) | 5496(1) | 3497(1) | 76(3) |
| F(20) | 3003(2) | 5568(2) | 3930(2) | 89(2) |
| F(21) | 3566(2) | 5889(2) | 3415(2) | 95(2) |
| F(22) | 3583(2) | 5119(2) | 3601(2) | 82(2) |
| C(26) | 3310(1) | 5447(1) | 2385(1) | 68(2) |
| F(23) | 3134(2) | 5161(2) | 1986(2) | 76(2) |
| F(24) | 3765(2) | 5321(2) | 2497(2) | 85(2) |
| F(25) | 3298(2) | 5905(2) | 2213(2) | 91(2) |
| C(27) | 1485(1) | 5567(1) | 2931(2) | 75(3) |
| F(29) | 1175(2) | 5832(2) | 3229(2) | 111(2) |
| F(30) | 1239(2) | 5270(2) | 2595(2) | 83(2) |
| F(31) | 1764(2) | 5858(2) | 2625(2) | 85(2) |
| C(28) | 1479(1) | 5041(1) | 3854(2) | 87(3) |
| F(26) | 1692(2) | 4646(2) | 4065(2) | 89(2) |
| F(27) | 1039(2) | 4924(2) | 3659(2) | 96(2) |
| F(28) | 1434(2) | 5377(2) | 4255(2) | 102(2) |
| F(1) | 4633(2) | 2695(2) | 1001(2) | 61(1) |
| F(2) | 3620(2) | 4382(2) | 1239(2) | 64(1) |
| F(3) | 3427(2) | 4498(2) | 2786(2) | 54(1) |
| F(4) | 1447(2) | 4388(2) | 2990(2) | 61(1) |
| F(5) | 5476(2) | 3902(2) | 1007(3) | 95(2) |
| F(12) | 4994(2) | 4524(2) | 628(3) | 103(2) |
| F(19) | 2661(2) | 5786(2) | 2897(2) | 70(1) |
| F(32) | 2097(2) | 5591(2) | 3630(2) | 76(2) |

**Table B.20**  Bond Lengths [Å] and Angles [°] for (F$_{64}$Pc)$_2$Dy

| | | | |
|---|---|---|---|
| Dy-N(3) | 2.417(6) | Dy-N(1)#1 | 2.421(6) |
| Dy-N(3)#1 | 2.417(6) | Dy-N(1) | 2.421(6) |
| Dy-N(3)#2 | 2.417(6) | Dy-N(1)#2 | 2.421(6) |
| Dy-N(3)#3 | 2.417(6) | Dy-N(1)#3 | 2.421(6) |
| | | | |
| N(1)-C(8) | 1.369(8) | C(8)-C(9) | 1.469(8) |
| N(1)-C(11) | 1.374(8) | C(11)-N(2)#3 | 1.345(9) |
| N(2)-C(8) | 1.312(8) | C(11)-C(10) | 1.460(8) |
| N(2)-C(11)#1 | 1.345(9) | C(9)-C(10) | 1.3900 |
| N(3)-C(22) | 1.378(10) | C(9)-C(15) | 1.3900 |
| N(3)-C(1) | 1.387(10) | C(10)-C(12) | 1.3900 |
| N(4)-C(1)#3 | 1.301(10) | C(12)-C(13) | 1.3900 |
| N(4)-C(22) | 1.290(10) | C(13)-C(14) | 1.3900 |
| C(1)-N(4)#1 | 1.301(10) | C(13)-C(24) | 1.590(8) |
| C(1)-C(2) | 1.463(8) | C(14)-C(15) | 1.3900 |
| C(2)-C(3) | 1.3900 | C(14)-C(23) | 1.582(8) |
| C(2)-C(7) | 1.3900 | C(16)-C(17) | 1.541(11) |
| C(3)-C(4) | 1.3900 | C(16)-C(18) | 1.678(13) |
| C(4)-C(5) | 1.3900 | C(19)-C(21) | 1.566(11) |
| C(4)-C(16) | 1.584(10) | C(19)-C(20) | 1.667(15) |
| C(5)-C(6) | 1.3900 | C(23)-C(25) | 1.576(9) |
| C(5)-C(19) | 1.567(11) | C(23)-C(26) | 1.607(8) |
| C(6)-C(7) | 1.3900 | C(24)-C(27) | 1.555(9) |
| C(7)-C(22) | 1.484(8) | C(24)-C(28) | 1.624(9) |
| N(3)-Dy-N(3)#1 | 70.55(15) | N(1)#2-Dy-N(1)#3 | 70.26(14) |
| N(3)-Dy-N(3)#2 | 109.5(3) | C(8)-N(1)-C(11) | 107.5(6) |
| N(3)#1-Dy-N(3)#2 | 70.55(15) | C(8)-N(1)-Dy | 123.5(4 |
| N(3)-Dy-N(3)#3 | 70.55(15) | C(11)-N(1)-Dy | 122.4(4) |
| | | | |
| N(3)#1-Dy-N(3)#3 | 109.5(3) | C(8)-N(2)-C(11)#1 | 123.7(7) |
| N(3)#2-Dy-N(3)#3 | 70.55(15) | C(22)-N(3)-C(1) | 109.4(6) |
| N(3)-Dy-N(1)#1 | 76.6(2) | C(22)-N(3)-Dy | 122.3(5) |
| N(3)#1-Dy-N(1)#1 | 89.3(2) | C(1)-N(3)-Dy | 123.0(5) |
| N(3)#2-Dy-N(1)#1 | 154.46(19) | C(1)#3-N(4)-C(22) | 124.4(6) |
| N(3)#3-Dy-N(1)#1 | 133.02(19) | N(4)#1-C(1)-N(3) | 128.2(7) |
| N(3)-Dy-N(1) | 89.3(2) | N(4)#1-C(1)-C(2) | 123.2(6) |
| N(3)#1-Dy-N(1) | 154.46(19) | N(3)-C(1)-C(2) | 108.6(6) |
| N(3)#2-Dy-N(1) | 133.02(19) | C(3)-C(2)-C(7) | 120.0 |
| N(3)#3-Dy-N(1) | 76.6(2) | C(3)-C(2)-C(1) | 133.1(4) |
| N(1)#1-Dy-N(1) | 70.26(14) | C(7)-C(2)-C(1) | 106.9(4) |
| N(3)-Dy-N(1)#2 | 133.02(19) | C(4)-C(3)-C(2) | 120.0 |
| N(3)#1-Dy-N(1)#2 | 76.6(2) | C(5)-C(4)-C(3) | 120.0 |
| N(3)#2-Dy-N(1)#2 | 89.3(2) | C(5)-C(4)-C(16) | 127.4(4) |
| N(3)#3-Dy-N(1)#2 | 154.46(19) | C(3)-C(4)-C(16) | 112.6(4) |
| N(1)#1-Dy-N(1)#2 | 70.26(14) | C(4)-C(5)-C(6) | 120.0 |
| N(1)-Dy-N(1)#2 | 108.9(3) | C(4)-C(5)-C(19) | 126.8(4) |
| N(3)-Dy-N(1)#3 | 154.46(19) | C(6)-C(5)-C(19) | 113.1(4) |
| N(3)#1-Dy-N(1)#3 | 133.02(19) | C(7)-C(6)-C(5) | 120.0 |
| N(3)#2-Dy-N(1)#3 | 76.6(2) | C(6)-C(7)-C(2) | 120.0 |
| N(3)#3-Dy-N(1)#3 | 89.3(2) | C(6)-C(7)-C(22) | 132.6(4) |
| N(1)#1-Dy-N(1)#3 | 108.9(3) | C(2)-C(7)-C(22) | 107.1(4) |
| N(1)-Dy-N(1)#3 | 70.26(14) | N(2)-C(8)-N(1) | 126.8(6) |
| N(2)-C(8)-C(9) | 123.1(6) | C(13)-C(14)-C(23) | 125.5(4) |
| N(1)-C(8)-C(9) | 110.0(5) | C(14)-C(15)-C(9) | 120.0 |

**Table B.20**   Bond Lengths [Å] and Angles [°] for (F$_{64}$Pc)$_2$Dy, Continued

| | | | |
|---|---|---|---|
| N(2)#3-C(11)-N(1) | 127.9(6) | C(17)-C(16)-C(4) | 111.6(8) |
| N(2)#3-C(11)-C(10) | 122.4(6) | C(17)-C(16)-C(18) | 108.7(6) |
| N(1)-C(11)-C(10) | 109.6(6) | C(4)-C(16)-C(18) | 115.1(6) |
| C(10)-C(9)-C(15) | 120.0 | C(21)-C(19)-C(5) | 118.4(8) |
| C(10)-C(9)-C(8) | 105.5(4) | C(21)-C(19)-C(20) | 109.7(7) |
| C(15)-C(9)-C(8) | 133.9(4) | C(5)-C(19)-C(20) | 108.0(7) |
| C(9)-C(10)-C(12) | 120.0 | N(4)-C(22)-N(3) | 128.0(7) |
| C(9)-C(10)-C(11) | 106.9(4) | N(4)-C(22)-C(7) | 124.2(6) |
| C(12)-C(10)-C(11) | 133.1(4) | N(3)-C(22)-C(7) | 107.5(7) |
| C(13)-C(12)-C(10) | 120.0 | C(25)-C(23)-C(14) | 112.2(5) |
| C(12)-C(13)-C(14) | 120.0 | C(25)-C(23)-C(26) | 110.9(5) |
| C(12)-C(13)-C(24) | 111.8(4) | C(14)-C(23)-C(26) | 116.0(5) |
| C(14)-C(13)-C(24) | 126.8(4) | C(27)-C(24)-C(13) | 116.2(6) |
| C(15)-C(14)-C(13) | 120.0 | C(27)-C(24)-C(28) | 109.8(5) |
| C(15)-C(14)-C(23) | 112.7(4) | C(13)-C(24)-C(28) | 114.5(5) |

Symmetry transformations used to generate equivalent atoms:
#1 y,-x+1/2,z    #2 -x+1/2,-y+1/2,z    #3 -y+1/2,x,z

**Table B.21** Anisotropic Displacement Parameters ($Å^2 \times 10^3$) for $(F_{64}Pc)_2Dy$. The Anisotropic Displacement Factor Exponent Takes the Form: $-2\pi^2[h^2a^{*2}U^{11} + ... + 2hka^*b^* \ U^{12}]$

| | $U^{11}$ | $U^{22}$ | $U^{33}$ | $U^{23}$ | $U^{13}$ | $U^{12}$ |
|---|---|---|---|---|---|---|
| Dy | 26(1) | 26(1) | 44(1) | 0 | 0 | 0 |
| N(1) | 30(4) | 27(3) | 45(4) | -4(3) | 6(2) | -1(2) |
| N(2) | 35(3) | 31(3) | 52(4) | -7(3) | 2(3) | 2(3) |
| N(3) | 39(4) | 38(4) | 62(4) | 2(3) | -1(3) | -5(3) |
| N(4) | 42(4) | 33(3) | 52(4) | 7(3) | 6(3) | -1(3) |
| C(1) | 35(4) | 47(5) | 46(4) | -2(3) | 7(3) | 6(4) |
| C(2) | 50(5) | 40(4) | 58(5) | 2(3) | 14(4) | -7(4) |
| C(3) | 32(4) | 57(5) | 58(5) | -13(4) | 17(3) | -8(4) |
| C(4) | 49(5) | 57(5) | 73(6) | -4(4) | 25(4) | -13(4) |
| C(5) | 49(5) | 56(5) | 66(5) | 9(4) | 16(4) | -6(4) |
| C(6) | 48(5) | 42(5) | 66(6) | 20(4) | 6(4) | -9(4) |
| C(7) | 43(4) | 58(5) | 45(5) | 5(4) | 6(3) | -6(4) |
| C(8) | 31(4) | 34(4) | 40(4) | -6(3) | 3(3) | -2(3) |
| C(11) | 40(4) | 27(4) | 52(4) | 1(3) | 7(3) | 10(3) |
| C(9) | 34(4) | 31(4) | 58(5) | -3(3) | 7(3) | -4(3) |
| C(10) | 35(4) | 34(4) | 53(4) | -5(3) | -1(3) | 0(3) |
| C(12) | 29(4) | 47(5) | 61(5) | -3(3) | 8(3) | -2(4) |
| C(13) | 58(5) | 25(4) | 55(5) | 0(3) | 8(3) | 6(4) |
| C(14) | 43(5) | 34(5) | 56(5) | -10(3) | 2(3) | 0(4) |
| C(15) | 49(5) | 40(5) | 46(4) | -2(3) | 1(3) | -8(4) |
| C(16) | 68(6) | 69(6) | 109(8) | -30(5) | 46(6) | -23(5) |
| C(17) | 93(9) | 205(16) | 77(8) | 16(9) | 49(7) | -59(10) |
| F(9) | 103(5) | 117(5) | 102(5) | -35(4) | 46(4) | -47(4) |
| F(10) | 97(5) | 156(6) | 146(7) | -35(5) | 70(5) | -32(5) |
| F(11) | 155(7) | 120(6) | 101(5) | 10(4) | 30(5) | -58(5) |
| C(18) | 46(5) | 78(7) | 98(8) | -6(6) | 9(5) | -2(5) |
| F(6) | 84(4) | 89(4) | 118(5) | -12(4) | -10(4) | 15(3) |
| F(7) | 66(4) | 103(5) | 178(7) | -37(4) | 0(4) | -18(3) |
| F(8) | 70(4) | 85(4) | 167(7) | -38(5) | 22(4) | -1(3) |
| C(19) | 56(6) | 72(7) | 125(10) | 18(6) | 43(6) | -11(6) |
| C(20) | 76(8) | 59(7) | 164(14) | -18(7) | 24(8) | -19(7) |
| F(16) | 102(5) | 69(4) | 290(12) | -35(6) | 41(6) | -35(4) |
| F(17) | 84(4) | 94(5) | 151(6) | -36(4) | 9(4) | -18(4) |
| F(18) | 69(4) | 122(6) | 162(6) | -54(5) | 31(4) | -23(4) |
| C(21) | 137(14) | 87(10) | 210(19) | 82(12) | 67(14) | -7(11) |
| F(13) | 117(5) | 129(6) | 127(6) | 63(5) | 4(4) | -2(5) |
| F(14) | 140(7) | 109(6) | 285(11) | 114(7) | 85(7) | 1(5) |
| F(15) | 90(5) | 61(4) | 276(11) | 36(5) | 54(6) | 0(4) |
| C(22) | 44(5) | 45(5) | 50(5) | 9(4) | 6(4) | -12(4) |
| C(23) | 51(5) | 34(4) | 70(6) | -12(3) | 8(4) | 2(4) |
| C(24) | 68(5) | 31(4) | 77(6) | -7(4) | 16(4) | 6(4) |
| C(25) | 82(7) | 66(7) | 82(7) | -9(5) | -5(6) | -16(6) |
| F(20) | 101(4) | 91(4) | 74(4) | -14(3) | 1(3) | -8(3) |
| F(21) | 98(4) | 74(4) | 114(4) | -27(3) | 7(3) | -45(3) |
| F(22) | 66(3) | 83(4) | 98(4) | -34(3) | -26(3) | -1(3) |

**Table B.21** Anisotropic Displacement Parameters ($\mathring{A}^2$x$10^3$)for (F$_{64}$Pc)$_2$Dy. The Anisotropic Displacement Factor Exponent Takes the Form: $-2\pi^2[h^2a^{*2}U^{11} + ... + 2hka^*b^* U^{12}]$, Continued

|  | $U^{11}$ | $U^{22}$ | $U^{33}$ | $U^{23}$ | $U^{13}$ | $U^{12}$ |
|---|---|---|---|---|---|---|
| C(26) | 67(6) | 58(6) | 80(7) | 6(5) | -1(5) | -5(5) |
| F(23) | 93(4) | 65(3) | 70(4) | -3(2) | 20(3) | 0(3) |
| F(24) | 64(3) | 64(3) | 127(5) | -15(3) | 21(3) | -13(3) |
| F(25) | 95(4) | 49(3) | 128(5) | 14(3) | 47(4) | -4(3) |
| C(27) | 70(7) | 60(6) | 96(8) | -15(5) | 5(5) | 12(6) |
| F(29) | 80(4) | 65(4) | 188(7) | 0(4) | 24(4) | 33(3) |
| F(30) | 66(3) | 74(3) | 110(4) | 16(3) | -4(3) | 6(3) |
| F(31) | 85(4) | 62(3) | 109(5) | 10(3) | 3(3) | 4(3) |
| C(28) | 71(7) | 44(5) | 145(10) | -5(6) | 45(7) | -5(5) |
| F(26) | 109(4) | 81(4) | 78(4) | 6(3) | 22(3) | -10(3) |
| F(27) | 66(3) | 71(3) | 150(5) | -25(3) | 40(4) | -9(3) |
| F(28) | 115(5) | 87(4) | 104(4) | -38(3) | 49(4) | -18(4) |
| F(1) | 38(2) | 56(3) | 90(3) | -12(2) | 28(2) | -1(2) |
| F(2) | 53(3) | 36(2) | 102(4) | 20(2) | 18(2) | -1(2) |
| F(3) | 36(3) | 35(2) | 89(3) | -13(2) | 1(2) | -3(2) |
| F(4) | 46(3) | 37(2) | 99(4) | -13(2) | 17(2) | 1(2) |
| F(5) | 56(3) | 90(4) | 139(5) | -30(4) | 25(3) | -33(3) |
| F(12) | 85(4) | 81(4) | 143(5) | 9(4) | 44(4) | -31(4) |
| F(19) | 75(3) | 44(3) | 90(4) | -1(2) | 23(3) | 0(3) |
| F(32) | 76(3) | 55(3) | 97(4) | -19(3) | 21(3) | -5(3) |

## NMR GRAPHS

This appendix contains the $^{19}$F NMR figures of complexes **[1], [3] and [4].**
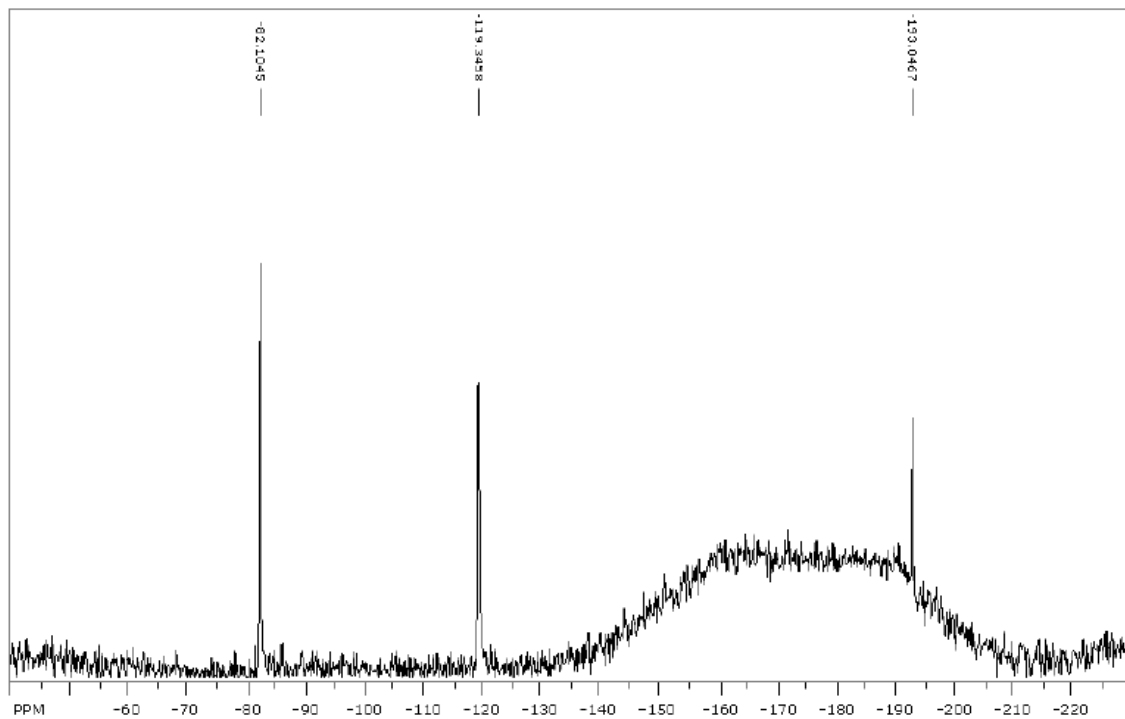


**Figure C.1**   $^{19}$F NMR of $(F_{64}Pc)_2TbH$ in acetone $D_6$.
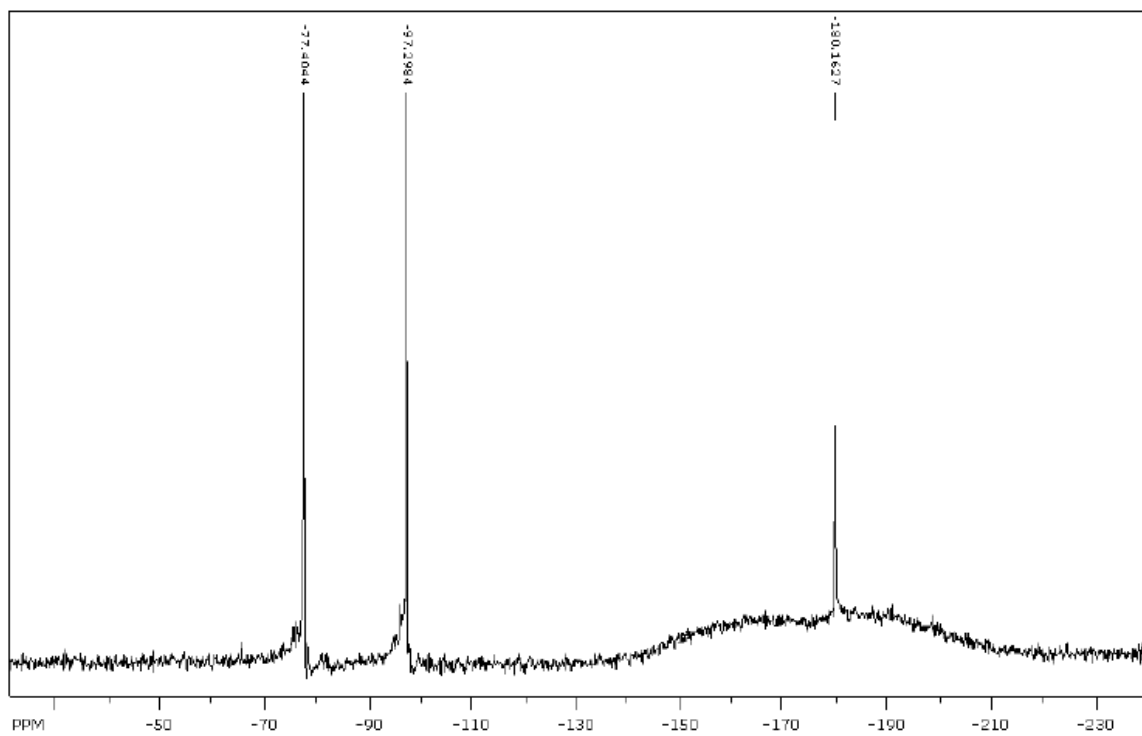
**Figure C.2** $^{19}$F NMR of $(F_{64}Pc)_2DyH$ in acetone $D_6$.
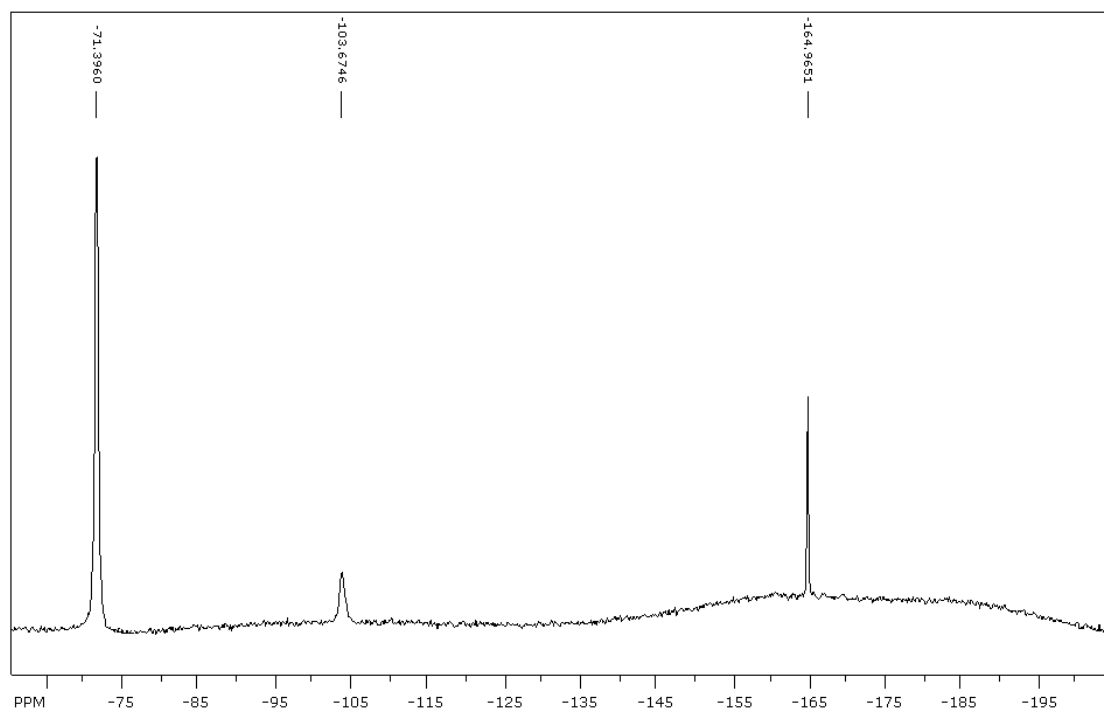
**Figure C.3** $^{19}$F NMR of $(F_{64}Pc)_2LuH$ in acetone $D_6$.

# APPENDIX D

## MAGNETISM HYSTERESIS AND AC MAGNETISM CURVES

This appendix contains Figure D.1, showing the DC magnetism hysteresis curve of $(F_{64}Pc)2LuH$ and Figures D.2-D.4 showing AC magnetism curves of $(F_{64}Pc)_2DyH$.
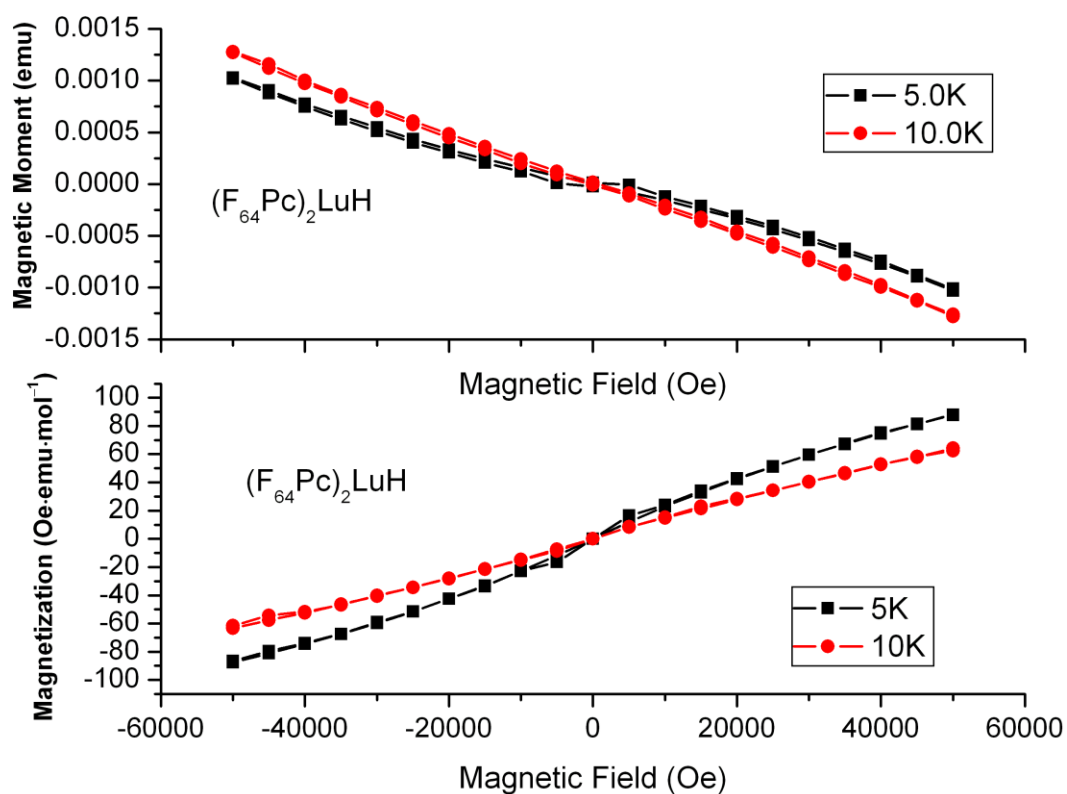


**Figure D.1** DC magnetic hysteresis of $(F_{64}Pc)_2LuH$. (top) Raw magnetic moment data. (bottom) Molar magnetization data corrected for capsule and diamagnetic contribution.
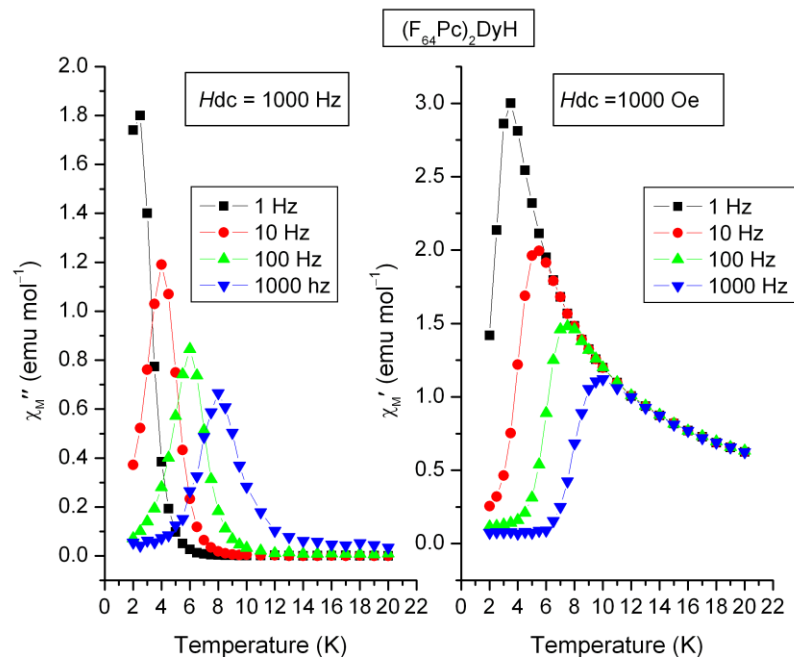
**Figure D.2** Temperature dependent out-of-phase susceptibility, $\chi_M{''}$ and in-phase susceptibility, $\chi_M{'}$ graphs of $(F_{64}Pc)_2DyH$ for static bias DC magnetic field, $H$dc of 1000 Oe.
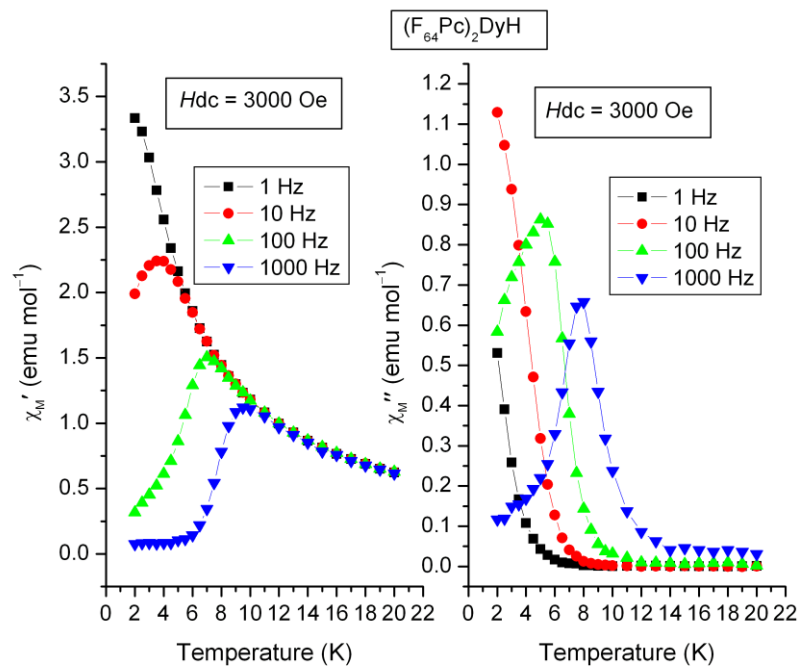


**Figure D.3** Temperature dependent out-of-phase susceptibility, $\chi_M{''}$ and in-phase susceptibility, $\chi_M{'}$ graphs of $(F_{64}Pc)_2DyH$ for static bias DC magnetic fields, $H$dc of 1000 Oe.
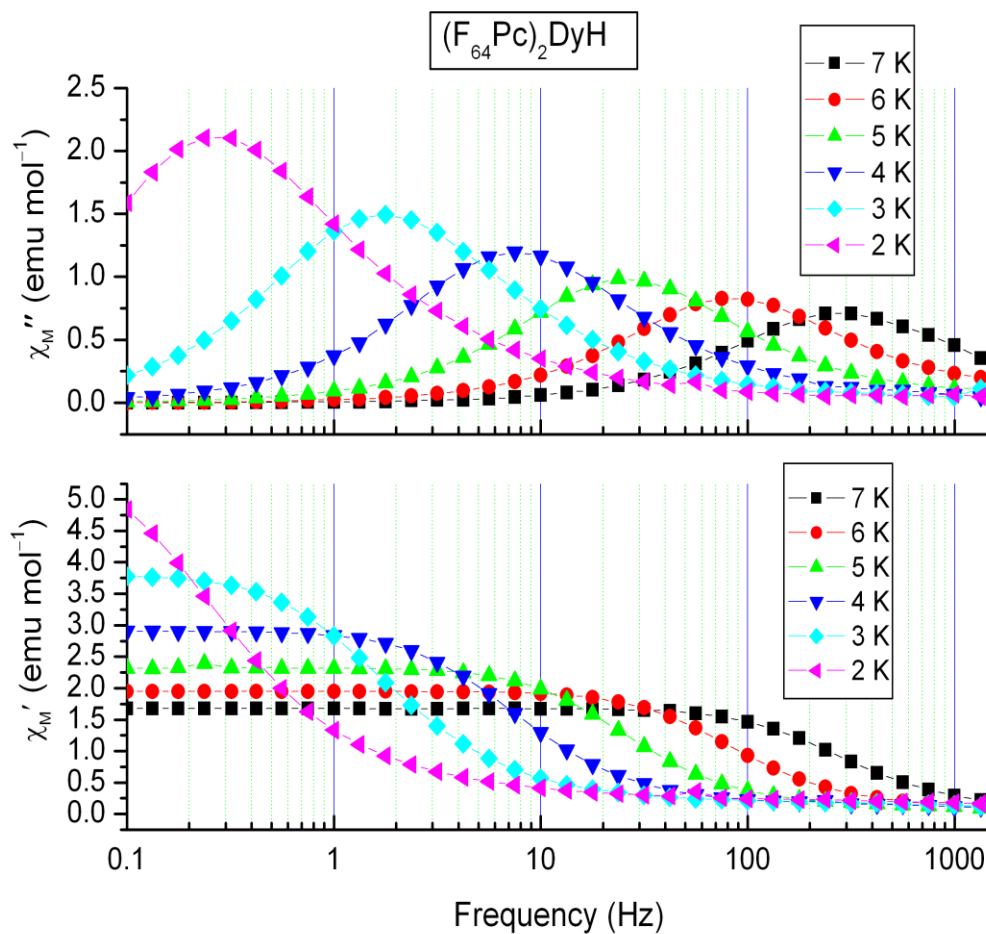
**Figure D.4** Frequency dependence of out-of-phase susceptibility, $\chi_M{}''$ and in-phase susceptibility, $\chi_M{}'$ graphs of $(F_{64}Pc)_2DyH$ in the temperature range 2-7 K for static bias DC magnetic fields, $H$dc of 500 Oe.

## ELECTRONIC SPECTRA

This appendix contains UV-visible and Near Infra-Red deconvolution spectral data and

figures. The Gaussian and Voigt functions are explained.

### E.1 The Gaussian and Voigt Functions

The Gaussian and Voigt functions contained in the Fityk® [160] program are given as
follows:

   a) Gaussian

$$y = a_0 \exp\left[-\ln(2)\left(\frac{x - a_1}{a_2}\right)^2\right]$$

   Where $a_0 = $ height of the curve's peak
      $a_1 = $ position of the centre of the peak
      $a_2 = $ parameter which controls the width of the bell and is related to
         the FWHM
   FWHM $= a_2(2\sqrt{2\ln(2)})$

   b) Voigt[267]

$$y = \frac{a_0 \int_{-\infty}^{+\infty} \frac{\exp(-t^2)}{a_3^2 + (\frac{x-a_1}{a_2} - t)^2} dt}{\int_{-\infty}^{+\infty} \frac{\exp(-t^2)}{a_3^2 + t^2} dt}$$

The Voigt function is a convolution of Gaussian and Lorentzian functions. $a_0 = $

height, $a_1 = $ center, $a_2$ is proportional to the Gaussian width, and $a_3$ is

proportional to the ratio of Lorentzian and Gaussian widths with

FWHM $= 0.5346 w_L + \sqrt{0.2169 w_L^2 + w_G^2}$ approximation[268] and where:

   $w_L = $ Lorentzian FWHM and $w_G = $ Gaussian FWHM.

**Table E.1** UV-Visible Deconvolution Data For $(F_{64}Pc)_2YH$ in Methanol

| Peak Type | Center | Height | Area | FWHM | Parameters | | |
|---|---|---|---|---|---|---|---|
| | | | | | $a_0$ | $a_1$ | $a_2$ |
| Gaussian | 877 | 0.122 | 16.1 | 124.1 | 0.122 | 877.2 | 62.0 |
| Gaussian | 776 | 0.079 | 6.9 | 81.3 | 0.079 | 775.5 | 40.6 |
| Gaussian | 705 | 0.095 | 2.7 | 26.2 | 0.095 | 704.8 | 13.1 |
| Gaussian | 683 | 0.372 | 9.8 | 24.7 | 0.372 | 683.1 | 12.3 |
| Gaussian | 676 | 0.793 | 65.1 | 77.1 | 0.793 | 675.8 | 38.5 |
| Gaussian | 608 | 0.207 | 8.6 | 39.2 | 0.207 | 608.1 | 19.6 |
| Gaussian | 559 | 0.367 | 17.2 | 44.2 | 0.367 | 558.7 | 22.1 |
| Gaussian | 548 | 0.210 | 3.9 | 17.6 | 0.210 | 547.5 | 8.8 |
| Gaussian | 522 | 0.083 | 5.7 | 64.0 | 0.083 | 522.0 | 32.0 |
| Gaussian | 434 | 0.244 | 5.8 | 22.4 | 0.244 | 434.1 | 11.2 |
| Gaussian | 415 | 0.088 | 1.7 | 18.2 | 0.088 | 415.1 | 9.1 |
| Gaussian | 386 | 0.349 | 9.1 | 24.5 | 0.349 | 385.7 | 12.2 |
| Gaussian | 342 | 0.807 | 93.8 | 109.2 | 0.807 | 341.5 | 54.6 |
| Gaussian | 337 | 0.091 | 1.5 | 15.7 | 0.091 | 337.4 | 7.8 |

**Table E.2** UV-Visible Deconvolution Data For $(F_{64}Pc)_2LuH$ in Methanol

| Peak Type | Center | Height | Area | FWHM | Parameters | | |
|---|---|---|---|---|---|---|---|
| | | | | | $a_0$ | $a_1$ | $a_2$ |
| Gaussian | 915 | 0.085 | 13.69 | 151 | 0.0854 | 915.2 | 75.3 |
| Gaussian | 801 | 0.049 | 4.81 | 93 | 0.0486 | 800.6 | 46.5 |
| Gaussian | 713 | 0.104 | 2.45 | 22 | 0.1041 | 713.3 | 11.0 |
| Gaussian | 688 | 0.671 | 21.45 | 30 | 0.6713 | 688.2 | 15.0 |
| Gaussian | 664 | 0.617 | 63.76 | 97 | 0.6170 | 663.8 | 48.5 |
| Gaussian | 548 | 0.253 | 15.59 | 58 | 0.2527 | 548.1 | 29.0 |
| Gaussian | 546 | 0.192 | 3.85 | 19 | 0.1925 | 545.5 | 9.4 |
| Gaussian | 495 | 0.034 | 1.06 | 29 | 0.0344 | 495.4 | 14.5 |
| Gaussian | 438 | 0.155 | 3.77 | 23 | 0.1553 | 438.3 | 11.4 |
| Gaussian | 421 | 0.034 | 0.77 | 21 | 0.0342 | 421.5 | 10.5 |
| Gaussian | 388 | 0.200 | 4.54 | 21 | 0.2001 | 388.4 | 10.6 |
| Gaussian | 346 | 0.741 | 96.20 | 122 | 0.7408 | 345.8 | 61.0 |
| Gaussian | 340 | 0.140 | 3.46 | 23 | 0.1404 | 340.0 | 11.6 |

**Table E.3** UV-Visible Deconvolution Data For $Pc_2Y$ in Chloroform

| Peak Type | Center | Height | Area | FWHM | Parameters | | | |
|-----------|--------|--------|------|------|------|------|------|------|
| | | | | | $a_0$ | $a_1$ | $a_2$ | $a_3$ |
| Voigt | 917 | 0.055 | 5.04 | 58 | 0.0551 | 917.2 | -2.92 | 9.91 |
| Voigt | 665 | 1.913 | 44.78 | 18 | 1.9134 | 665.0 | 8.15 | 0.50 |
| Voigt | 634 | 0.135 | 3.27 | 22 | 0.1352 | 634.3 | 13.22 | -0.03 |
| Voigt | 601 | 0.234 | 6.95 | 23 | 0.2342 | 601.3 | 9.77 | 0.57 |
| Voigt | 577 | 0.158 | 6.48 | 27 | 0.1583 | 576.8 | 4.69 | 2.61 |
| Voigt | 459 | 0.284 | 25.59 | 58 | 0.2840 | 459.3 | 4.70 | 6.02 |
| Voigt | 345 | 0.550 | 46.15 | 54 | 0.5501 | 344.9 | 3.72 | 7.11 |
| Voigt | 318 | 0.978 | 51.15 | 34 | 0.9778 | 318.1 | 3.11 | 5.26 |
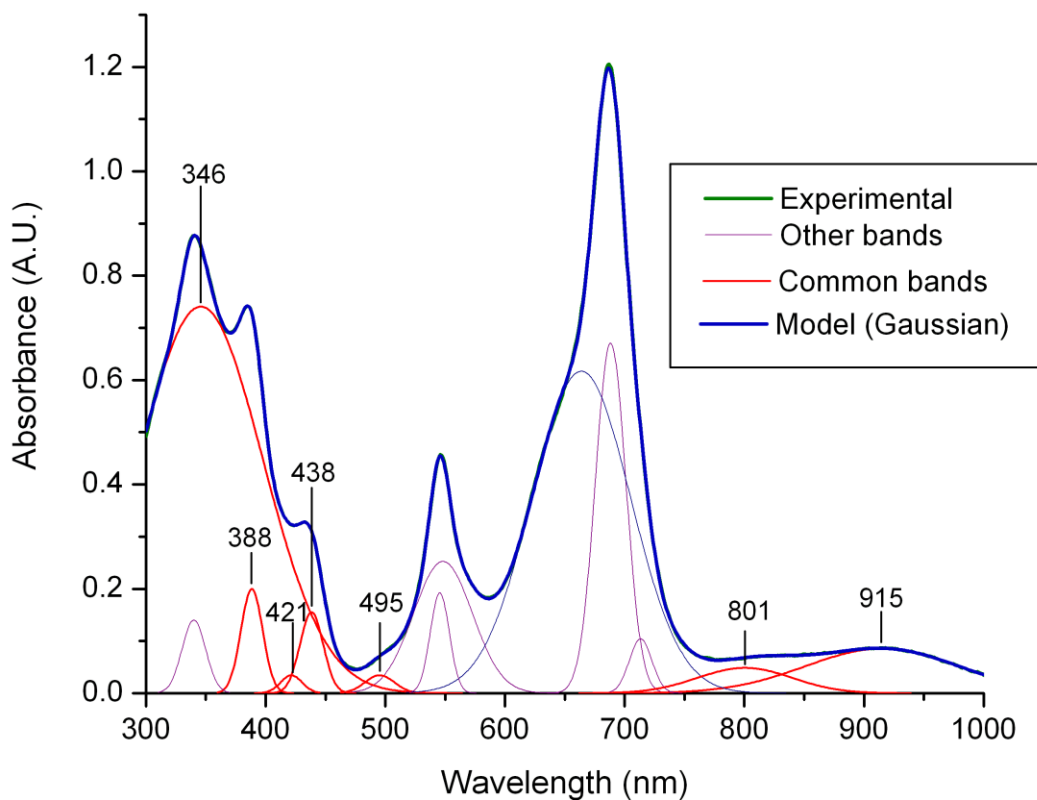


**Figure E.1** Deconvoluted UV-vis. and NIR (800-1000 nm) spectrum of $(F_{64}Pc)_2LuH$ in methanol.

**Table E.4** UV-Visible Data For $(F_{64}Pc)_2TbH$ in Methanol

| Peak Type | Center | Height | Area | FWHM | Parameters | | |
|---|---|---|---|---|---|---|---|
| | | | | | $a_0$ | $a_1$ | $a_2$ |
| Gaussian | 860 | 0.131 | 16.6 | 119.0 | 0.131 | 860.2 | 59.5 |
| Gaussian | 756 | 0.100 | 8.8 | 82.3 | 0.100 | 756.3 | 41.1 |
| Gaussian | 681 | 0.112 | 2.3 | 18.9 | 0.112 | 681.4 | 9.5 |
| Gaussian | 680 | 1.037 | 69.5 | 62.9 | 1.037 | 680.3 | 31.5 |
| Gaussian | 643 | 0.074 | 1.7 | 21.0 | 0.074 | 643.1 | 10.5 |
| Gaussian | 611 | 0.313 | 16.0 | 47.8 | 0.313 | 610.7 | -23.9 |
| Gaussian | 559 | 0.389 | 16.2 | 39.2 | 0.389 | 559.4 | 19.6 |
| Gaussian | 549 | 0.152 | 2.7 | 16.9 | 0.152 | 549.2 | 8.4 |
| Gaussian | 532 | 0.098 | 6.9 | 66.2 | 0.098 | 531.7 | 33.1 |
| Gaussian | 433 | 0.250 | 5.9 | 22.1 | 0.250 | 433.0 | 11.0 |
| Gaussian | 415 | 0.090 | 1.6 | 16.7 | 0.090 | 414.9 | 8.4 |
| Gaussian | 386 | 0.359 | 9.7 | 25.5 | 0.359 | 386.1 | 12.7 |
| Gaussian | 342 | 0.820 | 96.0 | 110.0 | 0.820 | 341.6 | 55.0 |
| Gaussian | 339 | 0.091 | 1.5 | 15.6 | 0.091 | 338.6 | 7.8 |

**Table E.5** UV-Visible Data For $(F_{64}Pc)_2DyH$ in Methanol

| Peak Type | Center | Height | Area | FWHM | Parameters | | |
|---|---|---|---|---|---|---|---|
| | | | | | $a_0$ | $a_1$ | $a_2$ |
| Gaussian | 871 | 0.084 | 12.3 | 137.2 | 0.084 | 871.3 | 68.6 |
| Gaussian | 764 | 0.053 | 5.0 | 87.9 | 0.053 | 763.7 | 44.0 |
| Gaussian | 682 | 0.532 | 32.3 | 57.0 | 0.532 | 682.2 | 28.5 |
| Gaussian | 682 | 0.222 | 5.6 | 23.8 | 0.222 | 681.5 | 11.9 |
| Gaussian | 644 | 0.323 | 36.2 | 105.3 | 0.323 | 644.5 | 52.7 |
| Gaussian | 608 | 0.019 | 0.3 | 15.1 | 0.019 | 608.2 | 7.5 |
| Gaussian | 554 | 0.245 | 10.9 | 41.8 | 0.245 | 553.9 | 20.9 |
| Gaussian | 547 | 0.105 | 1.9 | 17.1 | 0.105 | 547.2 | 8.5 |
| Gaussian | 513 | 0.051 | 3.0 | 55.4 | 0.051 | 512.9 | 27.7 |
| Gaussian | 434 | 0.167 | 4.1 | 23.2 | 0.167 | 433.7 | 11.6 |
| Gaussian | 415 | 0.062 | 1.2 | 18.4 | 0.062 | 415.3 | 9.2 |
| Gaussian | 387 | 0.217 | 5.8 | 25.0 | 0.217 | 386.8 | 12.5 |
| Gaussian | 342 | 0.634 | 75.3 | 111.6 | 0.634 | 342.2 | 55.8 |
| Gaussian | 339 | 0.085 | 1.7 | 18.7 | 0.085 | 338.8 | 9.4 |
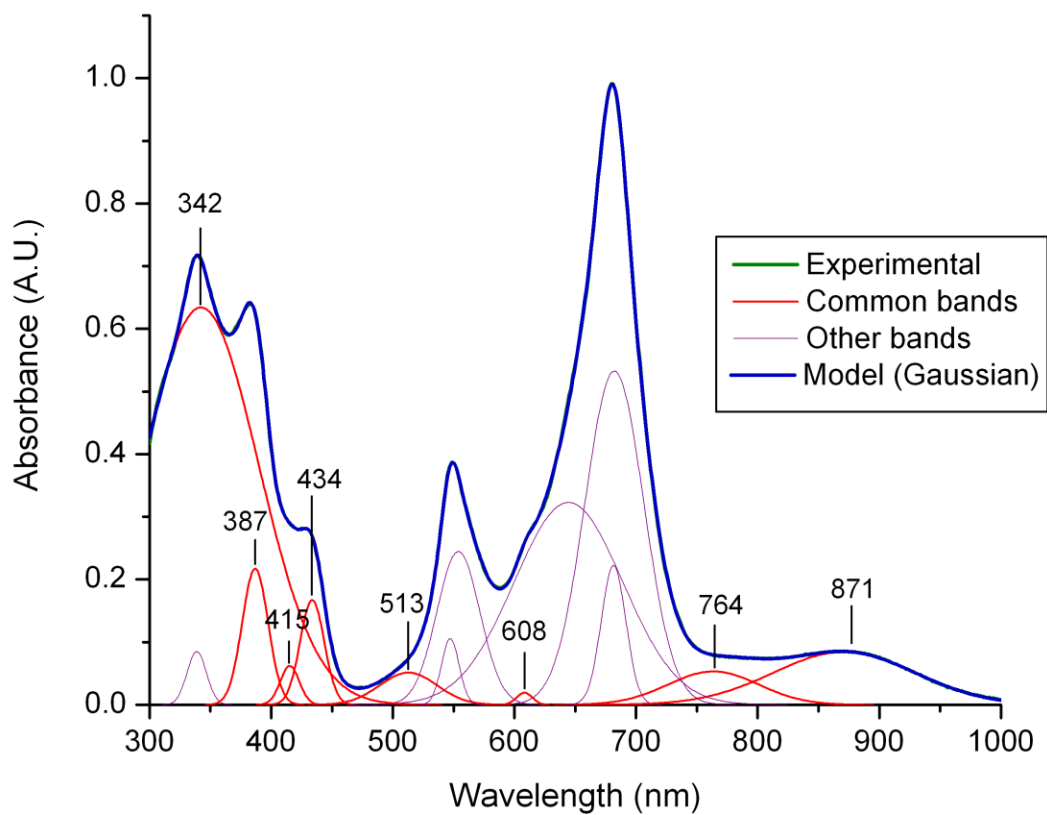
**Figure E.2** Deconvoluted UV-visible and NIR (800-1000 nm) spectrum of $(F_{64}Pc)_2DyH$ in methanol.
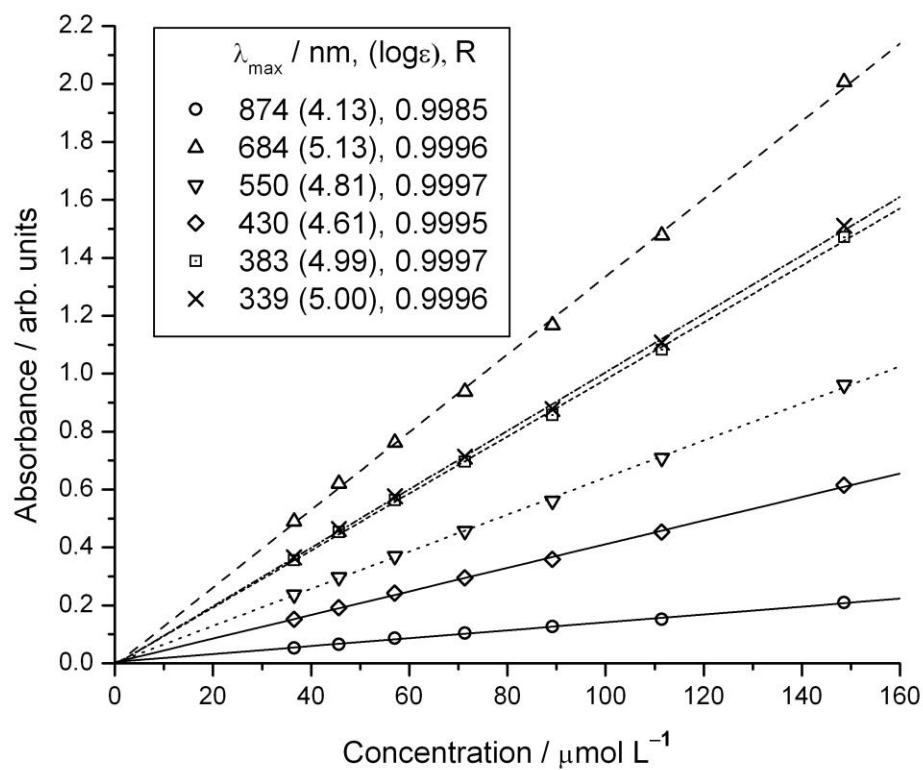
**Figure E.3** Example of aggregation probing via the Lambert-Beer law verification showing $(F_{64}Pc)_2YH$ in methanol, up to the saturation point. R is the goodness-of-fit.

# DENSITY FUNCTIONAL THEORY OF $(F_{64}Pc)_2MH$ ( M=Lu, Y)[109]

Selected tables and figures on Density Functional Theory (DFT) and Time Dependent Density Functional Theory TDDFT calculations for the $(F_{64}Pc)_2MH$ complexes ( M=Lu, Y) carried out by Liao et al.[109] This work is in the manuscript form at the time of writing this thesis.

**Table F.1** Calculated Properties[a] of the Protonated Forms of Double-Deckers $(H_{16}Pc)_2YH$, $(F_{16}Pc)_2YH$, $(F_{32}Pc)_2YH$, and $(F_{32}Pc)_2LuH$

|  | $(H_{16}Pc)_2YH$ | $(F_{16}Pc)_2YH$ | $(F_{32}Pc)_2YH$ | $(F_{32}Pc)_2LuH$ |
|---|---|---|---|---|
| $R_{Ct(N4)\cdots N}$, Å | 1.921, 1.993[b] | 1.922, 1.993 | 1.926, 1.994 | 1.924, 1.980 |
| $R_{Ct(N4)\cdots M}$, Å | 1.769, 1.228 | 1.762, 1.226 | 1.762, 1.221 | 1.709, 1.162 |
| $R_{M-N}$, Å | 2.611, 2.341 | 2.607, 2.340 | 2.611, 2.338 | 2.573, 2.296 |
| $R_{Ct(N4)\cdots Ct(C8)}$, Å | 0.450, 0.557 | 0.353, 0.352 | 0.279, 0.269 | 0.425, 0.361 |
| $R_{Pc\cdots Pc}$, Å | 2.997 | 2.988 | 2.983 | 2.871 |
| $R_{Ct(N4)\cdots H(ax)}$, Å | 0.516 | 0.531 | 0.539 | 0.530 |
| $R_{N-H(ax)}$, Å | 1.989 | 1.994 | 2.000 | 1.996 |
| $Q_M$ | 2.71 | 2.74 | 2.72 | 2.55 |
| μ, Debye | 1.93 | 2.15 | 1.78 | 1.62 |
| IP, eV | 6.23 | 7.22 | 7.96 | 7.92 |
| EA, eV | 2.87 | 3.95 | 4.83 | 4.83 |
| $E_{bind}(M-2Pc)$, eV | 18.47 | 18.14 | 18.40 | 18.68 |

[a]R, distance; Ct(N4), centroid of the plane defined by the four pyrrole nitrogen atoms; Ct(C8), centroid of the plane defined by the eight peripheral carbon atoms; $R_{Pc\cdots Pc} = 2 \times R_{Ct(N4)\cdots M}$; $Q_M$, Mulliken charge distribution on the M atom; μ, dipole moment; IP, vertical ionization potential; EA, vertical electron affinity; $E_{bind}$, binding energy, see text for the definition.
[b]The second set of values represents the structural parameters related to the other, lower-part, Pc ring which does not carry an axial H atom [see Figure 2(c)].
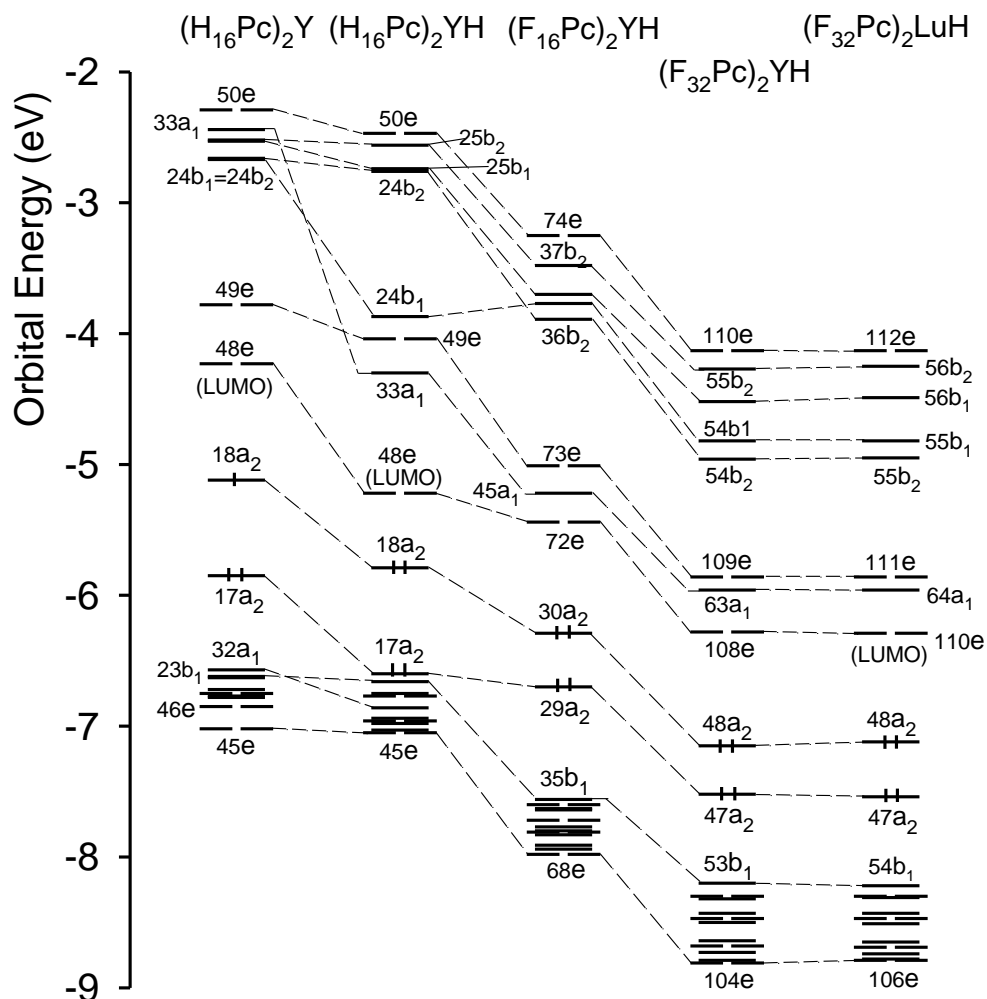
**Figure F.1** Orbital energy levels of various protonated yttrium bis(phthalocyanine)s Pc$_2$YH. The Orbital energy levels of (H$_{16}$Pc)$_2$Y are given here for comparison.
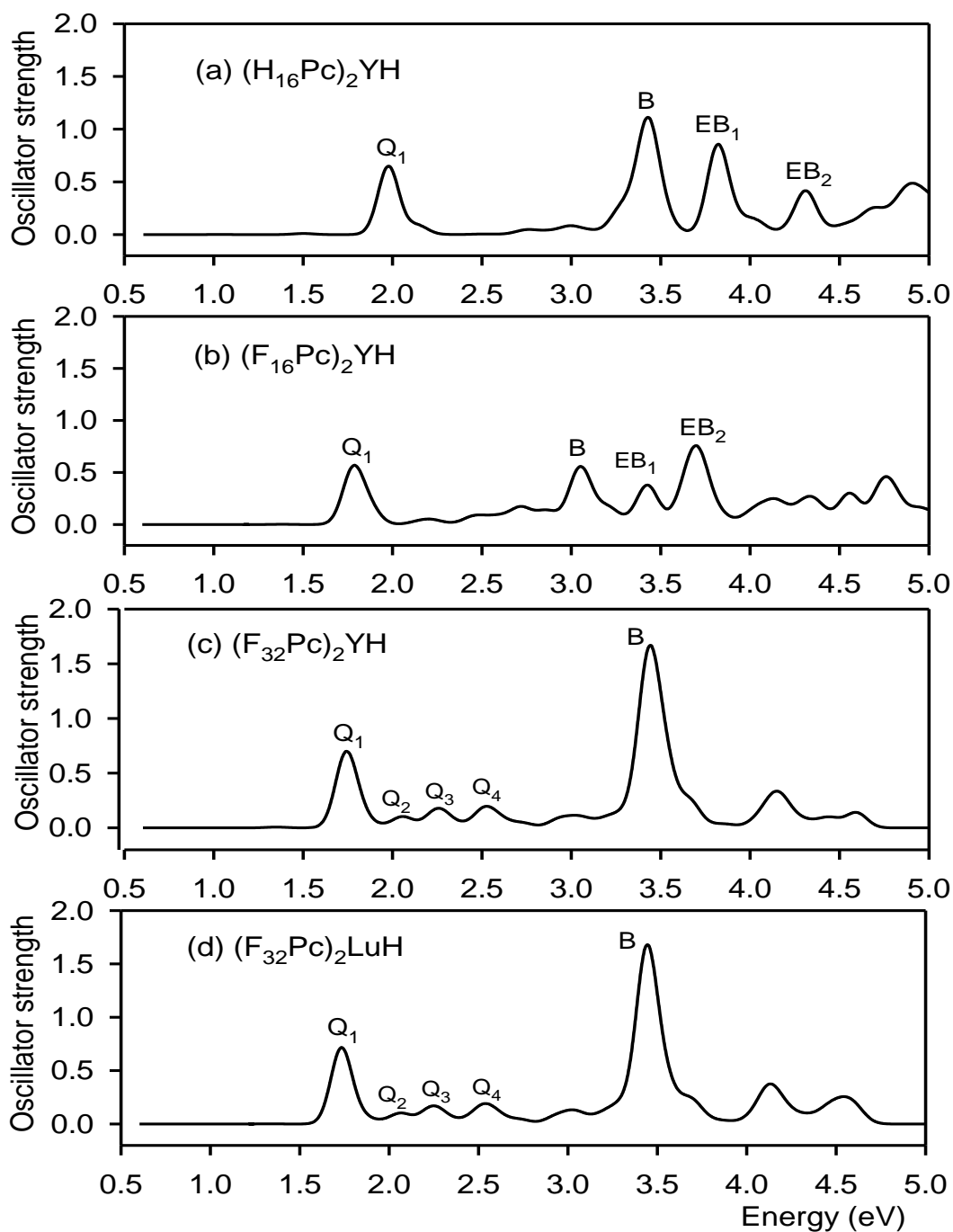
**Figure F.2** Simulated electronic absorption spectra for various protonated $Pc_2YH$ species and for $(F_{32}Pc)_2LuH$.

**Table F.2.** Calculated Excitation Energies ($E^{exc}$) and Oscillator Strengths ($f$) for $(F_{32}Pc)_2YH$

| State | Contribution (%) | $E^{exc}$, eV | | $f$ | Assignment |
|---|---|---|---|---|---|
| | | Calc | Exptl | | |
| $1^1E$ | 92 ($48a_2 \rightarrow 108e$) | 0.97 (0.95)[a] | | 0.0004 | |
| $2^1E$ | 50 ($47a_2 \rightarrow 108e$); 38 ($48a_2 \rightarrow 109e$) | 1.35 (1.33) | | 0.0070 | |
| $3^1E$ | 39 ($47a_2 \rightarrow 108e$); 38 ($48a_2 \rightarrow 109e$); 12 ($47a_2 \rightarrow 109e$) | 1.74 (1.73) | | 0.6540 | $Q_1$ |
| $4^1E$ | 75 ($47a_2 \rightarrow 109e$); 14 ($48a_2 \rightarrow 109e$) | 1.82 (1.84) | | 0.1158 | |
| $5^1E$ | 97 ($53b_1 \rightarrow 108e$) | 1.93 (1.95) | | 0.0164 | |
| $6^1E$ | 93 ($52b1 \rightarrow 108e$) | 2.06 (2.06) | | 0.0966 | $Q_2$ |
| $7^1E$ | 72 ($53b_2 \rightarrow 108e$); 26 ($52b_2 \rightarrow 108e$) | 2.22 (2.13) | | 0.0746 | |
| $8^1E$ | 73 ($52b_2 \rightarrow 108e$); 22 ($53b_2 \rightarrow 108e$) | 2.27 (2.28) | | 0.1208 | $Q_3$ |
| $10^1E$ | 97 ($53b_1 \rightarrow 109e$) | 2.38 (2.40) | | 0.0158 | |
| $13^1E$ | 69 ($52b_1 \rightarrow 109e$); 22 ($46a_2 \rightarrow 108e$) | 2.51 (2.51) | | 0.1438 | $Q_4$ |
| $16^1E$ | 88 ($53b_2 \rightarrow 109e$) | 2.59 (2.59) | | 0.0430 | |
| $17^1E$ | 84 ($61a_1 \rightarrow 108e$) | 2.63 (2.61) | | 0.0208 | |
| $20^1E$ | 86 ($51b_1 \rightarrow 108e$) | 2.74 (2.73) | | 0.0220 | |
| $23^1E$ | 48 ($51b_2 \rightarrow 109e$); 34 ($45a_2 \rightarrow 108e$) | 2.93 (2.94) | | 0.0378 | |
| $26^1E$ | 34 ($46a_2 \rightarrow 109e$); 34 ($61a_2 \rightarrow 109e$) | 3.03 (3.04) | | 0.0324 | |
| $28^1E$ | 61 ($48a_2 \rightarrow 110e$); 26 ($103e \rightarrow 63a_1$) | 3.05 (3.06) | | 0.0362 | |
| $30^1E$ | 90 ($51b_1 \rightarrow 109e$) | 3.12 (3.13) | | 0.0208 | |
| $31^1E$ | 76 ($102e \rightarrow 63a_1$) | 3.20 (3.21) | | 0.0604 | |
| $32^1E$ | 86 ($58a_1 \rightarrow 108e$) | 3.26 (3.29) | | 0.0570 | |
| $34^1E$ | 90 ($107e \rightarrow 54b_2$) | 3.34 (3.35) | | 0.0518 | |
| $37^1E$ | 15 ($59a_1 \rightarrow 109e$); 12 ($60a_1 \rightarrow 108e$); 11 ($102e \rightarrow 63a_1$) | 3.43 (3.44) | | 1.3720 | B |
| $38^1E$ | 46 ($57a_1 \rightarrow 108e$); 24 ($60a_1 \rightarrow 109e$) | 3.46 (3.46) | | 0.0470 | |
| $39^1E$ | 53 ($47a_2 \rightarrow 110e$); 15 ($57a_1 \rightarrow 108e$); 15 ($106e \rightarrow 54b_2$) | 3.48 (3.48) | | 0.1524 | |
| $41^1E$ | 56 ($59a_1 \rightarrow 109e$) | 3.53 (3.51) | | 0.4080 | |
| $45^1E$ | 41 ($58a_1 \rightarrow 109e$); 24 ($106e \rightarrow 54b_2$) | 3.66 (3.67) | | 0.2074 | |
| $59^1E$ | 41 ($48a_2 \rightarrow 113e$); 32 ($104e \rightarrow 54b_1$); 15 ($107e \rightarrow 55b_2$) | 4.04 (4.03) | | 0.0496 | |
| $65^1E$ | 38 ($101e \rightarrow 63a1$); 19 ($47a2 \rightarrow 112e$); 10 ($48a_2 \rightarrow 113e$); 10 ($107e \rightarrow 55b_2$) | 4.13 (4.12) | | 0.1802 | |
| $71^1E$ | 40 ($103e \rightarrow 54b_1$); 29 ($105e \rightarrow 55b_1$) | 4.19 (4.19) | | 0.1478 | |
| $78^1E$ | 95 ($104e \rightarrow 55b1$) | 4.28 (4.29) | | 0.0226 | |
| $79^1E$ | 80 ($102e \rightarrow 54b_2$); 11 ($47b_1 \rightarrow 108e$) | 4.30 (4.31) | | 0.0242 | |
| $90^1E$ | 64 ($98e \rightarrow 63a_1$); 10 ($97e \rightarrow 63a_1$) | 4.44 (4.44) | | 0.0518 | |
| $112^1E$ | 39 ($53a_1 \rightarrow 108e$); 14 ($44b_2 \rightarrow 108e$) | 4.60 (4.59) | | 0.0890 | |

[a]The values in parentheses are the results for $(F_{32}Pc)_2LuH$.

# APPENDIX G

## SPECTROELECROCHEMISTRY AND REDOX

Figures and data on chemical reductions, electrochemical reactions and magnetic circular dichroism for $(F_{64}Pc)_2MH$, (M=Lu, Y, Tb and Dy) are presented in this appendix.
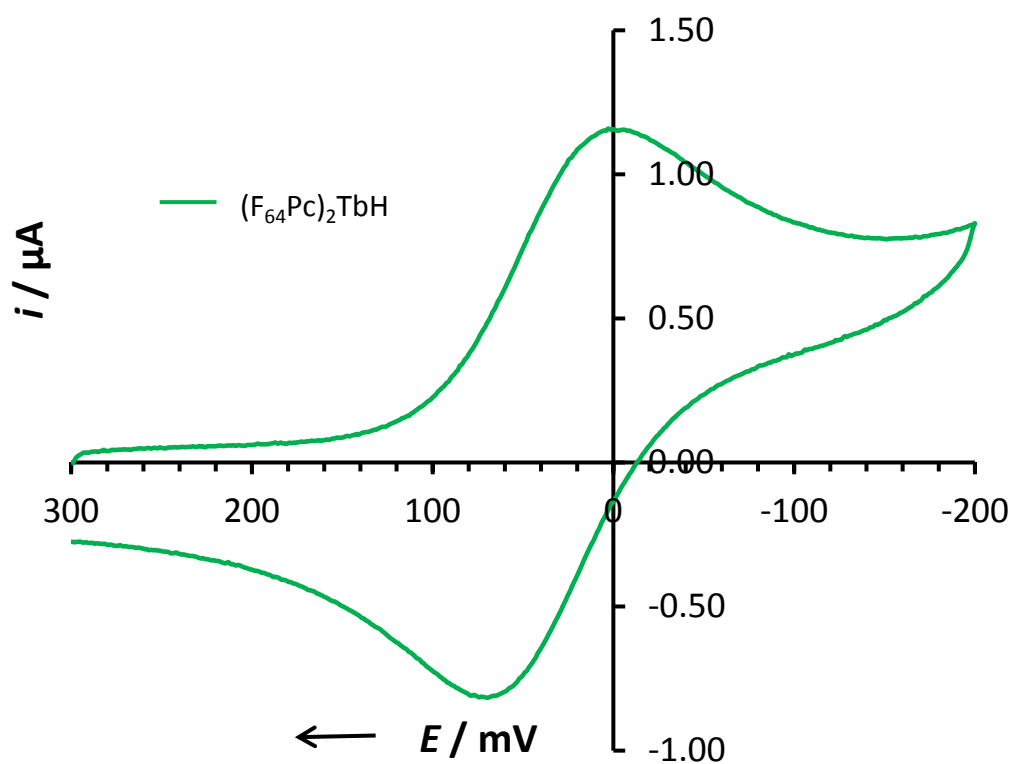


**Figure G.1** Cyclic voltammogram of $(F_{64}Pc)_2TbH$ in 0.1 mol $LiClO_4$/ethanol, platinum working electrode. The peak anodic and cathodic current separation is 67 mV with $E_0 = 36$ mV vs Ag/AgCl. No oxidation is observed. The first, one-electron reduction is highly reversible. Data was provided by BASi, USA.
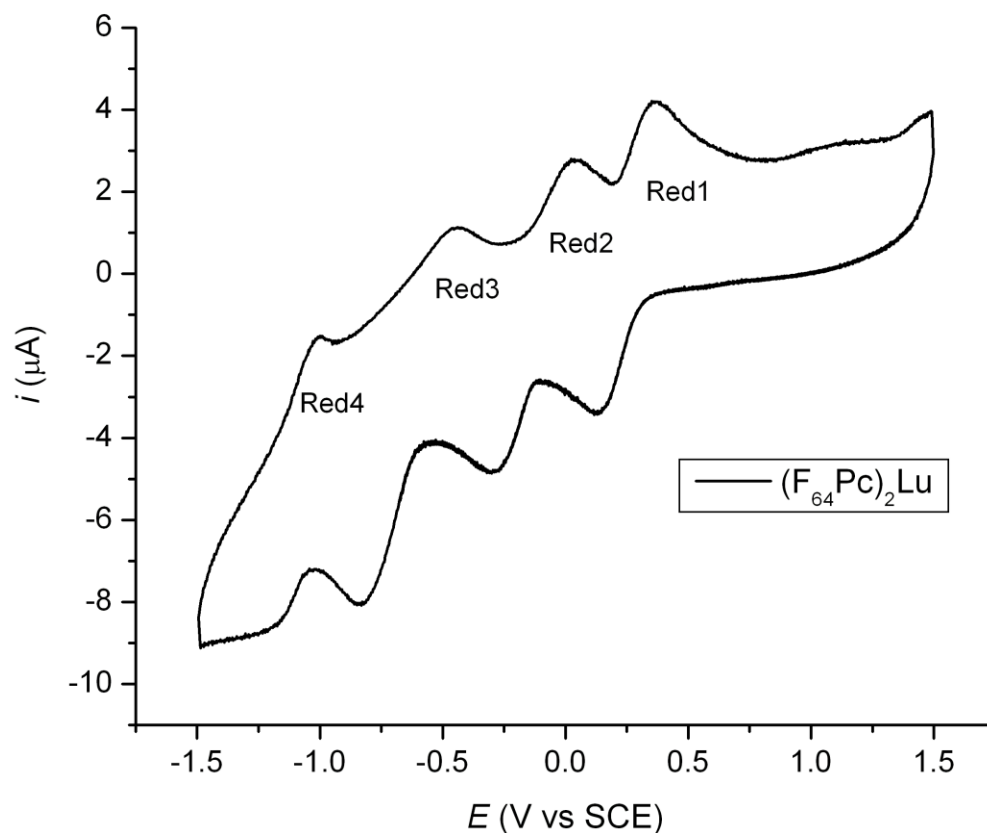
**Figure G.2** Cyclic voltammogram at 100 mV s$^{-1}$ of solution of **1$_{Lu}$** in a 0.1 M electrolyte solution of tetrabutylammonium hexafluorophosphate in acetone. The four reduction processes, Red*n, n* =1, 2, 3, 4 are shown occurring a 0.3 V, 0.03 V, −0.43 V and -1.00 V respectively. The processes occurring 0.3 V and 0.03 V were found to be reversible while the other two were quasi reversible. The oxidation process anticipated to occur beyond 1.5 V is not shown. SCE is Standard Calomel Electrode.
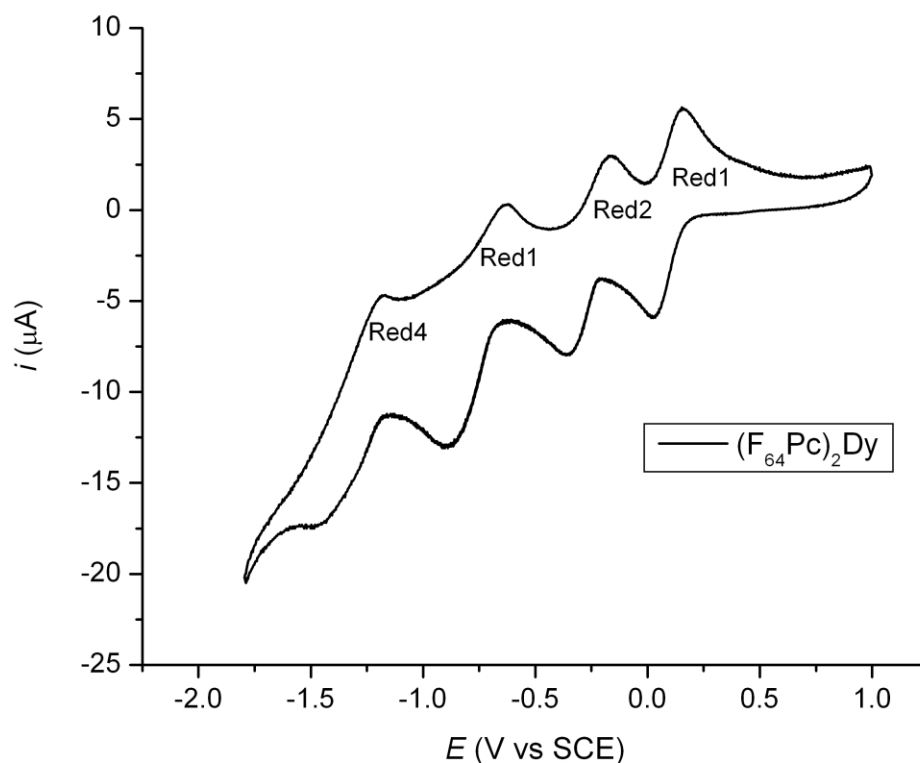
**Figure G.3** Cyclic voltammogram at 100 mV s$^{-1}$ of solution of **1$_{Dy}$** in a 0.1 M electrolyte solution of tetrabutylammonium hexafluorophosphate in acetone.   The four reduction processes, Red*n, n* =1, 2, 3, 4 are shown occurring a 0.15 V, −0.16 V, −0.63 V and −1.19 V, respectively.   The processes occurring 0.3 V and 0.03 V were found to be reversible while the other two were quasi reversible.   The oxidation process anticipated to occur beyond 1.5 V is not shown. SCE is Standard Calomel Electrode.
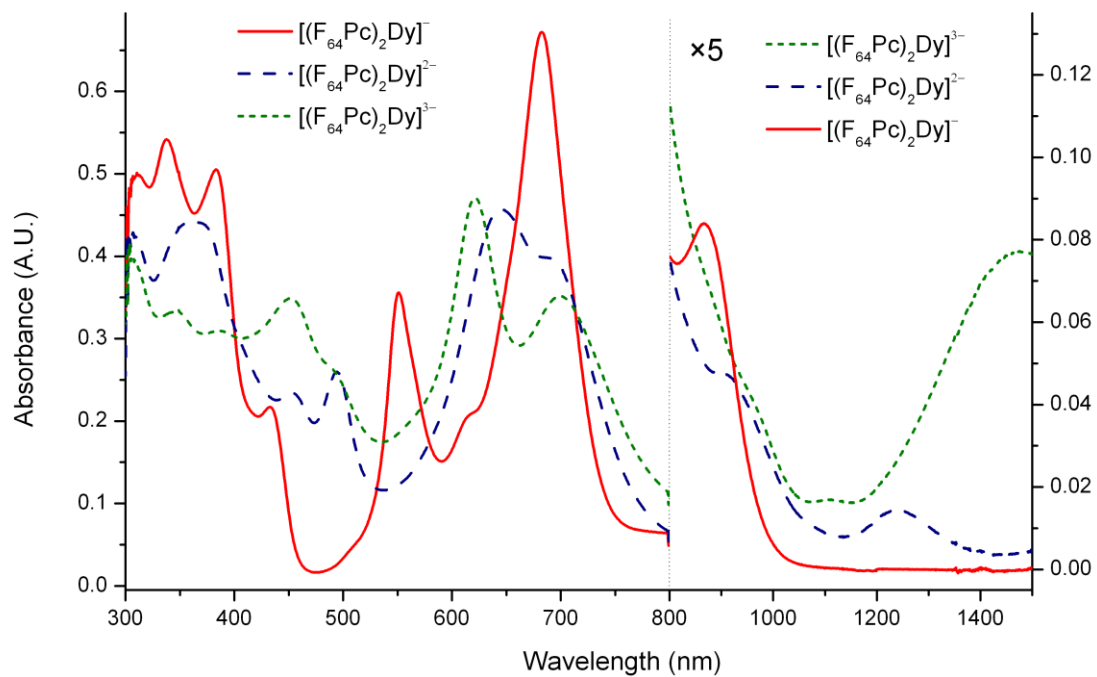
**Figure G.4** UV-visible and NIR absorption spectra of a solution of $[(F_{64}Pc)_2Dy]^-$ in 0.1 M electrolyte solutions of tetrabutylammonium hexafluorophosphate in acetone, and of solutions of $[(F_{64}Pc)_2Dy]^{2-}$ and $[(F_{64}Pc)_2Dy]^{3-}$ generated electrochemically from it.
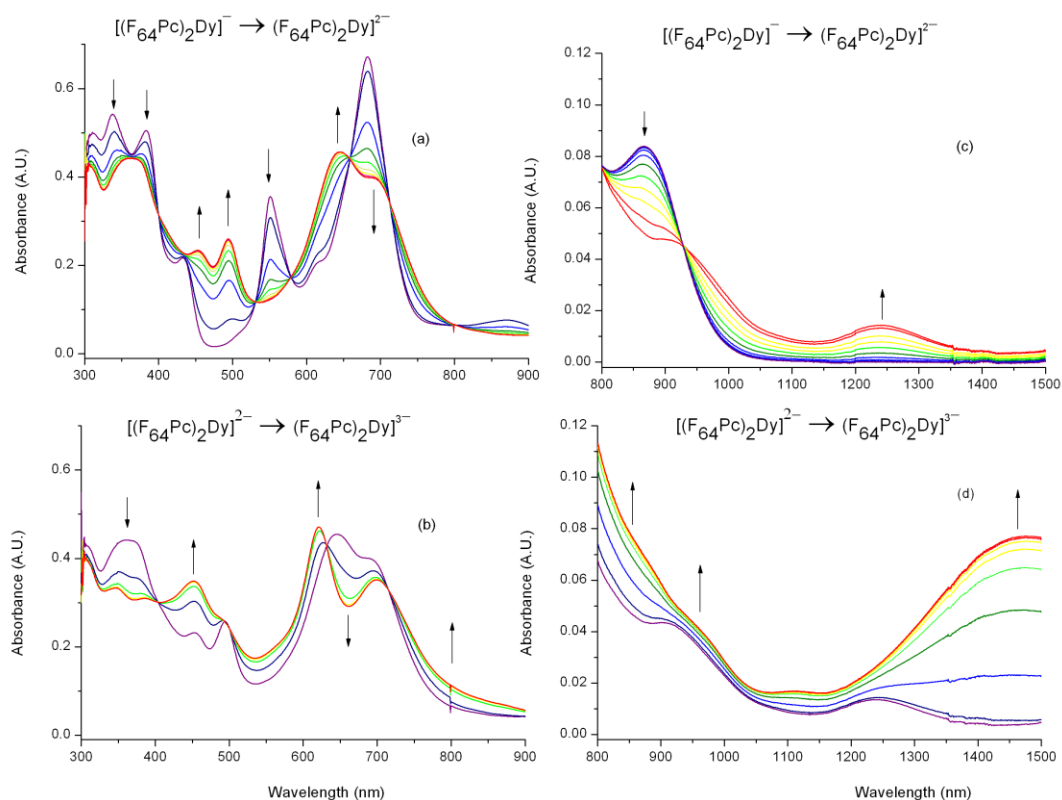
**Figure G.5** Successive UV-visible and NIR spectra during the electrochemical conversions of a solution of $\mathbf{1_{Dy}}^-$ to $\mathbf{1_{Dy}}^{2-}$ applying a potential of −0.25 V vs. Ag/AgCl (top (a) and (c)) and of $\mathbf{1_{Dy}}^{2-}$ to $\mathbf{1_{Dy}}^{3-}$ applying a potential of −0.70 V vs. Ag/AgCl (bottom (b) and (d)) in acetone with 0.1 M tetrabutylammonium hexafluorophosphate.
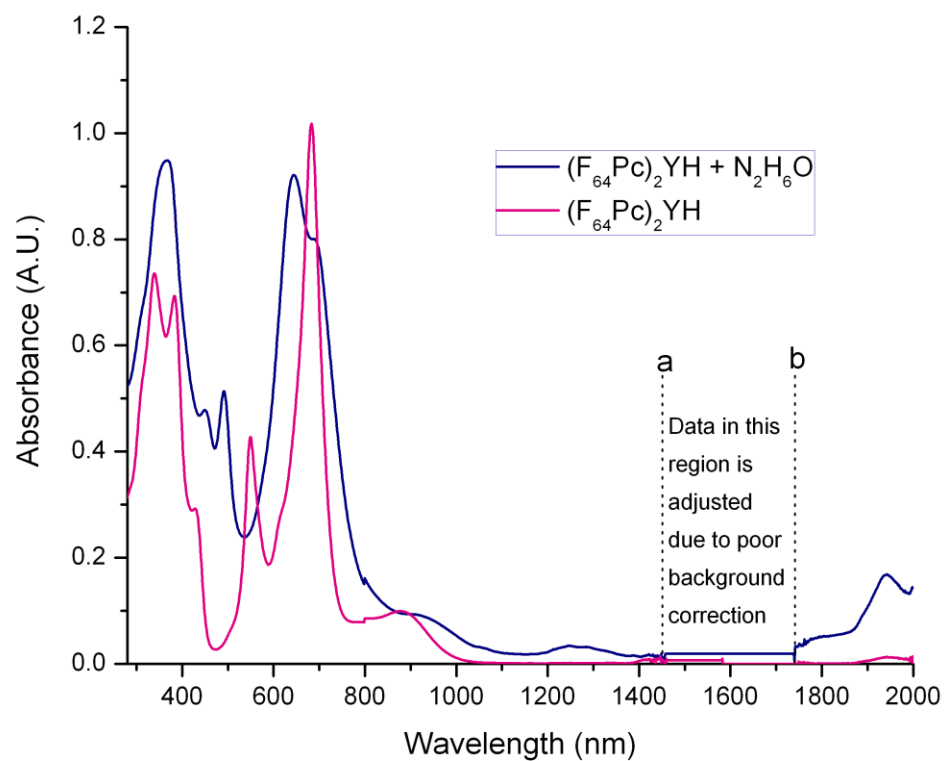
**Figure G.6** Electronic spectra of $(F_{64}Pc)_2YH$ and $(F_{64}Pc)_2YH$ reduced by hydrazine hydrate in methanol.  The spectra of the reduced complex is similar to the electrogenerated $[(F_{64}Pc)_2M]^{2-}$.

# APPENDIX H

## SPECTROSCOPY OF UNIDENTIFIED SYNTHESIS BYPRODUCTS

This appendix covers a summary of the properties of selected byproducts of synthesis for which neither structure nor empirical formula was confirmed.

### H.1 Reaction Byproducts

Several byproducts were synthesized in the microwave assisted reaction carried out to produce the $(F_{64}Pc)_2MH$ (M =Lu, Y, Tb, Dy) complexes. These were differentiated from the main products based on their color and migration rates on silica thin film chromatography (TLC) plates, during purification using flash chromatography and using standard spectroscopic methods such as UV-visible and MS spectroscopy, and NMR. In general, three separate colors of green byproducts were identified. They are referred to in this document as blue green, green and dark green and indexed as **[2-1]**, **[2-2]**, and **[2-3]** respectively.

### H.1.1 First Green Substances

During flash chromatography, the first colored product to elute is a light green product which is usually mixed in with some of the yellow and dark impurities and some un-reacted phthalonitrile. When this fraction was separated, dried and flash chromatography repeated on the said silica gel using a acetone/toluene mixture (20%/80%), two different green fractions were separated. The principal peaks in the UV-visible spectra of these green fractions are shown in the Table H.1. These green substances were separated purely on their mobility during flash chromatography.

**Table H.1** UV-Visible Spectra of "First Greens"

| Sample | Peaks (nm) | | | Shoulders (nm) | |
|---|---|---|---|---|---|
| First green | 692 | 622 | 313 | 361 | 658 |
| Second green | 691 | 623 | 385 | 665 | 421 |

From all indications, these first greens appear to be a mixture of the metal monophthalocyanines with different ligands attached, or may represent complexes which were formed from phthalocyanines that were formed from phthalonitriles that underwent various degrees of fractionation during the microwave synthesis. They were very difficult to separate and since initial MS and electronic spectral data indicated that they were not principally sandwich compounds, further analysis were curtailed.

### H.1.2 The Dark Green, [2-3] Compounds

This dark green colored material, **[2-3]** was obtained during the synthesis of the four identified sandwich compounds. Initially this compound was not identified because it travelled at the same rate as the blue sandwich metal complex on the chromatography column. It could not be adequately removed by flash chromatography. It was removed by dissolution of the sample in either ethyl acetate or acetone and after precipitation of this solution with toluene; some of it remained dissolved in the filtrate. Repeated cycles of this procedure removed more and more of this compound along with traces of the regular green, the metal free and the sandwich species. The UV-visible spectra of the **[2-3]** obtained from the $(F_{64}Pc)_2TbH$ synthesis reaction, $^{dg}$**Tb,** (Figure H.1) exhibited a broadened Q-band suggesting that it may be a sandwich compound. However the absence of the bands at 552 and around 430 nm resulted in a lack of interest these dark green compounds. The absence of the vibronic Q-band at 621 nm differentiates it from

the other green terbium complexes.    It was surmised that these compounds did not contain the $F_{64}Pc^{\bullet-}$ radical anion.  Furthermore, it was difficult to purify this compound using standard chromatography techniques.

A $^{19}F$ NMR spectrum of this compound failed to show the usual three peaks corresponding to the primary aliphatic $CF_3$, the aromatic F and the tertiary aliphatic F. The proton $^1H$ did show peaks.

Mass spectroscopy measurements of $^{dg}Tb$ using the MALDI-TOF negative mode gave a strong peak at 3676.92 amu.  This peak did not appear produce a structure or empirical formula consistent with a logical combination of the probable chemical components.    The combination of the proton NMR peaks, the broad Q-band, the absence of the charge transfer band was pointing to the possibility of the presence of a sandwich compound with some hydrocarbon groups attached.
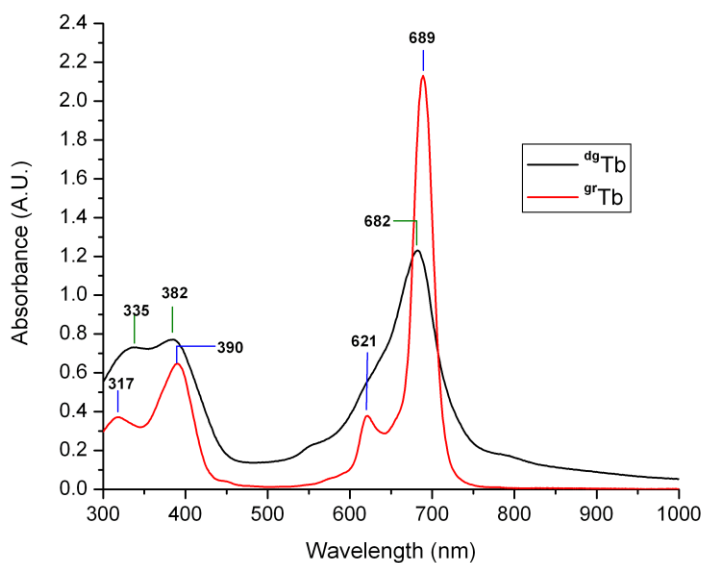


**Figure H.1**  UV-visible spectra of the unknown dark green **[2-3]** terbium phthalocyanine substance, $^{dg}Tb$ and the green **[2-2]** terbium phthalocyanine, $^{gr}Tb$ byproducts.

### H.1.3 The Blue-Green, [2-1] Compounds

After the main purple/bluish product elutes from the chromatography column, a bluish/green **[2-1]** product elutes. A feature of this product was that it initially appears blue on the TLC, but after drying for a few hours it turns green. It was called the blue green species. It was observed for three of the four metal phthalocyanine reactions carried out. A reasonable degree of purity was also achieved with some of these products, because it formed poor crystals in the same solvents as the main sandwich products. However, no X-ray structure was obtained. It also shared some of the UV-visible peaks in common with the **[1]**-**[4]** complexes. The UV-visible and NMR data are shown in Table H.2. There was some evidence to support a possible metal free sandwich structure for this molecule based on:

a) A mass spectroscopy done on two **[2-1]** obtained in the synthesis of **[2]** coded as $^{bg}$**Y** and obtained in the synthesis of **[4]** coded as $^{bg}$**Dy**, returned similar m/z peaks at 4041.65 and 4041.99 Da, respectively, suggesting the presence of a sandwich molecule, possibly attached with an acetate ion fragment. The mass spectroscopy data appeared to support the empirical formula $(F_{64}Pc)_2CH_2CO$. A summary of the data is given in Table H.2

**Table H.2** MALDI-TOF MS Data for the **[2-1]** Compounds ($^{bg}$**Y**) and ($^{bg}$**Dy**).

| Molecule | Matrix, Mode | Calculated Peak (m/z) | Observed Peak (m/z) | Comment |
|---|---|---|---|---|
| $^{bg}$Y | CCA, Negative | 4043.18 | 4041.99 | [M-H$^+$] |
| $^{bg}$Dy | CCA, Negative | 4043.18 | 4041.65 | [M-H$^+$] |

b) The UV-visible data on $^{bg}$**Dy** shows the presence of the Q-band at 688 nm and a main B-band at 404 nm. It shows the band and 552 nm in common with **[1]**-**[4]** complexes, but the band around 430 nm disappears and a new one at around 450 nm appears. The

band at 450 nm is interesting because it is now located in the region where the band associated with the radical $F_{64}Pc^{\bullet-}$ occurs. Another major difference is that the main B-band's absorbance is more intense than the Q-band.

Bench,[110] in her thesis, reported an unknown phthalocyanine of cobalt (III) which she suggested was a dimer and one having a UV-visible spectrum similar to the that of **[2-1]**. It was found to be diamagnetic and having no EPR signal with a $^{19}F$ NMR signal similar to that of the $F_{64}PcZn$. This would be consistent with a low spin $3d^6$ valence shell configuration of Co(III) with the presence of a pair of $F_{64}Pc^{2-}$ ligands in the complex. It was further suggested that the counter ion was a $Na^+$, based on the MS values obtained.
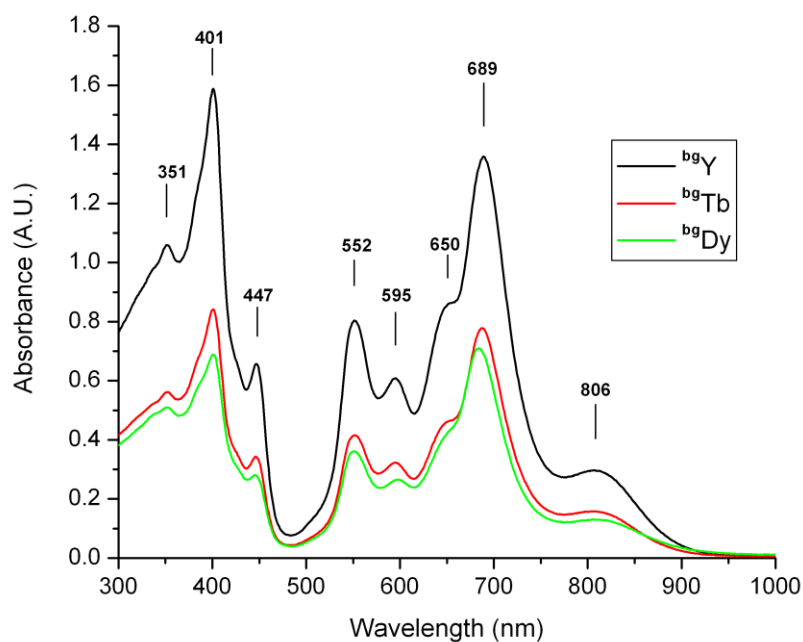


**Figure H.2** UV-visible spectra of some blue/green complexes obtained as byproducts in the synthesis of sandwich perfluoro phthalocyanine complexes of Y, ($^{bg}$Y), Tb, ($^{bg}$**Tb**) and Dy, ($^{bg}$**Dy**). The spectra were carried out in methanol solutions of the samples.

c) The $^{19}$F NMR of three of the **[2-1]** byproducts show the three main peaks found in the

$(F_{64}Pc)_2MH$ complexes.   However, the expected primary aliphatic $CF_3$ shifts, showed a

doublet similar to that found in $(F_{64}Pc)_2YH$.    There appeared to be no statistically

significant differences in shifts in the NMR spectra of **$^{bg}$Y**, **$^{bg}$Tb** and **$^{bg}$Dy** shown on

Table H.3.   They all showed a similar IR spectra which was similar to that of the

$(F_{64}Pc)_2MH$ and $(F_{64}Pc)_2LnH$ compounds.   A representative IR spectrum is shown in

Figure 3.7.

**Table H.3**   $^{19}$F NMR Spectra of  (**$^{bg}$Y**), (**$^{bg}$Tb**) and (**$^{bg}$Dy**) in Acetone $D_6$

| Complex | Primary Aliphatic $CF_3$ shifts, (ppm) and J (Hz) | Aromatic F shifts (ppm) | Tertiary Aliphatic CF shifts, (ppm) |
|---|---|---|---|
| **$^{bg}$Tb** | -71.3, -71.9   (J=170) | -104.7 | -165.1 |
| **$^{bg}$Dy** | -71.3, -71.9   (J=170) | -104.8 | -165.1 |
| **$^{bg}$Y** | -71.3, -71.8   (J=140) | -104.6 | -165.1 |

The $^1$H NMR showed the two shifts at 2.05 and 2.8 which were associated with

trace quantities of water and acetone $D_6$ solvents, respectively[269]  and, which were also

obtained for the $(F_{64}Pc)_2MH$ complexes.  However, it also showed other protons shifts at

3.28, 3.56 and 1.8 ppm.  A table of characteristics $^1$H NMR shifts[270]  lists the peaks for

HC-OH at 3.4-4 ppm, HC-O-R at 3.3-3.4 ppm and R-C-OH at 1-5.5 ppm.   These suggest

the presence of an oxygen atom in the form of ether or an alcohol.

**Table H.4** $^1$H NMR Spectra of  (**$^{bg}$Y**), (**$^{bg}$Tb**) and (**$^{bg}$Dy**) in Acetone $D_6$.

| Compound | Shifts (ppm) | | | | |
|---|---|---|---|---|---|
| **$^{bg}$Tb** | 1.8 | 2.04 | 2.8 | 3.28 | 3.57 |
| **$^{bg}$Dy** | 1.8 | 2.04 | 2.8 | 3.28 | 3.56 |
| **$^{bg}$Y** | 1.8 | 2.04 | 2.8 | 3.28 | 3.56 |

The foregoing analysis has opened two main possibilities. Since **[2-1]** is produced from the synthesis reactions of **[2]**, **[3]** and **[4]** and the UV-visible, IR, MS and NMR spectra are essentially similar for [bg]Y, [bg]Tb and [bg]Dy, then it appears that they are the same compound. Their solubility in polar solvents, while being insoluble less polar solvents such as toluene and hexane suggests possible ionization in these solvents via a proton.

### H.1.4 The Green, [2-2] Compounds

During flash chromatography a green substance, **[2-2]** was always left sticking to the silica gel. Initially it was coded last green. A 50:50 mixture of ethanol/acetone was required to remove most of it. However, further examination of this substance showed that it was a problem, because it appeared to stick to other products as well. The use of finer grained silica gel improved its removal from the other products, but it was time consuming and uneconomical to attempt to purify it. TLC showed it to be a mixture of several green compounds as exhibited by several spots on the plate. Despite these challenges, a level of separation was achieved, adequate enough to run some initial characterization tests. The UV-visible spectrum in Figure H.1, showed that it was different from the four characterized sandwich compounds. It has a narrow Q-band with no transitions in the BV or RV regions. The absence of these bands is supporting evidence of the absence of a π-radical electron. Mass spectroscopy done on the crude product was not conclusive. Despite the low purity of the compound, the MS of the Tb, **[2-2]** compound, [gr]Tb showed two major peaks; one at 2535 Da and the other at 4882 Da, and several lesser peaks, the major ones at 2347, 5137 and 741 Da. The peak at 4882 is a

sum of the peaks of 2347 and 2535 for example. This is suggesting that the bulk of **[2-2]** is monophthalocyanines.

The general structure of the monophthalocyanines, PcM is shown in Figure H.3. In order further elucidate the probable structure of any of the green compounds, an attempt was made to separate the $^{gr}$**Lu** as much as possible and measure the mass of one of its components using electrospray MS.  Again, the result of MS was inconclusive. Based on the synthesis and purification methods, the most likely bidentate/monodentate mono-anionic ligand was the acetate ion.  However, there are several other solvents such as chloroform, ethanol, water and 1-hexanol that could be possible neutral ligands.  There was no success in finding credible combination of ligands which would match the results of the MS of $^{gr}$**Lu** and $^{gr}$**Tb.**
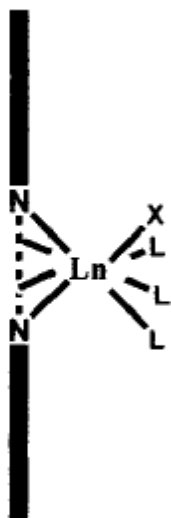


**Figure H.3**  Schematic representation of the octacoordinate  monophthalocyanine lanthanide/ metal(III) (Ln) mixed-ligand complex with X being monodentate and monoanionic and  L being  a monodentate neutral ligand.  In fact, ligand X may also form bi- or multidentate monoanionic units.[52]

For example, the empirical formula $C_{71}F_{64}H_{25}N_8O_3Lu$ representing $Lu(PcF_{64})(OAc)(ethanol)2(1\text{-hexanol})$ with a monoisotopic mass of 2428.0647 Da and an average mass of 2428.8758 Da looked workable. This was suggesting that the acetate ion was the mono-dentate mono-anionic ligand and ethanol and 1-hexanol are the neutral mono-dentate ligands. This overestimates the observed positive MS monoisotopic result of 2426.888 by approximately 1 Da, i.e., $[M+2H]^+$ but would be accurate in the estimate of a negative mode method as $[M-H]^-$.

It is known that monophthalocyanines may be anionic, such as in $[MPcX_2L_2]^-$ (where M is metal(III).[271] The combination of the peaks of the observed 2347 and 2535 to coincide with the observed 4882 peak to in the MS of $^{gr}$**Tb** is suggesting possibility of not only these anionic metal monophthalocyanine ions, but cationic ones as well. This further adds to the challenges of not only separating compounds with different combination of ligands, but ionic species, combinations and possible ligand exchanges during flash chromatography.

A $^{19}$F NMR spectrum of a **[2-2]** substance showed the usual three peaks corresponding to the primary aliphatic $CF_3$, the aromatic F and the tertiary aliphatic F. Further purification of these green colored substances was abandoned because of the challenges and cost and initial data suggested it was outside of the scope of the research.

## H.2 Synthesis Method of the Reduced form $N(C_4H_9)_4[(F_{64}Pc)_2Ln]$

Initially, when the synthesized sandwich compounds were thought to be neutral compounds, an attempt was made to synthesize the reduced form, $TBA[(PcF_{64})_2Tb]$ $TBA = [N(C_4H_9)_4]$ using the method by Moussavi et al.[64] This method was reported

successful in the synthesis of TBA[Pc$_2$Lu].[64]     It was also done because the sandwich (F$_{64}$Pc)$_2$TbH has been shown to have a reversible reaction when reduced by hydrazine in ethanol,  after analyzing the UV-visible spectrum before and after the treatment with hydrazine.   After confirmation of oxidation state of the original sandwich (F$_{64}$Pc)$_2$MH compounds, several attempts were made to synthesize, isolate and fully characterize the TBA[(PcF$_{64}$)$_2$Ln] class of compounds.   However, the attempts were now based on cation exchange in which the original H$^+$ counter-ion was to be replaced by the TBA ion.  The approach was to find synthetic methods which would foster an easy isolation of a TBA[(PcF$_{64}$)$_2$M] complex.

In general, the approach taken was to further reduce the (PcF$_{64}$)$_2$LnH by using either hydrazine hydrate in methanol or KOH in a 1:1 mixture of methanol and acetone. This reduced complex starting from (PcF$_{64}$)$_2$LnH, turned green in color and remained green until the reducing agent was removed.  Addition of TBA either as [TBA]Br or [TBA]ClO$_4$ in excess was expected to add the counter ion, even if the complex was more than one electron reduced.    It was observed that removal of the oxidizing agent and/or dilution resulted in a reversion to a blue colored compound.   However, this compound was much more soluble than the original compound.    The task of removing excess [TBA]Br or [TBA]CLO$_4$ using procedures such as filtration and chromatography, appeared to cause some reversion to (F$_{64}$Pc)$_2$MH as was observed through lowered migration rates during chromatography.  Crystals of the compound were formed from a acetone/chloroform solution, but the crystal structure was not obtained.  In the case of the reaction of the (F$_{64}$Pc)$_2$TbH complex, successive purification and recrystallization

resulted in a crystal structure of the parent $(F_{64}Pc)_2TbH$ complex. This suggested that the protonated form is more stable than the any of the forms produced with TBA.

UV-visible spectra of the blue colored, reverted compound coded as $^{TBA}Ln$ was the same as the respective $(F_{64}Pc)_2LnH$ compound. The IR spectra were also the same. The MS of $^{TBA}Tb$ using MALDI-TOF in negative ion mode, only gave large peaks at m/z of 4159.76 which was the value for the $(F_{64}Pc)_2TbH$ complex.

The $^{19}F$ NMR spectrum of $^{TBA}Y$ in acetone $D_6$ was not statistically different from $(F_{64}Pc)_2YH$. Proton ($^1H$) NMR of $^{TBA}Y$ in the same solvents did not show any statistical difference from the pure [TBA]ClO$_4$. The presence of the TBA ion was confirmed but whether it had replaced the proton was unknown. To further study the problem, the $^{19}F$ and $^1H$ NMR of the $^{TBA}Tb$ were carried out using the similar conditions as for the $^{TBA}Y$.

**Table H.5** Comparison of the NMR Values of $^{TBA}Y$ and $^{TBA}Tb$ with Those of the TBA$^+$ ion and $(F_{64}Pc)_2TbH$

| Compound/ Reaction | $^1H$ NMR in Acetone D$_6$ | | | |
|---|---|---|---|---|
| | δ (Np(C)-CH$_2$, 8H (ppm) | δ 8H, CH$_2$ (ppm) | δ 8H, CH$_2$ (ppm) | δ 12H, R-CH$_3$ (ppm) |
| [TBA]$^+$ (calc.) | *Triplet* 3.24 | *Doublets of triplets* 1.73 | *Doublet of quartets*, 1.33 | *Triplet* 0.96 |
| [TBA]ClO$_4$ (obs.) | 3.43 | 1.81 | 1.42 | 0.98 |
| $^{TBA}Y$ | 3.47 | 1.85 | 1.45 | 0.99 |
| $^{TBA}Tb$ | 3.31 | 1.67 | 1.28 | 0.83 |
| | | | | |
| Copound/ Reaction | $^{19}F$ NMR in Acetone D$_6$ Relative to CFCl$_3$ | | | |
| | δ, **Primary Aliphatic CF$_3$** ppm | δ, **Ar-F**, ppm | δ, **Tertiary Aliphatic CF,** ppm | |
| $^{TBA}Y$ | d, −71.5, −71.8 | s, −103.5 | s, −165.0 | |
| $^{TBA}Tb$ | s,−83.6 | s,−122.3 | s, −195.0 | |
| $(F_{64}Pc)_2TbH$ | s, −82.1 | s, −119.3 | s, −193.0 | |

Key: s = Singlet; d = doublet

Table H.5 which summarizes the data, shows statistically significant differences between the NMR of $^{\text{TBA}}$**Tb** and $(F_{64}Pc)_2TbH$. Notably, in the $^{19}F$ NMR, the differences between $^{\text{TBA}}$**Tb** and $(F_{64}Pc)_2TbH$ were: 1.5 ppm for the primary aliphatic $CF_3$, 3.0 ppm for the aromatic F and 2.0 ppm for the tertiary aliphatic CF. While these results provide some evidence of the presence of the $[TBA]^+$ ion attachment to the $[(F_{64}Pc)_2M]^-$ ion, the existence of the compound has not been confirmed.

# REFERENCES

1. Linert, W.; Verdaguer, M., *Molecular Magnets: Recent Highlights*. Springer: 2003.

2. Miller, J. S., *Dalton Transactions* **2006,** *2006*, 2742-2749.

3. Pilawa, B., *Annals of Physics* **1999,** *8* (3), 191-254.

4. Gómez-Segura, J.; Diéz-Pérez, I.; Ishikawa, N.; Nakano, M.; Veciana, J.; Ruiz-Molina, D., *Chemical Communications* **2006**, 2866-2868.

5. Lu, F.; Yang, Q.; Cui, J.; Yan, X., *Spectrochimica Acta Part A* **2006,** *65*, 221-228.

6. Ishikawa, N.; Lino, T.; Kiazu, Y., *Journal of the American Chemical Society* **2002,** *124*, 11440-11447.

7. Ishikawa, N.; Sugita, M.; Tanaka, N.; Ishikawa, T.; Koshihara, S.; Kaizu, Y., *Inorganic Chemistry* **2004,** *43* (18), 5498 - 5500.

8. Ishikawa, N., Phthalocyanine-Based Magnets. In *Functional Phthalocyanine Molecular Materials*, Jiang, J., Ed. Springer Berlin / Heidelberg: 2010; Vol. 135, pp 211-228.

9. Katoh, K.; Yoshida, Y.; Yamashita, M.; Miyasaka, H.; Breedlove, B. K.; Kajiwara, T.; Takaishi, S.; Ishikawa, N.; Isshiki, H.; Zhang, Y. F.; Komeda, T.; Yamagishi, M.; Takeya, J., *Journal of the American Chemical Society* **2009,** *131* (29), 9967-9976.

10. Kahlal, S.; Mentec, A.; Pondaven, A.; L'Her, M.; Saillard, J.-Y., *New Journal of Chemistry* **2009,** *33* (3), 574-582.

11. Braun, A.; Tcherniac, J., *Berichte Der Deutschen Chemischem Geselleschaft* **1907,** *40*, 2709.

12. Lever, A. P. B.; Hempstead, M. R.; Leznoff, C. C.; Liu, W.; Melnik, M.; Nevin, W. A.; Seymour, P., *Pure and Applied Chemistry* **1986,** *58* (11), 1467-1476.

13. Byrne, G. T.; P., L. R.; Lowe, A. R., *Journal of the Chemical . Society* **1934**, 1017.

14. Dent, C. E.; Linstead, R. P., *Journal of the Chemical Society* **1934**, 1027-31.

15. Dent, C. E.; Linstead, R. P.; Lowe, A. R., *Journal of the Chemical Society* **1934**, 1033-9.

16. Elvidge, J. A.; Linstead, R. P., *Journal of the Chemical . Society* **1955**, 3536.

17. Linstead, R. P., *Journal of the Chemical Society* **1934**, 1016-17.

18. Linstead, R. P.; Lowe, A. R., *Journal of the Chemical Society* **1934**, 1031-3.

19. Linstead, R. P.; Lowe, A. R., *Journal of the Chemical Society* **1934**, 1022-7.

20. Kobayashi, N.; Ashida, T.; Osa, T., *Chemistry Letters* **1992,** *21* (10), 2031-2034.

21. Kobayashi, N.; Sasaki, N.; Higashi, Y.; Osa, T., *Inorganic Chemistry* **1995,** *34* (7), 1636-7.

22. Takahashi, K.; Kawashima, M.; Tomita, Y.; Itoh, M., *Inorganica Chimica Acta* **1995,** *232*, 69-73.

23. Tomoda, H.; Saito, S.; Shiraishi, S., *Chemistry Letters* **1983**, 313-316.

24. Oksengendler, I. G.; Kondratenko, N. V.; Luk'yanets, E. A.; Yagupol'skii, L. M., *Zhurnal Organicheskoi Khimii* **1977,** *13* (7), 1554-8.

25. Yang, J.; Van De Mark, M., *Heterocyclic Chemistry* **1995,** *32,* (5), 1521-4.

26. Pawlowski, G.; Hanack, M., *Synthetic Communications* **1981,** *11* (5), 351-363.

27. Huheey, J. E., *Inorganic Chemistry: Principles of Structure and Reactivity*. 2nd ed.; John Wiley and Sons, Inc.: New York, 1978.

28. Cotton, F. A.; Wilkinson, G., *Advanced Inorganic Chemistry: A Comprehensive Text*. 4th ed.; John Wiley and Sons Inc.: New York, 1980.

29. Moeller, T., *Journal of Chemical Education* **1970,** *47*, 417.

30. Pitzer, K. S., *Accounts of Chemical Research* **1979,** *12* (8), 271-276.

31. Conway, J. G.; Wybourne, B. G., *Physical Review* **1963,** *130* (6), 2325.

32. Barbara, B.; Gunther, L. In *Quantum Tunneling of Magnetization*, QTM 94, 2005; Kluwer Academic Publishers: 1994.

33. Bohigas, X.; Hernandez, J. M.; Teheda, J.; Torres, F., *Applied Physics Letters* **2000,** *77* (20), 3248-3250.

34. Caneschi, A.; Gatteschi, D.; Pardi, L.; Sessoli, R., *Science* **1994,** *265* (5175), 1054-1058.

35. Chudnovsky, E. M., *Science* **1996,** *274* (8), 938-939.

36.     Dressel, M.; Gorshunov, B. Molecular Magnets. <http://www.pi1.physik.uni-stuttgart.de/Forschung/MolMagn_e.html> (accessed 12/26/2010).

37.     Gatteschi, D. QuantumTunneling in $Mn_{12}$-ac. <http://www.ln-w3.polycnrs-gre.fr/themes/nano/mn12/> (accessed 12/26/2010).

38.     Khanna, S. N.; Kortus, J.; Pederson, M. R.; Porezag, D. V., *Journal of Applied Physics* **2000,** *87* (9), 5487-5489.

39.     Miller, J. S., *Advanced Materials* **1992,** *4* (4), 298-300.

40.     Bogani, L.; Wernsdorfer, W., *Nature Materials* **2008,** *7* (3), 179-186.

41.     Romeike, C.; Wegewijs, M. R.; Hofstetter, W.; Schoeller, H., *Physical Review Letters* **2007,** *96* (19), 196601.

42.     Kahn, O., *Magnetism: A Supramolecular Function*. Kluwer Academic Publishing: Netherlands, 1996.

43.     Carretta, P.; Gatteschi, D.; Lascialfari, A., *Physica B.* **2000,** *289-290*, 94-105.

44.     Epstein, J. A.; Miller, J. S., *Journal of the American Chemical Society* **1995,** *6*, 161-185

45.     Miller, J. S., *Inorganic Chemistry* **2000,** *39*, 4392-4408.

46.     Kahn, O., *Nature* **1995,** *378* (14), 667-668.

47.     Miller, J. S., *The Philosophical Transactions of the Royal Society A* **1999,** *357*, 3159-3961.

48.     Mills, D. P.; Moro, F.; McMaster, J.; van Slageren, J.; Lewis, W.; Blake, A. J.; Liddle, S. T., *Nat Chem* **2011,** *3* (6), 454-460.

49.     Morton, J. J. L.; Tyryshkin, A. M.; Brown, R. M.; Shankar, S.; Lovett, B. W.; Ardavan, A.; Schenkel, T.; Haller, E. E.; Ager, J. W.; Lyon, S. A., *Nature* **2008,** *455* (7216), 1085-1088.

50.     Ahn, J.; Weinacht, T. C.; Bucksbaum, P. H., *Science* **2000,** *287* (5452), 463-465.

51.     Li, L.; Tang, Q.; Li, H.; Hu, W.; Yang, X.; Shuai, Z.; Liu, Y.; D., Z., *Pure and Applied Chemistry* **2008,** *80* (11), 2231-2240.

52.     Weiss, R.; Fischer, J., *Lanthanide Phthalocyanine Complexes*. Academic Press: San Diego, 2003; Vol. 16, p 171-246.

53.     Tomilova, L. G.; Dyumaev, K. M.; Tkachenko, O. P., *Russian Chemical Bulletin* **1995,** *44* (3), 410-415.

54. Kirin, I. S.; Moskalev, P. N.; Makashev, Y. A., *Zhurnal Neorganicheskoi Khimii* **1965,** *10* (8), 1951-3.

55. De Cian, A.; Moussavi, M.; Fischer, J.; Weiss, R., *Inorganic Chemistry* **1985,** *24* (20), 3162-7.

56. Sleven, J.; Görller-Walrand, C.; Binnemans, K., *Materials Science and Engineering. C* **2001,** *18*, 229-238.

57. L'Her, M.; Cozien, Y.; Courtot-Coupez, J., *Journal of Electroanalytical Chemistry and Interfacial Electrochemistry* **1983,** *157* (1), 183-187.

58. Lee, C.-H.; Ng, D. K. P., *Tetrahedron Letters* **2002,** *43*, 4211-4214.

59. Cook, M. J.; Dunn, A. J.; Howe, S. D.; Thomson, A. J.; Harrison, K. J., *Journal of the Chemical Society, Perkin Transactions 1:  Organic and Bio-Organic Chemistry* **1988,** *8*, 2453-8.

60. Shaabani, A.; Maleki, A., *Journal of Porphyrins and Phthalocyanines* **2006,** *10*, 1253-1258.

61. Liu, W.; Jiang, J.; Pan, N.; Arnold, D. P., *Inorganica Chimica Acta* **2000,** *310*, 140-146.

62. Pushkarev, V. E.; Breusova, M. O.; Nefedov, S. E.; Tomilova, L. G., *Mendeleev Communications* **2007,** *17*, 220-221.

63. Konami, H.; Hatano, M.; Tajiri, A., *Chemical Physics Letters* **1989,** *160* (2), 163-7.

64. Moussavi, M.; De Cian, A.; Fischer, J.; Weiss, R., *Inorganic Chemistry* **1988,** *27* (7), 1287-91.

65. Takamatsu, S.; Ishikawa, N., *Polyhedron* **2007,** *26* (9-11), 1859-1862.

66. Carnieri, N.; Harriman, A., *Inorganica Chimica Acta* **1982,** *62*, 103-107.

67. Gans, P.; Buisson, G.; Duée, E.; Marchon, J.-C.; Erler, B. S.; Scholz, W. F.; Reed, C. A., *Journal of the American Chemical Society* **1986,** *108* (6), 1223-1234.

68. Kasuga, K.; Ando, M.; Morimoto, H.; Isa, M., *Chemistry Letters* **1986**, 1095-1098.

69. Guyon, F.; Pondaven, A., *Journal of the Chemical Society, Chemical Communications* **1994,** *9*, 1125-6.

70. Takahashi, K.; Itoh, M.; Tomita, Y.; Nojima, K.; Kasuga, K.; Isa, K., *Chemistry Letters* **1993,** *11*, 1915-18.

71. Takahashi, K.; Shimoda, J.-I.; Itoh, M.; Fuchita, Y.; Okawa, H., *Chemistry Letters* **1998,** *2*, 173-174.

72. Guyon, F.; Pondaven, A.; Guenot, P.; L'Her, M., *Inorganic Chemistry* **1994,** *33* (21), 4787-93.

73. Ishikawa, N.; Kaizu, Y., *Chemical Physics Letters* **1994,** *228* (6), 625-32.

74. Ishikawa, N.; Kaizu, Y., *Chemical Physics Letters* **1995,** *1* (2), 50-6.

75. Ishikawa, N.; Okubo, T.; Kaizu, Y., *Inorganic Chemistry* **1999,** *38* (13), 3173-3181.

76. Jones, R.; Hunter, R. A.; Davidson, K., *Thin Solid Films* **1994,** *250*, 249-257.

77. Liu, Y.; Shigehara, K.; Hara, M.; Yamada, A., *Journal of the American Chemical Society* **1991,** *113* (2), 440-3.

78. Liu, Y.; Shigehara, K.; Yamada, A., *Thin Solid Films* **1989,** *179*, 303-8.

79. Lukas, B.; Lovett, D. R.; Silver, J., *Thin Solid Films* **1992,** *210-211* (1-2), 213-15.

80. Petty, M., Lovett, D. R.; O'Connor, J. M.; Silver, J., *Thin Solid Films* **1989,** *179*, 387-95.

81. Rodriguez-Mendez, M. L.; Aroca, R.; DeSaja, J. A., *Chemistry of Materials* **1992,** *4* (5), 1017-20.

82. Battisti, D.; Tomilova, L.; Aroca, R., *Chemistry of Materials* **1992,** *4* (6), 1323-8.

83. Ray, A. K.; Exley, J.; Ghassemlooy, Z.; Crowther, D.; Ahmet, M. T.; Silver, J., *Vacuum* **2001,** *61* (1), 19-27.

84. Bai, R.; Chen, H.-Z.; Zhou, H.-B.; Shi, M.-M.; Wang, M., *Journal of Crystal Growth* **2005,** *285*, 183-190.

85. Dhanabalan, A.; Gaffo, L.; Barros, A. M.; Moreira, W. C.; Oliveira, O. N., Jr., *Langmuir* **1999,** *15* (11), 3944-3949.

86. Trojan, K. L.; Kendall, J. L.; Kepler, K. D.; Hatfield, W. E., *Inorganica Chimica Acta* **1992,** *198-200*, 795-803.

87. Bernot, K.; Bogani, L.; Sessoli, R.; Gatteschi, D., *Inorganica Chimica Acta* **2007,** *360* (13), 3807-3812.

88. Ishikawa, N., *Polyhedron* **2007,** *26* (9-11), 2147-2153.

89. Ishikawa, N.; Sugita, M.; Tanaka, N.; Ishikawa, T.; Koshihara, S.; Kaizu, Y., *Journal of the American Chemical Society* **2003,** *125*, 8694 - 8695.

90.     Ishikawa, N.; Otsuka, S.; Kaizu, Y., *Angew Chem. Int. Ed* **2005,** *44*, 731 - 733.

91.     Ishikawa, N.; Sugita, M.; Wernsdorfer, W., *Angew Chem* **2005,** *44*, 2931-2935.

92.     Liu, Y.; Shigehara, K.; Hara, M.; Yamada, A., *Journal of the American Chemical Society* **1991,** *113* (2), 440-443.

93.     Nicholson, M. M., *Industrial & Engineering Chemistry Product Research and Development* **1982,** *21* (2), 261-6.

94.     Kirin, I. S.; Moskalev, P. N., *Zhurnal Fizicheskoi Khimii* **1967,** *41* (2), 497-9.

95.     de Saja, J. A.; Rodríquez-Méndez, M. L., *Advances in Colloid and Interface Science* **2005,** *116*, 1-11.

96.     Madru, R.; Guillaud, G.; Al Sadoun, M.; Maitrot, M.; Andre, J. J.; Simon, J.; Even, R., *Chemical Physics Letters* **1988,** *145* (4), 343-6.

97.     Madru, R.; Guillaud, G.; Al Sadoun, M.; Maitrot, M.; Schunck, J. P., *Chemical Physics Letters* **1990,** *168* (1), 41-4.

98.     Liu, M. O.; Tai, C.-H.; Hu, T. A.; Wei, T.-H., *Journal of Organometallic Chemistry* **2004,** *689*, 2138-2143.

99.     Belarbi, Z.; Sirlin, C.; Simon, J.; Andre, J.-J., *Journal of Physical Chemistry* **1989,** *93* (24), 8105-10.

100.    Toupance, T.; Bassoul, P.; Mineau, L.; Simon, J., *Journal of Physical Chemistry* **1996,** *100* (28), 11704-11710.

101.    Toupance, T.; Plichon, V.; Simon, J., *New Journal of Chemistry* **1999,** *23* (10), 1001-1006.

102.    Gorun, S. M.; Bench, B. A.; Carpenter, G.; Beggs, M. W.; Mague, J. T.; Ensley, H. E., *Journal of Fluorine Chemistry* **1998,** *91*, 37- 40.

103.    Jiang, J.; Xie, J.; Choi, M. T. M.; Yan, Y.; Sun, S.; Ng, D. K. P., *Journal of Porphyrins and Phthalocyanines* **1999,** *3* (4), 322-328.

104.    Clarisse, C.; Riou, M. T., *Inorganica Chimica Acta* **1987,** *130* (139-144).

105.    Allen, F., *Acta Crystallographica Section B* **2002,** *58* (3 Part 1), 380-388.

106.    Ostendorp, G.; Homborg, H., *Zeitschrift fuer Naturforschung, B: Chemical Sciences* **1995,** *50* (8), 1200-6.

107.    Buchler, J. W.; De Cian, A.; Fischer, J.; Kihn-Botulinski, M.; Paulus, H.; Weiss, R., *Journal of the American Chemical Society* **1986,** *108* (13), 3652-9.

108.  Buchler, J. W.; De Cian, A.; Fischer, J.; Kihn-Botulinski, M.; Weiss, R., *Inorganic Chemistry* **1988,** *27* (2), 339-45.

109.  Liao, M.-S.; Graham, W.; Gorun, S. M.; Huang, M.-J.; Watts, J. D., Electronic Structure, Bonding, and Optical Spectra of Unsubstituted and Fluorinated Yttrium and Lutetium Bis(phthalocyanine)s. A Theoretical Study. 2011.

110.  Bench, B. A. The Synthesis and Reactivity of Novel Perfluorinated Phthalonitriles and Phthalocyanines. Ph.D, Brown University, Rhode Island, USA, 2001.

111.  Derome, A. E., *Modern NMR Techniques for Chemistry Research*. Pergamon Press: Oxford, 1987.

112.  Buchanan, G. W.; Munteanu, E.; Dawson, B. A.; Hodgson, D., *Magnetic Resonance in Chemistry* **2005,** *43* (7), 528-534.

113.  Goecke, C. M.; Jarnot, B. M.; Reo, N. V., *Chemical Research in Toxicology* **1992,** *5* (4), 512-19.

114.  Ribeiro, A. A.; Umayahara, K., *Magnetic Resonance in Chemistry* **2003,** *41* (2), 107-114.

115.  Macrae, C. F.; Bruno, I. J.; Chisholm, J. A.; Edgington, P. R.; McCabe, P.; Pidcock, E.; Rodriguez-Monge, L.; Taylor, R.; van de Streek, J.; Wood, P. A., *Journal of Applied Crystallography* **2008,** *41* (2), 466-470.

116.  Marat, K. *SpinWorks Software Package for the Processing of 1D and 2D Data*, 3.1.6; Manitoba, 2009.

117.  Spyroulias, G. A.; Coutsolelos, A. G., *Inorganic Chemistry* **1996,** *35* (5), 1382-1385.

118.  Spyroulias, G. A.; Coutsolelos, A. G.; Raptopoulou, C. P.; Terzis, A., *Inorganic Chemistry* **1995,** *34* (9), 2476-9.

119.  Campbell, D.; Petrick, R. A.; White, J. R., *Polymer Characterization: Physical Techniques*. 2$^{nd}$ ed.; Stanley Thornes: Cheltenham, U.K., 2000.

120.  Jiang, J.; Bao, M.; Rintoul, L.; Arnold, D. P., *Coordination Chemistry Reviews* **2006,** *250* (3-4), 424-448.

121.  Bao, M.; Wang, R.; Rintoul, L.; Liu, Q.; Arnold, D. P.; Ma, C.; Jiang, J., *Polyhedron* **2006,** *25* (5), 1195-1203.

122.  Jiang, J.; Arnold, D. P.; Yu, H., *Polyhedron* **1999,** *18*, 2129-2139.

123.  Lu, F.; Zhang, L.; Liu, H.; Yan, X., *Vibrational Spectroscopy* **2005,** *39* (2), 139-143.

124. Ostendorp, G.; Homborg, H., *Zeitschrift fuer Anorganische und Allgemeine Chemie* **1996,** *622* (7), 1222-1230.

125. Haghighi, M. S.; Homborg, H., *Zeitschrift fuer Anorganische und Allgemeine Chemie* **1994,** *620* (7), 1278-84.

126. Socrates, G., *Infrared Characteristics Group Frequencies - Tables and Charts, 2nd Ed*. New York, 1994.

127. Nakanishi, K.; Solomon, P. H., *Infrared Absorption Spectroscopy*. 2nd ed.; Emerson-Adams Press Incorporated: Boca Raton, 1998.

128. Kim, J.-B.; Lim, S.-T., *Polymer Bulletin* **1996,** *37* (3), 297-303.

129. Kittel, C., *Introduction to Solid State Physics*. 5th ed.; John Wiley & Sons Inc.: New York, 1976.

130. Weckhuysen, B. M.; Heidler, R.; Schoonheydt, R. A., *Molecular Sieves* **2004,** *4*, 295-335.

131. Pilbrow, J. R., *Transition Ion Electron Paramagnetic Resonance*. Clarendon Press, Oxford: New York, 1990.

132. Atherton, N. M., *Electron Spin Resonance, Theory and Applications*. Ellis Horwood: Chichester, 1973.

133. Mabbs, F. E., *Chemical Society Reviews* **1993,** *22* (5), 313-324.

134. Agrawal, M. "Bruker ESR System" in Fundamental Physics in Nano-Structured Materials and Devices (Stanford University) 2008. http://www.stanford.edu/~mukul/tutorials. (accessed 1/23/2011).

135. Hatscher, S.; Schilder, H.; Lueken, H.; Urland, W., *Pure and Applied Chemistry* **2005,** *77* (2), 497-511.

136. Drago, R. S., *Physical Methods For Chemists*. 2nd ed.; Saunders College Publishing: Forth Worth, 1992.

137. Casey, A. T., Theoretical principles of Paramagnetism. In *Theory and Applications of Molecular Paramagnetism*, Boudreaux, E. A.; Mulay, L. N., Eds. Wiley-Interscience: New York, 1976

138. Clarke, J., *Scientific American* **1994,** *271* (2), 46.

139. Josephson, B. D., *Reviews of Modern Physics* **1974,** *46* (2), 251.

140. Barone, A.; Paterno, G., *Physics and Applications of the Josephson Effect*. John Wiley & Sons: New York, 1982.

141. Rohlf, J. W., *Modern Physics from Alpha to Z0*. 1st ed.; John Wiley & Sons: 1994.

142. Bouchiat, V.; Vion, D.; Joyez, P.; Esteve, D.; Devoret, M. H., *Physica Scripta* **1998,** *1998* (T76), 165-170.

143. McElfresh, M. Fundamentals of Magnetism and Magnetic Measurements. Featuring Quantum Design's Magnetic Property Measurement System. http://www.qdusa.com/sitedocs/appNotes/mpms/FundPrimer.pdf (accessed 1/29/11).

144. Bain, G. A.; Berry, J. F., *Journal of Chemical Education* **2008,** *85* (4), 532-536.

145. Haynes, W. M., *CRC Handbook of Chemistry and Physics*. 91 ed.; National Institute of Standards and Technology: Boulder, 2010.

146. Bleaney, B.; Bowers, K. D., *Proceedings of the Royal Society of London. Series A. Mathematical and Physical Sciences* **1952,** *214* (1119), 451-465.

147. Fisher, M. E., *American Journal of Physics* **1964,** *32* (5), 343-346.

148. Bonner, J. C.; Fisher, M. E., *Physical Review* **1964,** *135* (3A), A640.

149. Rueff, J.-M.; Masciocchi, N.; Rabu, P.; Sironi, A.; Skoulios, A., *European Journal of Inorganic Chemistry* **2001,** *2001* (11), 2843-2848.

150. Tyree, W. S. Correlation of Structure and Magnetic Properties in Charge-Transfer Salt Molecular Magnets Composed of Decamethylmetallocene Electron Donors and Organic Electron Acceptors. Virginia Polytechnic Institute and State University, Blacksburg, 2005.

151. Castaneda, F.; Piechocki, C.; Plichon, V.; Simon, J.; Vaxiviere, J., *Electrochimica Acta* **1986,** *31* (1), 131-133.

152. Paillaud, J. L.; Drillon, M.; De Cian, A.; Fischer, J.; Weiss, R.; Villeneuve, G., *Physical Review Letters* **1991,** *67* (2), 244.

153. Petit, P.; Spegt, P., *Journal de Physique (France)* **1990,** *51* (15), 1645-1654.

154. Vogt, O.; Mattenberger, K.; Löhle, J.; Rebizant, J., *Journal of Alloys and Compounds* **1998,** *271-273* (0), 508-512.

155. Dattelbaum, A. M.; He, L.; Tsui, F.; Martin, J. D., *Journal of Alloys and Compounds* **2002,** *338*, 173–184.

156. Van Vleck, J. H., *Electric and Magnetic Susceptibilities*. Oxford University Press: London, 1932.

157. Takahashi, K.; Tomita, Y.; Hada, Y.; Tsubota, K.; Handa, M.; Kasuga, K.; Sogabe, K.; Tokii, T., *Chemistry Letters* **1992,** *21* (5), 759-762.

158.    Markovitsi, D.; Tran-Thi, T.-H.; Even, R.; Simon, J., *Chemical Physics Letters* **1987,** *137* (2), 107-112.

159.    L'Her, M.; Cozien, Y.; Courtot-Coupez, J., *CR. Acad. Sci. Ser. II* **1986,** *302* (1), 9-14.

160.    Wojdyr, M., *Journal of Applied Crystallography* **2010,** *43* (5 Part 1), 1126-1128.

161.    Brown, A. J., *IEEE Transactions on Geoscience and Remote Sensing* **2006,** *44* (6), 1601-1608.

162.    VanCott, T. C.; Gasyna, Z.; Schatz, P. N.; Boyle, M. E., *The Journal of Physical Chemistry* **1995,** *99* (13), 4820-4830.

163.    Tomilova, L. G.; Chernykh, E. V.; Gavrilov, V. I.; Shelepin, I. V.; Derkacheva, V. M.; Luk'yanets, E. A., *Zhurnal Obshchei Khimii* **1982,** *52* (11), 2606-11.

164.    Tomilova, L. G.; Chernykh, E. V.; Ioffe, N. T.; Luk'yanets, E. A., *Zhurnal Obshchei Khimii* **1983,** *53* (11), 2594-601.

165.    Martynov, A. G.; Zubareva, O. V.; Gorbunova, Y. G.; Sakharov, S. G.; Nefedov, S. E.; Dolgushin, F. M.; Tsivadze, A. Y., *European Journal of Inorganic Chemistry* **2007,** *2007* (30), 4800-4807.

166.    Wyatt, M. F.; Stein, B. K.; Brenton, A. G., *Analytical Chemistry* **2006,** *78* (1), 199-206.

167.    Binnemans, K.; Görller-Walrand, C., *Chemical Reviews* **2002,** *102* (6), 2303-2346.

168.    Trojan, K. L.; Hatfield, W. E.; Kepler, K. D.; Kirk, M. L., *Journal of Applied Physics* **1991,** *69* (8), 6007-6009.

169.    Vajk, O. P.; Greven, M.; Mang, P. K.; Lynn, J. W., *Solid State Communications* **2003,** *126* (1-2), 93-101.

170.    Bordallo, H. N.; Chapon, L. C.; Cook, J. C.; Copley, J. R. D.; Goremychkin, E.; Kern, S.; Lee, S. H.; Yildirim, T.; Manson, J. L., *Applied Physics A: Materials Science & Processing* **2002,** *74* (0), s634-s636.

171.    Gonidec, M.; Davies, E. S.; McMaster, J.; Amabilino, D. B.; Veciana, J., *Journal of the American Chemical Society* **2010,** *132* (6), 1756-1757.

172.    Gonidec, M.; Luis, F.; Vílchez, À.; Esquena, J.; Amabilino, D. B.; Veciana, J., *Angewandte Chemie International Edition* **2010,** *49* (9), 1623-1626.

173.    Branzoli, F.; Carretta, P.; Filibian, M.; Graf, M. J.; Klyatskaya, S.; Ruben, M.; Coneri, F.; Dhakal, P., *Physical Review B* **2010,** *82* (13), 134401.

174.    Branzoli, F.; Filibian, M.; Carretta, P.; Klyatskaya, S.; Ruben, M., *Physical Review B* **2009,** *79* (22), 220404.

175.    Kharmouche, A., *Journal of Nanoscience and Nanotechnology* **2011,** *11* (6), 4757-4764.

176.    Yang, T.; Pradhan, N. R.; Goldman, A.; Licht, A. S.; Li, Y.; Kemei, M.; Tuominen, M. T.; Aidala, K. E., *Appl. Phys. Lett.* **2011,** *98* (24), 242505/1-242505/3.

177.    Miller, J. S.; Drillon, M., *Magnetism: Molecules to Materials III:Nanosized Magnetic Materials*. Wiley -VCH: Weinheim, 2002.

178.    Martien, D. Introduction to AC Susceptibility. *www.qdusa.com/resources/pdf/1078-201.pdf* (accessed 12/26/2010).

179.    Groenendijk, H. A.; van Duyneveldt, A. J.; Willett, R. D., *Physica B+C* **1980,** *101* (3), 320-328.

180.    Wang, Q.; Li, Y.; Yan, X.; Rathi, M.; Ropp, M.; Galipeau, D.; Jiang, J., *Applied Physics Letters* **2008,** *93* (7), 073303-3.

181.    Cole, K.; Cole, R., *Journal of Chemical Physics* **1941,** *9* (4), 341.

182.    Cole, K.; Cole, R., *Journal of Chemical Physics* **1942,** *10* (2), 98.

183.    Kent, A. D.; Christou, G. C.; Dalal, N.; Hendrickson, D. N.; Hill, S. In *Quantum Spin Dynamics in Molecular Nanomagnets,* NSF Nanoscale Science and Engineering Grantees Conference, Arlingon, VA, Dec 4-6, 2006; Arlingon, VA, 2006.

184.    Ishikawa, N.; Sugita, M.; Wernsdorfer, W., *Journal of the American Chemical Society* **2005,** *127* (11), 3650-3651.

185.    Friedman, J. R., *Resonant Magnetization Tunneling in Molecular Magnets*. Nova Science: New York, 2003; p 179-218.

186.    Friedman, J. R.; Sarachik, M. P.; Tejada, J.; Ziolo, R., *Physical Review Letters* **1996,** *76* (20), 3830.

187.    Schlegel, C.; van Slageren, J.; Manoli, M.; Brechin, E. K.; Dressel, M., *Physical Review Letters* **2008,** *101* (14), 147203.

188.    Wernsdorfer, W.; Sessoli, R., *Science* **1999,** *284* (5411), 133.

189.    Aubin, S. M. J.; Dilley, N. R.; Pardi, L.; Krzystek, J.; Wemple, M. W.; Brunel, L.-C.; Maple, M. B.; Christou, G.; Hendrickson, D. N., *Journal of the American Chemical Society* **1998,** *120* (20), 4991-5004.

190.    Brechin, E. K.; Boskovic, C.; Wernsdorfer, W.; Yoo, J.; Yamaguchi, A.; Sañudo, E. C.; Concolino, T. R.; Rheingold, A. L.; Ishimoto, H.; Hendrickson, D. N.; Christou, G., *Journal of the American Chemical Society* **2002,** *124* (33), 9710-9711.

191.    Christou, G.; Gatteschi, D.; Hendrickson, D. N.; Sessoli, R., *MRS Bulletin* **2000,** *66-71*.

192.    Leuenberger, M. N.; Meier, F.; Loss, D., *Monatshefte für Chemie / Chemical Monthly* **2003,** *134* (2), 217-233.

193.    Wang, B.; Jiang, S.; Wang, X.; Gao, S., *Science in China Series B: Chemistry* **2009,** *52* (11), 1739-1758.

194.    Leuenberger, M. N.; Loss, D., *Nature* **2001,** *410* (6830), 789.

195.    Boskovic, C.; Brechin, E. K.; Streib, W. E.; Folting, K.; Bollinger, J. C.; Hendrickson, D. N.; Christou, G., *Journal of the American Chemical Society* **2002,** *124* (14), 3725-3736.

196.    Giraud, R.; Wernsdorfer, W.; Tkachuk, A. M.; Mailly, D.; Barbara, B., *Physical Review Letters* **2001,** *87* (5), 057203.

197.    Takamatsu, S.; Ishikawa, T.; Koshihara, S.-y.; Ishikawa, N., *Inorganic Chemistry* **2007,** *46* (18), 7250-7252.

198.    Ishikawa, N.; Sugita, M.; Okubo, T.; Tanaka, N.; Iino, T.; Kaizu, Y., *Inorganic Chemistry* **2003,** *42* (7), 2440-2446.

199.    Gatteschi, D.; Sessoli, R., Magnetic Properties of Large Clusters. In *Magnetism: Molecules to Materials III:Nanosized Magnetic Materials*, Miller, J. S.; Drillon, M., Eds. Wiley-VCH: Weinheim, 2002.

200.    Ishikawa, N.; Sugita, M.; Ishikawa, T.; Koshihara, S.-y.; Kaizu, Y., *The Journal of Physical Chemistry B* **2004,** *108* (31), 11265-11271.

201.    Branzoli, F.; Carretta, P.; Filibian, M.; Zoppellaro, G.; Graf, M. J.; Galan-Mascaros, J. R.; Fuhr, O.; Brink, S.; Ruben, M., *Journal of the American Chemical Society* **2009,** *131* (22), 7934-7934.

202.    Ishikawa, N., Comment on AC Magnetism of $(F_{64}Pc)_2DyH$. Osaka University, Osaka, 2010.

203. Motulsky, H. Curvefit.com: A Complete Guide to Non-Linear Regression. <http://graphpad.com/curvefit/linear_regression.htm> (accessed 1/5/2012).

204. Marquardt, D. W., *Journal of the Society for Industrial and Applied Mathematics* **1963,** *11* (2), 431-441.

205. Levenberg, K., *Quarterly Journal of Applied Mathmatics* **1944,** *2* (2), 164-168.

206. Kissinger, P.; Heineman, W. R., *Laboratory Techniques in Electroanalytical Chemistry*. 2 ed ed.; CRC: 1996.

207. Zoski, C. G., *Handbook of Electrochemistry*. Elsevier Science: 2007.

208. Bard, A. J.; Faulkner, L. R., *Electrochemical Methods: Fundamentals and Applications*. 2 ed ed.; Wiley: 2000.

209. Heineman, W. R.; Hawkridge, F. M.; Blount, H. N., In *Electroanalytical Chemistry: A Series of Advances*, Bard, A. J., Ed. Marcel Dekker: New York, 1984; Vol. 13, p 285.

210. Kuwana, T.; Winograd, N., Spectroelectrochemistry at Optically Transparent Electrodes: I. Electrodes Under Semi-Infinite Diffusion Conditions. In *Electroanalytical Chemistry: A Series of Advances*, Bard, A. J., Ed. Marcel Dekker: New. York, 1974; Vol. 7, p 1.

211. Plieth, W.; Wilson, G. S.; de La Fe, C. G., *Pure and Applied Chemistry* **1998,** *70* (7), 1395-1414.

212. Strojek, J. W.; Kuwana, T., *Journal of Electroanalytical Chemistry and Interfacial Electrochemistry* **1968,** *16* (4), 471-483.

213. Pons, B. S.; Mattson, J. S.; Winstrom, L. O.; Mark, H. B., *Analytical Chemistry* **1967,** *39* (6), 685-688.

214. Yildiz, A.; Kissinger, P. T.; Reilley, C. N., *Analytical Chemistry* **1968,** *40* (7), 1018-1024.

215. Kuwana, T.; Darlington, R. K.; Leedy, D. W., *Analytical Chemistry* **1964,** *36* (10), 2023-2025.

216. Meyer, M. L.; DeAngelis, T. P.; Heineman, W. R., *Analytical Chemistry* **1977,** *49* (4), 602-606.

217. Murray, R. W.; Heineman, W. R.; O'Dom, G. W., *Analytical Chemistry* **1967,** *39* (13), 1666-1668.

218. Norvell, V. E.; Mamantov, G., *Analytical Chemistry* **1977,** *49* (9), 1470-1472.

219. Stotter, J.; Haymond, S.; Zak, J. K.; Show, Y.; Cvackova, Z.; Swain, G. M., *Electrochem. Soc. Interface* **2003,** *12* (1), 33-38.

220. Weber, C. M.; Eisele, D. M.; Rabe, J. P.; Liang, Y.; Feng, X.; Zhi, L.; Müllen, K.; Lyon, J. L.; Williams, R.; Bout, D. A. V.; Stevenson, K. J., *Small* **2009,** *6* (2), 184-189.

221. Zudans, I.; Paddock, J. R.; Kuramitz, H.; Maghasi, A. T.; Wansapura, C. M.; Conklin, S. D.; Kaval, N.; Shtoyko, T.; Monk, D. J.; Bryan, S. A.; Hubler, T. L.; Richardson, J. N.; Seliskar, C. J.; Heineman, W. R., *Journal of Electroanalytical Chemistry* **2004,** *565* (2), 311-320.

222. Richardson, J. N.; Osisek, A. J.; Dyer, A. L., *Electroanalysis* **2003,** *15* (19), 1567-1570.

223. Patel, M.; McGuire, M. E. In *Ruthenium(II) Complexes of a Bipyridine-Based Alloxazine Ligand Incorporated into TiO$_2$-Coated Electrodes*, American Chemical Society: 2003; pp INOR-114.

224. McIntyre, J. D. E., Specular reflection spectroscopy of the electrode-solution interphase. In *Advances in Electrochemistryand Electrochemical Engineering*, Muller, R. H., Ed. Wiley: New York, 1973; Vol. 9, p 61.

225. McGraw-Hill, *McGraw-Hill Dictionary of Scientific & Technical Terms, 6E*. McGraw-Hill Companies, Inc.: 2003.

226. Stephens, P. J.; Devlin, F. J., *Wiley/CSMP* **2007,** *21* ( 8 (c02)), 180-205.

227. Buckingham, A. D.; Stephens, P. J., *Annual Review of Physical Chemistry* **1966,** *17*, 399-432.

228. Mason, W. R., *A Practical Guide to Magnetic Circular Dichroism Spectroscopy*. John Wiley&Sons, Inc.: Hoboken, N. J, 2007; p 223

229. Drake, G. W. F., *Springer Handbook of Atomic, Molecular and Optical Physics*. Springer: 2006; Vol. 1, p 1504.

230. Stephens, P. J., *Annual Review of Physical Chemistry* **1974,** *25* (1), 201-232.

231. Hernandez-Marin, E.; Seth, M.; Ziegler, T., *Inorganic Chemistry 49* (13), 6066-6076.

232. Solomon, E. I.; Pavel, E. G.; Loeb, K. E.; Campochiaro, C., *Coordination Chemistry Reviews* **1995,** *144*, 369-460.

233. Lehnert, N.; George, S. D.; Solomon, E. I., *Current Opinion in Chemical Biology* **2001,** *5* (2), 176-187.

234. Neese, F.; Solomon, E. I., *Inorganic Chemistry* **1999,** *38* (8), 1847-1865.

235. Oganesyan, V. S.; George, S. J.; Cheesman, M. R.; Thomson, A. J., *Journal of Chemical Physics* **1999,** *110* (2), 762.

236. McInnes, E. J. L.; Pidcock, E.; Oganesyan, V. S.; Cheesman, M. R.; Powell, A. K.; Thomson, A. J., *Journal of the American Chemical Society* **2002,** *124* (31), 9219-9228.

237. Kadish, K. M.; Nakanishi, T.; Gürek, A.; Ahsen, V.; Yilmaz, I., *The Journal of Physical Chemistry B* **2001,** *105* (40), 9817-9821.

238. Zhu, P.; Lu, F.; Pan, N.; Arnold, Dennis P.; Zhang, S.; Jiang, J., *European Journal of Inorganic Chemistry* **2004,** *2004* (3), 510-517.

239. Pushkarev, V. E.; Tolbin, A. Y.; Borisova, N. E.; Trashin, S. A.; Tomilova, L. G., *European Journal of Inorganic Chemistry* **2010,** *2010* (33), 5254-5262.

240. Gonidec, M.; Davies, S. E.; Graham, W.; McMaster, J.; Vidal-Gancedo, J.; Gorun, S. M., Slow Magnetic Relaxation of Highly Reduced States of a Double-Decker Phthalocyanine Terbium (III) Complex. Barcelona, 2011; p 12.

241. Keizer, S. P.; Mack, J.; Bench, B. A.; Gorun, S. M.; Stillman, M. J., *Journal of the American Chemical Society* **2003,** *125* (23), 7067-7085.

242. Domingo, N.; Williamson, B. E.; Gomez-Segura, J.; Gerbier, P.; Ruiz-Molina, D.; Amabilino, D. B.; Veciana, J.; Tejada, J., *Physical Review B* **2004,** *69* (5), 052405.

243. Deutsch, D., *Proceedings of the Royal Society of London; Series A* **1985,** *400* (1818), 97-117.

244. Shor, P. W., *Physical. Review. A: At., Mol., Opt. Phys.* **1995,** *52* (4), R2493-R2496.

245. Grover, L. K., *Physical Review Letters* **1997,** *79* (23), 4709-4712.

246. Grover, L. K., *Physical Review Letters* **1998,** *80* (19), 4329-4332.

247. Nielsen, M. A.; Chuang, I. L., *Quantum Computation and Quantum Information*. Cambridge University Press: Cambridge, 2000.

248. Weber, J. R.; Koehl, W. F.; Varley, J. B.; Janotti, A.; Buckley, B. B.; Van de Walle, C. G.; Awschalom, D. D., *Proceedings of the National Academy of Sciences* **2010,** *107* (19), 8513-8518.

249. Milburn, G. J., *Science* **2010,** *330* (6008), 1188-1189.

250.    Martinis, J. M.; Nam, S.; Aumentado, J.; Urbina, C., *Physical Review Letters* **2002,** *89* (11), 117901.

251.    Jones, J. A.; Hansen, R. H.; Mosca, M., *Journal of Magnetic Resonance* **1998,** *135* (2), 353-360.

252.    Jones, J. A.; Mosca, M., *Journal of Chemical Physics* **1998,** *109* (5), 1648.

253.    Grover, L. K., *Physical Review Letters* **1997,** *79* (2), 325-328.

254.    Shor, P. W. In *Algorithms for Quantum Computation: Discrete Logarithms and Factoring*, Foundations of Computer Science, 1994 Proceedings., 35th Annual Symposium 20-22 Nov 1994; pp 124-134.

255.    Deutsch, D.; Jozsa, R., *Proceedings: Mathematical and Physical Sciences* **1992,** *439* (1907), 553-558.

256.    Komeda, T.; Isshiki, H.; Liu, J.; Zhang, Y.-F.; Lorente, N.; Katoh, K.; Breedlove, B. K.; Yamashita, M., *Nature Communications* **2011,** *2*, 217.

257.    Nakanotani, H.; Yahiro, M.; Adachi, C.; Yano, K., *Applied Physics Letters* **2007,** *90*, 262104.

258.    Vitali, L.; Fabris, S.; Conte, A. M.; Brink, S.; Ruben, M.; Baroni, S.; Kern, K., *Nano Letters* **2008,** *8* (10), 3364-3368.

259.    Riga, A. T.; Judovits, L., *Material Characterization by Dynamic and Modulated Thermal Analytical Techniques*. American Society for Testing and Materials: West Conshohocken, PA, **2001**; p 223.

260.    Thomas, L. C., *American Laboratory* **2001,** *33* (January), 26-31.

261.    Bench, B. A.; Beveridge, A.; Sharman, W. M.; Diebold, G. J.; van Lier, J. E.; Gorun, S. M., *Angewandte Chemie International Edition* **2002,** *41* (5), 747-750.

262.    Liu, W.; Jiang, J.; Du, D.; Arnold, D. P., *Australian Journal of Chemistry* **2000,** *53* (2), 131-135.

263.    Sheldrick, G. M. *SHELXL-97, Program for refinement of crystal structures*, University of Göttingen: Germany, 1997.

264.    Sheldrick, G. M. *SHELXTL, version 6.14; Bruker AXS, Inc*, Madison, WI., 2004.

265.    Barnes, P.; Vickers, M. Intensity of Diffraction: the Structure Factor Equation. http://pd.chem.ucl.ac.uk/pdnn/diff1/sfactor.htm (accessed 1/8/2012).

266. Müller, P.; Herbst-Irmer, R.; Spek, A. L.; Schneider, T. R.; Sawaya, M. R., *Crystal Structure Refinement: A Crystallographer's Guide to SHELXL*. Oxford University Press: Oxford, 2006.

267. Wells, R. J., *Journal of Quantitative Spectroscopy & Radiative Transfer* **1999,** *62*, 29-48.

268. Olivero, J. J.; Longbothum, R. L., *Journal of Quantitative Spectroscopy & Radiative Transfer* **1977** *17* (2), 233-236.

269. Gottlieb, H.; Kotlyar, V.; Nudelman, A., *Journal of Organic Chemistry* **1997,** *62*, 7512-7515.

270. Adminstrator Characteristic proton chemical shifts. <http://wwwchem.csustan.edu/Tutorials/NMRTABLE.HTM> (accessed 7/12/2009).

271. Nemykin, V. N.; Chernii, V. Y.; Volkov, S. V., *Journal of the Chemical Society, Dalton Transactions* **1998,** (18), 2995-3000.